

FERROELECTRIC THIN FILMS FOR MICROACTUATOR APPLICATIONS

*Thesis Submitted to the
Calicut University, Malappuram
in Partial Fulfillment of the Requirements
for the award of the degree of
Doctor of Philosophy
in Chemistry
under the Faculty of Science*

by

LAXMI PRIYA S.

**Under the supervision of
Dr. V. Kumar, Senior Scientist**



**Centre for Materials for Electronics Technology (C-MET)
(Scientific Society, Department of Information Technology,
Ministry of Communication and Information Technology, Govt. of India)
Shornur Road, M. G. Kavu, Athani P.O., Thrissur 680 581, Kerala, India.
Email: cmett@cmct.gov.in URL: wwwcmctt.gov.in**

April 2018

Ferroelectric Thin Films for Microactuator Applications

Ph D Thesis under the Faculty of Science

Submitted by

Laxmi Priya S.

Ambady, Kottayil Road

Kunnamkulam P.O.- 680 503

Kerala, India.

e-mail: laxmipriya.sm@gmail.com

Research Supervisor

Dr. V. Kumar

Scientist F

Centre for Materials for Electronics Technology (C-MET)

Thrissur- 680 581

Kerala, India

e-mail: vkumar@cmet.gov.in

April 2018

Format for plagiarism check certificate

**UNIVERSITY OF CALICUT
CERTIFICATE ON PLAGIARISM CHECK**

1.	Name of the research scholar	LAXMI PRIYA S.		
2.	Title of thesis/dissertation	FERROELECTRIC THIN FILMS FOR MICROACTUATOR APPLICATIONS		
3.	Name of the supervisor	Dr. V. KUMAR		
4.	Department/Institution	CENTRE FOR MATERIALS FOR ELECTRONICS TECHNOLOGY (C-MET), THRISSUR		
5.	Similar content (%) identified	Introduction/ Review of literature	Materials and Methods	Result/ Discussion/Summary/ Conclusion
		1%	4%	5%
	Acceptable maximum limit (%)	25 /35	25	10
6.	Software used	Vtrakund		
7.	Date of verification	10/4/2018		

*Report on plagiarism check, specifying included/excluded items with % of similarity to be attached.

Checked by (with name, designation & signature)

[Signature]

Dr. Vinod.V.M.
Assistant Librarian
University of Calicut

Name & Signature of the Researcher

[Signature] LAXMI PRIYA S.

Name & Signature of the Supervisor

[Signature]

Dr. V. Kumar
Scientist
Centre for Materials for Electronics Technology (C-MET), DIT, Govt. of India
Mulangunnathukavu, Athani,
Thrissur - 680 581

The Doctoral Committee* has verified the report on plagiarism check with the contents of the thesis, as summarized above and appropriate measures have been taken to ensure originality of the Research accomplished herein.

Name & Signature of the HoD/Hof (Chairperson of the Doctoral Committee)

[Signature]

डॉ. एन. राघु
Dr. N. RAGHU
In case of language other than Malayalam, Tamil, etc. on which no software is available for plagiarism check, a manual check shall be made by the Doctoral Committee, for which an additional certificate shall be attached.
C-MET (MET), Govt. of India
Mulangunnathukavu, Athani, Thrissur - 680 581 / Thrissur - 680 581
केरला / Kerala





सेन्टर फॉर मेटिरियल्स फॉर इलेक्ट्रॉनिक्स टेक्नोलॉजी (सी-मेट)

(वैज्ञानिक संस्था, इलेक्ट्रॉनिक्स और सूचना प्रौद्योगिकी मंत्रालय, भारत सरकार)

षोरनूर रोड, मुलंगुन्नतुकावु पोस्ट, अत्तानि, त्रिशूर - 680 581, केरला, भारत

CENTRE FOR MATERIALS FOR ELECTRONICS TECHNOLOGY

(Scientific Society, Ministry of Electronics and Information Technology, Government of India)

Shoranur Road, P.O. Mulangunnathukavu, Athani, Thrissur - 680 581, Kerala, India

Tel : EPABX : 91-487-2201156-59 (4 LINES). Fax : 91-487-2201347

E-mail : cmett@cmet.gov.in URL : www.cmet.gov.in

Dr. V. Kumar

Scientist F

Certificate

This is to certify that the thesis entitled “**Ferroelectric Thin Films for Microactuator Applications**” submitted to Calicut University in partial fulfilment of the requirements for the award of the degree of **Doctor of Philosophy in Chemistry** under the Faculty of Science, Calicut University, is a record of the authentic work carried out by Smt. Laxmi Priya S., at Centre for Materials for Electronics Technology, Thrissur, under my guidance. The work presented in this thesis has not been submitted for any other degree or diploma of this or any other University.

Thrissur
April 2018

Dr. V. Kumar
(Supervising Guide)

Declaration

I hereby declare that the thesis entitled “**Ferroelectric Thin Films for Microactuator Applications**” submitted to Calicut University, is based on the original research work carried out by me under the guidance and supervision of Dr. V. Kumar, Scientist, Centre for Materials for Electronics Technology, Thrissur. No part of this work has been presented for the award of any other degree from any other institution.

Thrissur
April 2018

Laxmi Priya S.

Dedicated to my family.....

Acknowledgments

I, personally wish to express my hearty gratitude towards God for his amazing grace of blessing in my life which cannot be expressed in a single word.

Firstly, I would like to express my sincere gratitude to my research supervisor, and former director, C-MET, Dr. V. Kumar for his critical and constructive comments, advices and suggestions during my entire research work. He was always an inspiration and encouragement to me and whenever I slipped down due to one or other reasons, the vibrational energy radiated by him helped to boost me. I am deeply grateful to him whose perceptiveness and astute suggestions made this thesis a different one.

I am grateful to the C-MET Executive Director Dr. N.R. Muniratnam, Director Dr. Raghu, former Executive Director Dr. D.P. Amelnekar and Former Director Dr. K.R. Dayas for permitting me to carry out research activities at this institution.

I would like to express my sincere gratitude to Dr. Ratheesh, Dr. N.C. Pramanik, Dr. S.N. Potty, Dr. A. Seema, Dr. Radhika, Dr. Stanly Jacob, Dr. K.P. Murali, Abhishek Choudhary and former scientist Dr. K.V. Baiju for their valuable suggestions and their support. I am also grateful to all technical staff of C-MET for their support and concern. I would like to thank Administrative staff of C-MET, Thrissur for their constant support.

The helping hands from different research laboratories are greatly acknowledged. I am indebted to Prof. Isaku Kanno (Kyoto University, Japan) for the piezoelectric measurements and valuable suggestions for my research work. I also acknowledge SAIIF, IIT Madras for recording the HRSEM images of thin film samples.

Financial support provided by University Grants Commission under UGC-JRF scheme is gratefully acknowledged.

My friends from different institutes have always helped me with literature survey and valuable suggestions. I remember Dr. Libu, Dr. Jai Kumar, Dr. Mothy

(Cusat), Miss. Archana (Cusat), Miss. veena, Mrs. Reshma (Calicut University), Mrs. Shaniba (SNGS College, Pattambi) for their valuable suggestions.

I am thankful to my colleagues of our lab Dr. Vani, Dr. Divya, Mr. Anil, Mrs. Vijila, Mr. Manoj and Mr. Satheeshan for their timely encouragement and support. I appreciate former group members Dr. Divya and Dr. K.P. Rema for their valuable suggestions. I am expressing my special thanks to Dr. D. Ambika and Dr. T. Anto Johny for their valuable suggestions in thin film area for my entire research work,

I remember the help received from Mr. Sivanandan and Mr. Packiaselvam for XRD measurements of thin films. I am also grateful to Mrs. Priyadarsini, and Mrs. Bindumol for their support and care.

I am also thankful for the continuous encouragement from my friends Miss. Swathy, Miss. Akhila, Mrs. Arathy, Mrs. Unnimaya, Mrs. Rahna, Mrs. Aparna, Mr. Prabeesh, Mr. Simson, Mr. Gopakumar, Mr. Rohith, Mr. Vinoj at C-MET. I am also grateful to all teachers of the department of Chemistry, Sree Narayana College, Nattika for their support. I acknowledge the sincere support of the management, Principal of Sree Narayana College, Nattika for helping me to continue the research. I am also grateful to all my teachers, especially the teachers of St. Thomas College for their constant motivation to pursue research. I would like to express my sincere thanks to my teacher Dr. Joby Thomas for his valuable suggestions and help during my career development. I am also indebted to my teacher Dr. E.A. Jose and his family for motivating me to pursue the best in my life.

Words really fail to express the love, support and encouragement that I enjoyed from my mother and Father. They motivated and encouraged me with their valuable advices, care and love throughout my life.

I am indebted to my husband for his full support and encouragement without which I was not able to do my research work, I am also grateful for the support and love received from my daughter and entire family. Above all, I thank almighty for all the blessings showered upon me.

Laxmi Priya S.

Preface

Ferroelectric oxides are actively researched due to their excellent properties like high piezoelectricity, high permittivity, tunability of dielectric permittivity and nonlinear optical property. Of the various ferroelectric oxides, lead based piezoelectrics acquire importance since they provide electrical properties suitable for multifunctionality. The quest for miniaturized products actually has led to increasing demands for the development of thin films. Advantages of ferroelectric thin films include lower operating voltages, device miniaturisation and easy integration to IC's. The electrical characteristics of ferroelectric thin films are mainly influenced by various factors such as processing conditions, preferential crystallographic orientation, film thickness etc whose underlying principles are not yet fully understood and explored. Ferroelectric Lead Zirconate Titanate (PZT) thin films have attracted considerable attention for microelectronic applications including ferroelectric memory devices. The properties of PZT can be tailored by appropriate doping mechanism and/or through the control of their crystallographic orientation. A-site substitution/doping in PZT forms complex perovskites which in turn receives greater attention due to their excellent electrostrictive, piezoelectric and electro optic characteristics above a threshold concentration of La^{3+} . PLZT compositions that lie very close to the morphotropic phase boundary (MPB) exhibits outstanding properties since there is the coexistence of rhombohedral, tetragonal and monoclinic phases.

We adopted Chemical solution deposition (CSD) method particularly Sol-gel for the precursor solution preparation since it offers excellent control of the stoichiometry, lower processing temperatures and is also economical.

The thesis is organised in to six chapters. Chapter-1 deals with the motivation for the present research work, general introduction, basic concepts, dielectric, piezoelectric and ferroelectric properties of normal ferroelectrics. This chapter also includes the charge compensation mechanisms that occur during acceptor and donor doping in PZT and also describes the path ways for achieving outstanding piezoelectric properties by preferential crystallographic orientation changes. The role of intrinsic and extrinsic factors in determining piezoelectric properties are also discussed in detail. A brief outline of the present research work is also given in this chapter.

Chapter-2 is dedicated to the discussions regarding the different deposition techniques and thin film properties. The Chemical solution deposition of ferroelectric thin films by Sol-gel method is discussed in detail on account of their ability to grow dense, crack-free films with precise stoichiometry. Also this chapter briefly explains the principles and theory behind major characterization techniques used in the present study such as XRD, dielectric, piezoelectric and ferroelectric characterization. The crystalline phase and preferential orientation of the prepared thin films were studied using an X-ray diffractometer (XRD, Model D-5005, Bruker, Germany) and a Raman spectrometer (Model:DXR, Thermoscientific, USA). The dielectric and ferroelectric measurements were carried out using an impedance-gain phase analyzer (Model, 4294A, Agilent Technologies, USA) and piezoelectric evaluation system (Model TF Analyser 2000, aixACCT, Germany) respectively. The transverse piezoelectric properties of PLZT thin films were evaluated using unimorph cantilevers of PLZT/Si. The application of sine wave voltage between the top and bottom electrodes generates deflection by inverse piezoelectric effect and the tip displacement was measured using a laser Doppler vibrometer (T-3500, Graphtec, Germany) and

a laser interferometer (AT-1100, Graphtec, Germany). The microstructural analysis of the prepared films was carried out using a high resolution Scanning electron microscope (HRSEM, Model, Genesis, Apex 2, Ametek, Japan).

Chapter-3 deals with the preparation of preferentially {100} and {110}-oriented PLZT thin films having compositions near the morphotropic phase boundary (MPB) that are suitable for microactuator applications. For micro actuator applications, fabrication of piezoelectric thin films within the thickness range of 0.5-2.0 μm is required for realizing maximum force and displacement. Also {100}-oriented films with rhombohedral structure offers high strain values preferable for electromechanical applications. Hence we prepared preferentially {100}-oriented thin films of Lead Lanthanum Zirconate Titanate, $(\text{Pb}_{1-x}\text{La}_x)(\text{Zr}_{0.65}\text{Ti}_{0.35})_{1-x/4}\text{O}_3$ [PLZT(x/65/35)], $x=0.06$, 0.07 and 0.08 near the morphotropic phase boundary (MPB) on silicon substrates (111)Pt/Ti/SiO₂/Si by sol-gel spin coating technique. It was found that optimum dielectric, piezoelectric and ferroelectric characteristics were obtained for PLZT (7/65/35) composition. Therefore using this as the basis, by varying the Zr/Ti ratios, three compositions viz, PLZT (7/65/35), (7/60/40) and (7/56/44) across the MPB were selected. For these compositions, {110}-preferentially oriented thin films were fabricated. We evaluated the transverse piezoelectric coefficient ($|e_{31,f}|$) through the tip deflection of unimorph cantilevers since it is the most important parameter to be considered regarding the geometry of thin films. We compared the electrical characteristics of both {100} and {110}-oriented PLZT thin films having compositions near MPB and selected a composition with the largest transverse piezoelectric coefficient ($|e_{31,f}|$), minimum nonlinearity in $|e_{31,f}|$ and minimum leakage current density that is most suitable for microactuator applications.

Chapter-4 deals with the fabrication of {110}-oriented acceptor-doped PLZT (8/65/35) thin films. PLZT (8/65/35) exhibits a rhombohedral structure very close to morphotropic phase boundary (MPB) and hence regarded as the ideal host system for B-site aliovalent acceptor doping since oxygen vacancies are neutralised by A-cation vacancies. The electromechanical properties suitable for MEMS applications can also be increased by structural distortions. We have selected Fe^{3+} , Mn^{3+} and Cu^{2+} B-site acceptor dopants, with a view to understand the influence of structural distortions on the transverse piezoelectric coefficient ($|e_{31,f}|$) and correlated them with their crystal structure. Mechanism for higher bipolar strain in Cu^{2+} and Mn^{3+} doped PLZT films have also been studied and are reported.

Most relaxor ferroelectric compositions come under the category of complex perovskites. The Lead based solid solutions of relaxor ferroelectrics may be either B-site substituted or A-site substituted complex perovskites. They are reported to exhibit excellent piezoelectric and electrostrictive properties suitable for micro electro mechanical systems. Solid solutions of Lead Indium Niobate (PIN) with ferroelectric Lead Titanate (PT) with the general formula $(1-x)\text{Pb}(\text{In}_{0.50}\text{Nb}_{0.50})\text{O}_{3-x}\text{PbTiO}_3$, with $0.34 < x < 0.38$ are at the MPB and can exhibit excellent piezoelectric applications. Also no reports are available on the electrical properties of PIN- x PT thin films. Hence Chapter 5 deals with the preparation of solid solutions consisting of Lead Indium Niobate (PIN) and Lead Titanate (PT), $(1-x)\text{PIN}-x\text{PT}$, $x = 0.36-0.40$ with compositions near the morphotropic phase boundary (MPB). We also established the stabilisation of discrete rhombohedral, monoclinic and tetragonal crystalline phases as the thin film composition is varied across the morphotropic phase boundary and also correlated the variation in transverse piezoelectric coefficient ($|e_{31,f}|$) while

moving from rhombohedral to monoclinic and tetragonal compositions with the domain switching mechanisms.

The extensive applications of ferroelectrics thin films in the field of non-volatile memories, microsensors, microactuators, random access memories, optical wave guides etc make them as ideal candidates for intense investigations for electronic applications. The increasing requirements for microactuators in MEMS made it necessary to develop thin films exhibiting high strain values. Hence excellent strain associated with electric field induced AFE→FE transition make them important for actuator applications due to the larger unit cell volume of the ferroelectric phase compared with the antiferroelectric phase and is described in detail in Chapter 6. We focussed on mainly three compositions in the antiferroelectric tetragonal region that lie in a line from left to right very close to the morphotropic phase boundary and investigate the influence of electric field induced phase transition on transverse piezoelectric coefficients of their thin film form on which no previous reports are available. We also investigated the variation of dielectric constant as a function of temperature for analysing AFE→FE transition. In addition to this, the structural evidence obtained from Raman spectra helped in confirming the electric field induced phase transitions in the antiferroelectric compositions.

The last section contains highlights of the present work. The major findings of the present research work have led to the following publications in international journals which are listed below.

- [1] **S. Laxmi Priya**, V. Kumar, Fumiya Kurokawa, Isaku Kanno, “Transverse piezoelectric properties of {100}-oriented PLZT [x/65/35] thin films,” **Materials Chemistry and Physics**, 151, (2015) 308-311.

- [2] **S. Laxmi Priya**, V. Kumar, Shogo Nishio, Isaku Kanno, "Composition dependence of transverse piezoelectric properties of preferentially {110}-oriented (1-x) PIN-x PT thin films," **Journal of Alloys and Compounds**, 688, (2016) 863-867.
- [3] **S. Laxmi Priya**, V. Kumar, Shogo Nishio, Isaku Kanno, "Improved piezoelectric response in {110}-oriented B-site acceptor doped PLZT (8/65/35) thin films," **Integrated Ferroelectrics**, 176, (2016) 210-219.
- [4] **S. Laxmi Priya**, V. Kumar, Isaku Kanno, "Influence of Zr/Sn ratio on the Transverse Piezoelectric Coefficient $|e_{31,f}|$ in Lanthanum doped Lead Zirconate Titanate Stannate Thin Films," **Journal of Materials Engineering and Performance** (communicated).
- [5] **S. Laxmi Priya**, V. Kumar, Takuya Teramoto, Isaku Kanno, "Transverse Piezoelectric properties of {110}-oriented PLZT thin films," **Integrated Ferroelectrics** (under review).

CONTENTS

1. Introduction to ferroelectric thin films -----	1
1.1 Motivation of the present study-----	2
1.2 Introduction-----	4
1.3 Basis of ferroelectricity -----	5
1.3.1 Ferroelectric domains and spontaneous polarization-----	10
1.3.2 Origin of hysteresis loop-----	13
1.3.2.1 Polarization-Electric field hysteresis loop -----	14
1.3.2.2 Strain –Electric field hysteresis in ferroelectrics -----	15
1.3.3 ABO ₃ Perovskite structure -----	17
1.3.3.1 Important ferroelectric oxides -----	19
1.3.3.2 Lead Zirconate Titanate (PZT)-----	19
1.3.3.3 Defect chemistry in PZT -----	23
1.3.3.3.1 Donor doping-----	24
1.3.3.3.2 Acceptor doping-----	24
1.3.3.4 Lanthanum doping in PZT (PLZT) -----	25
1.3.3.5 Relaxor ferroelectrics-----	26
1.3.4 Ferroelectric thin films -----	29
1.3.5 Domain wall contribution in determining properties of ferroelectric material -----	29
1.3.6 Intrinsic and extrinsic contributions -----	30
1.3.7 Dielectric properties -----	39
1.3.7.1 Dielectric permittivity -----	39
1.3.7.2 Dielectric loss-----	43
1.3.7.3 Dielectric tenability -----	44
1.3.7.4 Leakage current -----	44
1.3.8 Piezoelectric properties -----	46

1.3.8.1	Longitudinal piezoelectric constant (d_{33}) -----	54
1.3.8.2	Transverse piezoelectric constant (d_{31})-----	54
1.3.9	Domain engineering in thin films -----	59
1.3.10	Importance of film thickness and grain size in determining properties -----	59
1.3.11	Technological applications of ferroelectric thin films-----	66
1.4	Present research work -----	69
	References -----	73
2.	Thin film deposition and Characterisation techniques -----	83
2.1	Introduction-----	84
2.2	Thin film deposition techniques -----	85
2.2.1	Vacuum evaporation -----	86
2.2.2	Sputter deposition-----	86
2.2.3	Ion beam deposition -----	87
2.3	Chemical deposition -----	88
2.3.1	Chemical vapour deposition (CVD) -----	88
2.3.2	Atomic layer deposition (ALD)-----	89
2.3.3	Metallo-Organic Decomposition (MOD)-----	89
2.3.4	Sol-gel -----	90
2.4	Selection of chelating agents for thin film precursor solution preparation -----	92
2.5	Preparation of precursor solutions-----	96
2.5.1	PLZT precursor $[(\text{Pb}_{1-x}\text{La}_x)(\text{Zr}_{0.65}\text{Ti}_{0.35})_{1-x/4}\text{O}_3]$ -----	96
2.5.2	Acceptor doped PLZT precursor -----	96
2.5.3	$(1-x)\text{PIN}- x\text{PT}$ precursor solution-----	97
2.5.4	Tin doped lead lanthanum zirconate titanate (PLSnZT) solution -----	97
2.6	Processing equipments -----	97

2.6.1	Substrates for thin film deposition -----	97
2.6.2	Spin coating-----	98
2.6.3	Tubular furnace -----	99
2.6.4	High vacuum coating unit -----	99
2.7	Thin film growth process -----	100
2.8	Characterization techniques -----	101
2.8.1	X-ray diffraction (XRD) -----	101
2.8.2	Spectroscopic reflectometer -----	103
2.8.3	Raman spectroscopy-----	104
2.8.4	Scanning electron microscope -----	106
2.8.5	UV-Visible spectrophotometry -----	108
2.8.6	Impedance Analyser-----	109
2.9	Measurement of leakage current-----	111
2.10	Measurement of ferroelectric properties-----	112
2.11	Measurement of piezoelectric properties-----	116
	References -----	119

3. Preferentially oriented PLZT thin films suitable for MEMS applications -----123

3.1	Introduction -----	124
3.2	Preferentially 100}-oriented $(\text{Pb}_{1-x}\text{La}_x)(\text{Zr}_{0.65}\text{Ti}_{0.35})_{1-x/4}\text{O}_3$ thin films -----	124
3.2.1	Experimental work-----	131
3.2.2	Results and discussion -----	135
3.3	Transverse piezoelectric properties of {110}-oriented PLZT thin films -----	140
3.3.1	Experimental -----	141
3.3.2	Results and discussion -----	142
3.4	Conclusion -----	147
	References -----	149

4. Improved piezoelectric response in {110}–oriented B – site acceptor doped PLZT (8/65/35) thin films-----	155
4.1 Introduction-----	156
4.2 Experimental -----	159
4.3 Results and Discussion-----	161
4.4 Conclusion-----	172
References -----	173
5 Composition dependence of Transverse Piezoelectric properties of preferentially {110}– oriented (1 – x) PIN- x PT thin films-----	177
5.1 Introduction-----	178
5.2 Experimental -----	182
5.3 Results and Discussions -----	185
5.5 Conclusion-----	192
References -----	193
6 Influence of Zr/Sn ratio on the transverse piezoelectric Coefficient $e_{31,f}$ in Lanthanum doped Lead Zirconate Titanate Stannate Thin Films -----	199
6.1 Introduction-----	200
6.2 Experimental -----	202
6.3 Results and discussion -----	203
6.4 Conclusion-----	211
References -----	212
Highlights of the Present Work -----	217
List of Research Publications -----	219

LIST OF TABLES

Table 3.1	Electrical characteristics of PLZT thin films-----	138
Table 4.1	Dielectric and piezoelectric properties of acceptor doped PLZT (8/65/35) thin films -----	167
Table 5.1	Dielectric and piezoelectric characteristics of $(1-x)$ PIN- x PT thin films-----	189
Table 6.1	Dielectric and piezoelectric properties of thin films -----	207

LIST OF FIGURES

Figure 1.1:	Schematic diagram of the classification of crystal based on symmetry-----	6
Figure 1.2:	Piezoelectric effects in ferroelectric ceramics-----	7
Figure 1.3:	Changes that occur in a two-axial ferroelectric material when it transforms from a paraelectric cubic into a ferroelectric tetragonal phase (only two axes are shown)-----	9
Figure 1.4:	Change with temperature of dielectric permittivity of BaTiO ₃ single crystal -----	10
Figure 1.5:	(a) Dielectric polarisation, (b) Paraelectric polarisation and (c) Ferroelectric polarization -----	11
Figure 1.6:	Perovskite ABO ₃ unit cell demonstrating 180 ⁰ polarisation reversal for two of the six possible polarisation states caused by the displacement of central ion in a tetragonal plane -----	11
Figure 1.7:	Illustration of (a) 180 ⁰ and (b) 90 ⁰ ferroelectric domains and domain wall regions in a tetragonal perovskite ferroelectric. The change of polarization across domain wall for a 180 ⁰ wall is given in (a) and tetragonal distortion in (b) -----	12
Figure 1.8:	Three phases of domain reversal; 1. Nucleation (fast) 2. Forward growth (fast) 3. Sideways growth (slow)-----	13
Figure 1.9:	Polarization-Electric field hysteresis loop. Circles with arrows represent the polarization state of the material at the indicated fields-----	15
Figure 1.10:	Strain-Electric field (S-E) hysteresis loop in ferroelectrics -----	16
Figure 1.11:	A typical ABO ₃ unit cell structure -----	17
Figure 1.12:	The low temperature phase diagram of lead zirconate titanate (PZT) phase diagram illustrating cubic paraelectric phase and tetragonal and rhombohedral phases-----	20

Figure 1.13:	PbZrO ₃ -PbTiO ₃ phase diagram according to Woodward et al -----	22
Figure 1.14:	Mirror planes of monoclinic phase found in MPBs of PZT -----	23
Figure 1.15:	Piezoelectric d strain coefficients versus composition for PZT system -----	23
Figure 1.16:	Phase diagram of PZT and PLZT solid-solution systems -----	26
Figure 1.17:	Domain engineered structure in [001] _c oriented rhombohedral crystals of PMN-xPT and PZN-xPT on application of electric field along [001] _c direction -----	28
Figure 1.18:	Illustration of 180 ⁰ domain switching in ferroelectric materials -----	30
Figure 1.19:	Illustration of non-180 ⁰ domain switching in ferroelectrics -----	31
Figure 1.20:	Possible orientations of polarization vectors in (a) tetragonal and (b) rhombohedral PZT film -----	32
Figure 1.21:	P-E hysteresis loop of PZT thin films on (a) Pt/MgO and (b) on Si -----	32
Figure 1.22:	Tip deflection of cantilevers as a function of applied voltage in (a) Pt/MgO and (b) PZT film on Si -----	33
Figure 1.23:	Tip displacement as a function of applied voltage in (a) epitaxial PZT film on Pt/MgO substrate, (b) polycrystalline PZT film on Pt/Ti/Si substrate -----	34
Figure 1.24:	Piezoelectric coefficient e ₃₁ of PZT film deposited on (a) Pt/MgO and (b) Pt/Si substrate -----	35
Figure 1.25:	Single domain PZT ferroelectric single crystal -----	36
Figure 1.26:	The nonlinear behaviour of the dielectric permittivities ε ₁₁ and ε ₃₃ with the applied AC field in a soft PZT ceramic -----	38
Figure 1.27:	Effect of composition on dielectric constant ε _r and electromechanical coupling factor K _p in PZT -----	42

Figure 1.28:	Intercept and slope of linear logarithmic fits at various bias field for extrinsic (blue) and intrinsic (black) contributions -----	43
Figure 1.29:	Leakage current density (J) curves of PZT thin films for different orientations-----	45
Figure 1.30:	Direction of forces acting on a piezoelectric element-----	47
Figure 1.31:	(a) Effective piezoelectric constant d_{33} of rhombohedral PZT 52/48. (b) Cross sectional curve when figure in (a) is cut by Y-Z plane -----	48
Figure 1.32:	Experimental evidence regarding the variation of d_{33} as a function of composition and concentration -----	49
Figure 1.33:	Possible spontaneous polarization directions for (a) (111) and (b) (001) oriented films -----	51
Figure 1.34:	Theoretical polarization and induced strain curves for (a) (111) and (b) (001) oriented rhombohedral PZT 60/40 -----	52
Figure 1.35:	Domains along various directions in (a) Tetragonal and (b) Rhombohedral PZT (i) {001}, (ii) {110} and (iii) {111}-----	53
Figure 1.36:	Displacement as a function of thickness of piezoelectric layer-----	60
Figure 1.37:	DC electrical breakdown for various PZT film thickness -----	61
Figure 1.38:	(a) Permittivity, (b) remanent polarization and (c) coercive field of PZT films on SRO/Si substrate. ○ indicates that films were deposited and annealed, ▲ indicates films grinded from 64- μ m-thick sample-----	62
Figure 1.39:	Variation of permittivity with two-dimensional compression for specimens of different grain sizes -----	65
Figure 1.40:	Typical hysteresis loops from various ferroelectric ceramics: (A) BaTiO ₃ capacitor, (B) easily switchable soft PZT, (C) PLZT 8.6/65/35 relaxor and (D) PSZT antiferroelectric material -----	66
Figure 1.41:	Applications of ferroelectric materials -----	67
Figure 2.1:	Molecular structure of tetravalent metal alkoxide -----	93

Figure 2.2:	Molecular structure of $Ti(OPr^i)_3(OAc)$ -----	94
Figure 2.3:	Molecular structure of $Ti(OPr^i)_3(acac)$ -----	95
Figure 2.4:	Spin coater-----	98
Figure 2.5:	High vacuum coating unit-----	100
Figure 2.6:	Scheme of the crystal growth observed in single and multilayer sol gel PZT coatings. Thick gel films lead to spherical crystallites randomly oriented whereas thin gel films lead to a columnar growth-----	101
Figure 2.7:	Schematic stretching of Bragg's law derived from triangle ABC-----	102
Figure 2.8:	X-ray diffractometer-----	103
Figure 2.9:	Spectroscopic reflectometer-----	104
Figure 2.10:	(A) Inelastic Rayleigh scattering, (B) Elastic Stokes lines and (C) Elastic anti stokes lines in Raman spectra-----	105
Figure 2.11:	Raman spectrometer-----	106
Figure 2.12:	UV-Visible spectrophotometer-----	108
Figure 2.13:	Impedance analyser for CV determination Model: 4294A, Agilent, USA-----	109
Figure 2.14:	Behavior of dielectric permittivity ϵ_r with different characteristic temperatures T_B , T_m , T_C and T_f in (a) normal ferroelectrics, (b) relaxors with a transition to ferroelectric phase and (c) canonical relaxors-----	111
Figure 2.15:	Leakage current plots of $(Pb_{1-3x/2}La_x)(Zr_{0.53}Ti_{0.47})O_3$ thin films. Here (a) $x = 0.0$, (b) $x = 0.001$, (c) $x = 0.004$, (d) $x = 0.008$ and (e) $x = 0.010$ -----	112
Figure 2.16:	Set up for the measurement of P-E hysteresis using TF analyser (Model: aix ACCT 2000, Germany)-----	113
Figure 2.17:	Ferroelectric P-E hysteresis loop-----	114
Figure 2.18:	Schematic diagram of sample preparation for investigating optimum crystallographic orientation-----	115
Figure 2.19:	Hysteresis is plotted as a function of α , where α is the degree of deviation from $\langle 001 \rangle$ toward $\langle 111 \rangle$ -----	116

Figure 2.20:	Measurement system of the transverse piezoelectric properties of PLZT thin films-----	117
Figure 3.1:	Schematic diagram of domain configurations in <001> oriented rhombohedral crystals under bias-----	125
Figure 3.2:	(a) Dielectric constant of tetragonal PZT 40/60. (b) shows the cross section curve when fig (a) is cut by (010) plane. Here maximum value of ϵ_{33} is obtained in a direction perpendicular to [001]-----	126
Figure 3.3:	Dielectric constant of rhombohedral PZT 60/40. (b) shows the cross section curve when the figure is cut by Y-Z plane -----	127
Figure 3.4:	(a) shows the piezoelectric constant d_{33} of tetragonal PZT 40/60. (b) gives the cross section curve when fig (a) is cut by (010) plane. (c) gives the electromechanical coupling factor k_{33} of tetragonal PZT 40/60 and (d) gives the cross section curve when fig (c) is cut by (010) plane -----	127
Figure 3.5:	(a) shows the piezoelectric constant d_{31} of tetragonal PZT 40/60. (b) shows the electromechanical coupling factor k_{31} of tetragonal PZT 40/60 -----	128
Figure 3.6:	(a) Piezoelectric constant d_{33} of rhombohedral PZT 60/40, (b) Cross section curve when Fig in (a) is cut by Y-Z plane, (c) Electromechanical coupling factor K_{33} , (d) Cross section curve when fig in (c) is cut by Y-Z plane -----	129
Figure 3.7:	(a) Piezoelectric constant d_{31} of rhombohedral PZT 60/40. (b) Electro mechanical coupling factor k_{31} of rhombohedral PZT 60/40-----	130
Figure 3.8:	Room temperature phase diagram of PLZT system-----	131
Figure 3.9:	Synthesis of PLZT precursor solution-----	132
Figure 3.10:	(A) XRD patterns and (B) Raman spectra of PLZT films with varying lanthanum concentrations (a) 6/65/35, (b) 7/65/35, and (c) 8/65/35 on Pt/Ti/SiO ₂ /Si substrate -----	135
Figure 3.11:	HRSEM of the PLZT (a) 6/65/35, (b) 7/65/35, and (c) 8/65/35 thin films-----	136

Figure 3.12:	Transverse piezoelectric response in {100} - oriented PLZT (a) (6/65/35), (b) (7/65/35), and (c) (8/65/35) thin films as a function of applied voltage-----	137
Figure 3.13:	Domains in {100} - oriented PLZT thin film having (A) rhombohedral and (B) tetragonal structure -----	138
Figure 3.14:	Leakage current of PLZT thin films (a) 6/65/35, (b) 7/65/35, and (c) 8/65/35 on TiO ₂ /ST/Pt/Ti/SiO ₂ /Si substrate-----	139
Figure 3.15:	(A) P-E hysteresis loop and (B) S-E curve under bipolar excitation in PLZT thin films (a) 6/65/35, (b) 7/65/35, and (c) 8/65/35 -----	140
Figure 3.16:	XRD patterns of PLZT thin films (a) 7/60/40, (b) 7/56/44, and (c) 7/65/35 on Pt/Ti/SiO ₂ /Si substrate -----	142
Figure 3.17:	Raman spectra of PLZT thin films (a) 7/60/40 (b) 7/56/44 and (c) 7/65/35 on Pt/Ti/SiO ₂ /Si substrate-----	143
Figure 3.18:	HRSEM images of (a) 7/60/40, (b) 7/56/44, and (c) 7/65/35 thin films on Pt/Ti/SiO ₂ /Si substrate-----	144
Figure 3.19:	Transverse piezoelectric coefficient, $ e_{31,f} $ in {110} - oriented PLZT thin films (a) (7/60/40), (b) (7/56/44), and (c) (7/65/35) as a function of applied voltage-----	146
Figure 3.20:	Domains in {110} - preferentially oriented PLZT thin films having (A) rhombohedral and (B) tetragonal structure-----	146
Figure 3.21:	P-E characteristics of {110}-oriented PLZT thin films (a) 7/60/40, (b) 7/56/44, (c) 7/65/35 -----	147
Figure 4.1:	EPR spectra of $[Fe'_{Ti}-\ddot{V}_O]$ defect dipole in PSZTFe -----	157
Figure 4.2:	(A) XRD patterns of acceptor (X) doped PLZT (8/65/35) thin films; X= (a) Fe ³⁺ , (b) Cu ²⁺ , (c) Mn ³⁺ and (d) Pure PLZT (Inset shows the XRD of ST buffer layer on Pt (111)/Ti/SiO ₂ /Si substrate) and (B) Raman spectra of (a) Fe ³⁺ -doped, (b) Cu ²⁺ -doped, (c) Mn ³⁺ -doped and (d) undoped PLZT thin films on (111)Pt/Ti/SiO ₂ /Si substrate-----	161
Figure 4.3:	Character table and symmetry modes of rhombohedral phase (R3m)-----	162

Figure 4.4:	Character table and symmetry modes of monoclinic phase (Pm)-----	163
Figure 4.5:	Character table and symmetry modes of tetragonal phase (P4mm)-----	164
Figure 4.6:	Deconvoluted Raman spectra of (A) Fe ³⁺ doped PLZT (8/65/35), (B) Cu ²⁺ doped PLZT (8/65/35), (C) Mn ³⁺ doped PLZT (8/65/35) and (D) undoped PLZT (8/65/35) -----	166
Figure 4.7:	Transverse piezoelectric coefficient ($ e_{31,f} $) in {110} – oriented films of PL _x ZT where x = (a) Fe ³⁺ , (b) Cu ²⁺ , (c) Mn ³⁺ and (d) pure PLZT (8/65/35)-----	168
Figure 4.8:	Domains in {110} - preferentially oriented PLZT thin films having (A) rhombohedral and (B) tetragonal structure-----	169
Figure 4.9:	S-E curve under bipolar excitation in acceptor (X) doped PLZT (8/65/35) thin films; X= (a) Fe ³⁺ , (b) Cu ²⁺ , (c) Mn ³⁺ and (d) Pure PLZT -----	170
Figure 4.10:	P-E hysteresis loop under bipolar excitation in acceptor (X) doped PLZT (8/65/35) thin films; X= (a) Fe ³⁺ , (b) Cu ²⁺ , (c) Mn ³⁺ and (d) Pure PLZT -----	170
Figure 4.11:	Absorption spectra obtained for (A) Cu ²⁺ , (B) Mn ³⁺ and (C) Fe ³⁺ - doped PLZT (8/65/35) thin films-----	171
Figure 4.12:	Crystal field splitting in (A) Cu ²⁺ , (B) Mn ³⁺ and (C) Fe ³⁺ - doped PLZT thin films -----	172
Figure 5.1:	Phase diagrams of (1-x)PIN-xPT system-----	178
Figure 5.2:	Two possible paths <i>R-T</i> and <i>R-O-T</i> for polarization direction to change from [111] in the rhombohedral <i>R</i> phase to [001] in the tetragonal <i>T</i> phase. The thickest lines represent path followed by polarization in PZN-8%PT upon electric field application. The solid arrows demonstrate the orientation of polarization in a particular domain with and without electric field-----	179
Figure 5.3:	New PZT diagram around MPB-----	180
Figure 5.4:	PZT phase diagram close to MPB reported by Jaffe et al -----	181

Figure 5.5:	Synthesis of $(1-x)$ PIN- x PT precursor solution -----	184
Figure 5.6:	(A) XRD patterns and (B) Raman spectra of $\{110\}$ -oriented $(1-x)$ PIN- x PT thin films (a) $x = 0.36$, (b) $x = 0.38$, (c) $x = 0.40$ on (111) Pt/Ti/SiO ₂ /Si substrate -----	185
Figure 5.7:	Deconvoluted Raman spectra of (a) PIN- 0.36PT, (b) PIN- 0.38PT and (c) PIN-0.40PT -----	186
Figure 5.8:	HRSEM of the cross-section of the (a) PIN- 0.36PT, (b) PIN- 0.38PT and (c) PIN-0.40PT thin films -----	187
Figure 5.9:	Transverse piezoelectric coefficient ($ e_{31,f} $) in $\{110\}$ -oriented $(1-x)$ PIN- x PT films where (a) $x = 0.36$, (b) $x = 0.38$ and (c) $x = 0.40$ -----	188
Figure 5.10:	Domains in $\{110\}$ -preferentially oriented $(1-x)$ PIN- x PT thin film having (A) rhombohedral (B) monoclinic and (C) tetragonal structure-----	189
Figure 5.11:	Temperature and frequency dependence of dielectric properties in (A) PIN-0.30PT, (B) PIN-0.40PT. Frequencies from top to bottom are 100 Hz, 1 kHz, 10 kHz and 100 kHz respectively -----	190
Figure 5.12:	S-E curves under bipolar excitation in $\{110\}$ -oriented $(1-x)$ PIN- x PT thin films (a) $x = 0.36$, (b) $x = 0.38$, (c) $x = 0.40$ -----	191
Figure 5.13:	P-E hysteresis loop under bipolar excitation in $\{110\}$ -oriented $(1-x)$ PIN- x PT thin films (a) $x = 0.36$, (b) $x = 0.38$, (c) $x = 0.40$ -----	192
Figure 6.1:	Tolerance factor versus averaged electronegativity difference for various perovskites. Here BT = BaTiO ₃ , KN = KNbO ₃ , BZN = Ba(Zn _{1/3} Nb _{2/3})O ₃ , BZ = BaZrO ₃ , SZ = SrZrO ₃ , CZ = CaZrO ₃ , ST = SrTiO ₃ , CT = CaTiO ₃ , PT = PbTiO ₃ , PMN = Pb(Mg _{1/3} Nb _{2/3})O ₃ , PSN = Pb(Sc _{1/2} Nb _{1/2})O ₃ , PZ = PbZrO ₃ , PFN = Pb(Fe _{1/2} Nb _{1/2})O ₃ , PNN = Pb(Ni _{1/3} Nb _{2/3})O ₃ , PZN = Pb(Zn _{1/3} Nb _{2/3})O ₃ , PIN = Pb(In _{1/2} Nb _{1/2})O ₃ , PCN = Pb(Cd _{1/3} Nb _{2/3})O ₃ , BF = BiFeO ₃ , NF = NdFeO ₃ , BNF = Bi _{0.8} Nd _{0.2} FeO ₃ , LF = LaFeO ₃ , SF = SmFeO ₃ , GF = GdFeO ₃ , BS = BiScO ₃ , BM = BiMnO ₃ -----	201

Figure 6.2:	PZT-PZSn-PZ ternary phase diagram showing antiferroelectric orthorhombic (A_0), antiferroelectric tetragonal (A_T) and ferroelectric rhombohedral (FE_R) phases. Compositions studied in the present work are marked B, C and D respectively -----	204
Figure 6.3:	X-ray diffraction pattern of $Pb_{0.97}La_{0.02}(Zr_xSn_yTi_z)O_3$ thin films. (B) $x = 0.750, y = 0.150, z = 0.10$; (C) $x = 0.775, y = 0.125, z = 0.10$ and (D) $x = 0.80, y = 0.10, z = 0.10$ on (111)Pt/Ti/SiO ₂ /Si substrate -----	204
Figure 6.4:	Raman spectra of $Pb_{0.97}La_{0.02}(Zr_xSn_yTi_z)O_3$ thin films. (B) $x = 0.750, y = 0.150, z = 0.10$; (C) $x = 0.775, y = 0.125, z = 0.10$ and (D) $x = 0.80, y = 0.10, z = 0.10$ on (111)Pt/Ti/SiO ₂ /Si substrate -----	205
Figure 6.5:	HRSEM of $Pb_{0.97}La_{0.02}(Zr_xSn_yTi_z)O_3$ thin films. (B) $x = 0.750, y = 0.150, z = 0.10$; (C) $x = 0.775, y = 0.125, z = 0.10$ and (D) $x = 0.80, y = 0.10, z = 0.10$ on (111)Pt/Ti/SiO ₂ /Si substrate -----	205
Figure 6.6:	Temperature dependence of dielectric permittivity of (B) $x = 0.750, y = 0.150, z = 0.10$; (C) $x = 0.775, y = 0.125, z = 0.10$ and (D) $x = 0.80, y = 0.10, z = 0.10$ on (111)Pt/Ti/SiO ₂ /Si substrate -----	206
Figure 6.7:	Tip displacement of PLSnZT/Si unimorph cantilever and $ e_{31,f} $ as a function of applied unipolar voltage. (B) $x = 0.750, y = 0.150, z = 0.10$; (C) $x = 0.775, y = 0.125, z = 0.10$ and (D) $x = 0.80, y = 0.10, z = 0.10$ on (111)Pt/Ti/SiO ₂ /Si substrate -----	208
Figure 6.8:	Domains in {110} - preferentially oriented PLZT thin films having (A) rhombohedral and (B) tetragonal structure -----	209
Figure 6.9:	P-E hysteresis loop under bipolar excitation in PLSnZT thin films. (B) $x = 0.750, y = 0.150, z = 0.10$, (C) $x = 0.775, y = 0.125, z = 0.10$ and (D) $x = 0.80, y = 0.10, z = 0.10$ on (111)Pt/Ti/SiO ₂ /Si substrate -----	210

LAXMI PRIYA S. "FERROELECTRIC THIN FILMS FOR MICROACTUATOR APPLICATIONS". THESIS. CENTRE FOR MATERIALS FOR ELECTRONICS TECHNOLOGY (C-MET), UNIVERSITY OF CALICUT, 2018.

Introduction to ferroelectric thin films

• Contents •

- 1.1 Motivation of the present study
- 1.2 Introduction
- 1.3 Basis of ferroelectricity
- 1.4 Present research work
- References

1.1 Motivation of the present study

The urge for integration and miniaturization of bulk electronic components has generated widespread interest in ferroelectric thin films. Ferroelectric thin films are ideal in Micro electro mechanical systems (MEMS) applications. Their applications include piezoelectric microsensors, microactuators etc. Piezoelectric microactuators offer advantages such as small size, low cost and low energy consumption. Still there is sufficient scope for improving the piezoelectric characteristics of ferroelectric thin films to meet the increasing demands of electronic industry. Fabrication of preferentially oriented piezoelectric thin films and correlating with their piezoelectric properties is gaining importance due to their potential device application. We have therefore aimed to improve the piezoelectric properties of different compositions by preparing preferentially oriented thin films particularly for actuator applications. Estimation of the transverse piezoelectric coefficient, $|e_{31,f}|$ of the thin films has also been carried out to evaluate their suitability for MEMS applications.

The widely used material for piezoelectric applications is $\text{Pb}(\text{Zr,Ti})\text{O}_3$ [PZT] with compositions near the morphotropic phase boundary (MPB) due to the excellent properties offered by them. Also high quality PZT films can be grown on silicon substrates even at moderate temperatures of 500-600⁰C. Since Lanthanum (La^{3+}) is a donor dopant, the easy domain switching offered by ‘soft’ PLZT compositions near MPB can provide increased strain values due to the coexistence of rhombohedral, tetragonal and monoclinic phases. We have therefore selected PLZT compositions at or near the MPB to fabricate

preferentially {001}-oriented thin films and also through appropriate doping/substitution at the B-site with a view to improve their properties.

A major obstacle regarding the utilization of Pb-based relaxor solid solutions is the lack of a simple reproducible fabrication technique with which a single phase material, without the undesirable pyrochlore phase, can be readily obtained. Eventhough literature reviews are readily available on Lead Magnesium Niobate (PMN) – Lead Titanate (PT) and Lead Zinc Niobate (PZN) – Lead Titanate (PT), no reports are available on the piezoelectric properties of preferentially oriented thin films of lead based relaxor ferroelectric solid solutions of Lead Indium Niobate (PIN) – x Lead Titanate (PT), $(1-x)$ PIN- x PT $0.36 < x < 0.40$. Hence we have chosen PIN- x PT compositions near MPB and investigated the influence of different crystallographic orientations of their thin films on their piezoelectric, ferroelectric and dielectric properties.

The study will be incomplete without a look at the antiferroelectric-ferroelectric phase boundary compositions since the antiferroelectric materials have potential applications in microactuators due to the electric field induced AFE \rightarrow FE phase transition which is associated with high strains. No study has yet been reported on the transverse piezoelectric characteristics, especially $|e_{31,f}|$, of antiferroelectric PLSnZT thin films. Hence, we have selected compositions near the phase boundary in the PbZrO_3 - PbSnO_3 - PbTiO_3 ternary phase diagram, that undergo a field induced phase transition to the ferroelectric phase.

1.2 Introduction

The discovery of ferroelectricity in Rochelle salt ($\text{NaKC}_4\text{H}_4\text{O}_6 \cdot 4\text{H}_2\text{O}$) by J. Valasek in 1921 and its extension to Barium Titanate (BT), which is the first ferroelectric structure without hydrogen bonds and with more than one ferroelectric phase created much curiosity in the scientific world to fabricate new ferroelectric materials. Piezoelectric materials are generally classified as lead based and lead free materials. Out of these two, lead based piezoelectric materials acquire importance since they offer excellent electrical properties that are reliable and repeatable^{1,2}. The discovery of lead zirconate titanate (PZT) in the late 1950s and transparent lanthanum doped lead zirconate titanate (PLZT) ceramics in late 1960s opened a broad window offering excellent piezoelectric applications better than BT. PZT was also found to be an effective material for energy harvesting. PZT has been the leading material for ferroelectric memories and it also finds extensive applications in gas sensors, pyroelectric thin film sensors, infra red sensors, imaging etc. Relaxors like Lead Zinc Niobate (PZN), Lead Magnesium Niobate (PMN) can also form solid solutions with ferroelectrics such as Barium Titanate (BT), Lead Titanate (PT) thereby exhibiting ultra-high piezo properties³. Later 1970s actually witnessed the emergence of thin films. The increased demand of the electronic industry for miniaturised products paved the way for emergence of thin film technology. The advantages offered by piezoelectric thin films in MEMS and NEMS have provided dramatic advances in the field of non volatile memory devices, sensors, actuators etc. Epitaxial thin films also emerged as a fast track in information technology electronics due to advantages offered by thin films over bulk materials in electromechanical devices. In addition to device miniaturization, thin films provide easier integration to integrated circuit technology and require lower processing

temperatures only. The lower operating voltages and small inertia makes them unique for high frequency applications. They are economically viable and fabrication of unique micro level structures is possible. They offer rapid speed in polarisation switching and high energy densities can be achieved as a result of higher dielectric strengths⁴.

1.3 Basis of ferroelectricity

According to symmetry considerations, there are 230 space groups among which 32 crystalline classes or point groups are found in crystals that are subdivisions of seven basic crystal systems (Figure 1.1). Out of this 32 point groups, 21 are non-centrosymmetric classes, within which 20 are piezoelectrics that can be polarized under stress. Piezoelectricity which was discovered by Jacques and Pierre Curie in 1880 is exhibited by a specific group of materials like quartz, tourmaline, Zinc blende etc. According to Cady⁵, “Piezoelectricity is defined as the electric polarization produced by mechanical strain in crystals belonging to certain classes, the polarization being proportional to strain and changing sign with it”. The piezoelectric effect is linear and reversible and for the presence of piezoelectricity, a lack of centre of symmetry (non-centrosymmetry) is an essential factor. The magnitude of piezoelectric polarization will depend upon the magnitude of stress and the sign of charge produced will depend on the type of stress. Piezoelectric properties are mainly influenced by stoichiometry and morphology and hence proper monitoring of nucleation, growth, crystallization and seed layer introduction are important.

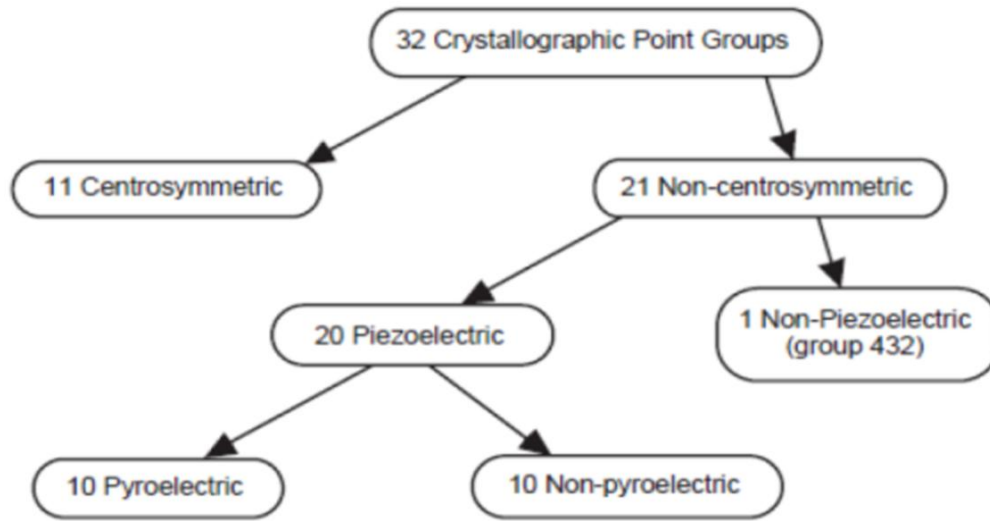


Figure 1.1: Schematic diagram of the classification of crystal based on symmetry

[Source: *Piezoelectric and acoustic materials for transducer applications*, Edited by A. Safari and E.K. Akdoğan, Springer (2008) 40].

Piezoelectric materials are defined as those materials that can convert mechanical signals to electrical signals and vice versa. Thus two effects are operative in piezoelectric crystals (a) direct effect designated as generator and (b) converse effect designated as motor. During direct effect, there occurs the production of a voltage/charge upon stress application as in the case of sensors and in converse effect, stress is produced upon electric field application as in the case of actuators⁶. Since piezoelectricity is reversible, a material that exhibits the direct piezoelectric effect can also exhibit the converse effect. The basic equations describing these two effects with regard to directional properties are depicted in equations (1.1) and (1.2) respectively

$$D = dT + \varepsilon^T E \quad (1.1)$$

$$S = s^E T + dE \quad (1.2)$$

where D is dielectric displacement (Polarisation), T is stress, E is electric field, S is strain, d is piezoelectric coefficient and ϵ is dielectric constant (permittivity). ϵ^T denote stress is held constant which implies that piezoelectric element is mechanically unconstrained, s^E indicates electric field is held constant which means that the electrodes on the element are shorted together⁶. Both these effects are illustrated as cartoons in Figure 1.2.

The quantities specified in equations (1.1) and (1.2) are directional quantities and have to be expressed with subscripts in order to specify the conditions under which they are determined. For example, d_{31} indicates that when stress is applied in 1 or lateral direction, polarization is generated in 3 or perpendicular direction, d_{33} indicates when stress is applied in 3 direction, polarization is also generated in the same direction.

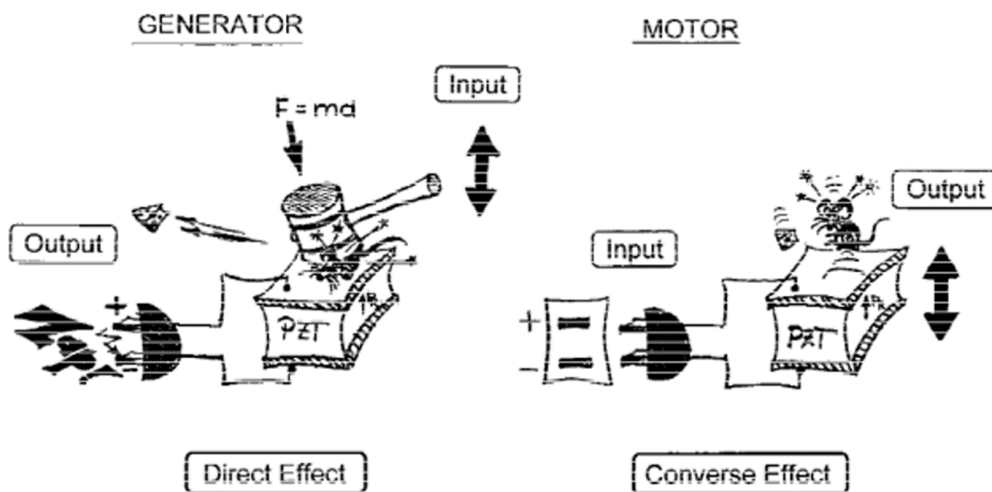


Figure 1.2: Piezoelectric effects in ferroelectric ceramics.

[Source: G. H. Haertling, "Ferroelectric ceramics: History and technology", *J. Am. Ceram. Soc.*, 82 (1999) 797]

Piezoelectrics offer various advantages such as good actuating range, good signal-to-noise ratio, high generated force, wide frequency range of operation and low power consumption which makes them ideal for use in

sensors, actuators and transducers and their pyroelectricity are utilised in IR detectors. Piezoelectric materials find extensive applications in portable micro electromechanical systems (MEMS). Also power harvesting and energy storage in such systems opened new areas for active research.

Among 20 piezoelectrics, 10 have spontaneous polarization that can vary with temperature and are pyroelectric⁷. Also the polarization change in pyroelectric materials can be reversed on heating and cooling. Ferroelectrics are a subclass of pyroelectrics ie, among pyroelectrics, some will be ferroelectric. All ferroelectric materials will be essentially pyroelectric and all pyroelectric materials will be piezoelectric. Ferroelectrics possess the property of spontaneous polarisation similar to pyroelectrics. But apart from this, ferroelectrics also possess reversibility of spontaneous polarisation upon electric field application. Thus two conditions that is mandatory for a material to be ferroelectric are (i) *Spontaneous polarization and (ii) electrically switchable reversibility of spontaneous polarization.*

The non-centrosymmetric crystal structure resulting from the distortion of ideal cubic perovskite structure is responsible for the outstanding property of ferroelectrics⁸. All ferroelectric materials possess a transition temperature called Curie point (T_C). When temperature of the crystal is greater than T_C , the crystal do not exhibit ferroelectricity and exists as paraelectric. Paraelectric phase can be piezoelectric or nonpiezoelectric⁹. Ferroelectricity ceases above the Curie temperature since heat agitates the dipoles to overcome the forces that spontaneously align them.

But on decreasing the temperature through the Curie point, the ferroelectric material undergoes a phase transition from a non-ferroelectric to a ferroelectric phase where many phases like tetragonal, orthorhombic and

rhombohedral phases can exist depending on temperature. The distortion of the ideal cubic structure to a non-centrosymmetric structure induces a permanent internal dipole moment and is the basic reason for the origin of excellent dielectric properties in ferroelectrics. Thus Ferroelectrics are dielectrics that exhibit spontaneous polarization below the Curie point (T_C) and possess nonlinear polarization upon electric field application thereby producing Polarisation-Electric field hysteresis loop which is the finger print of the material. The phase transition from paraelectric (non ferroelectric, high temperature) to ferroelectric phase (low temperature) can also bring strong anomalies in thermal, elastic and dielectric properties of the material. Dimensional changes that can occur in a ferroelectric material when it transform from a paraelectric cubic to a ferroelectric tetragonal phase is depicted in Figure 1.3.

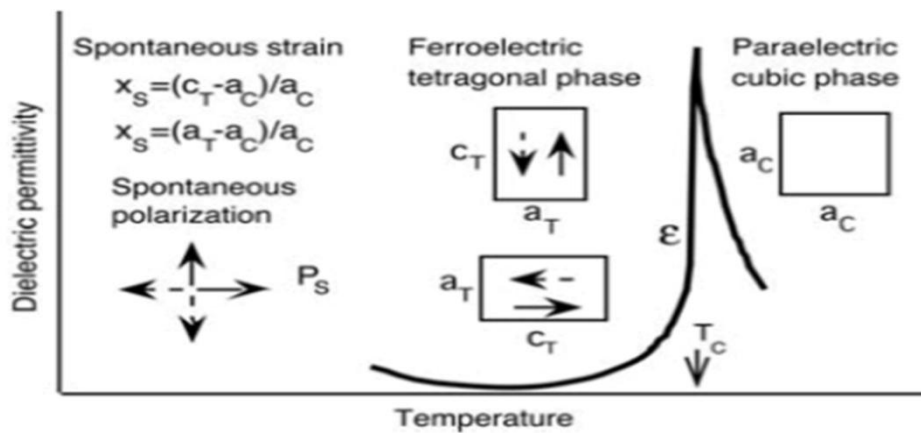


Figure 1.3: Changes that occur in a two-axial ferroelectric material when it transforms from a paraelectric cubic into a ferroelectric tetragonal phase (only two axes are shown)

[Source: Chapter 4, *The science of Hysteresis, volume 3*; I.Mayergoyz and G. Bertotti (Eds.); Elsevier (2005)].

Figure 1.4 demonstrates the changes in dielectric permittivity with temperature in BaTiO_3 single crystal. Here the displacement of Ti ion from the

centre of TiO_6 octahedron results in spontaneous polarization along $\langle 001 \rangle$, $\langle 101 \rangle$ and $\langle 111 \rangle$ set of directions for tetragonal, orthorhombic and rhombohedral phases respectively and maximum dielectric constant is obtained near the Curie point.

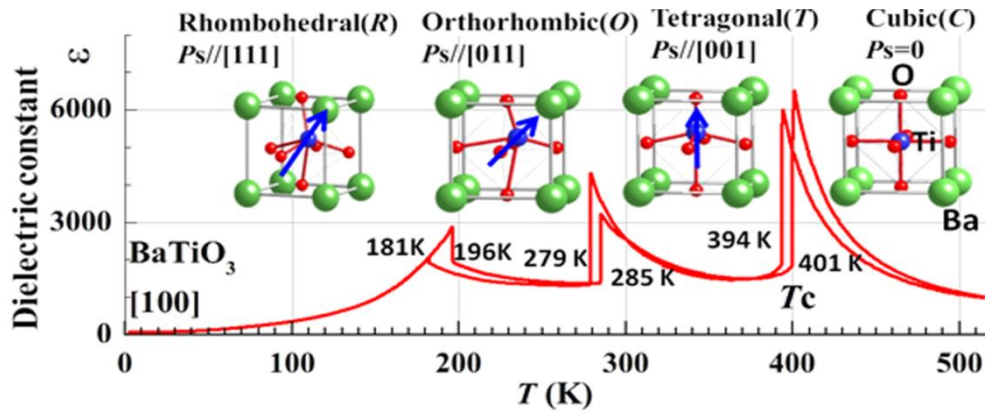


Figure 1.4: Change with temperature of dielectric permittivity of BaTiO_3 single crystal.

[Source: D. Fu and M. Itoh, "Ferroelectric Materials – Synthesis and Characterization", Chapter 5, Edited by Aime Pelaiz Barranco, InTech Publisher (2015)].

1.3.1 Ferroelectric domains and spontaneous polarization

Mainly three types of polarization can exist in materials: Dielectric polarization, Paraelectric polarization and Ferroelectric polarization as illustrated in Figure 1.5. During dielectric polarisation, the polarisation induced will be exactly proportional to the applied electric field. Paraelectric material shows a nonlinear polarisation where electrical permittivity corresponding to the slope of the polarisation curve is a function of external electric field. In addition to being nonlinear, ferroelectric materials also shows a spontaneous non zero polarisation even when the applied electric field is zero.

For a cubic perovskite structure, when electric field is applied to the unit cell, the centrally placed Ti^{4+} or Zr^{4+} ion (B-site ion) moves to a new position along the direction of the applied field. Such movement of ions can

bring about macroscopic change of unit cell and the ceramic as a whole. Figure 1.6 demonstrates polarisation reversal brought about by the displacement of centrally placed Ti^{4+} or Zr^{4+} ion. In tetragonal unit cell, the spontaneous polarization can rise along six equivalent directions, in an orthorhombic unit cell along twelve directions and in a rhombohedral unit cell along eight equivalent directions⁷.

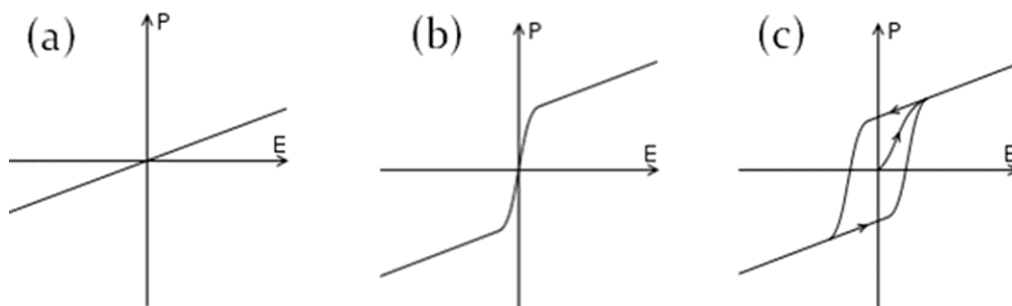


Figure 1.5: (a) Dielectric polarisation, (b) Paraelectric polarisation and (c) Ferroelectric polarisation.

[Source: Chiang, Y. et al.: *Physical Ceramics*, John Wiley & Sons (1997) New York].

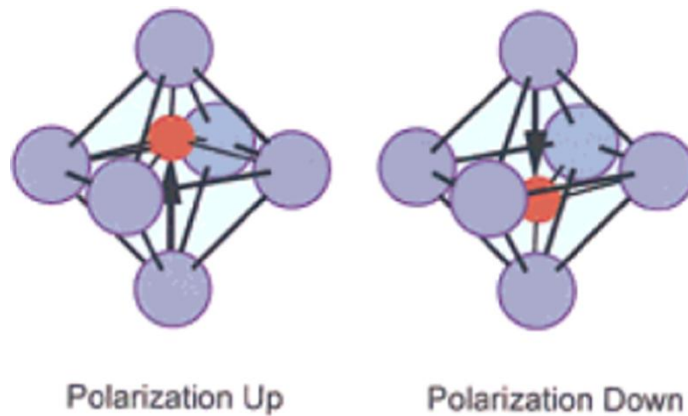


Figure 1.6: Perovskite ABO_3 unit cell demonstrating 180° polarisation reversal for two of the six possible polarisation states caused by the displacement of central ion in a tetragonal plane.

[Source: G. H. Haertling, "Ferroelectric ceramics: History and technology," *J. Am. Ceram. Soc.*, 82 (1999) 797].

Ferroelectric domains are regions in a crystal with uniformly oriented spontaneous polarization. The polarization within a domain will be aligned in the same direction for minimizing energy and the boundary separating two adjacent domains are termed as domain walls. Walls separating domains with oppositely oriented polarization are 180° domain walls and those separating regions with mutually perpendicular polarization are 90° domain walls¹⁰. 180° and 90° ferroelectric domains and domain wall regions in a tetragonal perovskite ferroelectric are illustrated in Figure 1.7.

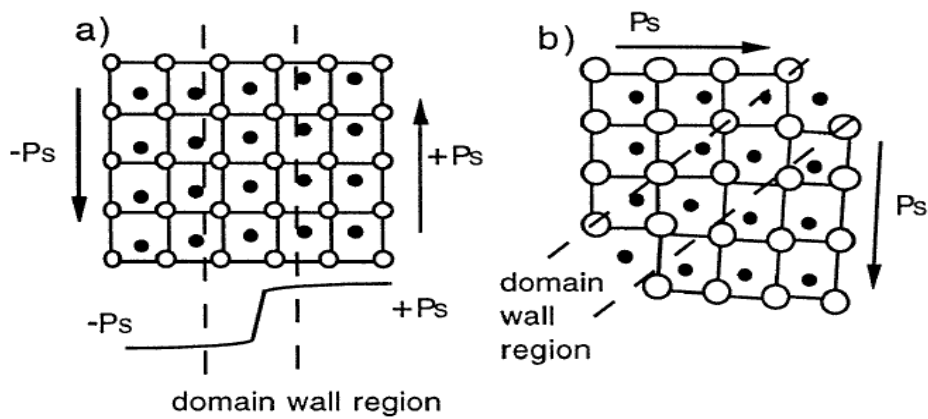


Figure 1.7: Illustration of (a) 180° and (b) 90° ferroelectric domains and domain wall regions in a tetragonal perovskite ferroelectric. The change of polarization across domain wall for a 180° wall is given in (a) and tetragonal distortion in (b).

[Source: D. Damjanovic, "Ferroelectric, dielectric and piezoelectric properties of ferroelectric thin films and ceramics," *Rep. Prog. Phys.*, 61 (1998) 1267].

Polarization changes from one domain to another, both continuously and steeply. Ferroelectric domain walls are narrower than ferromagnetic domain walls¹¹. Ferroelectric domain walls differ in orientation from the spontaneous polarization vector and ferroelastic domain walls differ in orientation from the spontaneous strain tensor. In thin films, domain wall contribution to the piezoelectric effect mainly depends on film thickness, crystal orientation and microstructure^{12,13}. Films with thickness greater than

5 μm and large grain size are reported to exhibit domain wall contribution comparable to bulk materials¹⁴.

When many unit cells that are adjacent to each other switch like those given in Figure 1.6, it can be called as domain switching. In tetragonal materials, there occurs both 90⁰ (strain-producing domains) and 180⁰ domain switching (nonstrain-producing domains) whereas in rhombohedral materials, the strain producing domains are 71⁰ and 109⁰ and nonstrain producing domains are 180⁰ domains. Macroscopic changes are produced in the dimensions of the material when strain producing domains are switched⁷.

1.3.2 Origin of hysteresis loop

Ferroelectric polarization (P-E) and strain field (S-E) hysteresis loops were mainly influenced by nucleation, propagation and switching of domains.

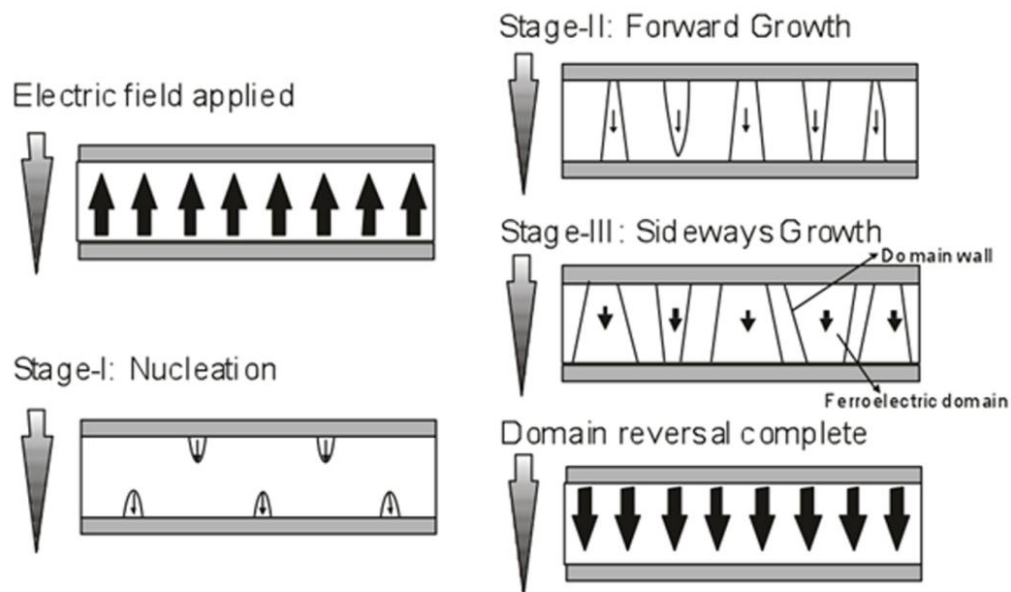


Figure 1.8: Three phases of domain reversal; 1. Nucleation (fast) 2. Forward growth (fast) 3. Sideways growth (slow).

[Source: M. Dawber, K. M. Rabe and J. F. Scott, *Physics of thin-film ferroelectric oxides, reviews of modern physics*, 77 (2005)]

The first stage, the nucleation of domains, starts with its propagation across the film and slower widening of domains¹⁵ (Figure 1.8). In perovskite oxides, the sideways growth (final stage) is slower than the other two stages and hence it will be the rate determining step. But in other materials, nucleation (stage 1) can be the rate determining step.

1.3.2.1 Polarization-Electric field hysteresis loop

The polarisation reversal can be analysed from the ferroelectric hysteresis loop since it arises from the domain structure of the ferroelectric material¹⁶. On applying small ac field to the material in positive direction, the material will behave as a normal dielectric since the electric field is not enough to overcome the energy barrier. This is indicated by the segment A-B in Figure 1.9. When electric field is increased, the domains get aligned in the positive direction giving rise to a rapid increase in polarisation as indicated by segment B-C. Then all domains get aligned with the direction of the electric field giving the saturation polarization along C-D. Saturation polarisation can be defined as the maximum polarization that can be reached. When electric field is reduced and reversed, the direction of dipoles get switched and will follow the path D-F-G-H for reaching the saturation polarization H. The reversal of polarization will occur again following the H-I-D path giving a well developed hysteresis loop. P_R (remanent polarisation) is the polarisation present when no electric field is applied indicated by A-F. The external field needed to bring the polarisation to zero is called coercive field (E_c) indicated by A-G. The extrapolation of linear portion C-D to $E=0$, gives the spontaneous polarization P_S .

For an ideal symmetric hysteresis loop, $+E_c = -E_c$ and $+P_R = -P_R$. The thickness of the material, presence of charged defects, mechanical stress, preparation condition and thermal treatment are the major factors determining

the extent of remanent polarisation, coercive field, spontaneous polarization and shape of the material. On comparing the bulk and thin film ferroelectrics, the major difference in hysteresis loop arises in the magnitude of coercive field (E_C) that are usually larger in films than in bulk materials¹⁷. Also hysteresis loops in films will be more tilted with lower remanent polarizations. The tilt of the loop may be due to the presence of low dielectric constant layer in series with the ferroelectric layer. Also differences in switching properties of films from bulk materials can arise due to difference in preparation conditions.

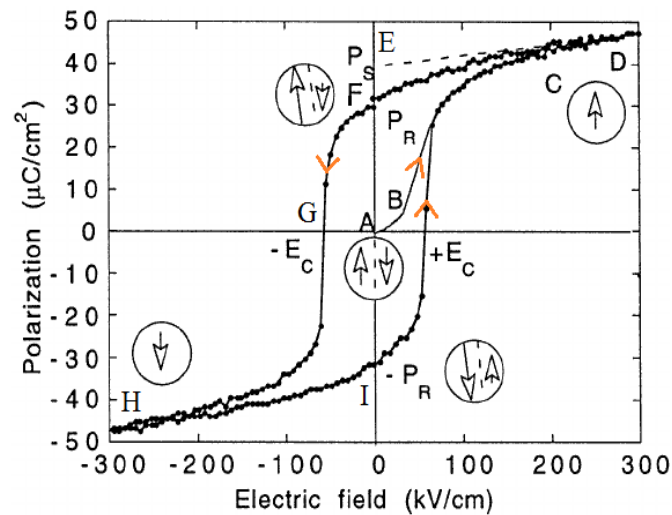


Figure 1.9: Polarization-Electric field hysteresis loop. Circles with arrows represent the polarization state of the material at the indicated fields.

[Source: D. Damjanovic, "Ferroelectric, Dielectric and Piezoelectric properties of Ferroelectric thin films and ceramics," *Rep. Prog. Phys.*, 61 (1998) 1267].

1.3.2.2 Strain –Electric field hysteresis in ferroelectrics

Electric field induced polarization switching in ferroelectric materials can also lead to Strain-Electric field (S-E) hysteresis. Such S-E hysteresis loops mainly arise due to three types of effects- normal converse piezoelectric effect, switching of domain walls and movement of domain walls. When

electric field is zero, the strain of crystal is taken as zero. On applying electric field along the direction of spontaneous polarization (Figure 1.10), the material will expand along A-B-C due to piezoelectric effect and the expansion continues until maximum field is reached (point C)¹⁰.

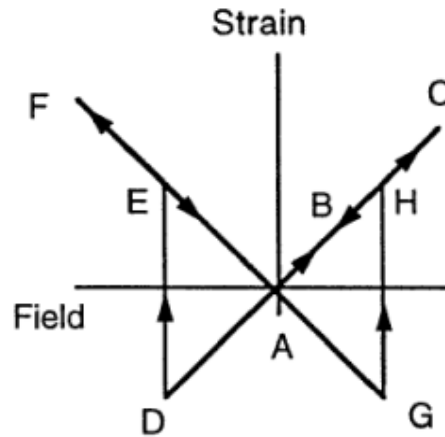


Figure 1.10: Strain-Electric field (S-E) hysteresis loop in ferroelectrics.

[Source: D. Damjanovic, "Ferroelectric, Dielectric and Piezoelectric properties of Ferroelectric thin films and ceramics," *Rep. Prog. Phys.*, 61 (1998) 1267].

At point C, the field begin to decrease, but found to be parallel to P_S . The strain traces the same line A-C but will be in the opposite direction and becomes again zero at point A. The field then changes its direction and becomes anti parallel to P_S . When the electric field increases in the negative direction, the crystal gets contracted with respect to point A. When strain reaches point D, electric field is strong enough for switching the direction of polarization. After switching, the polarization become parallel to the applied electric field and the strain becomes positive at point E. On further increasing electric field in the negative direction, strain increases to point F and then decreases to A on decreasing the field. The polarization reversal and change of strain again occurs at point G. When dc field is low, the strain curves will follow linear relationship

according to piezoelectric effect. But large hysteresis and large negative strain are mainly contributed by ferroelastic domain wall switching.

1.3.3 ABO₃ Perovskite structure

Out of four categories of ferroelectrics viz Tungsten Bronze, Oxygen Octahedral, Pyrochlore and Layer structure, we have focussed on oxygen octahedral possessing ABO₃ simple cubic unit cell structure. ABO₃ Perovskite structure provides a wide range of lattice substitutions thereby making an excellent platform for studying correlation between structure and property. A typical ABO₃ unit cell structure is given in Figure 1.11.

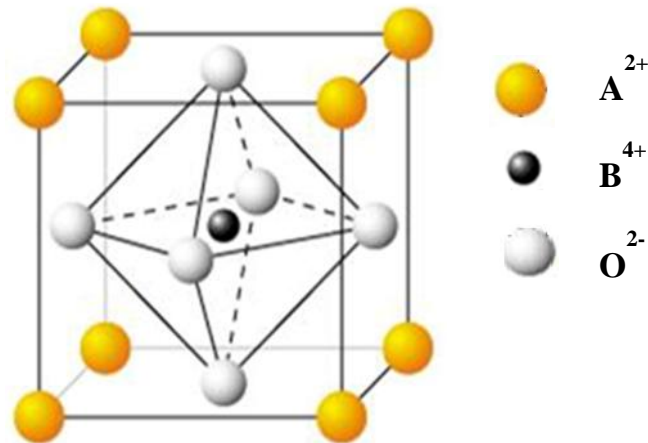


Figure 1.11: A typical ABO₃ unit cell structure.

In perovskites, larger A cations occupy the eight corners of the unit cell, smaller B cations occupy the body centre and the oxygen anion occupy the centres of six faces. The A site ion has a dodecahedral coordination with oxygen anions at the face centres. Generally large cations like Na⁺, K⁺, Rb⁺, Ca²⁺, Sr²⁺, Ba²⁺, Pb²⁺ etc occupy the corners. The smaller B cation (Ti⁴⁺, Sn⁴⁺, Zr⁴⁺, Nb⁵⁺, Ta⁵⁺ or W⁶⁺) is octahedrally coordinated with oxygen atoms forming [BO₆] octahedral which is the heart of the unit cell. The oxygen anion satisfies a six coordination number, four with the neighbouring A cations and

two with the B cations. Apart from O^{2-} in the adjacent unit cells, other large ions such as F^- and Cl^- are possible⁶. The simultaneous substitution of ions in A and B sites can be used for tailoring the properties of perovskites. The $[BO_6]$ octahedral units form a three-dimensional array by corner linking. This high symmetry offered by the perovskite structure is useful since it forms equivalent but differently oriented domains when it transforms to a ferroelectric phase. Hence large remanent polarization and substantial piezoelectric and electro optic coefficients are offered by them¹⁸.

Stability of the Perovskite structure can be determined from the radius ratio rule called the Goldschmidt's tolerance factor ' t '. It also helps to estimate the degree of distortion and can be applied for compounds with a higher degree of ionic bonding. Let us consider a BO_6 octahedra made of rigid spheres which are in contact with each other. If a is the cubic unit cell parameter, then B-O will be equal to $a/2$ and A-O will be equal to $a/\sqrt{2}$. Then the ionic radius of cations and anions can be related by the equation (1.3) and (1.4),

$$r_A + r_o = \sqrt{2}(r_B + r_o) \quad (1.3)$$

$$\text{Also } t = \frac{r_A + r_o}{\sqrt{2}(r_B + r_o)} \quad (1.4)$$

where r_A , r_B and r_o are the relative ionic radii of A-site cation, B-site cation and the oxygen anion respectively⁶.

For an ideal cubic perovskite structure, $t = 1$. But when A cation is smaller than the ideal value, t becomes smaller than 1 and hence $[BO_6]$ octahedra will tilt for filling space. On the other hand, when t is larger than 1, A cation will be larger or B cation will be smaller resulting in hexagonal variants of the Perovskite structure. Hence t can be considered as a measure of the degree of distortion of Perovskites from ideal cubic structure. When

tolerance factor is about 0.95-1.0, the structure is cubic, those with lower values will be non-ferroelectric and slightly higher values than 1 will be ferroelectric⁶. In addition to ionic radii, polarisation and nature of bonds are also important factors that should be taken in to account. For compositions satisfying the above condition, the valency of A-cation usually ranges from 1 to 3 while B cation will be from 3 to 5.

1.3.3.1 Important ferroelectric oxides

BaTiO ₃ -based materials	(Ba,Sr)TiO ₃
Pb-based materials	Pb(Zr,Ti)O ₃
Layered perovskites	SrBi ₂ Ta ₂ O ₉ , Bi ₄ Ti ₃ O ₁₂

Eventhough piezoelectric applications have been reported from a number of solid solutions such as BaTiO₃, Pb(Zr,Ti)O₃, (Pb,La)(Zr,Ti)O₃, PMN, (Na,K)NbO₃ etc, PZT and PLZT composition offers the following advantages⁷:

- i. higher electromechanical coupling coefficients than BaTiO₃.
- ii. higher T_c values permitting higher temperature operation.
- iii. compositions at or near MPB can be well poled.
- iv. possess a wide range of dielectric constants.
- v. forms solid-solution compositions with different constituents thereby providing a wide range of properties.

1.3.3.2 Lead Zirconate Titanate (PZT)

PZT (Lead Zirconate Titanate) is a binary solid solution of antiferroelectric PbZrO₃ (orthorhombic structure) and ferroelectric PbTiO₃ (tetragonal structure). At high temperatures, PZT exhibits a cubic perovskite structure that is paraelectric and on cooling below the curie point, it undergoes a phase transition to the

ferroelectric tetragonal or rhombohedral phases as depicted in phase diagram (Figure 1.12). In tetragonal phase, the spontaneous polarisation is along $\langle 100 \rangle$ set of directions while in rhombohedral phase, it is along $\langle 111 \rangle$ set of directions. The boundary between the rhombohedral and tetragonal phases is referred to as the morphotropic phase boundary (MPB) which is independent of temperature. Excellent dielectric and piezoelectric properties can be obtained for compositions at or near the phase boundary as a result of polarization rotation between the two phases. Poling of PZT ceramics is also easy in this region since the spontaneous polarisation within each grain can be switched to one of the 14 possible orientations (eight along $\langle 111 \rangle$ directions for the rhombohedral and six along $\langle 100 \rangle$ directions for the tetragonal phases)⁶.

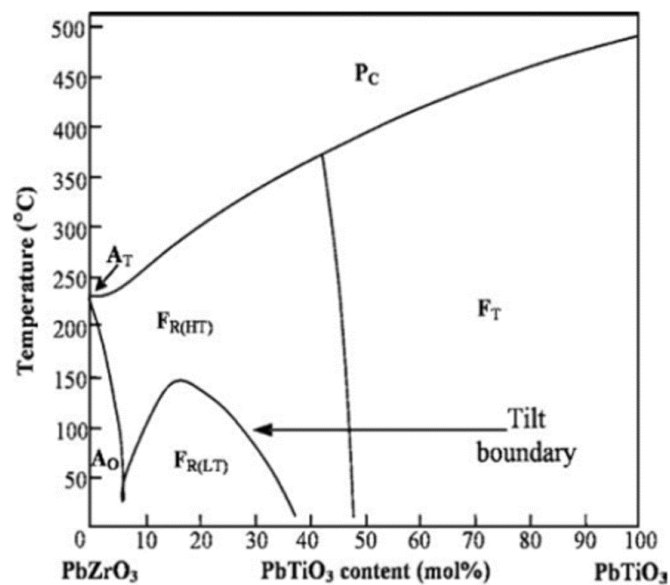


Figure 1.12: The low temperature phase diagram of lead zirconate titanate (PZT) phase diagram illustrating cubic paraelectric phase and tetragonal and rhombohedral phases.

[Source: B. Jaffe, W. R. Cook and H. Jaffe, *Piezoelectric Ceramics*, Academic press, 1971].

For Ti-rich compositions, the symmetry changes from cubic $m\bar{3}m$ to tetragonal $4mm$ at the curie temperature. Hence titanium rich compositions in the

PZT system favour tetragonal phase formation with elongation and spontaneous polarisation along $\langle 001 \rangle$ direction. Also there are 6 equivalent polar axes corresponding to $[100]$, $[\bar{1}00]$, $[010]$, $[0\bar{1}0]$, $[001]$ and $[00\bar{1}]$ directions of the cubic paraelectric phase. For Zr-rich compositions, rhombohedral ferroelectric phase is favoured with the polarisation along $\langle 111 \rangle$ direction giving eight possible domain states as $[111]$, $[\bar{1}11]$, $[1\bar{1}1]$, $[11\bar{1}]$, $[1\bar{1}\bar{1}]$, $[\bar{1}\bar{1}1]$, $[\bar{1}1\bar{1}]$ and $[\bar{1}\bar{1}\bar{1}]$. Hence the structure and the preferential orientation of PZT films are very important while considering their specific applications.

The enhanced property at MPB was only supposed to be the coexistence of tetragonal and rhombohedral phases. But recent studies on PZT revealed the presence of a monoclinic phase at the morphotropic phase boundary separating the tetragonal and rhombohedral phases. The revised phase diagram incorporating the monoclinic phase proposed by Woodward *et al.*¹⁹ is depicted in Figure 1.13. This monoclinic phase in PZT was observed by Noheda *et al.*²⁰ using a high resolution X-ray diffractometer with a PT content of 48 mol%. The monoclinic phase M_A in PZT acts as a structural bridge between the tetragonal and rhombohedral phases allowing polarization rotation leading to enhanced piezoelectric properties. Hence in the ferroelectric monoclinic phase, the remaining symmetry element $\{1\bar{1}0\}_c$ mirror plane and the polar vector P_S is found to rotate within this plane between $[111]_c$ and $[001]_c$ directions as indicated in Figure 1.14.

Figure 1.15 shows the values of piezoelectric constant d obtained for composition near MPB. The highest d value is obtained near MPB due to increased ease of reorientation of polarisation on application of electric field. But the actual polarization is found to be lower than the expected one since the electric field within the grains and the internal stress will prevent the reorientation of domains^{10,21}.

When PZT material is doped with donor or acceptor dopants, its properties are changed dramatically since the dopants have a valence different from those of ions in the lattice. Donor dopants (Nb^{5+} , Ta^{5+}) will enhance domain reorientation resulting in ‘soft’ PZTs and are compensated by Pb-vacancies. ‘Soft’ PZT is characterised by larger value of susceptibilities (piezoelectric coefficient d , dielectric constant ϵ , material compliance s). Acceptor dopants (lower valence than the host atom like Fe^{3+} , Sc^{3+} on Ti^{4+} sites in PZT) produce hard PZTs since oxygen vacancies pin domain wall motion. ‘Hard’ compositions are characterised by lower value of susceptibilities (piezoelectric coefficient d , dielectric constant ϵ , material compliances) conductivity and nonlinearity⁶.

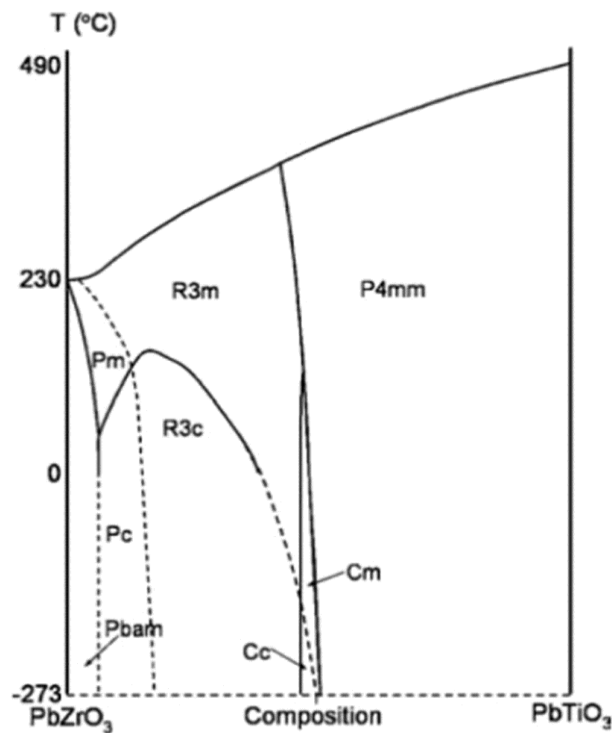


Figure 1.13: PbZrO_3 - PbTiO_3 phase diagram according to Woodward et al.

[Source: D. I. Woodward, J. Knudsen and I. M. Reaney, “Review of crystal and domain structures in the $\text{PbZr}_x\text{Ti}_{1-x}\text{O}_3$ solid solution”, *Phys. Rev. B.*, 72 (2005) 104110].

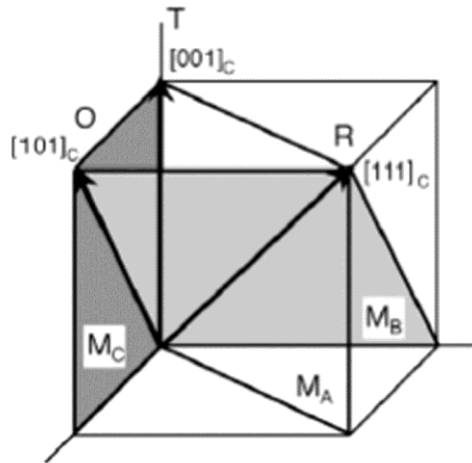


Figure 1.14: Mirror planes of monoclinic phase found in MPBs of PZT.

[Source: D. Vanderbilt and M. H. Cohen, "Monoclinic and triclinic phases in higher-order Devonshire theory," *Phys. Rev. B.*, 63 (2001) 094108].

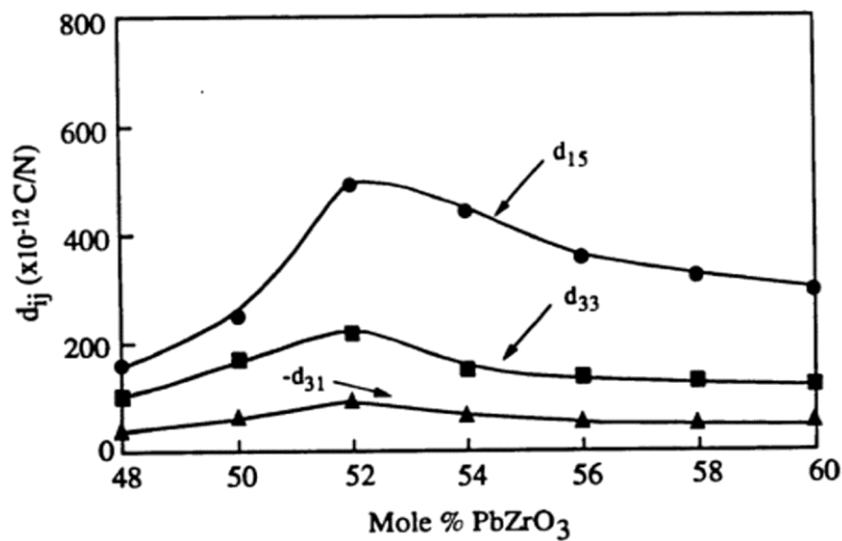


Figure 1.15: Piezoelectric d strain coefficients versus composition for PZT system.

[Source: D. Damjanovic, "Ferroelectric, dielectric and piezoelectric properties of ferroelectric thin films and ceramics," *Prog. Phys.*, 61 (1998) 1267].

1.3.3.3 Defect chemistry in PZT

Defects in PZT are mainly due to lead and oxygen vacancies. Since PbO is volatile, PZT can accommodate lead and oxygen vacancies.

Undoped PZT exhibits *p*-type conductivity due to the presence of holes created by A-site vacancies as a result of the higher volatility of Pb^{2+} ions. This is shown in equation (1.5).



1.3.3.3.1 Donor doping

During donor-doping, a positive ion will replace another ion having lower valence thereby contributing extra electrons. In PZT, donor dopants (La^{3+}) on A-site are more common due to the lower volatility of trivalent ions. The trivalent donors (D) on A-site provide electrons as per equation (1.6) or can be compensated by A-site vacancies as per equation (1.7) respectively.



Here D_{Pb}' represents a donor dopant/substituent in the A-site which is positively charged, V_{Pb}'' shows a doubly negatively charged A-site vacancy with respect to the neutral lattice and O_o^x is the neutral lattice oxygen.

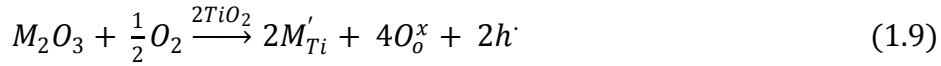
1.3.3.3.2 Acceptor doping

During acceptor doping, a positive ion replaces higher valence ion creating holes. In PZT, acceptors on the B-site are more common. A trivalent acceptor in the B-site could be compensated by the formation of oxygen vacancy as per equation (1.8).



Here \check{V}_o is a doubly positively charged oxygen vacancy and M_{Ti}' is a negatively charged acceptor at the B-site with respect to the neutral lattice.

When $[\ddot{V}_O]$ formation is suppressed under rich O_2 atmospheres, charge compensation is achieved by hole formation as per equation (1.9).



1.3.3.4 Lanthanum doping in PZT (PLZT)

PLZT is a transparent ferroelectric oxide formed by doping La^{3+} ion in the A-site of PZT. On adding lanthanum to PZT system, extensive solid solution is maintained throughout the system and the stability of ferroelectric phase is decreased in favour of paraelectric and antiferroelectric phases. The phase diagram of PZT and PLZT are given in Figure 1.16. In a PLZT unit cell, there is a corner linked network of oxygen octahedra with Zr^{4+} and Ti^{4+} ions occupying B-site within the octahedral cage and Pb^{2+} , La^{3+} ions occupying the 12-fold coordination site formed in the middle of the cube of eight such octahedra⁶. Due to variable valency of Pb^{2+} and La^{3+} in the structure, in order to maintain electrical neutrality, some of A and B-sites are kept vacant. Since perovskite structure offers compositional flexibility, a large number of perovskite related structures are also possible by varying A and B cations.

Various compositions suitable for specific applications are illustrated in the phase diagram given in Figure 1.16. Since we are interested in making materials suitable for actuator applications, we mainly concentrated in the MPB compositions shown in green colour.

On adding lanthanum to lead zirconate titanate solid solution, noticeable changes are observed in the phase diagram as proposed by Haertling and Land²². (1) Small changes in Lanthanum content produce large changes in areas of phase stability, (2) The antiferroelectric phase is extended at the expense of the ferroelectric phase for increasing Lanthanum content and

(3) increased La^{3+} content favours ferroelectric tetragonal phase over the rhombohedral phase. Since lanthanum is a donor dopant, its addition to PZT helps in getting ‘soft’ compositions where domain switching takes place easily thereby achieving increased dielectric and piezoelectric characteristics.

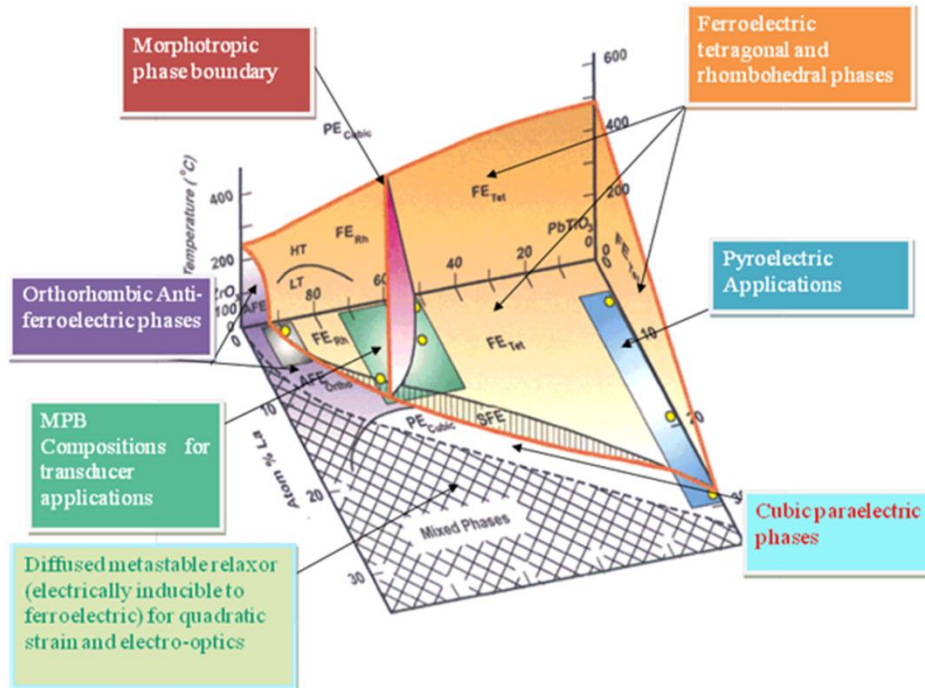


Figure 1.16: Phase diagram of PZT and PLZT solid-solution systems.

[Source: G. H. Haertling, “Ferroelectric Ceramics: History and Technology,” *J. Am. Ceram. Soc.*, 82 (1999) 797].

1.3.3.5 Relaxor ferroelectrics

The era of relaxor ferroelectrics began with the discovery of the unusual high dielectric behaviour in complex Perovskites by Smolenskii and Agranovskaya²³ in 1958. Relaxor ferroelectrics are similar to ferroelectrics but possess randomness associated with one or more atoms within the unit cell. The A or B atom within the ABO_3 cubic perovskite structure will get replaced with other atoms such as A' , A'' etc. Complex Perovskites having the general

formulae $(\text{Pb},\text{A}')(\text{Zr},\text{Ti})\text{O}_3$ or $\text{Pb}(\text{B}'\text{B}'')\text{O}_3$ are well known. Thus the origin of relaxor properties will be mainly due to the charge as well as site disorder within the Perovskite structure that is caused by the substitution of cations with different valence²⁴. They exhibit slim ferroelectric hysteresis loop near T_C with large saturation polarization and small remanent polarization in addition to large electrostrictive coefficients and electrooptical constants²⁵. Previous reports^{26,27} revealed the interesting nature of $\text{Pb}(\text{Mg}_{1/3}\text{Nb}_{2/3})\text{O}_3$ [PMN] due to high dielectric constant at room temperature above a broad dielectric maximum at around 0°C . The dielectric constant can further be increased by forming solid solutions with another Perovskite material such as Lead Titanate (PT). Lead-based solid solutions of relaxor ferroelectrics of the type $(1-x)\text{Pb}(\text{B}'\text{B}'')\text{O}_3-x\text{PbTiO}_3$, where $\text{B}' = \text{Mg}, \text{Zn}, \text{In}$; $\text{B}'' = \text{Nb}, \text{Ta}$ are extensively used in actuators due to their excellent piezoelectric and electrostrictive properties. Examples of relaxor ferroelectrics include PMN-PT, PZN-PT, PIN-PT etc. They exhibit a diffuse frequency-dependent phase transition over a temperature range and a broad frequency dispersive behaviour of dielectric permittivity. The electrostrictive coefficients of PMN- x PT was found to increase with increasing PT contents²⁸ and large pyroelectric coefficients were obtained for poled PMN- x PT which make them ideal for pyroelectric detector applications²⁹.

Solid solutions of $\text{Pb}(\text{Zn}_{1/3}\text{Nb}_{2/3})\text{O}_3$ [PZN] relaxor ferroelectric single crystal (PZN- x PT) proposed by Nomura and co-workers^{29,30} in early 1970s exhibited morphotropic phase boundary between the rhombohedral and tetragonal phases at 9 wt.% PT. This solid solution poled along the pseudo-cubic [001] axis exhibited giant piezoelectric coefficients of $1500 \times 10^{-12} \text{ C/N}$ in rhombohedral phase at room temperature. In this system, Shrout *et. al*³¹ studied compositions having $0.3 \leq x \leq 0.4$ near MPB and his findings also supported Kuwata³⁰.

In 1997, Park and Shrout³ jointly worked on single crystals of PMN- x PT and PZN- x PT poled and cut along different crystallographic directions. They obtained enhanced piezoelectric and electromechanical properties in $\langle 001 \rangle$ oriented rhombohedral crystals. The concept of engineered domain structure with eight possible ferroelectric domain variants coalescing into a tetragonal one at higher electric fields was found to be the reason for the excellent properties of $[001]$ oriented rhombohedral crystals (Figure 1.17).

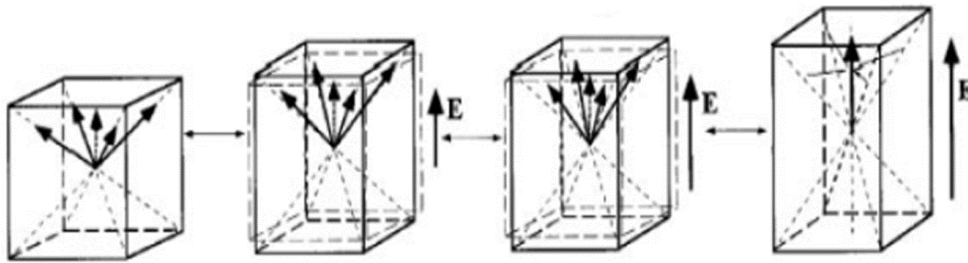


Figure 1.17: Domain engineered structure in $[001]_c$ oriented rhombohedral crystals of PMN- x PT and PZN- x PT on application of electric field along $[001]_c$ direction.

[Source: S. F. Liu, S. E. Park, T. R. Shrout and L. E., Cross, "Electric field dependence of piezoelectric properties for rhombohedral $0.955\text{Pb}(\text{Zn}_{1/3}\text{Nb}_{2/3})\text{O}_3-0.045\text{PbTiO}_3$ single crystals," *J. Appl. Phys.*, 85 (1999) 2810].

The presence of monoclinic phase M_C was also discovered in the MPBs of PMN- x PT and PZN- x PT with high resolution X-ray and neutron diffraction studies^{30,32,33}. Hence new phase diagrams were proposed for PMN- x PT³⁴ and PZN- x PT³³. The presence of M_A phase along with M_C phase was later proposed by Singh and Pandey³⁵. Thus polarization rotation in presence of one or more monoclinic phases was considered as the reason for giant piezoelectric responses offered by PMN- x PT and PZN- x PT single crystals oriented along $\langle 001 \rangle_c$ direction. Later Alberta and Bhalla³⁶ proposed a phase diagram for $(1-x)$ PIN- x PT and the morphotropic phase boundary provide a wide range of compositions with excellent electrical properties.

1.3.4 Ferroelectric thin films

Ferroelectrics in thin film form started in 1960s and 1970s and have been used in sensors, actuators, Rf devices, tunable microwave devices, microelectronics and so on. For dynamic random access memory applications, high capacitance and switching of polarisation offered by thin films are highly advantageous. Thin film ferroelectrics can be synthesised with excellent compositional control, high crystal quality and excellent strain control. By fixing all synthesis parameters, film thickness can be varied and size effects can be investigated. Thin films can be synthesised by various methods such as chemical solution deposition (CSD)^{37,38,39} pulsed laser ablation^{40,41} sputtering^{42,43,44} molecular beam epitaxy^{45,46} and metal-organic chemical vapour deposition (MOCVD)^{47,48} including sol-gel^{49,50} and metal-organic decomposition (MOD)^{51,52}. The main advantage of integration of films on to silicon is the prospect of non-volatile, radiation-robust memories. For thin films, with low voltages, it is possible to switch the polarisation making them suitable for integrated electronic applications.

1.3.5 Domain wall contribution in determining properties of ferroelectric material.

The displacement of domain walls under weak and moderate fields has a prominent influence on dielectric, piezoelectric and mechanical properties of ferroelectric materials. Very small displacements of domain walls are also capable of contributing to polarization of material. In addition to the intrinsic contribution from lattice defects, the extrinsic contribution like the displacement of non-180° domain walls at weak to moderate fields are also significant contributors to the elastic, dielectric and piezoelectric properties of ferroelectric materials. But the movement of domain wall gets pinned or

clamped by the presence of defects and imperfections like oxygen vacancies and electron trapped in the domain wall. In addition to this, the grain size, nature of dopants, crystal structure, preferential orientation and preparation conditions of films may also adversely affect domain wall motion¹⁰.

1.3.6 Intrinsic and extrinsic contributions

Domain formation in ferroelectric thin films are governed by two factors a) mechanical clamping of the substrate that leads to the formation of ferroelastic domains and b) the depolarising effect which leads to non-ferroelastic 180° domains.

Perovskite-structured ferroelectrics show both intrinsic and extrinsic contribution to piezoelectric response. Intrinsic contribution due to lattice defects originates in all individual ferroelectric domains as a result of relative ion/cation shift and deformation within a domain. The displacement of 180° domain walls is the intrinsic contributor to piezoelectricity. An electrically induced 180° domain switch of the central metal cation in perovskite structure is illustrated in Figure 1.18. Such domain switches are mainly achieved by single domain crystals like PZT films on (100) Pt/MgO substrate.

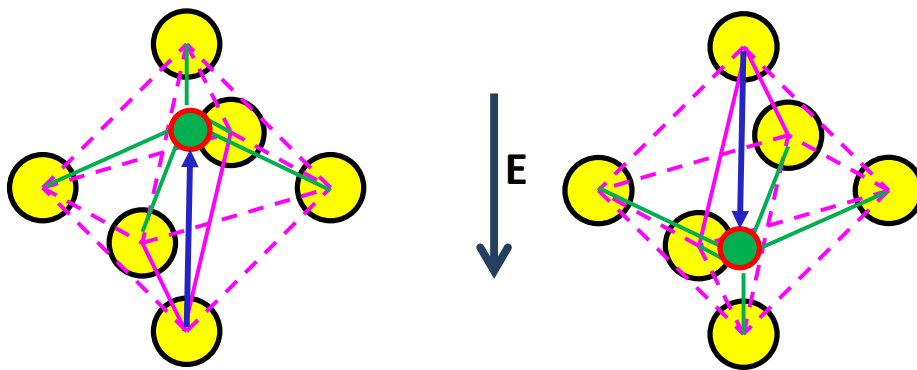


Figure 1.18: Illustration of 180° domain switching in ferroelectric materials. (The arrow shown by red colour is aligned at an angle of 90° from the film normal.)

Displacement of non-180° domain is the extrinsic contributor to piezoelectricity. Figure 1.19 illustrates a tetragonal structure where 90° domain switching can take place. When electric field is applied along the film normal (given in blue coloured arrow), the red coloured arrow get switched at an angle of 90° towards the film normal leading to increased piezo responses.

Various types of non-180° domain switches are possible in preferentially oriented films. In PZT having MPB composition, where tetragonal, monoclinic and rhombohedral phases coexist, 45° (domain \vec{a}) and 35°16' (domain \vec{c}) domain switches are possible in {110}-oriented films as given in Figure 1.20. Such 180° and non-180° domain switching lead to differences in P-E and S-E characteristics as shown in Figures 1.21 and 1.22 respectively.

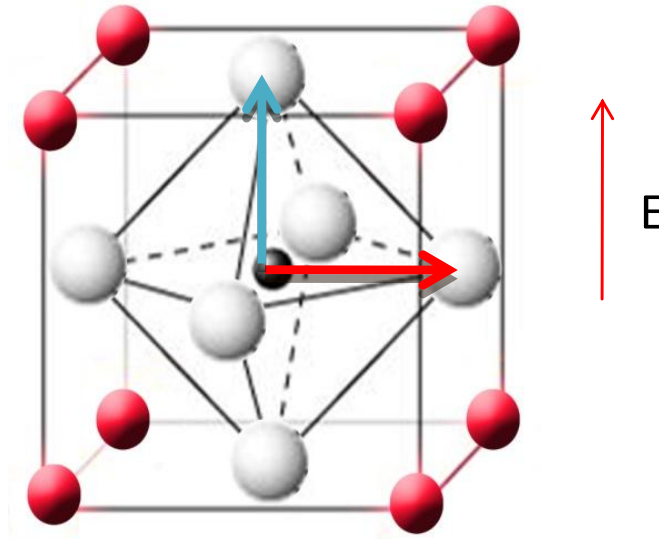


Figure 1.19: Illustration of non-180° domain switching in ferroelectrics.

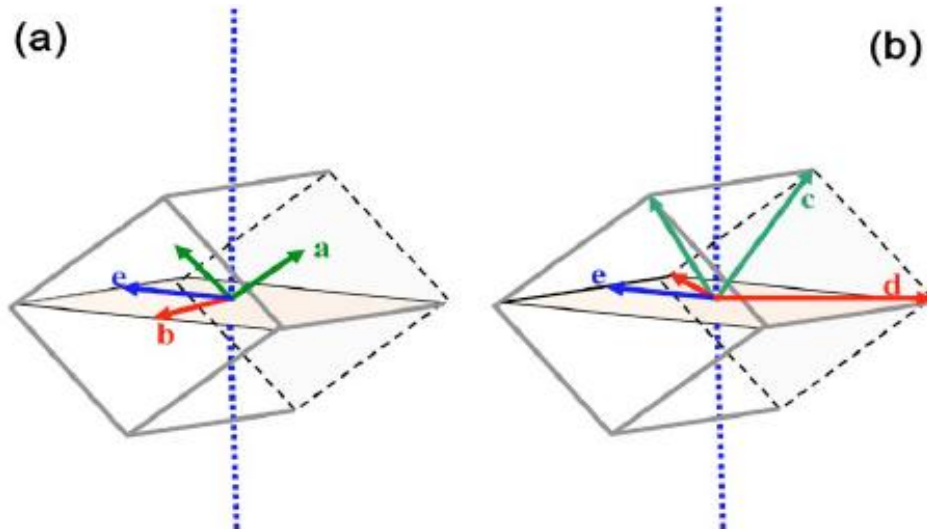


Figure 1.20: Possible orientations of polarization vectors in (a) tetragonal and (b) rhombohedral PZT film.

[Source: D. Ambika, V. Kumar, H. Imai and I. Kanno, "Sol-gel deposition and piezoelectric properties of {110}-oriented $\text{Pb}(\text{Zr}_{0.52}\text{Ti}_{0.48})\text{O}_3$ thin films," *Appl. Phys. Lett.*, 96 (2010) 031909].

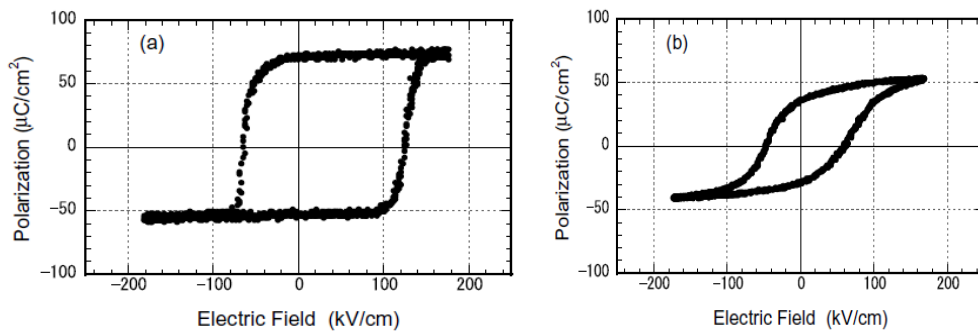


Figure 1.21: P-E hysteresis loop of PZT thin films on (a) Pt/MgO and (b) on Si.

[Source: I. Kanno, H. Kotera and K. Wasa, "Measurement of transverse piezoelectric properties of PZT thin films," *Sens. Actuators, A.*, 107 (2003) 68].

Figure 1.21 (a) shows P-E hysteresis loop of c-axis oriented PZT film on Pt/MgO substrate. It is a clear square shaped one indicating abrupt polarization reversal due to c-axis orientation of PZT films. But for polycrystalline PZT film on Pt/Si substrate, polarization reversal occurred

gradually with applied field as given in Figure 1.21 (b) due to the off-axis polar domain motion corresponding to the nonlinear piezoelectric properties of PZT films⁵³.

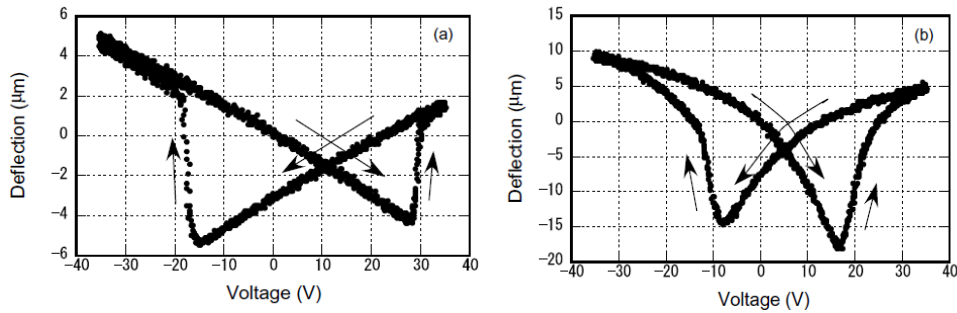


Figure 1.22: Tip deflection of cantilevers as a function of applied voltage in (a) Pt/MgO and (b) PZT film on Si.

[Source: I. Kanno, H. Kotera and K. Wasa, "Measurement of transverse piezoelectric properties of PZT thin films," *Sens. Actuators, A.*, 107 (2003) 68].

The deflection curve of c-axis oriented PZT film on MgO substrate given in Figure 1.22 (a) which is an ideal butterfly loop with clear 180⁰ domain switching. Except for 180⁰ switching, the cantilever made of c-axis oriented PZT film on Pt/MgO substrate shows linearity due to the perfect c-axis orientation of PZT thin films. But the curve in Figure 1.22 (b) showed large displacement hysteresis since piezoelectric strain arises not only from lattice motion but also due to off-axis domain motion like the reorientation of 90⁰ domains⁵³. For both intrinsic and extrinsic contribution, strain is proportional to electric field. In the first case, it is linear and for the extrinsic contribution, it is nonlinear.

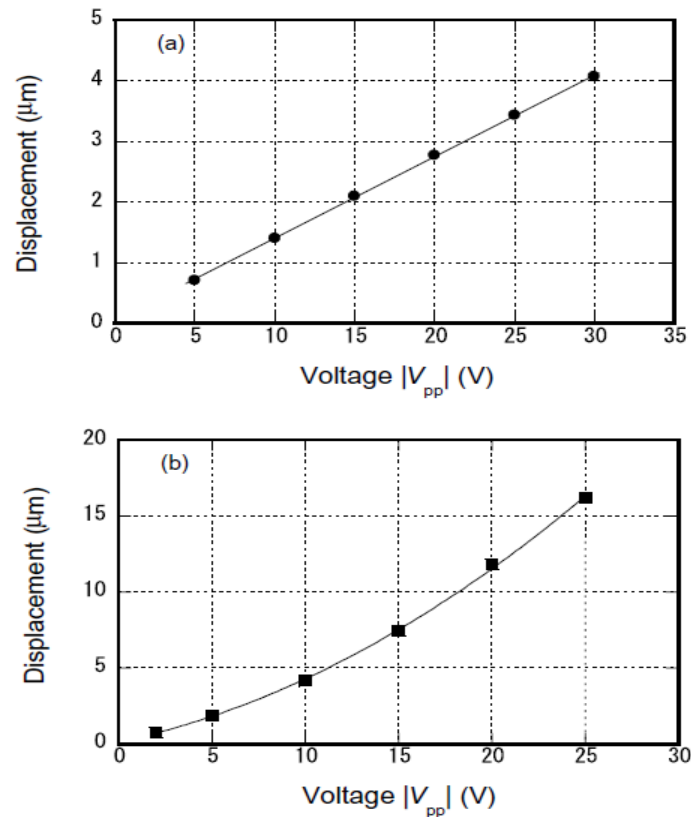


Figure 1.23: Tip displacement as a function of applied voltage in (a) epitaxial PZT film on Pt/MgO substrate, (b) polycrystalline PZT film on Pt/Ti/Si substrate.

[Source: I. Kanno, H. Kotera and K. Wasa, "Measurement of transverse piezoelectric properties of PZT thin films," *Sens. Actuators, A.*, 107 (2003) 68].

Figure 1.23 shows the relationship between tip displacement of a cantilever and applied voltage. In Figure 1.23 (a), tip displacement showed excellent proportional relationship (linearity) since the piezoelectric strain is caused by simple lattice motion of elongation and shrinkage along the polar axis. But in Figure 1.23 (b), the relationship is nonlinear for polycrystalline PZT thin films since domain wall motion which is not parallel to the electric field is superimposed on the lattice motion under the high voltage⁵³. Hence both intrinsic and extrinsic effects are significant contributors to piezo effect and dielectric permittivity.

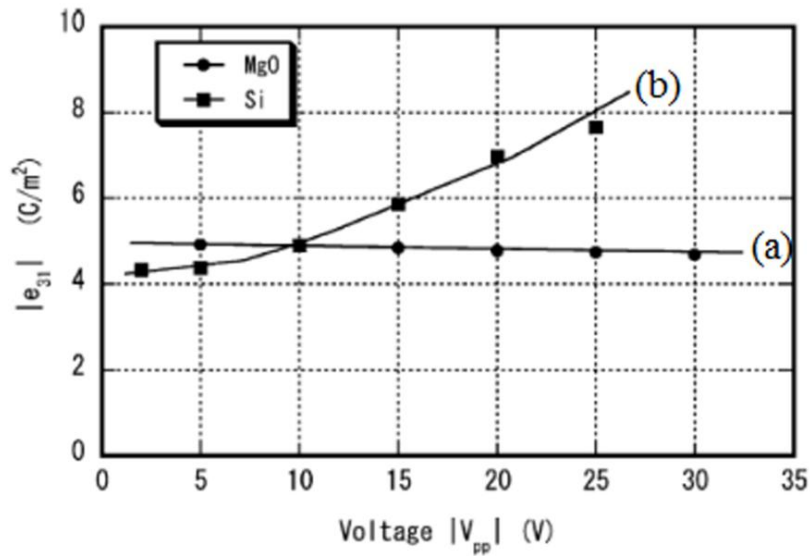


Figure 1.24: Piezoelectric coefficient $|e_{31}|$ of PZT film deposited on (a) Pt/MgO and (b) Pt/Si substrate.

[Source: I. Kanno, H. Kotera and K. Wasa, "Measurement of transverse piezoelectric properties of PZT thin films," *Sens. Actuators, A.*, 107 (2003) 68].

Figure 1.24 shows the dependence of transverse piezoelectric coefficient of PZT film on Pt/MgO and (b) Pt/Si substrate. The absolute value of $|e_{31}|$ of PZT on Pt/MgO is higher than that on Pt/Si especially at higher voltage. In (a), $|e_{31}|$ value seems to be linear and stable due to c-axis orientation and absence of off-axis domain motion. But large $|e_{31}|$ value of polycrystalline PZT films on Si (Figure 1.24 (b)) is due to off-axis domain motion superimposed on lattice motion. Thus substrate used for film growth provides a profound influence on piezo properties⁵³. Hence by modifying texture and crystal structure, the intrinsic and extrinsic effects contributing to the piezoelectric properties of thin films can be engineered.

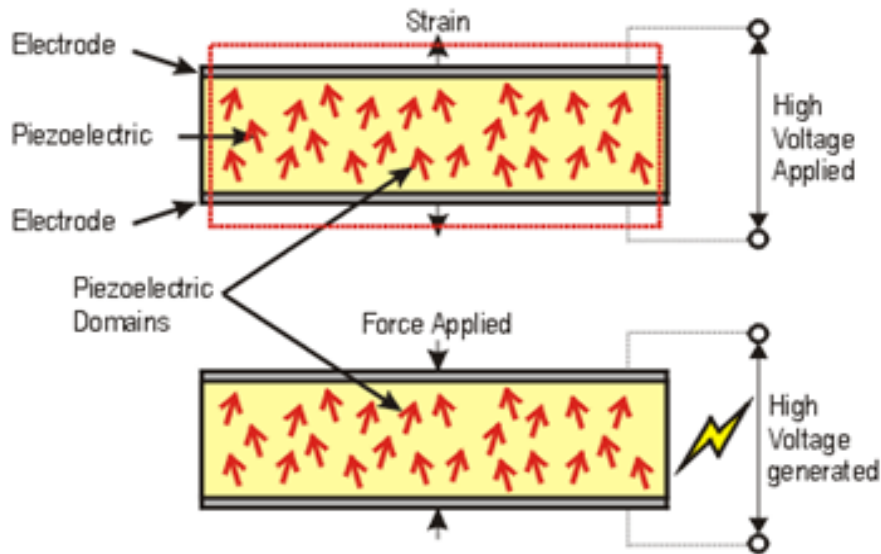


Figure 1.25: Single domain PZT ferroelectric single crystal

[Source: <https://www.greenoptimistic.com/nano-piezo-electric-generator-20081202/#.WeDJf1uCzIU>]

For a single domain PZT ferroelectric single crystal (Figure 1.25), the piezoelectric property can be defined as

$$d_{33} = 2Q_{11}\epsilon_0\epsilon P \quad (1.10)$$

Where ϵ_0 is the permittivity of free space

Q_{11} is the hydrostatic electrostriction coefficient

ϵ is the dielectric constant and

P is polarisation

On averaging, this equation can also be applied for polycrystalline ferroelectrics. This equation can also give evidence on whether intrinsic or extrinsic factor is the predominant contributor to piezoelectric property. Intrinsic factor (which corresponds to the response observed in a single domain single crystal) will be major contributor if the measured piezo property coincides with the above equation.

Intrinsic factors contributing to piezoelectricity in thin films is mainly affected by substrate clamping and misfit strains^{54,55,56}. During ferroelectric phase transition, when there is formation of ferroelastic domains, partial release of substrate-induced stress occurs in films and the total permittivity of films include contribution from these domains⁵⁷. The main difference in respect of this contribution between a bulk material and a thin film is that in bulk materials, the domain contribution to permittivity is influenced by defect pinning of domain wall whereas for films with ferroelastic domain pattern, the contribution is minimised by clamping effect induced by the substrate. Main extrinsic factor that contributes to ferroelectric phase transition are depolarisation resulting from imperfect screening of divergence in polarisation, interfacial charge compensation, impurities, non-stoichiometry, line and plane defects etc. Also many extrinsic factors are size dependent^{58,59}. Normally in the low temperature domain engineered phase, intrinsic reversible contribution will be larger than the extrinsic factor. This is because the extrinsic factor is a temperature activated process that can be frozen at very low temperature. Thus the intrinsic part can be determined by freezing the material at 0 K temperature⁶⁰. The extrinsic contribution can be divided into two, the in phase component and out of phase component of which the out of phase component is the major contributor to dielectric loss.

Films with different crystallographic orientation will have different domain wall contributions and hence their intrinsic and extrinsic contributions to piezoelectric responses will also be different. Thus the dielectric, piezoelectric and nonlinear responses in ferroelectrics are due to intrinsic and extrinsic components associated with it. Rayleigh's law can be used to analyze quantitatively the intrinsic and extrinsic contributions to dielectric and piezoelectric response. This law was originally applied for ferromagnetic materials. But now it has been

successfully used to understand the dielectric, piezoelectric and nonlinear behaviour of ferroelectric ceramics as well as thin films.

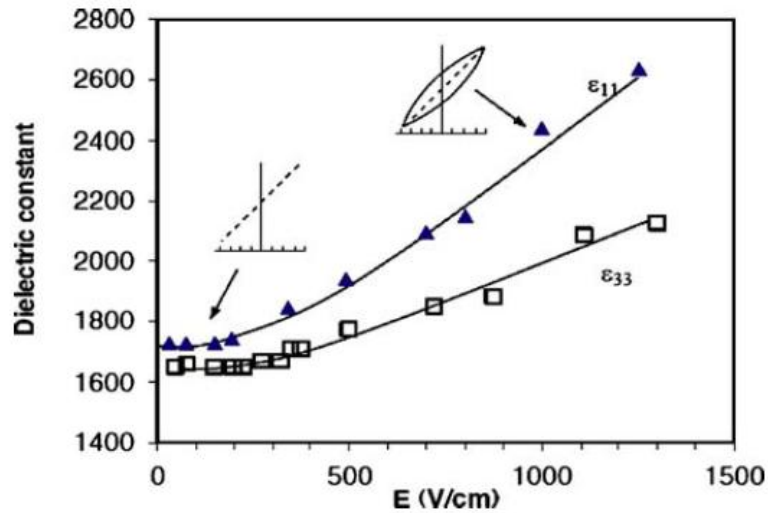


Figure 1.26: The nonlinear behaviour of the dielectric permittivities ϵ_{11} and ϵ_{33} with the applied AC field in a soft PZT ceramic.

[Source: N. B. Gharb, I. Fujii, E. Hong, S. Trolier-McKinstry, D. V. Taylor and D. Danjanovic "Domain wall contributions to the properties of piezoelectric thin films," *J. Electroceram*, 19 (2007) 47]

The dielectric and piezoelectric responses of a ferroelectric material is due to the average response of intrinsic and extrinsic contributions. The intrinsic and extrinsic contributions can be distinguished by studying the field amplitude dependence⁶¹. At lower AC field, the relative dielectric permittivity is a proportionality constant as a result of linear relationship between dielectric displacement D and electric field E (Figure 1.26)⁶². But on increasing ac field, ϵ_r varies with applied field's amplitude. This is dielectric nonlinearity⁶³. Likewise, piezoelectric nonlinearity is also observed. Hence for most ferroelectric ceramics and thin films, the linear relationship does not exist beyond a certain threshold field. This nonlinear response is caused by both the intrinsic and extrinsic components. Rayleigh law is mainly used in

ferroelectrics to include the behaviour of dielectric permittivity and piezoelectric coefficient for AC field amplitude higher than the threshold field. For ferroelectrics, Rayleigh law translates in to a linear AC electric field dependence of permittivity and piezoelectric coefficients in sub switching conditions with the density and structure of domain walls remaining unchanged⁶⁴. The importance of Rayleigh relations is that they link the hysteresis and nonlinearity, ie, the same mechanism is responsible for nonlinearity and hysteresis at which Rayleigh behaviour is observed.

1.3.7 Dielectric properties

The electrical properties of thin films mainly depend upon composition, crystallographic structure, preferential orientation and nature of the substrate.

1.3.7.1 Dielectric permittivity

Dielectric permittivity (ϵ_r) is defined as the ratio between the charge stored on an electrode slab of material brought to a given voltage to the charge stored on a set of identical electrodes separated by vacuum. With altering voltages, the charge stored on a dielectric has both the in phase (real) and out of phase (imaginary) components, caused by resistive leakage or dielectric absorption⁶⁵.

Hence on inserting a material between the parallel plates, the capacitance gets increased.

$$K = \frac{\epsilon}{\epsilon_0} \quad (1.11)$$

Where K is the relative permittivity and ϵ is the permittivity of dielectric material.

Dielectric permittivity shows a sharp peak near the paraelectric-ferroelectric transition temperature, Curie point T_C . Above the Curie Point, dielectric permittivity obeys Curie-Weiss law.

$$\text{The law states that } \epsilon_r = \frac{C}{T-T_C} \quad (1.12)$$

where ϵ_r is the dielectric permittivity, C is a constant, T is the absolute temperature and T_C is the Curie point. The value of constant C can be determined by plotting $\frac{1}{\epsilon_r}$ against T . The plot thus obtained will give a straight line with a slope of $\frac{1}{C}$ and an intercept of $T_0(\theta)$ which is slightly different from T_C . Thus Curie –Weiss law can be written as,

$$\epsilon_r = \frac{C}{T-T_0}, \text{ where } T_0(\theta) \text{ is the Curie temperature}$$

The dielectric constant of a material arises from polarization of the material under applied electric field. Polarization is the total dipole moment per unit volume given as

$$P = N\alpha_e E \quad (1.13)$$

Where N is the number of molecules per unit volume, α_e is the polarizability of the material and E is the electric field. There are four types of polarization mechanisms: electronic polarisation, ionic polarisation, dipolar polarisation and space charge polarisation that contributes to dielectric permittivity of a material depending on the exciting frequency^{66,67}.

- i. Electronic polarisation: It involves shifting and/or polarisation of valence electron cloud of ion of the material with regard to the nucleus thereby creating a dipole moment. The extent of the shift will be proportional to field strength. It occurs mainly in the ultraviolet region.

- ii. Ionic polarisation (atomic polarisation): Here the oppositely charged ions are shifted from their equilibrium position by the application of an electric field. It occurs in the infrared region.
- iii. Dipolar (orientation) polarisation: It involves the rotation of internal dipole moments for aligning along with an applied force and this polarisation is mainly exhibited by ferroelectric materials. It occurs in the microwave region.
- iv. Space charge polarization: The movement of charged internal defects with applied force is involved in space charge polarisation. It occurs due to the accumulation of charges at the electrodes or at interfaces in a multiphase material.

The sum of all these polarization mechanism contributes to permittivity,

$$P_{total} = P_e + P_i + P_o + P_s \quad (1.14)$$

PZT ceramics with MPB compositions are found to exhibit excellent dielectric and electromechanical properties as shown in Figure 1.27. This behaviour is due to the coexistence of phases at the boundary causing larger number of reorientable polarization directions and also due to maximum in mechanical compliance permitting maximum domain reorientation⁶⁸. PZT ceramics can also be easily poled in this composition since the spontaneous polarization within each grain can be switched to one of the 26 possible orientations ie, eight along $\langle 111 \rangle$ direction in the rhombohedral phase, twelve along $\langle 110 \rangle$ direction in the monoclinic phase and six along $\langle 100 \rangle$ direction in the tetragonal phase.

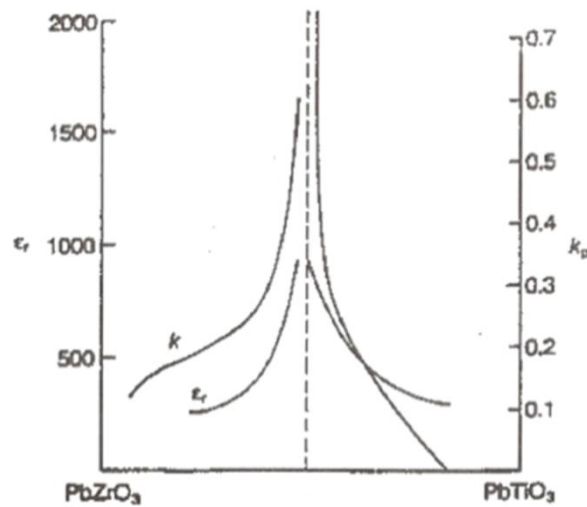


Figure 1.27: Effect of composition on dielectric constant ϵ_r and electromechanical coupling factor K_p in PZT.

[Source: K. P. Rema, "Structure-property relationship in PZT based piezoelectric systems," Ph.D Thesis, January (2010)].

In ferroelectrics, dielectric permittivity and piezoelectric coefficients have contributions from intrinsic (lattice) and extrinsic (domain wall motion) factors. The intrinsic permittivity was found to have a weak dependence on bias field and frequency whereas the extrinsic permittivity has a strong dependence on bias field and temperature. Narayanan *et. al*⁶⁹ developed a method to separate the lattice and domain wall contribution to dielectric response. According to him, domain wall motion could be effectively suppressed by high bias field that enables to measure directly the lattice contribution. As per the data illustrated in Figure 1.28, an electric field of $\sim 20\text{-}25\text{MV/m}$ was required to suppress the extrinsic contribution (domain wall motion) completely in PLZT (8/52/48) and the intrinsic permittivity due to lattice contribution measured at the same field was found to be about $\sim 300\text{-}350$.

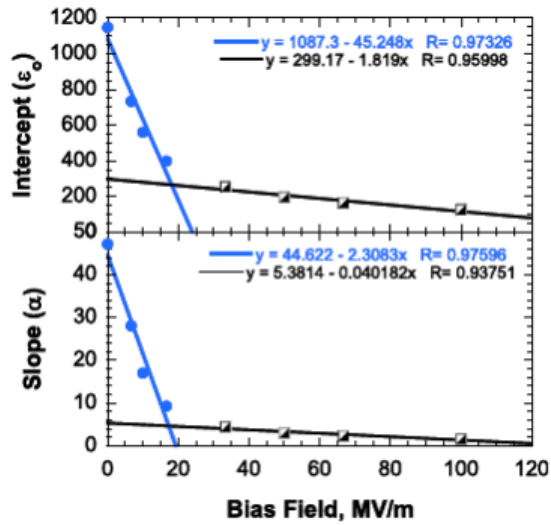


Figure 1.28: Intercept and slope of linear logarithmic fits at various bias field for extrinsic (blue) and intrinsic (black) contributions.

[Source: M. Narayanan, S. Tong, S. Liu, B. Ma, U. Balachandran, "Estimation of intrinsic contribution to dielectric response of $Pb_{0.92}La_{0.08}Zr_{0.52}Ti_{0.48}O_3$ thin films at low frequencies using high bias fields," *Appl. Phys. Lett.*, 102 (2013) 062906].

1.3.7.2 Dielectric loss

Dielectric loss is defined as the ratio of out of phase component to the in phase component in a dielectric material. It is also called dissipation factor or loss tangent ($\tan \delta$). When the period of applied voltage is much larger than the relaxation time of polarisation, polarisation will be completed at any instant. The charging current will be 90° advanced to the voltage. Hence electrical energy will not be lost during charging. When the period of the applied voltage is in the same range as relaxation, resonance occurs, then current leads voltage by $90-\delta$. δ is the loss angle and $\tan \delta$ is the electrical loss due to resonance.

Dielectric loss in a material is given as

$$\tan \delta = \frac{\epsilon''}{\epsilon'} \quad (1.15)$$

1.3.7.3 Dielectric tunability

Dielectric tunability is defined as $\frac{\epsilon_{r0} - \epsilon_r V}{\epsilon_{r0}}$. Here ϵ_{r0} and $\epsilon_r V$ are the dielectric permittivities of the ferroelectric material at 0 and V volts. It is an important parameter for designing tunable devices and arises mainly due to the switching of dipoles upon electric field application.

1.3.7.4 Leakage current

Leakage current is an important factor that badly affects the performance of a dielectric and can adversely affect the long-term reliability of storage equipments⁷⁰. The magnitude of leakage current mainly depends on material parameters, processing and testing conditions (voltage and temperature)⁷¹. Possible mechanisms of conduction in ferroelectric dielectric films are Schottky and Poole-Frenkel emissions, the Fowler-Nordheim tunnelling, the ohmic, space-charge limited, hopping conductivity and conductivity via the grain boundaries^{72,73}.

Undoped PZT exhibits p-type conductivity attributed to lead vacancies in the PZT unit cell. They possess perovskite structure with built around oxygen octahedron. Since interstitial cationic defects are absent in such structures, oxygen vacancies and cation vacancies become prominent.

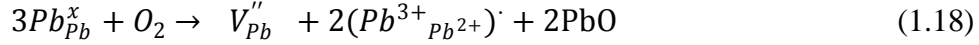


Where O_o^x represent an oxygen atom sitting on an oxygen lattice site with neutral charge, \dot{V}_o represent doubly positively charged oxygen vacancy.

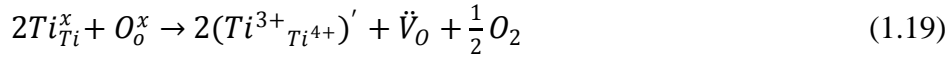
These electrons will be neutralised by the majority charge carriers 'holes'. Hence the oxygen vacancies are capable of decreasing the concentration of holes. Also lead vacancies and oxygen vacancies will be created in PZT as a result of PbO volatility.



Pb^{2+} ions can be oxidised to Pb^{3+} ions creating a lead site vacancy for every two oxidised Pb ions.



Pb^{3+} ions are singly positively charged holes compared with the neutral lattice. The mobile holes can lower the electrical resistivity of the film thereby causing poor performance of devices. Also some Ti^{4+} ions can occur in Ti^{3+} state due to loss of oxygen.



Such defects, which are charge carriers, should be considered as important while analysing the leakage current mechanism of PZT^{74,75}.

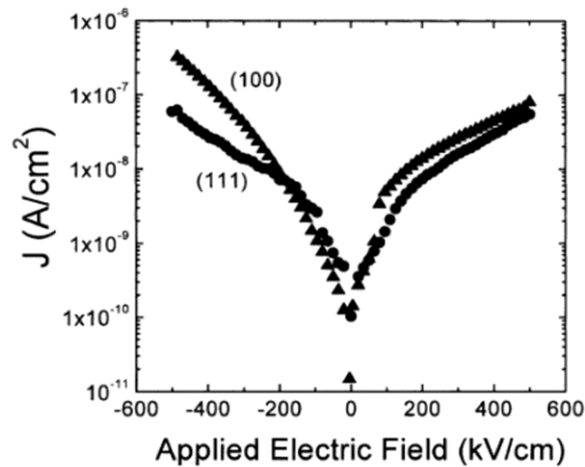


Figure 1.29: Leakage current density (J) curves of PZT thin films for different orientations.

[Source: Seung-Hyun Kim, D. Y. Park, H. J. Woo, D. S. Lee, J. Ha, C. S. Hwang, I. B. Shim, A. I. Kingon, "Orientation effects in chemical solution derived $Pb(Zr_{0.3}Ti_{0.7})O_3$ thin films on ferroelectric properties," *Thin Solid Films*, 416, (2002) 264].

In lead based system, an effective method to improve the leakage current characteristics is controlled A-site donor doping⁷⁶.

But on adding low levels of lanthanum, $0 \leq x \leq 0.004$, the number of vacancies will be partly compensated by the A-site donor dopant,



In PLZT system, the process of such electronic charge compensation is found to exist till $x=0.004$. But above $x=0.004$, V_{Pb}'' state gets dominated which in turn increases the leakage current density as per equation (1.21) given below



Leakage current characteristics obtained for (100) and (111) oriented films are shown in Figure 1.29. For (111) and (100)-oriented PZT thin films, the leakage current density (J) was found to be gradually increased with increasing applied voltage. The leakage current density is found to be almost similar regardless of film orientation. This suggests that it is the film microstructure and not the orientation that plays a prominent role in leakage current characteristics⁷⁷.

1.3.8 Piezoelectric properties

Since a piezoelectric material is anisotropic, the physical constants relate to both the direction of applied electrical or mechanical force and the direction parallel and perpendicular to the applied force. For relating both the electrical and mechanical quantities, double subscripts are used like d_{ij} . Here 'i' represents the direction of excitation and "j" represents the direction of the response of the system. Important piezoelectric constants in thin films are longitudinal piezoelectric constant (d_{33}) and transverse piezoelectric constant (d_{31}). The direction of forces acting on the piezoelectric material is depicted in Figure 1.30.

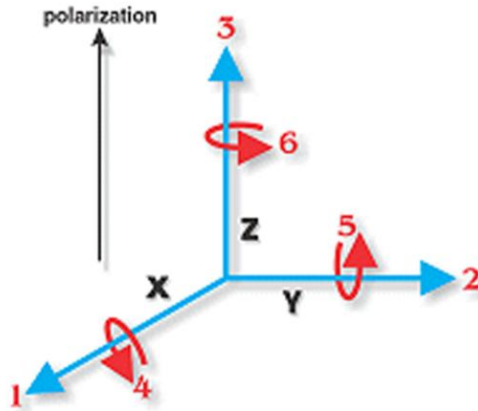


Figure 1.30: Direction of forces acting on a piezoelectric element.

Quartz (SiO_2), lithium niobate (LiNbO_3) and lithium tantalate (LiTaO_3) are some of the widely used single crystal piezoelectrics employed for specific applications. But these single crystals are found to exhibit inferior piezoelectric properties than PZT ceramics. As single crystal PZT is difficult to prepare, high performance material can be devised by preparing preferentially oriented films. Preferential crystallographic growth is necessary for optimising the electrical properties and can be achieved by controlling the nucleation and growth mechanisms. Ferroelectric and piezoelectric properties of thin films are largely dependent on the crystal orientation⁷⁸. Epitaxial growth of ferroelectric thin films on suitable substrates improves the quality of films by lowering the dislocation density of films. Epitaxial films are more advantageous than polycrystalline since the former can be polarised only in one direction. Epitaxial films exhibit superior electrical properties since they have the full component of their polarization vector normal to the film. Uchino *et. al*⁷⁹ proposed a theoretical model for the piezoelectric coefficient in PZT with Zr/Ti ratio 60/40 and 40/60 (rhombohedral PZT 60/40 with 60% PZ and 40% PT, tetragonal PZT 40/60 with 40% PZ and 60% PT) obtained for [001] and [111] orientation. Properties of films with different orientations were explained on the basis of domain stability. It was seen that the piezoelectric

coefficient d_{33} exhibits the highest value at an angle of 59.4° from the Z-axis on Y-Z plane in {100}-oriented rhombohedral films (Figure 1.31). Also {100} textured tetragonal compositions with Zr/Ti ratio 40/60 shows maximum value of d_{33} along the film normal (along Z-axis). The value of d_{33} obtained for different film orientation is plotted as a function of composition and concentration and is given in Figure 1.32.

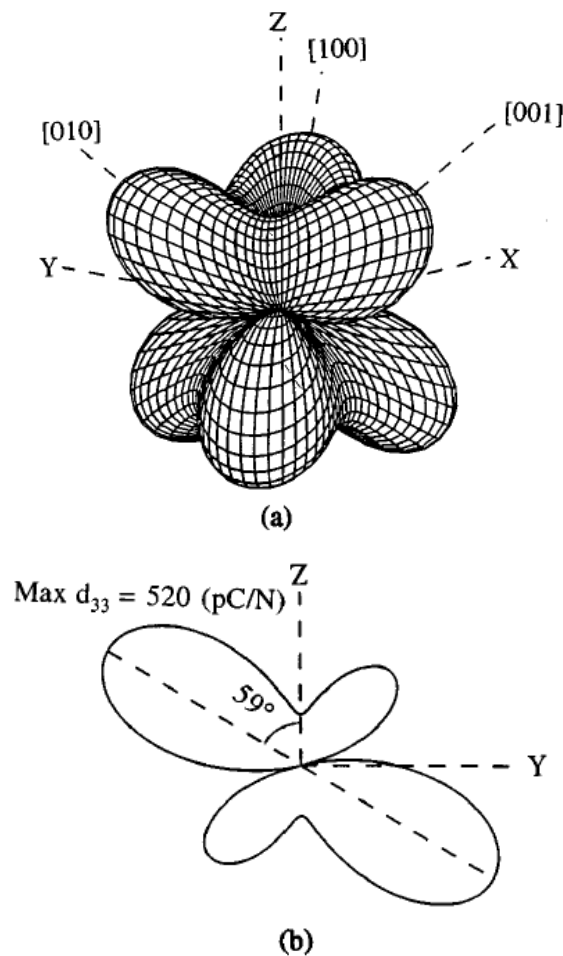


Figure 1.31: (a) Effective piezoelectric constant d_{33} of rhombohedral PZT 52/48. (b) Cross sectional curve when figure in (a) is cut by Y-Z plane.

[Source: Xiao-hong Du, U. Belengundu and K. Uchino, "Crystal orientation dependence of piezoelectric properties of lead zirconate titanate near morphotropic phase boundary," *Appl. Phys. Lett.* 72 (1998) 2424].

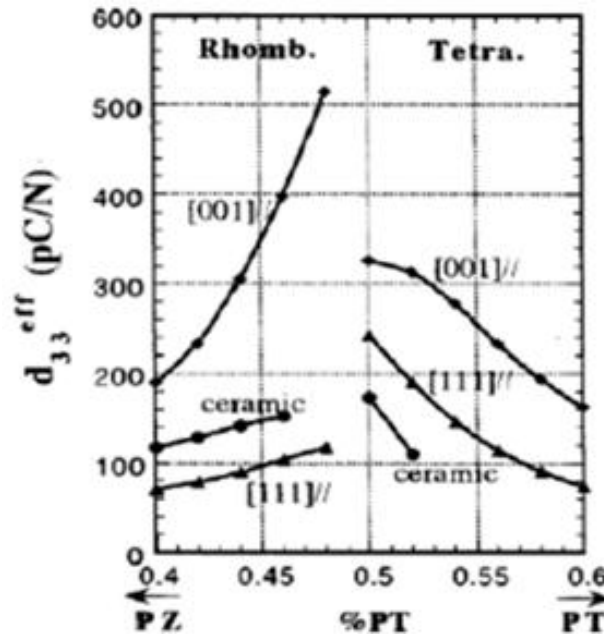


Figure 1.32: Experimental evidence regarding the variation of d_{33} as a function of composition and concentration.

[Source: Xiao-hong Du, U. Belengundu and K. Uchino, "Crystal orientation dependence of piezoelectric properties of lead zirconate titanate near morphotropic phase boundary," *Appl. Phys. Lett.* 72 (1998) 2424].

Selection of proper electrode material is also very important for specific applications since it will determine the quality, texture and properties of piezoelectric films. The nucleation controlled growth allows one to choose film texture by selecting substrates with buffer layers or by reducing the deposition temperatures. The bottom electrode used for thin film preparation should not oxidise or become insulating. Mostly used metal electrodes are platinum⁸⁰ and the widely used sequence is PZT/Pt/Ti/SiO₂/Si with Ti as the adhesion layer. For preparing PZT films with higher quality, buffer layers can be grown initially on the silicon substrate⁸¹⁻⁸³. Buffer layers on the electrode materials can switch the crystal orientation of PZT films on silicon and can prevent inter diffusion and oxidation reactions⁸⁴. SrTiO₃ (ST) is mostly used as

the buffer layer for the growth of PZT thin films since it has a perovskite structure and only a smaller lattice mismatch with PZT. In addition to this, ST layer can also reduce the crystallization temperature since only small activation energy is required for inducing nucleation between the two perovskites. Thus by properly choosing the substrate, buffer layer and by carefully controlling the annealing conditions, different preferentially oriented films can be prepared.

(111)-textured Pt electrodes are available for preparing (111)-oriented thin films and (100)-textured substrates provide (100)-preferential orientation through the electrode-interface controlled nucleation⁸⁵. The possible spontaneous polarization directions of (111) and (100) oriented rhombohedral PZT composition 60/40 was calculated by Uchino *et. al*⁷⁹ and is depicted in Figure 1.33. For (111) oriented films [Figure 1.33 (a)], the polarization directions 2, 3 and 4 are equivalent and are about 70.5° away from the polarization direction 1. When electric field changes its direction from upward to downward direction, the domain along direction 1 will be reversed first since it is parallel to the field. Later the domains along 2, 3 and 4 will be reversed. Hence the reverse-segments on polarization and induced strain hysteresis curves will be inclined as in the Figure 1.34 (a). For (100) oriented films having rhombohedral crystal structure, there are two sets of equivalent polarization directions namely (1,2,3,4) and (5,6,7,8) inclined at an angle of 54.7° from the film normal as given in Figure 1.33 (b). On changing the direction of electric field from upward to downward direction, the domains along 1,2,3,4 directions will get reversed at the same time.

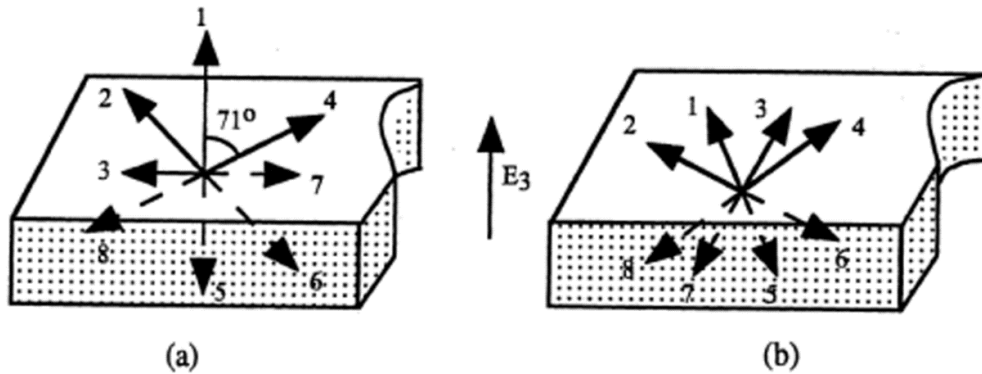


Figure 1.33: Possible spontaneous polarization directions for (a) (111) and (b) (001) oriented films.

[Source: Xiao-hong, U. Belegundu and K. Uchino, "Crystal orientation dependence of piezoelectric properties in Lead Zirconate Titanate: Theoretical expectation for thin films," *Jpn. J. Appl. Phys.*, 36, (1997), 5580.]

In the case of piezoelectric thin films having rhombohedral structure, out of the (100) and (111) orientations, the (100) orientation can provide higher piezo and lower dielectric properties⁴. Also improved fatigue endurance of {100}-oriented PZT thin films provide potential advantages in MEMS technology⁸⁶. The crystal orientation dependence of piezoelectric properties of PZT in three dimensional space has been calculated by Uchino *et. al*⁷⁹. There are two equivalent polarization directions [Figure 1.33 (b)] (1, 2, 3, 4) and (5, 6, 7, 8) which are about 54.7° away from the film normal. When electric field changes direction from upward to downward, the domains along direction (1, 2, 3, 4) will also be reversed at the same time. The reverse segment of polarization and strain induced hysteresis curve is abrupt as indicated in Figure 1.34 (b).

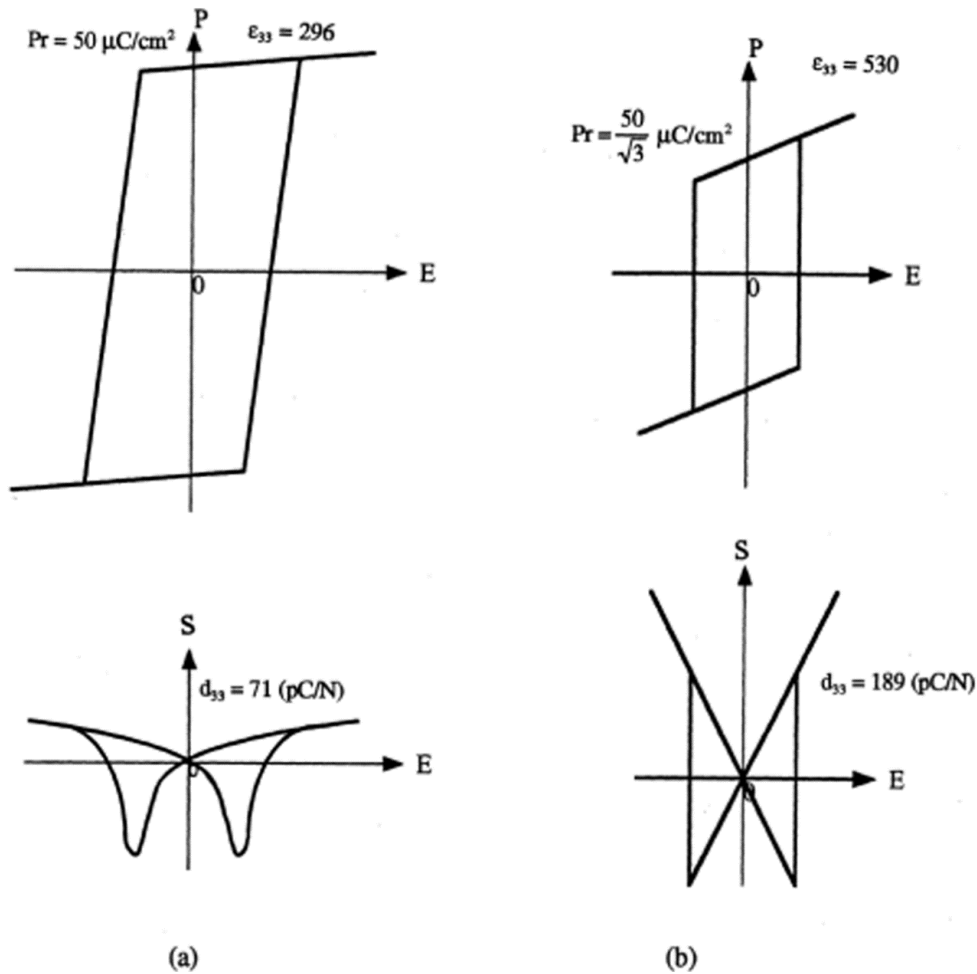


Figure 1.34: Theoretical polarization and induced strain curves for (a) (111) and (b) (001) oriented rhombohedral PZT 60/40.

[Source: Xiao-hong, U. Belegundu and K. Uchino, "Crystal orientation dependence of piezoelectric properties in Lead Zirconate Titanate: Theoretical expectation for thin films," *Jpn. J. Appl. Phys.*, 36, (1997) 5580].

The domain directions in $\{001\}$, $\{110\}$ and $\{111\}$ oriented PZT films with tetragonal and rhombohedral structure reported by Ambika *et. al*⁸⁶ are shown in Figure 1.35. For PZT films with MPB composition, there is the coexistence of both tetragonal and rhombohedral phases. For $\{100\}$ -oriented PZT films with tetragonal phase, there exists two types of domains- 90° domains (\vec{a}) and 180° domains (\vec{b}) with respect to the film normal (N) as in

Figure 1.35 (a)(i). For $\{110\}$ -oriented films, there exists 45° (\vec{c}) and 90° (\vec{d}) domains [Figure 1.35 (a)(ii)] whereas for $\{111\}$ -orientation, three domains (\vec{e}) are at an angle of $54^\circ 44'$ with respect to N [Figure 1.35 (a)(iii)]. For rhombohedral PZT compositions with $\{100\}$ -orientation, there are four $54^\circ 44'$ domains (\vec{f}) [Figure 1.35 (b)(i)]. The domains associated with $\{110\}$ -orientation are at an angle of $35^\circ 16'$ (\vec{g}) and 90° (\vec{h}) [Figure 1.35 (b)(ii)] whereas for $\{111\}$ -orientation there are three 71° domains (\vec{j}) and one 180° domain (\vec{i}) w.r.t film normal [Figure 1.35 (b)(iii)]⁸⁶.

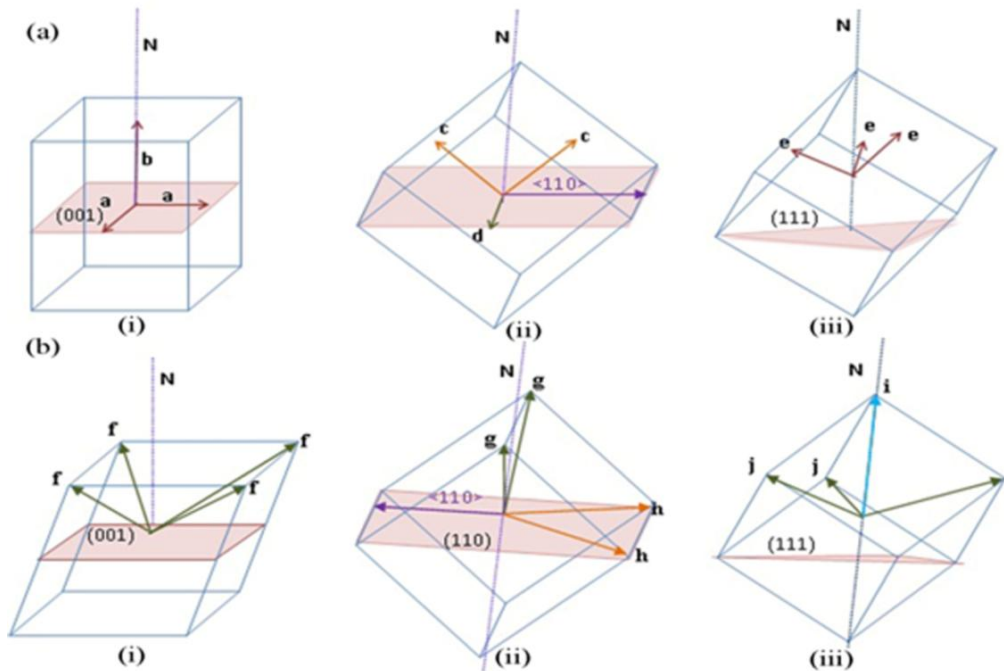


Figure 1.35: Domains along various directions in (a) Tetragonal and (b) Rhombohedral PZT (i) $\{001\}$, (ii) $\{110\}$ and (iii) $\{111\}$.

[Source: D. Ambika, V. Kumar, K. Tomioka, I. Kanno, "Deposition of PZT thin films with $\{001\}$, $\{110\}$, and $\{111\}$ crystallographic orientations and their transverse piezoelectric characteristics," *Adv. Mat. Lett.*, 3(2) (2012)102].

1.3.8.1 Longitudinal piezoelectric constant (d_{33})

Longitudinal piezoelectric constant is defined as out of plane strain to the electric field applied normal to the plane.

$$\text{Mathematically, } d_{33} = \left(\frac{\partial S_3}{\partial E_3}\right)_T = \left(\frac{\partial D_3}{\partial T_3}\right)_E \quad (1.22)$$

Where S is the strain

E is electric field

D is the displacement and

T is the stress

The subscript 3 indicates the axis perpendicular to the film surface. Due to the clamping of the film on the substrate, the above equation gives only an effective value for thin films.

1.3.8.2 Transverse piezoelectric constant (d_{31})

d_{31} is defined as the in-plane strain to the electric field applied normal to the plane.

$$d_{33,f} = d_{33} - 2d_{31} \frac{(s_{13}^E + \nu/Y)}{s_{11}^E + s_{12}^E} \quad (1.23)$$

$$d_{33,f} = -\frac{2d_{31}s_{13}^E}{s_{11}^E + s_{12}^E} \quad (1.24)$$

where s_{11}^E , s_{12}^E and s_{13}^E are the mechanical compliances of the piezoelectric film under constant electric field. Here Y denotes Young's modulus and ν represents Poisson's ratio of substrate. Out of d_{33} and d_{31} , the transverse piezoelectric coefficient d_{31} is more important for device applications since large deformation can be obtained perpendicular to the electric field due to longer lateral dimension when compared with the small

thickness of piezoelectric film. But for thin film, one problem while determining d_{31} is the difficulty to estimate independently the contribution of compliance from the piezoelectric film. In this context arise the importance of the transverse piezoelectric coefficient, $e_{31,f}$ which is almost independent of Young's modulus of the piezoelectric film. $e_{31,f}$ is the most important piezoelectric coefficient in case of thin film actuators driven with top and bottom electrodes.

$e_{31,f}$ relates an applied electric field out of plane to the resultant in-plane stress. When the direction of applied electric field is parallel to the direction of spontaneous polarization, the piezoelectric material is found to expand parallel to the polarization and gets contracted laterally⁸⁷.

$$e_{31,f} = \frac{d_{31}}{s_{11,p}^E + s_{12,p}^E} \cong - \frac{h_s^2}{3s_{11,s}(1-\nu_s)L^2} \frac{\delta}{V} \quad (1.25)$$

Here h_{si} is the thickness of the substrate, δ is the tip displacement, V is the applied voltage, L is the length of the cantilever and S_{11}^S is the elastic compliance of the substrate.

Evaluation of e_{31}

A heterogeneous bimorph is a cantilever beam with an upper piezoelectric element, sandwiched between a pair of metal electrodes and a lower non-piezoelectric element.

Here the polarisation vector defines 3- or z -direction which is perpendicular to the large surface of piezo film and x - and y - directions (1- and 2- respectively) are mutually perpendicular to the z -direction (Figure 1.30). Upon electric field application across the piezoelectric material, deformation of the material occurs. When electric field is applied parallel with the polarization direction of element (ie, along the z -axis), the element will try to

contract in the planes perpendicular to the applied field (ie, along x and y planes) and will expand along the z axis. On the other hand, when electric field is applied anti parallel with the polarization direction of the element, it will try to expand along the planes perpendicular to the electric field and will contract along the direction of the field.

When an external voltage, \bar{A} , is applied across the electrodes, then the electric field E_3 will be anti parallel to the polarisation of the piezoelectric material and hence it will expand in the plane perpendicular to E_3 if $d_{31} < 0$ and will contract in the direction of E_3 if $d_{31} > 0$. Since the piezoelectric material will be adhered to the lower silicon substrate, the reaction forces at the interface from the silicon will oppose the expansion of the piezoelectric material. This will restrict the downward curling of the bender and by changing the polarity of external voltage, the beam will bend in the opposite direction⁸⁸. The constituent equations of piezoelectric effect for the upper element with anti parallel polarisation can be reduced from the tensor form as

$$s_1^P = s_{11}^{E,P} T_1^P - d_{31} \quad (1.26)$$

$$-D_3^P = d_{31} T_1^P - \epsilon_{33}^T E_3 \quad (1.27)$$

Where P is the piezoelectric element, $s_{11}^{E,P}$, ϵ_{33}^T and d_{31} are the compliance at constant electric field, permittivity at constant stress and the piezoelectric constant respectively. $s_{11}^{E,P}$ is be written as s_{11}^P for distinguishing the elastic modulus of piezoelectric element from non-piezoelectric material.

For non-piezoelectric silicon element,

$$s_{11}^{Si} = s_{11}^{Si} T_1^{Si} \quad (1.28)$$

s_{11}^{Si} is the compliance under mechanical stress and superscript Si denotes the lower silicon element. Any non-piezoelectric but suitably elastic material can be used as substitutes for silicon.

T_1^P and T_1^{Si} are transverse stresses acting on y - z planes of the element and are linear functions of distances from the neutral axis, z_p and z_{Si} as given in the following equations (1.18) and (1.19)

$$T_1^P = -\Gamma^P z_p \text{ and} \quad (1.29)$$

$$T_1^{Si} = -\Gamma^{Si} z_{Si} \quad (1.30)$$

Here Γ^P and Γ^{Si} are the proportionality constants. Since the upper and lower elements are composed of different material and different thickness, the neutral axis of the bender will not coincide with the joined surface.

The internal energy density of an infinitesimally small volume element in the piezoelectric material in thermodynamic equilibrium is given by

$$u^p = \frac{1}{2} s_1^P T_1^P + \frac{1}{2} D_3^P E_3 \quad (1.31)$$

Substituting (1.26) and (1.27) in (1.31) gives,

$$u^p = \frac{1}{2} s_{11}^P (T_1^P)^2 - d_{31} E_3 T_1^P + \frac{1}{2} \epsilon_{33}^T E_3^2 \quad (1.32)$$

For silicon element,

$$u^{Si} = \frac{1}{2} s_1^{Si} T_1^{Si} \quad (1.33)$$

$$\text{By using (a), } u^{Si} = \frac{1}{2} s_{11}^{Si} (T_1^{Si})^2 \quad (1.34)$$

By determining the energy density of each element, the total energy of the bender is obtained by volume integration as given in equation (1.24)

$$U = U^P + U^{Si} = \iiint (u^p + u^{Si}) dx dy dz \quad (1.35)$$

The electromechanical characteristics of the bimorph such as displacement (f), rotation (α) of the tip and volume displacement (v) along with charge (Q) on the electrode can be obtained by considering the canonical conjugates namely, force (F), moment (M), external load (P) and voltage (\dot{A}) respectively and also by the application of boundary conditions as detailed⁸⁹.

The resulting constituent equations are represented by the matrix E :

$$\begin{pmatrix} \alpha \\ \delta \\ \gamma \\ Q \end{pmatrix} = \begin{pmatrix} e_{11} & e_{12} & e_{13} & e_{14} \\ e_{21} & e_{22} & e_{23} & e_{24} \\ e_{31} & e_{32} & e_{33} & e_{34} \\ e_{41} & e_{42} & e_{43} & e_{44} \end{pmatrix} \begin{pmatrix} M \\ F \\ P \\ V \end{pmatrix} \quad (1.36)$$

Applying boundary conditions and on solving

$$\begin{pmatrix} \alpha \\ \delta \\ \gamma \\ Q \end{pmatrix} = \begin{pmatrix} \frac{12L}{KW} & \frac{6L^2}{KW} & \frac{2L^3}{K} & \frac{-6d_{31}BL}{K} \\ \frac{6L^2}{KW} & \frac{4L^3}{4L^3} & \frac{3L^4}{3L^4} & \frac{-3d_{31}BL^2}{K} \\ \frac{KW}{2L^3} & \frac{KW}{3L^4} & \frac{2K}{3L^5W} & \frac{-3d_{31}BL^3W}{K} \\ \frac{K}{-6d_{31}BL} & \frac{2K}{-3d_{31}BL^2} & \frac{5K}{-3d_{31}BL^3W} & \frac{LW}{Ah_p} (\epsilon_{33}^T - \frac{d_{31}^2 h_{Si} (s_{11}^{Si} h_p^3 + s_{11}^p h_{Si}^3)}{K}) \end{pmatrix} \begin{pmatrix} M \\ F \\ P \\ V \end{pmatrix} \quad (1.37)$$

$$\text{Where } A = s_{11}^{Si} s_{11}^p (s_{11}^p h_{Si} + s_{11}^{Si} h_p)$$

$$B = \frac{h_{Si} (h_{Si} + h_p)}{(s_{11}^p h_{Si} + s_{11}^{Si} h_p)}$$

$$K = (s_{11}^{Si})^2 (h_p)^4 + 4 s_{11}^{Si} s_{11}^p h_{Si} (h_p)^3 + 6 s_{11}^{Si} s_{11}^p (h_{Si})^2 (h_p)^2 + 4 s_{11}^{Si} s_{11}^p (h_{Si})^3 + (s_{11}^p)^2 (h_{Si})^4 \quad (1.38)$$

Considering external moment (M), external force (F) and external load (P) are absent, the above matrix gets reduced to

$$\delta = \frac{-3d_{31} s_{11}^{Si} s_{11}^p h_{Si} (h_{Si} + h_p) L^2}{K} V \quad (1.39)$$

$$e_{31} = \frac{d_{31}}{\delta_{11}^p} \approx \frac{-(h_{Si})^2}{3s_{11}^{Si} L^2 V} \delta \quad (1.40)$$

1.3.9 Domain engineering in thin films

The control of desirable domain configuration called domain engineering is used for achieving enhanced ferroelectric properties for the conventional ferroelectric materials. The engineered domain configurations will contain domain structure with equivalent polar vectors lying along the electric field direction. Various domain engineering techniques were already proposed⁹⁰. Acceptor doping in PZT ceramics produce hard PZT with inhibited domain wall motion is one among them. Donor doping in PZT forms soft PZT with enhanced domain wall motion is another. Others include domain engineering using crystallographic anisotropy. Out of these techniques, crystal structure and crystallographic orientation are required for best engineered domain configuration, where the number of equivalent domains constructing the engineered domain configuration, the angle θ between the polar direction and the electric field direction are important factors responsible for the piezoelectric performance⁹⁰.

The following are the characteristics of engineered domain configuration for piezoelectric performance.

- i. hysteresis free strain Vs electric field behaviour due to inhibited domain wall motion.
- ii. higher piezoelectric constant along the non-polar direction.
- iii. change in macroscopic symmetry of crystals.

1.3.10 Importance of film thickness and grain size in determining properties

For actuators, maximum displacement with a higher breakdown electrical field can be achieved by using the piezoelectric layer as thin as possible (2-5 μ m). Also for maximum displacement, the thickness of the piezoelectric layer should be 0.3-1.0 that of the nonpiezoelectric layer. Films

possessing thickness less than $0.5\mu\text{m}$ impart residual stress that adversely affects the actuator applications since the domains get clamped, and thereby cannot undergo free switching on application of electric field thereby leading to decreased piezoproperties⁹⁰.

The value of leakage current does not depend on PZT film thickness in the range of 1-100 μm and changes from 10^{-10} up to 10^{-7} A/cm^2 on applying an external electric field from 10 to 500 kV/cm . On the other hand, higher the thickness, lower will be the electric field and hence lower will be the piezo responses since actuators are based on inverse piezoelectric effect. In Figure 1.36, curve 1 indicates that at a fixed voltage, the maximum displacement of the actuator occurs when the piezoelectric layer is so thin. Also the breakdown electrical field is a prominent factor that restricts the piezo layer thickness selection. The dielectric breakdown is reported to be lower for thicker films as indicated in Figure 1.37⁹⁰.

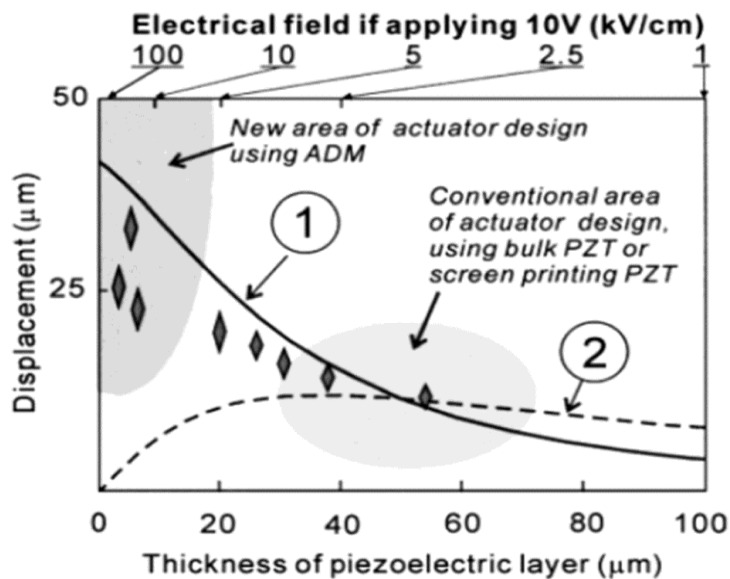


Figure 1.36: Displacement as a function of thickness of piezoelectric layer.

[Source: M. Lebedev and J. Akedo, "What thickness of the piezoelectric layer with High breakdown voltage is required for the microactuator," *Jpn. J. Appl. Phys., Part 1*, 41 (2002) 3344].

For films with higher thickness, porosity will be greater and may lead to decreased electrical breakdown. Since our requirement is to achieve maximum insulating character for a film, by fabricating piezo films with decreased thickness higher breakdown properties can be achieved.

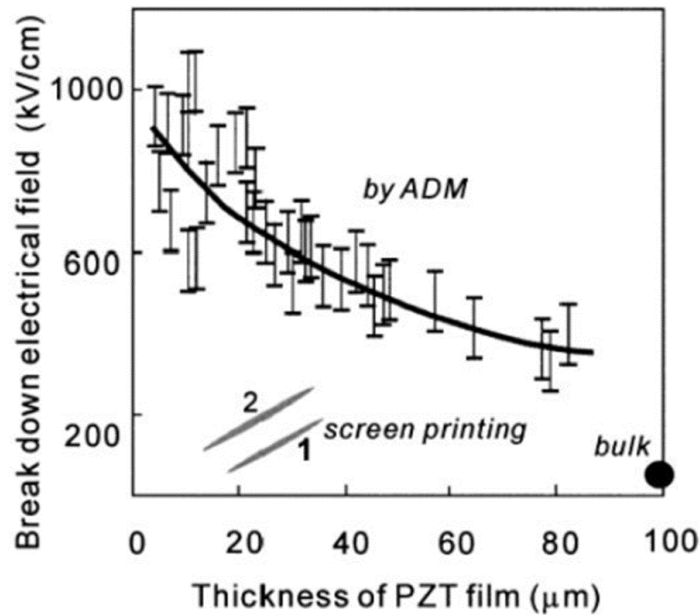


Figure 1.37: DC electrical breakdown for various PZT film thickness

[Source: M. Lebedev and J. Akedo, "What thickness of the piezoelectric layer with High breakdown voltage is required for the microactuator," *Jpn. J. Appl. Phys.*, 41 (2002) 3344].

The influence of thickness on permittivity, remanent polarization and coercive field are given in Figure 1.38. Dielectric permittivity is found to be increased with film thickness and the remanent polarisation decreases when the film thickness is less than $7\mu\text{m}$. The coercive field is found to be increased when sample thickness is less than $20\mu\text{m}$ ⁹¹. Regarding energy consumption, thinner piezo layer has no advantage over thicker ones. But on decreasing ten-folds the thickness of the layer, two fold decrease of applied voltage can be attained and the cost of driving circuit can be minimised.

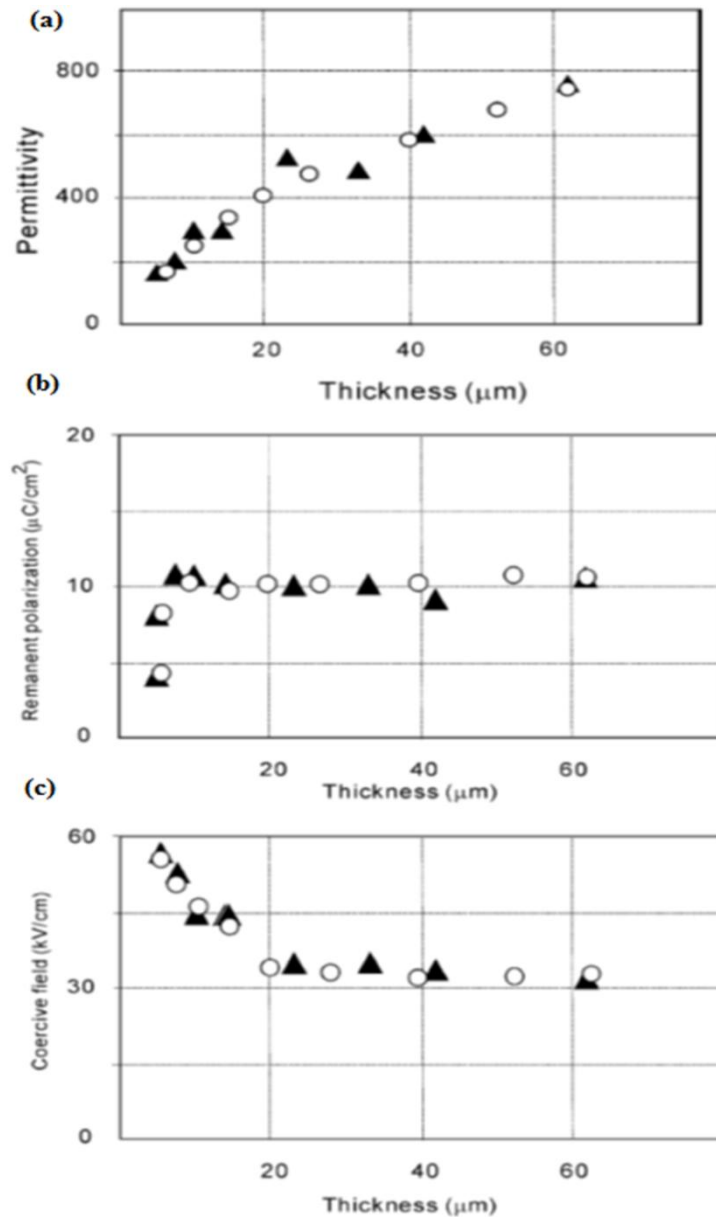


Figure 1.38: (a) Permittivity, (b) remanent polarization and (c) coercive field of PZT films on SRO/Si substrate. \circ indicates that films were deposited and annealed, \blacktriangle indicates films grinded from 64- μm -thick sample.

[Source: M. Lebedev and J. Akedo, "Effect of thickness on the piezoelectric properties of lead zirconate titanate films fabricated by aerosol deposition method," *Jpn. J. Appl. Phys.*, 41 (2002) 6669].

Grain size also had a strong influence on film properties. The grains within a material will be under varying amounts of internal stress. In coarse-grained materials or when the stress is above a critical level, the extrinsic contribution will dominate and the internal stress is found to be minimized by repeated 90° twinning. As a result there will be reduction in dielectric permittivity. But in fine-grained materials with grain size $\leq 1 \mu\text{m}$, absence of 90° twinning within the grains give rise to internal stress below the Curie temperature with a prominent intrinsic effect. The maximum room temperature permittivity of BaTiO_3 was obtained at a grain size of about $1 \mu\text{m}$. When external applied stress is low, the coercive force will prevent domain reorientation and hence coarse and fine-grained materials will behave in a similar manner, ie the permittivity increases with stress. The increase of internal stress in ferroelectric materials makes the domain switching difficult and this may lead to an increase in the coercive field. Such an increased stress can also cause asymmetrical hysteresis and increase of electrical breakdown. The stress inside the film will be localized in some parts of the film and can act as a defect thereby reducing ferroelectric properties. But above a critical stress, domains began to reorient, the very high spontaneous anisotropy dominates the weaker intrinsic effect thereby causing the permittivity level to fall with increasing stress in coarse-grained material^{92,93,94}. The following feature of the fine-grained material is also consistent with the suggested internal stress model.

- i. Aging process is associated with 90^0 domain motion. Aging in fine-grained material is found to be lesser than that in corresponding coarse-grained ceramic due to reduction in 90^0 walls.
- ii. Lower remanence and piezoelectric effects in fine-grained material suggests a decrease in wall motion.
- iii. Comparable density is formed in fine-grained ceramics at room temperature by high pressure compaction, but high permittivity does not occur.

The application of two dimensional stress for the coarse and fine grained specimens in the range of 0 to 8000 psi is illustrated in Figure 1.39. Specimen 4 was found to have an approximate grain size of 1μ and the permittivity was found to be increased with increase in pressure. For specimen 6 having a grain size of 15μ , permittivity showed a slight increase at small load and later decreased continuously with increase in pressure. For specimen 9 with an intermediate grain size, permittivity was found to be almost independent of pressure. Films with smaller grain size grown on platinised silicon substrate were reported to exhibit better fatigue characteristics. In such cases only a small fraction of grains will touch the platinised electrode surface with decreased pinning of domain walls^{95,96}.

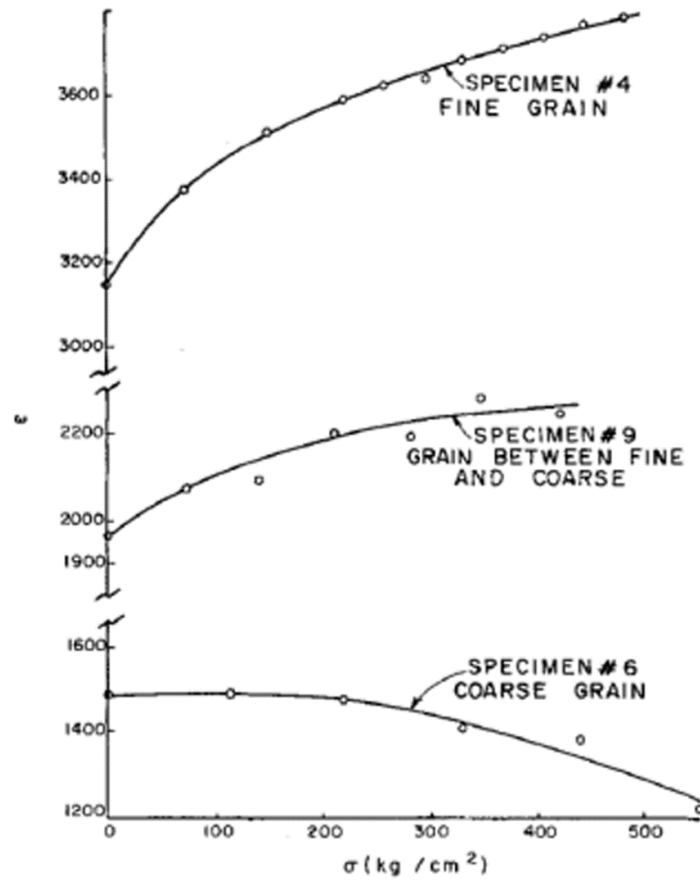


Figure 1.39: Variation of permittivity with two-dimensional compression for specimens of different grain sizes.

[Source: W. R. Buessem, L. E. Cross and A. K. Goswami, "Effect of two-dimensional pressure on the permittivity of fine- and coarse-grained barium titanate," *J. Am. Ceram. Soc.*, 49 (1966) 33].

Residual stress is a function of film thickness. Hence thickness dependence on the properties of epitaxial thin films is used to analyse the strain effects in such materials. Mechanical strain can be controlled by choosing substrates with different lattice constants and thermal expansion coefficients, by varying deposition conditions or by inserting a thin layer of a material of different chemical composition in between the film and the substrate⁹⁷.

1.3.11 Technological applications of ferroelectric thin films

The applications of ferroelectrics cover all areas of our workplaces especially the electronic industry. The important property of ferroelectrics, especially switchable spontaneous polarization gives rise to electrical hysteresis loop which is the finger print of the ferroelectric material.

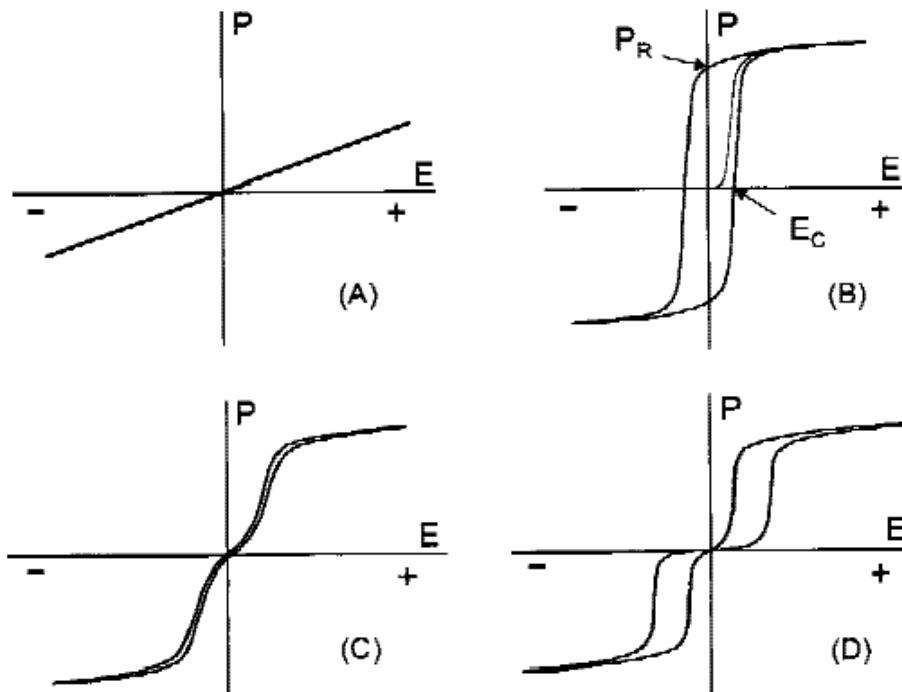


Figure 1.40: Typical hysteresis loops from various ferroelectric ceramics: (A) BaTiO₃ capacitor, (B) easily switchable soft PZT, (C) PLZT 8.6/65/35 relaxor and (D) PSZT antiferroelectric material.

[Source: G. H. Haertling, "Ferroelectric ceramics: History and technology", *J. Am. Ceram. Soc.*, 82 (1999) 797]

The hysteresis loop given in Figure 1.40 (B) indicates that the material has memory whereas in (C) shows no memory. The large remanent polarisation (P_R) obtained for (C) indicates high internal polarizability, strain, electromechanical coupling and electrooptic activity. The switching field (E_C) gives an idea regarding the grain size of a material. Smaller E_C indicates larger

grain size and larger E_C indicates smaller grain size. Higher the loop squareness, better the homogeneity and uniformity of grain size. The off-centered loop from zero voltage point indicates some degree of internal electrical bias caused by internal space charge or aging. The sharpness of the loop tip indicates higher electrical resistivity $> 10^9 \Omega \text{ cm}$. Hence variations in domain switching can be utilised for different applications⁷. Since domain configuration can influence the device functioning, knowledge of domain configuration and switching mechanism are important for developing FE devices.

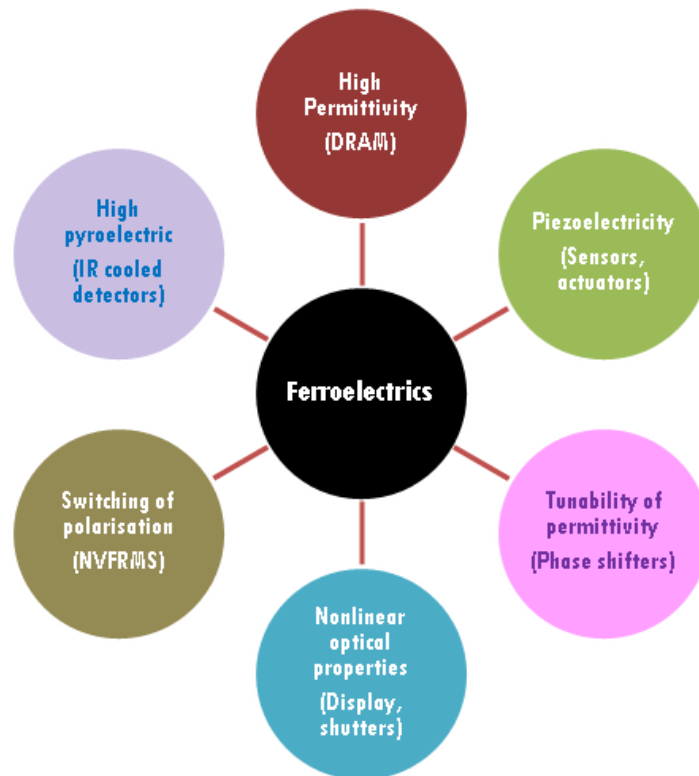


Figure 1.41: Applications of ferroelectric materials.

Figure 1.41 gives a detailed picture of the various applications of ferroelectric materials. Because ferroelectric materials are piezoelectric, they

find applications in sensors and actuators. The direct piezoelectric effect is the underlying principle of a sensor. The electric field induced strain known as the inverse piezoelectricity is the parameter determining the property of actuators. PZT, $\text{Pb}(\text{Zr}_{1-x}\text{Ti}_x)\text{O}_3$ compositions in the MPB region with a Zr/Ti ratio of 52/48 is most suitable for actuator applications.

The direct piezoelectric effect is given as

$$D_i = d_{ijk} X_{jk} \quad (1.41)$$

Here d_{ijk} is the tensor of piezoelectric coefficients. D_i is the charge density induced by applying a stress X_{jk} .

In the converse piezoelectric effect,

$$X_{ij} = d_{ijk} E_k \quad (1.42)$$

Where X_{ij} is the strain developed due to an applied electric field E_k .

The dielectric tunability of ferroelectrics can be varied by the application of dc bias voltage. This makes them applicable in dielectric tunable devices which are of significant importance in microwave engineering. The electrically tunable microwave devices include tunable oscillators, phase shifters etc. The wide range of band gap offered by ferroelectrics makes them useful for nonlinear optical applications. The nonlinear optical devices are mainly important for protecting from intense laser pulses⁹⁸.

The presence of an electric dipole moment with two different polarizations that can be switched by applying an external electric field is utilised for non-volatile memory applications. The pyroelectric effect in polar materials occurs as a result of change in polarization as a function of temperature and can be utilised in IR cooled detectors.

1.4 Present research work

The present research work mainly concentrates on lead based ferroelectric thin films since they offer considerable interest for microelectronic applications including ferroelectric memory devices. Eventhough many perovskite structured materials such as SBT ($\text{SrBi}_2\text{Ta}_2\text{O}_9$), BST ($\text{Ba}_x\text{Sr}_{1-x}\text{TiO}_3$), BLT ($\text{Bi}_{4-x}\text{La}_x\text{Ti}_3\text{O}_{12}$) are reported, lead based materials are important due to their lower processing temperatures, excellent thin film quality and economical viability. The electrical characteristics of ferroelectric thin films are mainly influenced by various factors such as the precursor solution chemistry, nature of substrate, film thickness, heat treatment conditions which are not yet fully understood. Also lead zirconate titanate (PZT) compositions near morphotropic phase boundary (MPB) are already reported to exhibit outstanding piezoelectric properties due to polarization rotation offered by coexisting rhombohedral and tetragonal phases. Hence we fabricated piezoelectric thin films of compositions at or near MPB having fine grained microstructure and studied the influence of preferential crystallographic orientation of thin films on their electrical characteristics, correlated the structure with the electrical properties. Chemical modification was achieved through appropriate doping/substitution at A and B-site of perovskite structure. We adopted chemical solution deposition (CSD) methods like sol-gel for the precursor solution preparation since this method is excellent in controlling the stoichiometry of the precursor. The lower processing temperature, economy and high quality of the prepared films are additional benefits offered by sol-gel method. The structural, microstructural and electrical characteristic of PLZT was studied as a function of thin film composition and preferential orientation.

Preferentially {100}-oriented thin films having rhombohedral symmetry near MPB are reported to be suitable candidates for electromechanical applications. So we have selected the compositions lead lanthanum zirconate titanate, $(\text{Pb}_{1-x}\text{La}_x)(\text{Zr}_{0.65}\text{Ti}_{0.35})_{1-x/4}\text{O}_3$ [PLZT(x/65/35)], $x = 0.06, 0.07$ and 0.08 near the morphotropic phase boundary (MPB) and prepared preferentially {100}-oriented thin films on silicon substrates (111)Pt/Ti/SiO₂/Si by Sol-gel spin coating technique. The influence of thin film composition on $|e_{31,f}|$ has been determined since it is the most important parameter for piezoelectric applications as it can be measured precisely in both direct and converse modes.

Next we focussed our attention on compositions having fixed La³⁺-content viz PLZT (7/60/40), (7/56/44) and (7/65/35) across the morphotropic phase boundary and prepared preferentially {110}-orientated thin films. Preferential {110} orientation facilitates polarisation rotation between the [111] rhombohedral and [100] tetragonal polar axis leading to enhanced field induced strain values. We investigated the dielectric, piezoelectric and ferroelectric properties as a function of thin film composition and texture.

PLZT (8/65/35) exhibited a rhombohedral structure very close to MPB and are ideal host systems for B-site aliovalent acceptor doping. In A-site La³⁺ doped systems, as charge compensation occurs through A-cation vacancies, oxygen vacancies are not formed. They are represented by the following equations;



where M'_{Ti} is a negatively charged acceptor at the B-site, \check{V}_O , is a doubly positively charged oxygen vacancy, V''_{pb} is a doubly negatively charged A-site vacancy and La_{pb} represents a positively charged A-site with respect to the neutral lattice according to Kröger and Vink notation.

B-site aliovalent acceptor dopants can induce structural distortions in the BO_6 octahedra in PLZT. This can lead to increase in the electromechanical properties for MEMS applications. Hence we studied the influence of Fe^{3+} , Mn^{3+} and Cu^{2+} acceptor dopants on B-site in $\{110\}$ -oriented PLZT(8/65/35) thin films. Transverse piezoelectric coefficient, $|e_{31,f}|$ of thin films has been correlated with their crystal structure.

Lead based solid solutions of relaxor ferroelectrics are reported to exhibit excellent piezoelectric and electrostrictive properties suitable for microelectro mechanical systems. Since no reports were available on the electrical properties of PIN- x PT thin films, we prepared solid solutions consisting of lead indium niobate (PIN) and lead titanate (PT), $(1-x)$ PIN- x PT, $x = 0.36-0.40$ with compositions near the morphotropic phase boundary (MPB). Through Raman spectral investigation, we have attempted to study the stabilisation of discrete rhombohedral, monoclinic and tetragonal crystalline phases as the thin film composition is varied across the morphotropic phase boundary. The transverse piezoelectric coefficient ($|e_{31,f}|$) have been correlated with the crystal structure.

Tin-modified $PbZrO_3$ - $PbTiO_3$ ferroelectric and antiferroelectric thin films with higher piezoelectric coefficients offer advantages for various applications. The excellent strain associated with electric field induced AFE \rightarrow FE transition is important for actuator applications. We selected specific compositions, in the $PbZrO_3$ - $PbSnO_3$ - $PbTiO_3$ ternary phase diagram

in the antiferroelectric tetragonal region having constant Titanium content very close to the morphotropic phase boundary and investigated the influence of electric field induced phase transition on transverse piezoelectric coefficient $|e_{31,f}|$ of their thin films which have not yet been previously reported. We also investigated the variation of dielectric constant as a function of temperature for analysing AFE→FE transition.

In short, the thesis describes our studies on the following;

1. Transverse piezoelectric properties of {100}-oriented PLZT (x/65/35) thin film having compositions near the morphotropic phase boundary $0.06 \leq x \leq 0.08$ and {110}-oriented PLZT (7/65/35), (7/60/40) and (7/56/44) suitable for MEMS applications. Detailed discussions are given in Chapter 3.
2. Influence of B-site aliovalent acceptor dopants on the structure, dielectric and piezoelectric properties of {110}-oriented PLZT (8/65/35) thin films. Detailed discussions are given in Chapter 4.
3. The composition dependence on transverse piezoelectric coefficient, $|e_{31,f}|$ of {110}-oriented lead based relaxor ferroelectric solid solutions of (1-x)PIN-xPT near MPB are discussed in Chapter 5 and
4. The influence of electric field induced antiferroelectric → ferroelectric phase transition in Lanthanum doped Lead Zirconate Titanate Stannate thin films having compositions near MPB in Chapter 6.

References

- [1] W. Liu and X. Ren, "Large piezoelectric effect in Pb-free ceramics," *Phys. Rev. Lett.*, **103** (2009) 257602.
- [2] J. Rodel, W. Jo, K. T. P. Seifert, E.M. Anton, T. Granzow and D. Damjanovic, "Perspective on the development of lead-free piezoceramics," *J. Am. Ceram. Soc.*, **92** (2009) 1153.
- [3] S. E. Park and T. R. Shrout, "Ultrahigh strain and piezoelectric behavior in relaxor based ferroelectric single crystals," *J. Appl. Phys.*, **82** (1997) 1804.
- [4] L. Lian and N. R. Sottos, "Effects of thickness on the piezoelectric and dielectric properties of lead zirconate titanate thin films," *J. Appl. Phys.*, **87** (2000) 3941.
- [5] W. G. Cady, "Piezoelectricity," *McGraw-Hill, New York*, (1946) 1.
- [6] B. Jaffe, W. R. Cook and H. Jaffe, "Piezoelectric ceramics," *Academic, New York*, (1971) 1.
- [7] G. H. Haertling, "Ferroelectric ceramics: History and technology," *J. Am. Ceram. Soc.*, **82** (1999) 797.
- [8] IEEE Standard definitions of primary ferroelectric terms ANSI/IEEE Std.180-1986, *IEEE, New York* (1986) 1.
- [9] M. E. Lines and A. M. Glass, *Principles and Applications of Ferroelectrics and Related Materials*, Oxford: Clarendon (1979).
- [10] D. Damjanovic, "Ferroelectric, dielectric and piezoelectric properties of ferroelectric thin films and ceramics," *Rep. Prog. Phys.*, **61** (1998) 1267.
- [11] D. Damjanovic, "Hysteresis in piezoelectric and Ferroelectric materials, The science of Hysteresis," *I. Mayergoyz and G. Bertotti (Eds): Elsevier.*, **3** (2005).
- [12] V. V. Shvartsman, N. A. Pertsev, J. M. Herrero, C. Zaldo and A. L. Kholkin, "Nonlinear local piezoelectric deformation in ferroelectric thin films studied by scanning force microscopy," *J. Appl. Phys.*, **97** (2005) 104105.

- [13] S. Trolier-McKinstry, N. B. Gharb and D. Damjanovic, "Piezoelectric nonlinearity due to motion of 180 domain walls in ferroelectric materials at subcoercive fields: a dynamic poling model," *Appl. Phys. Lett.*, **88** (2006) 202901.
- [14] F. Xu, S. Trolier-McKinstry, W. Ren and B. Xu, "Domain wall motion and its contribution to the dielectric and piezoelectric properties of lead zirconate titanate films," *J. Appl. Phys.*, **89** (2001) 1336.
- [15] M. Dawber K. M. Rabe and J. F. Scott, "Physics of thin -film ferroelectric oxides," *Rev. Mod. Phys.*, **77** (2005) 1083.
- [16] N. Izyunskaya, Y. -I Alivov, S. -J Cho, H. Morkoe, H. Lee and Y. -S Kang, "Processing, structure, properties and Applications of PZT thin films," *Crit. Rev. Solid State.*, **32** (2007) 111.
- [17] A. K. Tagantsev, K. Alexander, "Mechanisms of polarization switching in ferroelectric thin films," *Ferroelectrics.*, **184** (1996) 79.
- [18] L. E. Cross and S. Trolier-McKinstry, "Thin-film integrated ferroelectrics," *Enc. Appl. Phys.*, **21**, (1997) 429.
- [19] D. I. Woodward, J. Knudsen and I. M. Reaney, "Review of crystal and domain structures in the $(\text{PbZr}_x\text{Ti}_{1-x})\text{O}_3$ solid solution," *Phys. Rev. B.*, **72** (2005) 104110.
- [20] B. Noheda, "Structure and high-piezoelectricity in lead oxide solid solutions," *Curr. Opin. Solid. St. M.*, **6** (2002) 27.
- [21] D. Damjanovic, "A morphotropic phase boundary system based on polarization rotation and polarization extension," *Appl. Phys. Lett.*, **97** (2010) 062906.
- [22] G. H. Haertling and C. E. Land, "Hot-pressed $(\text{Pb,L a})(\text{Zr,T i})\text{O}_3$ ferroelectric ceramics for electrooptic applications," *J. Am. Ceram. Soc.*, **54** (1971) 1.
- [23] G. A. Smolenskii and A. I. Agranovskaya, "Dielectric polarization of a number of complex compounds," *Sov. Phys. Solid State.*, **1** (1959) 1429.
- [24] L. E. Cross, "Relaxor ferroelectrics," *Ferroelectrics.*, **76** (1987) 241.

- [25] R. A. Cowley, S. N. Gvasaliya, S. G. Lushnikov, B. Roessli and G. M. Rotaru, "Relaxing with relaxors: a review of relaxor ferroelectrics," *Adv. Phys.*, **60** (2011) 229.
- [26] S. W. Choi, T. R. Shrout, S. J. Jang and A. S. Bhalla, "Morphotropic Phase Boundary in $\text{Pb}(\text{Mg}_{1/3}\text{Nb}_{2/3})\text{-PbTiO}_3$ System," *Mater. Lett.*, **8** (1989) 253.
- [27] S. J. Jang, K. Uchino, S. Nomura and L. E. Cross, "Electrostrictive behavior of lead magnesium niobate based ceramic dielectrics," *Ferroelectrics.*, **27** (1980) 31.
- [28] D. J. Taylor, D. Damjanovic and A. S. Bhalla, "Pyroelectric and dielectric properties of PMN-based ceramics under dc bias," *Ferroelectrics.*, **118** (1991) 143.
- [29] J. Kuwata, K. Uchino and S. Nomura, "Phase Transitions on the $\text{Pb}(\text{Zn}_{1/3}\text{Nb}_{2/3})\text{O}_3$ - PbTiO_3 System," *Ferroelectrics.*, **37** (1981) 579.
- [30] J. Kuwata, K. Uchino and S. Nomura, "Dielectric and Piezoelectric Properties of $0.91\text{Pb}(\text{Zn}_{1/3}\text{Nb}_{2/3})\text{O}_3$ - 0.09PbTiO_3 Single Crystals," *Jpn. J. Appl. Phys.*, **21** (1982) 1298.
- [31] S. Wada, S. E. Park, L. E. Cross and T. R. Shrout, "Engineered domain configuration rhombohedral PZN-PT single crystals and their ferroelectric related properties," *Ferroelectrics.*, **221** (1999) 147.
- [32] Z. -G. Ye, B. Noheda, M. Dong, D. Cox and G. Shirane, "Monoclinic phase in the relaxor-based piezoelectric/ferroelectric $\text{Pb}(\text{Mg}_{1/3}\text{Nb}_{2/3})\text{O}_3\text{-PbTiO}_3$ system," *Phys. Rev. B.*, **64** (2001) 184114.
- [33] B. Noheda, D. E. Cox, G. Shirane, J. Gao and Z. G. Ye, "Phase diagram of the ferroelectric relaxor $(1-x)\text{PbMg}_{1/3}\text{Nb}_{2/3}\text{O}_3\text{-xPbTiO}_3$," *Phys. Rev. B.*, **66** (2002) 054104.
- [34] D. La-Orauttapong, B. Noheda, Z.-G. Ye, P.M. Gehring, J. Toulouse, D. E. Cox and G. Shirane, "Phase diagram of the relaxor ferroelectric $(1-x)\text{Pb}(\text{Zn}_{1/3}\text{Nb}_{2/3})\text{O}_3\text{-xPbTiO}_3$," *Phys. Rev. B.*, **65** (2002) 144101.

- [35] A. K. Singh and D. Pandey, "Evidence for M_B and M_C phases in the morphotropic phase boundary region of $(1-x)[Pb(Mg_{1/3}Nb_{2/3})O_3] - xPbTiO_3$: A Rietveld study", *Phys. Rev. B.*, **67** (2003) 064102.
- [36] E. F. Alberta and A. S. Bhalla "Piezoelectric properties of $Pb(InNb)_{1/2}O_3$ - $PbTiO_3$ solid solution ceramics," *J. Korean Phys. Soc.*, **32** (1998) 1265.
- [37] A. I. Kingon and S. Srinivasan, "Lead zirconate titanate thin films directly on copper electrodes for ferroelectric, dielectric and piezoelectric applications," *Nat. Mater.*, **4** (2005) 233.
- [38] M. D. Losego, L. H. Jimison, J. F. Ihlefeld and J. P. Maria, "Ferroelectric response from lead zirconate titanate thin films prepared directly on low-resistivity copper substrates," *Appl. Phys. Lett.*, **86** (2005) 172906.
- [39] R. W. Schwartz, "Chemical solution deposition of perovskite thin films," *Chem. Mater.*, **9** (1997) 2325.
- [40] L. M. Doeswijk, G. Rijnders and D. H. A. Blank, "Pulsed laser deposition: metal versus oxide ablation," *Appl. Phys. A: Mater. Sci. Process. A.*, **78** (2004) 263.
- [41] D. A. Muller, N. Nakagawa, A. Ohtomo, J. L. Grazul and H. Y. Hwang, "Atomic-scale imaging of nanoengineered oxygen vacancy profiles in $SrTiO_3$," *Nature.*, **430** (2004) 657.
- [42] S. D. Bu, M. K. Lee, C. B. Eom, W. Tian, X. Q. Pan, S. K. Streiffer and J. J. Krajewski, "Perovskite phase stabilization in epitaxial $Pb(Mg_{1/3} Nb_{2/3})O_3$ - $PbTiO_3$ films by deposition onto vicinal (001) $SrTiO_3$ substrates," *Appl. Phys. Lett.* **79** (2001) 3482.
- [43] T. Maeder, P. Muralt and L. Sagalowicz, "Growth of (111)-oriented PZT on RuO_2 (100)/Pt (111) electrodes by in-situ sputtering," *Thin solid Films.*, **345** (1999) 300.

- [44] P. Muralt, T. Maeder, L. Sagalowicz, S. Hiboux, S. Scalese, D. Naumovic, R. G. Agostino, N. Xanthopoulos, H. J. Mathieu, L. Patthey and E. L. Bullock, "Texture control of PbTiO_3 and $\text{Pb}(\text{Zr},\text{Ti})\text{O}_3$ thin films with TiO_2 seeding," *J. Appl. Phys.*, **83** (1998) 3835.
- [45] J. H. Haeni, P. Irvin, W. Chang, R. Uecker, P. Reiche, Y. L. Li, S. Choudhury, W. Tian, M. E. Hawley, B. Craigo and A. K. Tagantsev, "Room-temperature ferroelectricity in strained SrTiO_3 ," *Nature* ., **430** (2004) 758.
- [46] C. D. Theis, J. Yeh, D. G. Schlom, M. E. Hawley and G. Brown, "Adsorption-controlled growth of PbTiO_3 by reactive molecular beam epitaxy," *Thin Solid Films.*, **325** (1998) 107.
- [47] G. R. Bai, L.-F. Tsu, A. Wang, C. M. Foster, C. E. Murray and V. P. Dravid, "In situ growth of highly oriented $\text{Pb}(\text{Zr}_{0.5}\text{Ti}_{0.5})\text{O}_3$ thin films by low-temperature metal-organic chemical vapor deposition," *Appl. Phys. Lett.*, **72** (1998) 1572.
- [48] M. De. Keijser and G. J. M. Dormans, "Modelling of organometallic chemical vapour deposition of lead titanate," *J. Cryst. Growth.*, **149** (1995) 215.
- [49] K. D. Budd, S. K. Dey and D. A. Payne, "Sol-gel processing of PT, PZ, PZT and PLZT thin films," *Br. Ceram. Proc.*, **36** (1985) 107.
- [50] S. K. Dey, K. D. Budd and D. A. Payne, "Thin film ferroelectrics of PZT by sol-gel processing," *IEEE T Ultrason Ferr.*, **35** (1988) 80.
- [51] G. A. C. M. Spierings, M. J. E. Ulenaers, G. L. M. Kampschöer, H. A. M. Van Hal, and P. K. Larsen, "Preparation and ferroelectric properties of $\text{PbZr}_{0.53}\text{Ti}_{0.47}\text{O}_3$ thin films by spin coating and metal organic decomposition," *J. Appl. Phys.*, **70** (1991) 2290.
- [52] B. A. Tuttle, T. J. Headley, B. C. Bunker, R. W. Schwartz, T. J. Zender, C. L. Hernandez, D. C. Goodnow, R. J. Tissot, J. Michael, and A. H. Carim, "Microstructural evolution of $\text{Pb}(\text{Zr},\text{Ti})\text{O}_3$ thin films prepared by hybrid metallo-organic decomposition," *J. Mater Res.*, **7** (1992)1876.

- [53] I. Kanno, H. Kotera and K. Wasa, "Measurement of transverse piezoelectric properties of PZT thin films," *Sens. Actuators, A.*, **107** (2003) 68.
- [54] V. G. Koukhar, N. A. Pertsev and R. Waser, "Thermodynamic theory of epitaxial ferroelectric thin films with dense domain structures," *Phys. Rev. B.*, **64** (2001) 214103.
- [55] L. Chen, V. Nagarajan, R. Ramesh and A. L. Roytburd, "Nonlinear electric field dependence of piezoresponse in epitaxial ferroelectric lead zirconate titanate thin films," *J. Appl. Phys.*, **94** (2003) 5147.
- [56] D. V. Taylor, D. Damjanovic and N. Setter, "Nonlinear contributions to dielectric and piezoelectric properties in lead zirconate titanate thin films," *Ferroelectrics.*, **224** (1999) 299.
- [57] N. Setter, D. Damjanovic, L. Eng, G. Fox, S. Gevorgian, S. Hong, A. Kingon, H. Kohlstedt, N. Y. Park, G. B. Stephenson, I. Stolitchnov, A. K. TagansteV, D. V. Taylor, T. Yamada and S. Streiffer, "Ferroelectric thin films: Review of materials, properties and applications," *J. Appl. Phys.*, **100** (2006) 051606.
- [58] T. Mitsui and J. Furuichi, "Domain Structure of Rochelle Salt and KH_2PO_4 ," *Phys. Rev.* **90** (1953) 193.
- [59] I. P. Batra, P. Wurfel and B. D. Silverman, "Phase Transition, Stability, and Depolarization Field in Ferroelectric Thin Films" *Phys. Rev. B.*, **8** (1973) 3257.
- [60] C. A. Randall, N. Kim, J. P. Kucera, W. Cao and T. R. Shrout, "Intrinsic and extrinsic size effects in fine-grained morphotropic-phase boundary lead zirconate titanate ceramics," *J. Am. Ceram. Soc.*, **81** (1998) 677.
- [61] D. A. Hall, "Review Nonlinearity in Piezoelectric Ceramics," *J. Mater. Sci.*, **36** (2001) 4575.
- [62] M. E. Lines, A. M. Glass, "Principles and Applications of ferroelectrics and related materials (Oxford University Pres, New York," (1977)

- [63] S. Li, W. Cao, L. E. Cross, "The extrinsic nature of nonlinear behavior observed in lead zirconate titanate ferroelectric ceramic," *J. Appl. Phys.*, **69** (1991) 7219.
- [64] D. Damjanovic, in *Hysteresis in Pieoelectric and ferroelectric materials*, eds. By G. Bertotti, I. Mayergoyz. Science of Hysteresis, vol III (2005) 337.
- [65] L. B. Kong, S. Li, T. S. Zhang, J. W. Zhai, F. Y. C. Boey and J. Ma, "Electrically tunable dielectric materials and strategies to improve their performance," *Prog. Mater Sci.*, **5** (2010) 840.
- [66] W. D. Kingery, H. K. Bowen, D. R. Uhlmann, "Introduction to ceramics," *John Wiley and Sons, New York* (1976).
- [67] L. L. Hench, J. K. West, "Principles of electronic ceramics," John Wiley and Sons, New York (1990).
- [68] K. P. Rema, "Structure-property relationship in PZT based piezoelectric systems," *Ph.D Thesis*, (2010).
- [69] M. Narayanan, S. Tong, S. Liu, B. Ma and U. Balachandran, "Estimation of intrinsic contribution to dielectric response of $\text{Pb}_{0.92}\text{La}_{0.08}\text{Zr}_{0.52}\text{Ti}_{0.48}\text{O}_3$ thin films at low frequencies using high bias fields," *Appl. Phys. Lett.*, **102** (2013) 062906.
- [70] B. Nagaraj, S. Aggarwal, T. K. Song, T. Sawhney and R. Ramesh, "Leakage current mechanisms in lead based thin-film ferroelectric capacitors," *Phys. Rev. B.*, **59**, (1999) 16022.
- [71] A. Sigov, Yu. Podgorny, K. Vorotilov and A. Vishnevskiy; "Leakage currents in ferroelectric thin films," *Phase transitions.*, **86** (2013) 1141.
- [72] M. Dawber K. M. Rabe and J. F. Scott, "Physics of thin -film ferroelectric oxides," *Rev. Mod. Phys.*, **77** (2005) 1083.
- [73] R. Waser and M. Klee, "Theory of conduction and breakdown in perovskite thin films," *Integr. Ferroelectr.*, **2** (1992) 23.

- [74] R. L. Holman and R. M. Fulrath, "Intrinsic nonstoichiometry in the lead zirconate-lead titanate system determined by Knudsen effusion," *J. Appl. Phys.*, **44** (1973) 5227.
- [75] S. Fushimi and T. Ikeda, "Phase Equilibrium in the System PbO-TiO₂-ZrO₂," *J. Am. Ceram. Soc.*, **50** (1967) 129.
- [76] S. M. Sze and K. K. Ng, "Physics of semiconductor devices," *Hoboken, NJ: John Wiley & Sons* (2006).
- [77] S. wada, H. Kakemoto and T. Tsurumi, "Enhanced piezoelectric properties of piezoelectric single crystals by domain engineering," *Mater. Trans.*, **45** (2004) 178.
- [78] M. Dekkers, Minh D. Nguyen, R. Steenwelle, Paul M. Te Riele, Dave H. A. Blank and G. Rijnders, "Ferroelectric properties of epitaxial Pb(Zr,Ti)O₃ thin films on silicon by control of crystal orientation," *Appl. Phys. Lett.*, **95**, (2009) 012902.
- [79] X. Hong, U. Belegundu and K. Uchino, "Crystal orientation dependence of piezoelectric properties in Lead Zirconate Titanate: Theoretical expectation for thin films," *Jpn. J. Appl. Phys.*, **36** (1997) 5580.
- [80] H. N. Al-Shareef, K. D. Gifford, S. H. Rou, P. D. Hren, O. Auciello and A. I. Kingon, "Electrodes for ferroelectric thin films," *Integr Ferroelectr.*, **3** (1993) 321.
- [81] G. J. Willems, D. J. Wouters, H. E. Maes and R. Nouwen, "Nucleation and orientation of Sol-gel PZT thin films on Pt electrodes," *Integr Ferroelectr.*, **15** (1997) 19.
- [82] K. Sreenivas, I. Reaney, T. Maeder, N. Setter, C. Jagadish and R. G. Elliman, "Investigation of Pt/Ti bilayer metallization on silicon for ferroelectric thin film integration," *J. Appl. Phys.*, **76** (1994) 466.
- [83] P. Revesz, J. Li, N. Szabo, J.W. Mayer, D. Caudillo and E. R. Myers, "PZT Interaction with Metal and Oxides Studied by Rutherford Backscattering Spectrometry," *Mater. Res. Symp. Proc.*, **243** (1991) 101.

- [84] P. Muralt, "Ferroelectric thin films for micro-sensors and actuators: a review," *J. Micromech. Microeng.*, **10** (2000) 136.
- [85] S. H. Kim, D. Y. Park, H. J. Woo, D. S. Lee, J. Ha, C. S. Hwang, I. B. Shimand and A. I. Kingon, "Orientation effects in chemical solution derived $\text{Pb}(\text{Zr}_{0.3}\text{Ti}_{0.7})\text{O}_3$ thin films on ferroelectric properties," *Thin solid films.*, **416** (2002) 264.
- [86] D. Ambika, V. Kumar, K. Tomioka, I. Kanno, "Deposition of PZT thin films with {001}, {110}, and {111} crystallographic orientations and their transverse piezoelectric characteristics," *Adv. Mat. Lett.*, **3** (2012) 102.
- [87] S. Trolier-Mc Kinsty, F. Griggio, C. Yaeger, P. Jousse, D. Zhao, S. S. Bharadwaja, T. N. Jackson, S. Jesse, S. V. Kalinin, K. Wasa, "Designing piezoelectric films for micro electromechanical systems," *IEEE Trans. Ultrason., Ferroelect. Freq. Control.*, **58** (2011).
- [88] J. G. Smith and S. I. Dalke and T. K. Cooney, "The constituent equations of piezoelectric bimorphs," *Sens. Actuators, A.*, **28** (1991) 41.
- [89] J. G. Smits and W. Choi, "The constituent equations of piezoelectric heterogeneous bimorphs," *IEEE Trans. Ultrason. Ferroelect. Freq. Control.*, **38** (1991) 256.
- [90] M. Lebedev and J. Aakedo, "What thickness of the piezoelectric layer with High breakdown voltage is required for the microactuator," *Jpn. J Appl. Phys.*, **41** (2002) 3344.
- [91] M. Lebedev and J. Aakedo, "Effect of thickness on the piezoelectric properties of Lead Zirconate Titanate films fabricated by aerosol deposition method," *Jpn. J. Appl. Phys.*, **41** (2002) 6669.
- [92] W. R. Buessem, L. E. Cross and A. K. Goswami, "Effect of two-dimensional pressure on the permittivity of fine- and coarse-grained barium titanate," *J. Am. Ceram. Soc.*, **49** (1966) 36.
- [93] W. R. Buessem, L. E. Cross and A. K. Goswami, "Phenomenological theory of high permittivity in fine-grained barium titanate," *J. Am. Ceram. Soc.*, **49** (1966) 33.

- [94] G. Arlt, D. Hennings and G. De With, "Dielectric properties of fine grained barium titanate ceramics," *J. Appl. Phys.*, **58** (1985) 1619.
- [95] J. K. Yang, W. S. Kim and H. H. Park, "Effect of grain size of $\text{Pb}(\text{Zr}_{0.4}\text{Ti}_{0.6})\text{O}_3$ sol-gel derived thin films on the ferroelectric properties," *Appl. Surf. Films.*, **169** (2001) 544.
- [96] F. Yan, P. Bao, H. L. W. Chan, C. L. Choy and Y. Wang, "The grain size effect of $\text{Pb}(\text{Zr}_{0.3}\text{Ti}_{0.7})\text{O}_3$ thin films," *Thin Solid Films.*, **406** (2002) 282.
- [97] B. H. Park, E. J. Peterson, Q. X. Jia, J. Lee, X. Zeng, W. Si and X. X. Xi, "Effects of very thin strain layers on dielectric properties of epitaxial $\text{Ba}_{0.6}\text{Sr}_{0.4}\text{TiO}_3$ films," *Appl. Phys. Lett.*, **78** (2001) 533.
- [98] O. Auciello, J. F. Scott and R. Ramesh, "The Physics of ferroelectric memories," *Phys. Today.*, **51** (1998) 22.

LAXMI PRIYA S. “FERROELECTRIC THIN FILMS FOR MICROACTUATOR APPLICATIONS”. THESIS. CENTRE FOR MATERIALS FOR ELECTRONICS TECHNOLOGY (C-MET), UNIVERSITY OF CALICUT, 2018.

Thin film deposition and Characterisation techniques

● Contents ●	2.1 Introduction
	2.2 Thin film deposition techniques
	2.3 Chemical deposition
	2.4 Selection of chelating agents for thin film precursor solution preparation
	2.5 Preparation of precursor solutions
	2.6 Processing equipments
	2.7 Thin film growth process
	2.8 Characterization techniques
	2.9 Measurement of leakage current
	2.10 Measurement of ferroelectric properties
	2.11 Measurement of piezoelectric properties
	References

2.1 Introduction

The preliminary process during film growth is the selection of a suitable substrate that facilitates the deposition and formation of good quality oxide layer or hetero structures with minimised stress and defects¹. Since stress accompanied differences in lattice parameters and thermal expansion coefficients causes deformation of crystal structure and deterioration of film properties, selection of suitable substrates with minimised stress in the layers acquires importance. Mainly there are two groups of substrates (i) insulating bulk substrate and (ii) conducting metal or oxide substrate depending on specific applications. Insulating single crystal substrates like MgO and SrTiO₃ are suitable for electro-optic applications whereas conducting metal substrates serves as bottom electrodes for preparing PZT films especially for non volatile random access memory devices. For MEMS applications, deposition of PZT films on metal substrates like Pt is required¹.

The necessary requirements for potential electrodes to serve for good device performance are depicted below,

1. To get crystalline epitaxial ferroelectric films on conductive electrodes, the bottom electrode should be epitaxial with lattice parameter close to the ferroelectric material, should have compatible crystalline structure and chemistry. In case if the bottom electrode is not having similar structure with the material, it should atleast allow the ferroelectric material to assume its lattice structure during the growth process.
2. In order to prevent interdiffusion and post growth annealing, the bottom electrode should be impervious to the constituents of both the ferroelectric layer and the substrate.

3. For achieving lower leakage currents, the electrodes should possess a higher work function.

2.2 Thin film deposition techniques

Thin film deposition technology has grown tremendously over the last few years extending its applications over electronics, thin film coating industries etc. Thin film deposition process can be generally classified as physical deposition and chemical deposition. The purpose of both methods is to produce thin films with desired properties in a controlled reproducible manner. The most important requisite for thin film precursors is that the solution should be a true/stable solution and hence the deposition method should not cause segregation of the metallo-organic compound. Since different metallo-organic compounds in a precursor have different solubilities, the solvent evaporation during deposition step should be rapid for minimizing segregation. Also the deposition method should have the ability to control both the magnitude and uniformity of film thickness since the properties of films are related to a single layer thickness.

During physical deposition, the atoms or molecules of the source material gets vaporised by physical processes such as thermal evaporation or by bombardment of the source by an energetic beam of electrons, photons or ions. Usually the process is carried out at high vacuum or ultra high vacuum in order to avoid contamination of film by the ambient atmosphere. Chemical deposition is accompanied by chemical reaction with vapour species containing the film constituents that are incident on a substrate producing film with desired composition. It mainly utilizes an inert carrier gas maintained at atmospheric pressure.

The major physical deposition techniques are

2.2.1 Vacuum evaporation

High purity films are obtained by vacuum evaporation. It can be applied for a wide range of materials including highly refractory metals with very low vapour pressure. The method includes the transfer of atoms from a heated source (either solid or liquid) to a substrate for the growth of film. The source is heated directly or indirectly up to the point where it gets sublimed or evaporated.

On heating the source, when the temperature reaches the evaporation temperature, atoms or molecules gets ejected from the surface of source and gets travel in a straight path till they reach the substrate. Since the substrate is at a much lower temperature, the molecules will transfer their energy to the substrate, thereby lowering their temperature². The thickness of deposited film depends on the rate of evaporation, time of evaporation and the geometry of source and the substrate. The deposition rate depends on the evaporation rate and also on the angle and distance between the source and the substrate.

2.2.2 Sputter deposition

Sputtering deals with the ejection of atoms or molecules from a target bombarded by energetic ions^{3,4,5,6,7,8}. The main steps in this process are the generation of a beam of inert gas ions, accelerating the beam to few kV energies and directing the beam to a target composing the material to be deposited with the transfer of momentum from the incident beam to the substrate. Sputtering offers several advantages for the controlled deposition of films. The main advantages are

- i. Any thermally stable conducting material including alloys or compounds can be sputtered with one component having a much larger vapour pressure than the other.

- ii. Since the target temperature is slightly increased by the impact of incident ion beam, the power radiated to the substrate will be much less than that from a hot evaporating source.
- iii. The arriving atoms or molecules have larger kinetic energies than evaporated atoms and this improves step coverage by enhancing surface migration.
- iv. For refractory metals or oxides which have low evaporation rates, sputtering can produce more useful deposition rates.
- v. Sputtered films will have finer grain size than evaporated films.
- vi. Since ion bombardment of the substrate occur before deposition, it is possible to enhance adhesion of the film by removing surface impurities and also by increasing surface topography.

There are different types of magnetron sputtering depending on application. Planar magnetron sputtering is the most common one due to greater ion density and fast sputtering rate. Reactive-ion sputtering is normally used to deposit oxides, carbides, nitrides etc for the deposition of insulator films^{9,10}.

2.2.3 Ion beam deposition

In this method, material for deposition is ionized, focussed in to a fine beam and directed electrostatically to a desired location. By this method, it is possible to deposit small amounts of film material at precise locations.

The main advantage of this technique is that by increasing the ion beam energy, it is possible to change the operational mode from deposition to ion beam etching. Focussed ion beams obtained from sharpened tips by using field-enhanced ionization offers localized etching and deposition with high-brightness point source of ions.

2.3 Chemical deposition

Chemical deposition method involves chemical reaction between a compound vapour containing the element comprising the film and the substrate. In most cases, substrate acts as a catalyst to mediate energy involved in the reaction between two vapour species. The energy required for initiating the reaction is supplied either thermally or by an electron or photon beam incident on substrate¹¹.

2.3.1 Chemical vapour deposition (CVD)

Chemical vapour deposition (CVD) includes the deposition of thin film materials from vapour phase by means of a chemical reaction. The deposition conditions can be UHV-CVD (Ultrahigh vacuum CVD), low pressure CVD, atmospheric pressure CVD and sub atmospheric pressure CVD. Thermal controlling of chemical reactions is achieved by the application of heat or plasma.

CVD offers many advantages such as ability to deposit films in a broad range of deposition rates, flexibility to utilize a range of pressure conditions, uniform deposition and ability to control thin film properties. The main requisite for CVD is that the vapour pressure of the precursor should be sufficient allowing transportation to growth surface with no association or reaction in the gas phase and the material should undergo facile decomposition to the product at appropriate temperature¹². Prominent factors influencing the processing conditions and deposition techniques are the chemistry and conditions selected for deposition and the nature and quality of the required film.

At low temperature, the most appropriate method for film deposition is Plasma-enhanced chemical vapour deposition (PECVD) which uses plasma to couple electrical energy in to the gas thereby generating ions, radicals, excited

state neutrals and electrons. PECVD is specifically used for the deposition of insulating films on integrated circuits. Also it is able to achieve uniform film thickness by PECVD despite of electrical non-uniformities¹³.

2.3.2 Atomic layer deposition (ALD)

ALD is a deposition technique which involves the sequential use of a gas phase chemical process. ALD is a subclass of CVD. Here the precursors are inserted as a series of sequential, non-overlapping pulses. The precursor molecules will react with the surface in a self-limiting way, and will get terminated when all the reactive sites on the surface are consumed. By means of this technique, it is possible to control both the composition and thickness of the film even at atomic level¹⁴.

2.3.3 Metallo-Organic Decomposition (MOD)

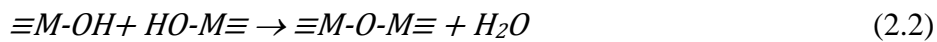
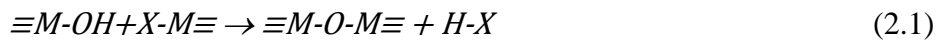
MOD is the simplest technique available for preparing pure stoichiometric thin films. It involves a non-gelling chemistry process with the molecular homogeneity attained in the liquid phase^{15,16}. The MOD is a technique for producing inorganic films by dissolving metal organic compounds of required elements in appropriate solvents. This method offers several advantages such as yielding the equilibrium phases of the desired system at low temperatures which overcomes the problem of selective volatility of various species and also allows precise control of grain size by annealing after the preparation of films. These advantages are obtained since the mixing of ingredients occurs in a molecular level. The ultimate mixing and high reactivity also helps to get very dense films. In addition to this, high purity and cost effectiveness are also attractions of MOD method.

The main intrinsic limitation of MOD processing is the large volume change in going from deposited wet film to fired inorganic film, which causes

decrease in fired film thickness. This limitation can be overcome by the process of multilayer deposition. MOD method is typical since it can control the composition of multi component systems. Most frequently reported solvents for MOD processing are 2-ethyl hexanoic acid and neodecanoic acid.

2.3.4 Sol-gel

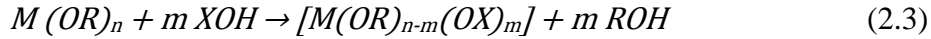
Sol-gel process includes the synthesis of amorphous inorganic network by means of a chemical reaction at low temperature. Precursors that can form inorganic monomers or oligomers or peptised finely divided silica particles can be used for sol-gel technique¹⁷. Since the solution has to be kept stabilized for a long time, analysis of sol-gel chemistry is very important. Alkoxides are mainly used as precursors for sol-gel preparation since they are soluble in common solvents and also due to the possibility of controlling hydrolysis and condensation by chemical methods¹⁸.



Equations (2.1) and (2.2) are the most important condensation reactions of combination of two M-OH groups or the fraction of M-X with an M-OH group, X may be halogen, OR, NR₂, acylate etc. The reactivity of metal alkoxides towards hydrolysis, condensation and complexation is strongly influenced by the electronegativity of metal atom, its coordination number and the steric hinderance exhibited by alkoxide groups. When electronegativity of the metal atom decreases, the size increase and the chemical reactivity of the corresponding alkoxide increase on going down the periodic table. Since transition metal alkoxides are highly reactive, they can be stabilized by complexation thereby avoiding fast condensation. The precursors used for sol-

gel preparation should be soluble in the reaction medium and they have to be reactive enough to participate in gel formation process.

Most sol-gel reactions are nucleophilic substitutions represented as,

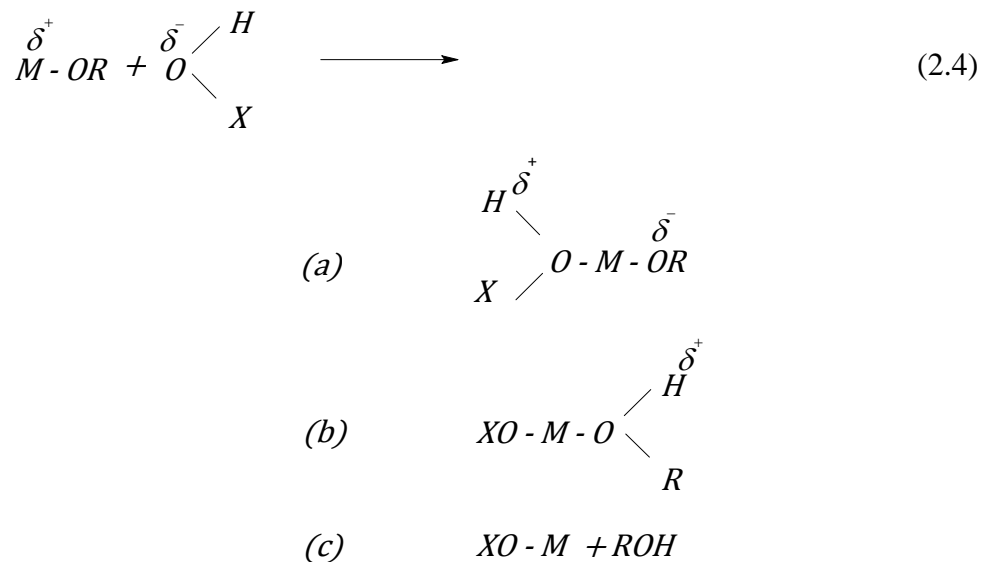


Where X represents H ie, hydrolysis

M represents condensation and

L represents complexation with organic or inorganic ligands.

The above reactions can be described according to SN² mechanism,



Here 2.4(a) represent the product formed by the nucleophilic addition of $OH^{\delta-}$ group on $M^{\delta+}$ (metal atom) which causes an increase in the coordination number of metal atom in transition state^{19,20}. Product (b) represent the transfer of a positively charged proton towards negatively charged OR group within the transition state and product (c) illustrate the departure of positively charged protonated alkoxide ligand ROH.

Hydrolysis process is the most crucial step influencing the sol and gel properties. The important thermodynamic parameters affecting the hydrolysis process are solvent, temperature, complex ligands or pH values and the order of compound addition. The condensation step is the most important step with respect to the structure and processing properties of the synthesised material. It is also a nucleophilic substitution reaction. Condensation is inseparable from hydrolysis and the consumption rate of reactive monomers by condensation can influence the production rate by equilibrium¹⁷.

The metal alkoxides are generally very reactive and their coordination expansion plays a vital role in preventing hydrolysis reaction. Use of complexing ligands can effectively change the behaviour of metal alkoxides towards hydrolysis and condensation. Less electronegative alkoxide ligands are hydrolysed preferentially whereas strongly bonded complexing groups are difficult to remove. Coordination expansion is the tendency of positively charged metal atoms to increase their coordination number by using their vacant orbitals to accept electrons from nucleophilic ligands. Coordination expansion can occur either by alkoxide bridging or by solvation. Hence the choice of solvent is also very important. When alkoxides are dissolved in the parent alcohol, coordination expansion by solvate formation occurs and the stability of such solvates increases with size and electropositive character of the metal. Also intramolecular hydrogen bonding between alcohol and alkoxide ligand are witnessed in solvated alkoxides²¹. By choosing appropriate solvents, molecular complexity of metal alkoxides can also be controlled²².

2.4 Selection of chelating agents for thin film precursor solution preparation

Since metal alkoxides are reactive towards hydrolysis and condensation, in order to avoid fast precipitation, complexing reagents that can react with metal

alkoxides at the molecular level should be used for getting molecular species with different structure, reactivity and functionality²³. $Ti(OPr^i)_4$ is coordinatively unsaturated as illustrated in Figure 2.1, hence it is more reactive towards hydrolysis. But by using chelating agents such as diethanolamine, acetylacetonone etc the coordination number of Ti can be increased from 4 to 6 as depicted in Figure 2.2. Hence by making Ti coordinatively saturated, hydrolysis rate can be considerably decreased thereby avoiding precipitation and allowing the formation of homogeneous sols and gels.

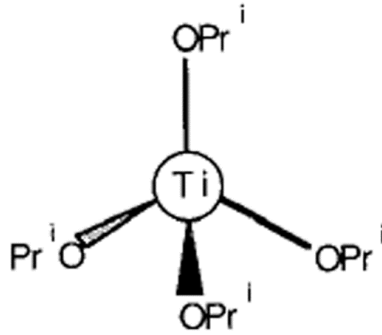
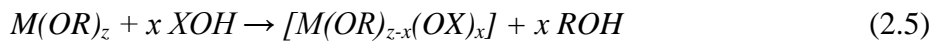


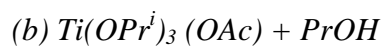
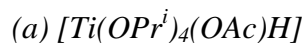
Figure 2.1: Molecular structure of tetraivalent metal alkoxide.

[Source: J. Livage and C. Sanchez, "Sol-gel Chemistry," *J. Non-Cryst. Solids.*, 145(1992) 11].

Usually hydroxylated nucleophilic ligands such as carboxylic acids, β -diketones are used for making chemical modifications as indicated in equation (2.5).



Addition of small amounts of acetic acid prevents precipitation since acetate group OAc^- behaves as nucleophilic complexing agent while reacting with titanium alkoxides²⁴.



The transition state formed during the reaction between titanium alkoxide and acetic acid is given in equation 2.6(a). Since AcOH is negatively charged ($\delta_{AcOH} = -0.7$) and PrOH is positively charged ($\delta_{PrOH} = +0.1$), PrOH group will be better leaved giving rise to products indicated in equation 2.6(b). Here acetate group behaves as bidentate ligand and the coordination number of Ti increases from 4 to 6 forming $[Ti(OPr^i)_3(OAc)]_n$ where $n = 2$ or 3. The Molecular structure of $Ti(OPr^i)_3(OAc)$ is given in Figure 2.2.

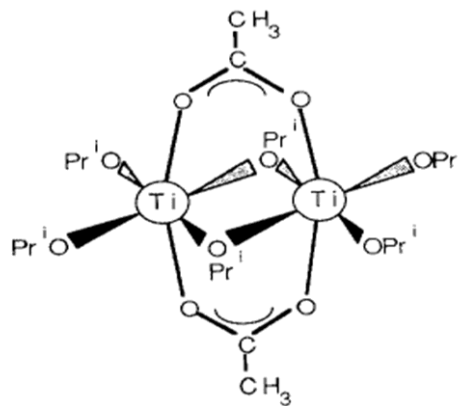


Figure 2.2: Molecular structure of $Ti(OPr^i)_3(OAc)$.

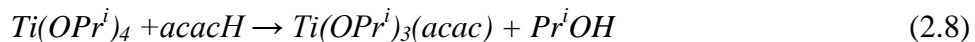
[Source: J. Livage and C. Sanchez, "Sol-gel Chemistry," *J. Non-Cryst.Solids.*, 145 (1992) 1].

Less negative alkoxide ligands are preferentially hydrolysed and more strongly bonded complexing groups are difficult to remove.

Upon hydrolysis, $Ti(OPr^i)_3(OAc) + H_2O \rightarrow Ti(OH)(OPr)_2(OAc) + PrOH$ (2.7)

Here $\delta_{PrOH} = +0.3$ and $\delta_{AcOH} = -0.6$. Hence PrOH is better leaved and complexing ligands act as termination reagents for condensation and precipitation.

Similarly by using acetyl acetone as the chelating agent, the following reaction occurs,



Oligomers are not readily formed and for a stoichiometric ratio $acac/Ti = 1$, monomer with five fold co-ordinated Ti is formed by nucleophilic substitution as given in Figure 2.3²⁵.

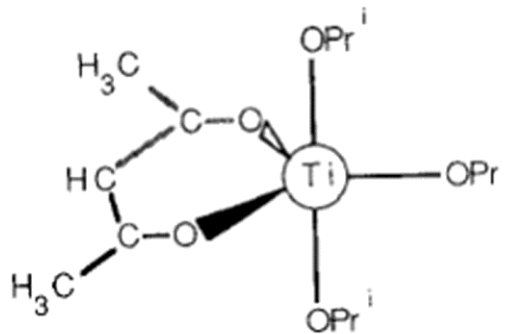


Figure 2.3: Molecular structure of $Ti(OPr^i)_3(acac)$.

[Source: J. Livage and C. Sanchez, "Sol-gel Chemistry," *J. Non-Cryst. Solids*, 145 (1992) 11].

With acetyl acetone, titanium alkoxide form several molecular compounds. An excess of acetyl acetone or upon hydrolysis of $Ti(acac)_2(OR)_2$, $TiO(acac)_2$ is formed²⁶. Large molecular species are generally obtained with smaller amounts of acetyl acetone. But addition of more than one mole of $AcOH$ to one mole of titanium alkoxide brings about esterification. Acetic acid in excess will react with alcohol molecules released during complexation leading to the generation of water giving clear transparent gels. Water produced by esterification reaction with excess acid leads to slow hydrolysis of alkoxide groups which are then replaced by oxo bridges. As a result, complexation provides chemical control of hydrolysis and condensation process by modifying structure, reactivity and functionality of molecular species.

The main advantages of sol-gel method are listed below,

- i. Provides the easiest way to purify precursors to achieve homogeneous precursors.
- ii. Makes use of chemistry to control reactions with the formation of a "pre" inorganic network in solution and hence the densification of inorganic solids.
- iii. Provides the way to adjust the viscosities for coating.

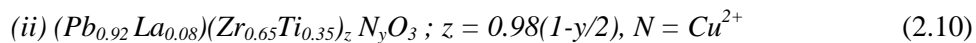
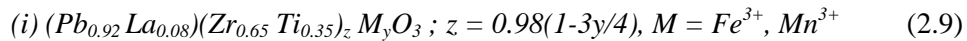
2.5 Preparation of precursor solutions

2.5.1 PLZT precursor [(Pb_{1-x}La_x)(Zr_{0.65}Ti_{0.35})_{1-x/4}O₃]

For PLZT solution preparation, we adopted sol-gel method²⁷. The reactants, lead acetate (99%, Merck, India), lanthanum acetyl acetonate hydrate (Sigma Aldrich, India) and zirconium acetyl acetonate (98%, Merck, India) were refluxed in ethanol at 50°C for 1 hr. 10% excess lead was used to compensate lead loss during annealing. A clear solution was obtained which was then mixed with titanium (IV) isopropoxide (97%, Sigma Aldrich, India) in isopropyl alcohol containing equimolar amounts of diethanolamine (98%, Merck, India) as the chelating agent. The resulting PLZT solution was then stirred well to obtain homogeneous and transparent precursor for spin coating.

2.5.2 Acceptor doped PLZT precursor

We used acceptor dopants Fe³⁺, Mn³⁺ and Cu²⁺ in stoichiometric amounts as per the formula depicted below,



The reactants, lead acetate (99%, Merck, India), lanthanum acetyl acetonate hydrate (Sigma Aldrich, India), zirconium acetyl acetonate (98%, Merck, India) were refluxed with different acceptor dopants such as Iron (III) acetyl acetonate (tech.-grade, Sigma Aldrich, Germany), Manganese (III) acetyl acetonate (tech.-grade, Sigma Aldrich, Germany) and Copper (II) acetyl acetonate (tech.-grade, Sigma Aldrich, Germany). The three clear solutions thus obtained were mixed individually with solution of titanium (IV) isopropoxide (97%, Sigma Aldrich, India) in isopropyl alcohol with equimolar amounts of acetyl acetone ($\geq 98\%$, Merck, India) as the chelating agent, thereby producing stable precursors.

2.5.3 (1-x)PIN- xPT precursor solution

A hybrid Metallo-Organic Decomposition (MOD)²⁸ and Sol-gel process²⁹ were adopted to prepare highly stable (1-x)PIN-xPT solution. The reactants, lead acetate (99%, Merck, India) and Indium acetyl acetonate were refluxed in 2-ethyl hexanoic acid (99%, Sigma Aldrich, India). Excess 2-ethyl hexanoic acid was removed by distillation and the resulting residue was dissolved in Isopropyl alcohol containing titanium (IV) isopropoxide (97%, Sigma Aldrich, India) and niobium (V) ethoxide (99.999%, Alfa Aesar, India) with acetyl acetone ($\geq 98\%$, Merck, India) as the chelating agent to yield a highly stable precursor solution.

2.5.4 Tin doped lead lanthanum zirconate titanate (PLSnZT) solution

The reactants lead acetate (99%, Merck, India), lanthanum acetyl acetonate (Sigma Aldrich, India) and zirconium acetyl acetonate (98% ,Merck, India) were refluxed in ethanol for 1 hr. Tin (IV) isopropoxide (98%, Merck, India) was then dissolved separately in an equimolar mixture of acetic acid and ethanol. This mixture was then treated with titanium (IV) isopropoxide (97%, Sigma Aldrich, India) in isopropyl alcohol with equimolar amounts of acetyl acetone ($\geq 98\%$, Merck, India) as the chelating agent. The resulting mixture was then added to the previously made residue obtained after refluxing for 1hr to get a highly stable precursor solution.

2.6 Processing equipments

2.6.1 Substrates for thin film deposition

In our work, platinised silicon was used as the substrate for thin film deposition. Platinum is preferred since it exhibits lattice mismatch of $\sim 3\%$ with PZT. Since Platinum is inert, it never forms a stable oxide and also offers

a lower leakage current. Usually Ti is used as the adhesion layer and it forms Pt/Ti/SiO₂/Si configuration with Platinum. The adhesion layer plays a prominent role in determining the orientation, microstructure and ferroelectric properties of PZT films.

2.6.2 Spin coating

Spin coating is a technique used to produce uniform thin films of a few nanometer or micron thickness on flat substrates. Spin coater model KW-4A, Chemat technologies, USA given in Figure 2.4 was used for our work. A small amount of the precursor solution is introduced at the centre of the substrate which is either spinning at a low speed or not spinning at all. The substrate is then rotated at high speed for spreading the precursor on it by centrifugal force. Spin coater has a dual speed controller with an initial low speed for preset time of 6 seconds and then automatically switches to high speed for a preset time of 20 seconds. The speed is adjusted at the rate of 4000 rpm for getting a homogeneous thin film layer. The substrate can be fixed on the spinner by means of vacuum suction applied with the help of a rotary pump.



Figure 2.4: Spin coater

2.6.3 Tubular furnace

A tubular furnace is a heating electrical device for conducting synthesis and purification of inorganic and rarely organic compounds. It consists of a cylindrical cavity surrounded by heating coils embedded in thermally insulating matrix and is used to improve the crystalline quality of the prepared thin films. The furnace can maintain temperature accurately and with stability. Temperature inside the furnace can be controlled from the thermocouple feedback. The tubular furnace used in our laboratory is manufactured by Indfur, Chennai, India and the cylindrical cavity has a diameter of 100 mm which in turn is surrounded by heating elements. The furnace can be operated at 1000⁰C and in our study it was set at 650⁰C.

2.6.4 High vacuum coating unit

High vacuum coating unit is employed to deposit gold top electrodes on to thin films for doing electrical measurements and is given in Figure 2.5. A shadow mask is placed on the required area of the thin film and is then placed in the coating chamber. Usually a 1 cm length and 1mm diameter gold rod is inserted into the tungsten filament and evaporated under a vacuum of 10⁻⁶ mbar. The vacuum is achieved in the bell jar with a rotary pump and diffusion pump. The substrate can be cleaned by the collision of energetic ions generated during high tension (HT) voltage environment. Under the vacuum environment, a blue colour is observed. The tungsten filament is then heated under vacuum environment by using a low tension (LT) voltage mode. Golden yellow colour is observed within the chamber due to the evaporation of gold rod which is then deposited on the exposed area of the thin film. The model of the coating unit used for deposition is 124AD, Hind High Vacuum, India.



Figure 2.5: High vacuum coating unit.

2.7 Thin film growth process

Thin films prepared by any deposition technique starts with nucleation process followed by growth step. These processes mainly depend upon the chemistry of the material and substrate, growth temperature, growth rate etc.

A model was proposed by Schuler and Aegerter³⁰ for the growth of crystallites in sol gel multilayer coatings. Single layers are made by agglomeration of spherical particles having a high void fraction. A schematic representation of crystal growth in single and multilayer sil gel PZT coatings is given in Figure 2.6. When the thickness of individual layers is small (smaller or equal to 20 nm), formation of heterogeneously nucleated crystals is enhanced at the interface of the last sintered layer and gel film that inturn results in a columnar growth. Such a columnar growth increases the crystallite size perpendicular to the surface resulting in increased density of the film^{30,31}.

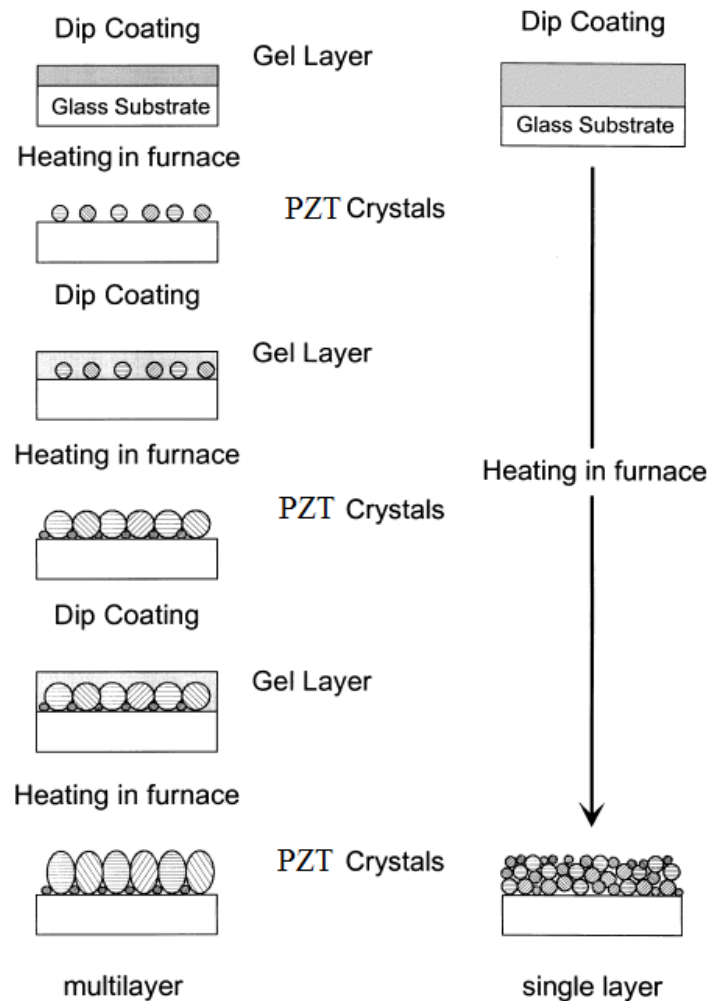


Figure 2.6: Scheme of the crystal growth observed in single and multilayer sol gel PZT coatings. Thick gel films lead to spherical crystallites randomly oriented whereas thin gel films lead to a columnar growth.

[Source: T. Schuler and M. A. Aegerter, "Optical, electrical and structural properties of sol gel ZnO:Al coatings," *Thin Solid Films*; 351 (1999) 125].

2.8 Characterization techniques

2.8.1 X-ray diffraction (XRD)

X-ray diffraction technique is the most powerful non destructive technique used for the analysis of crystallinity, phase purity, preferential

orientation, phase composition, lattice defects etc with in a solid material. When X-rays are incident on a sample, the electrons present in the sample will diffract X-rays. If atoms within the material are arranged in a regular crystalline structure, the scattering results in maxima and minima in the diffracted intensity as given in Figure 2.7. X-ray diffraction is based on the constructive interference of monochromatic X-rays with a crystalline sample. ie, when there is constructive interference from X-rays that is scattered by the atomic planes in a crystal, diffraction peak is observed. The interpretation of XRD is done using Bragg's law, $n\lambda = 2d \sin\theta$. Here λ is the wavelength of X-rays, n is an integer known as the order of reflection. Thus by knowing the angle of diffraction (2θ), we can calculate the distance between two planes. For thin films, the most beneficial use of XRD is the analysis of preferential crystallographic orientation.

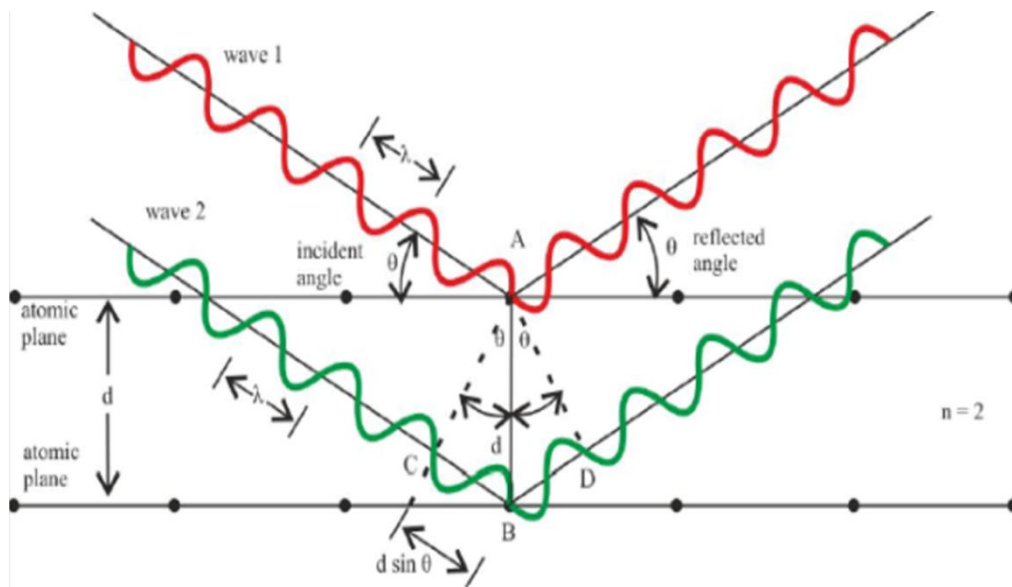


Figure 2.7: Schematic stretching of Bragg's law derived from triangle ABC.

[Source: N. Waesemann, Hamburg: "Structural transformations in complex perovskite-type relaxor and relaxor-based ferroelectrics at high pressures and temperatures- Dissertation" (2012)].



Figure 2.8: X-ray diffractometer.

The diffraction patterns of the sample were obtained from an XRD machine Model D-5005, Bruker, Germany given in Figure 2.8 with Ni filtered $\text{CuK}\alpha$ radiation having λ value 1.54 \AA . The intensity of the X-ray beam is plotted against 2θ values and the scan rate was between $20^\circ - 60^\circ$. Formation of crystalline phase is confirmed by comparing the measured intensity with that of International Crystallographic Diffraction data.

2.8.2 Spectroscopic reflectometer

Spectroscopic reflectometer (Figure 2.9) is used to measure the thickness of thin film samples when the film surface is highly reflected or when transparency is a problem. An interference pattern is observed due to the interaction of the reflected beam of light from top and bottom surfaces of the film. The interference pattern thus obtained is interpreted to determine the thickness of the film. TF Probe 2.2 is the software used to operate the system.



Figure 2.9: Spectroscopic reflectometer

Light source used is a medium power deuterium and halogen lamps that can be operated in the UV and Visible-IR regions respectively. A highly polished silicon wafer (100% reflection) is used as the reflecting surface whose data is stored in the computer. The thin film having reflection from the top and bottom surface is placed in front of the Xenon lamp light source. Path difference between the reflected rays from top and bottom of the film interfere to form interference pattern. A red coloured interference pattern is obtained for theoretically fitted one for a probable thickness and a blue coloured one for the actual interference pattern of the film from the reflected data. When theoretically fitted and actual fringes are matched, it will be the thickness of the sample.

2.8.3 Raman spectroscopy

Raman spectroscopic technique named in honour of Sir C.V Raman is used to study the rotational, vibrational and other lower frequency modes in condensed matter physics and chemistry. The Raman effect occur when electromagnetic radiation impinges upon a molecule and interacts with the electron density and the bonds of the molecule. The incident photon excites the molecule to a virtual energy state for a short period before an inelastically scattered photon results. The inelastically scattered photon which is emitted or

scattered will be either lower energy or higher energy than the incident photon resulting in Stokes or anti-Stokes line respectively (Figure 2.10). Hence the resulting rotational and vibrational state of the molecule after interacting with the electromagnetic radiation will be different from the previous one. The energy difference between the original rovibronic state and the resulting rovibronic state leads to a shift in the emitted photon's frequency away from the excitation wavelength resulting in the formation of Rayleigh line.

Raman spectroscopy reveals information regarding local lattice structures and phase transitions in ferroelectric materials. Each Raman mode will have a Raman tensor depending on the Raman selection rules. The intensities and shapes of modes in Raman spectra depend on crystal orientation. Also phase transitions can be witnessed from new Raman scattering peaks and from the splitting of existing peaks. Phonon modes represent the quanta of vibrational energy within a crystal. The atoms in acoustic phonon modes vibrate in-plane while those in optical phonon mode vibrates out-of-phase.

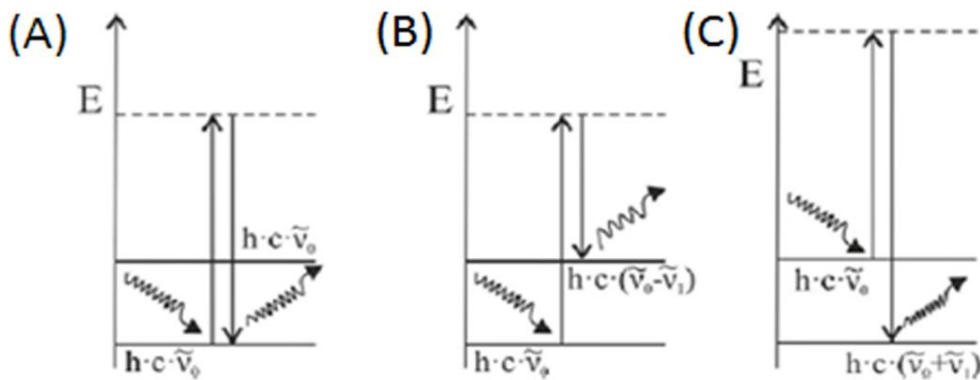


Figure 2.10: (A) Inelastic Rayleigh scattering, (B) Elastic Stokes lines and (C) Elastic anti Stokes lines in Raman spectra.

[Source: L. Nasdala, D. C. Smith, R. Kaindl, M. A. Ziemann, "Spectroscopic methods in Mineralogy," *EMU Notes in Mineralogy, Chapter Raman spectroscopy: Analytical perspectives in mineralogical research, European Mineralogical Union, 6 (2004)281*].



Figure 2.11: Raman spectrometer.

The optical and acoustic phonon modes are further differentiated into longitudinal and transverse modes. Longitudinal modes show atomic displacements where the polarization of elastic wave is parallel to the wave propagation while transverse mode shows perpendicular displacement with respect to wave propagation. Raman spectra were taken and recorded using a Raman spectrometer Model: DXR, Thermo scientific, USA shown in Figure 2.11.

2.8.4 Scanning electron microscope

Scanning electron microscopy makes visual inspection of the surface of a material by means of secondary and backscattered electrons. In addition to providing better resolution, information regarding characteristics at and near the surface of a specimen can be provided by variety of signals produced as a result of nature of electron beam specimen interactions. Secondary electrons with energies generally less than 50eV are produced as a result of inelastic collision and due to scattering of incident electrons with specimen electrons. Fabrication of highly dense ferroelectric materials is necessary for the excellent performance

of that material. They can provide details regarding the surface structure of a material with a resolution of 10 nm or even better³². Backscattered electrons are produced as a result of elastic collision and due to the scattering between incident electrons with specimen electrons/nuclei. They can resolve topographical contrast and atomic number contrast with a resolution of more than 1 micron. Eventhough many types of signals are generated by a specimen on application of electron beam, X-ray signal which is produced by recombination interaction between free electrons and positive electron holes generated within the material are typically used for SEM. These signals were originated from deeper portions of the specimen surface and provide elemental analysis through energy dispersive X-ray spectroscopy or EDS analysis.

Proper choice of accelerating voltage is crucial for obtaining a good clear image and it mainly depends on the type of material being examined. High voltage of about 15-30KV are generally used for high resolution at high magnification. But this can cause damage to the specimen easily if the material is not highly conductive. In addition to this, right choice of working distance and spot size are critical parameters influencing image quality. Generally, a working distance of 10 mm will give a good depth of field thereby maintaining good resolution. At lower accelerating voltage; working distance is reduced for achieving better resolution. Typically smaller spot sizes allows higher resolution and hence a greater depth of field.

Image disturbances that occur while imaging can badly affect the image quality. This may be due to defects within the instrument, improper sample preparation, instrument vibration or operator's lack of experience. These can be corrected by a systematic approach based on their appearance. Micro structural analysis of thin films was carried out using a High Resolution Scanning Electron Microscope (HRSEM, Model: Genesis Apex 2, Ametek, Japan).

2.8.5 UV-Visible spectrophotometry

UV-Visible spectrophotometer measures the amount of ultraviolet or visible radiation absorbed or transmitted by photons within the material. Spectrophotometric methods are relatively simple, rapid and applicable to small quantities of material. The fundamental law governing the quantitative spectrophotometric analysis is Beer-Lamberts law. This law states linear relationship between absorbance and concentration of an absorbing species and is usually written as, $A = a(\lambda)bc$, where A is the measured absorbance, $a(\lambda)$ is the wavelength-dependent absorptivity coefficient, b is the path length, and c is the analyte concentration. Working in concentration units of molarity, the Beer-Lambert law is written as: $A = \varepsilon bc$, where ε is the wavelength-dependent molar absorptivity coefficient in units of $M^{-1}cm^{-1}$.



Figure 2.12: UV-Visible spectrophotometer.

The UV-Visible spectrophotometer (Figure 2.12) consists of a source, a sample compartment, optics to focus the beam on the sample and detectors. When light from the source falls on the sample, a portion of the incident light is absorbed by the material, another portion is reflected and the remaining

balance will get transmitted. Since a portion of energy of incident photon is absorbed by the electron, it gets excited to a higher energy level. Electronic transitions are of two types: d-d transitions and charge transfer (CT) transitions. d-d transition provides information regarding oxidation state and coordination environment whereas CT spectra which are more intense reveals information regarding the nature of acceptor and donor atoms.

2.8.6 Impedance Analyser

Dielectric permittivity (ϵ), dielectric loss tangent ($\tan \delta$) and dielectric tunability are the important parameters that determine the dielectric properties of a material. Dependence of temperature on dielectric properties can also be measured by attaching a furnace to the impedance analyser. An impedance analyzer Model: 4294A, Agilent, USA is used in our laboratory for dielectric measurements and is depicted in Figure 2.13.

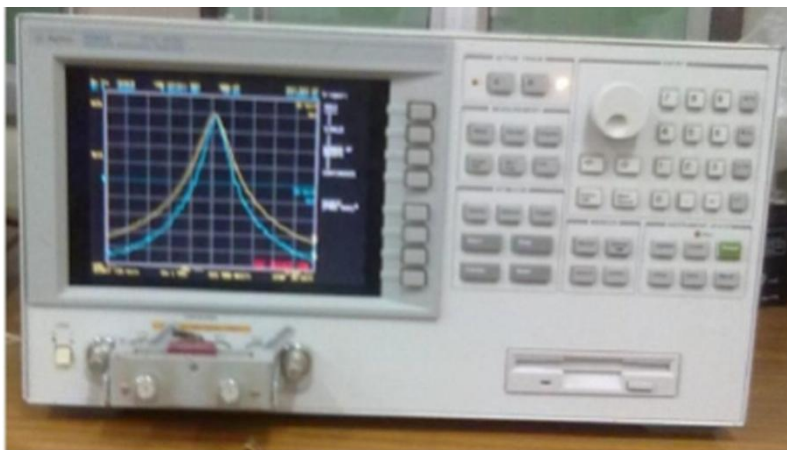


Figure 2.13: Impedance analyser for CV determination Model: 4294A, Agilent, USA.

Parallel plate method is used to measure the dielectric constant of a thin film using an impedance analyser. It consists of a thin sheet of material sandwiched between two metal electrodes thus forming a capacitor. Since we

used platinised silicon substrate, Pt is employed as the bottom electrode. Gold is used as the top electrode. The dielectric measurements were carried out at a frequency of 1 kHz.

$$\text{Dielectric permittivity } K = \frac{Ct}{A\epsilon_0} \quad (2.11)$$

Where C is the capacitance in farads, t is the distance between electrodes in metres, A is the area of the electrode in square metre and ϵ_0 is the permittivity of free space.

The large dielectric response exhibited by ferroelectric thin films is due to the combination of intrinsic and extrinsic factors as a result of domain wall and phase boundary motion. The domain wall motion in perovskites can be induced by the application of electric field, stress or both.

The behavior of dielectric permittivity (ϵ_r) with different characteristic temperatures in normal ferroelectrics, relaxors and canonical relaxors are given in Figure 2.14. Relaxors possess a broad and frequency dispersive dielectric permittivity (ϵ) at T_m that distinguishes relaxors from normal ferroelectrics. Figure 2.14(b) shows relaxors that develop long-range ferroelectric order at T_C and Figure 2.14(c) shows canonical relaxors that does not shows a macroscopic phase transition and remain isotropic. ie, the polar-nano regions (PNRs) or domains freeze at T_f thereby causing a change in translational symmetry. The dielectric permittivity of relaxors is large and the value is found to be changed slowly with temperature³³.

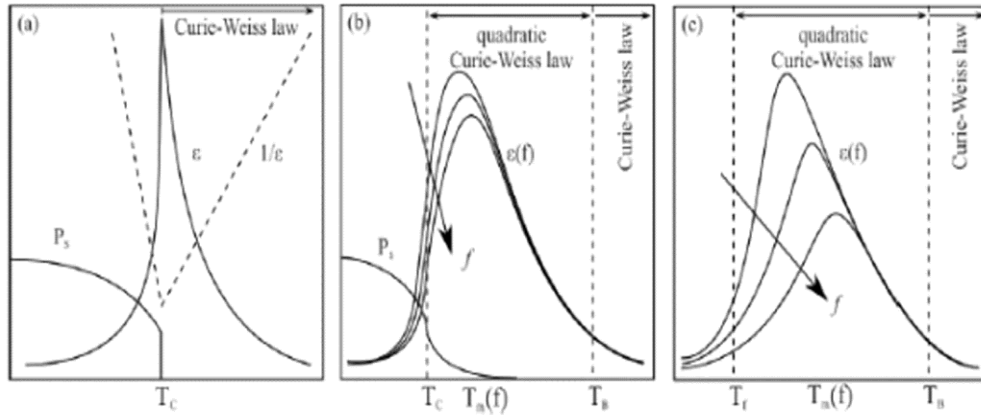


Figure 2.14: Behavior of dielectric permittivity ϵ_r with different characteristic temperatures T_B , T_m , T_C and T_f in (a) normal ferroelectrics, (b) relaxors with a transition to ferroelectric phase and (c) canonical relaxors.

[Source: K. Hirota, S. Wakimoto and D. E. Cox, "Neutron and X-ray scattering study of relaxors," *J. Phys. Soc. Jpn*, 75, (2006) 111006].

$$\text{Dielectric tunability is defined as } \text{tunability} = \left(\frac{\epsilon_{r0} - \epsilon_{rv}}{\epsilon_{r0}} \right) \times 100 \quad (2.12)$$

Where ϵ_{r0} is the dielectric constant at zero applied field,

ϵ_{rv} is the dielectric constant at V applied voltage.

Dielectric loss ($\tan \delta = \frac{\epsilon''}{\epsilon'}$) is defined as the ratio of imaginary part to real part of complex permittivity at a given frequency.

2.9 Measurement of leakage current

In pure PZT, the leakage current is due to the conductivity of holes as per equation 2.13

$$V_{pb} \rightarrow V_{pb}'' + 2h' \quad (2.13)$$

This case is depicted in Figure 2.15 (a).

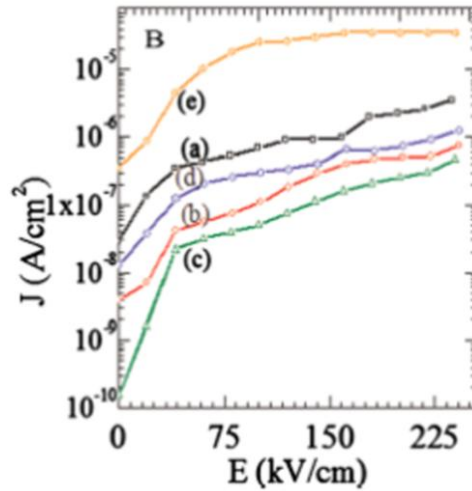


Figure 2.15: Leakage current plots of $(\text{Pb}_{1-3x/2}\text{La}_x)(\text{Zr}_{0.53}\text{Ti}_{0.47})\text{O}_3$ thin films. Here (a) $x = 0.0$, (b) $x = 0.001$, (c) $x = 0.004$, (d) $x = 0.008$ and (e) $x = 0.010$.

[Source: D. Ambika, V. Kumar, C. S. Suchand Sandeep, R. Philip, "Tunability of third order nonlinear absorption in (Pb, La)(Zr, Ti) O_3 thin films," *Appl. Phys. Lett.* 98 (2011), 011903].

Upon adding lanthanum in concentrations of $0 < x \leq 0.004$, the resistivity increases as illustrated in Figure 2.15 (b) and (c). This occurs due to electron-hole compensation mechanism as given in equation 2.14.



For $x = 0.004$, the lowest leakage current density was observed as a result of the low concentration of defect states. On further increasing La^{3+} concentration, the leakage current was found to be increased as there is increase in $[\text{V}_{\text{Pb}}'']$ defect state as shown in Figure 2.15 (d) and (e)²⁹.

2.10 Measurement of ferroelectric properties

The main consequence of domain wall switching in ferroelectric materials is the formation of ferroelectric hysteresis loop. Ferroelectric materials are characterised by measuring their polarization as a function of

applied electric field. Thus Polarization vs Electric field hysteresis loop is a good indicator to measure the degree of ferroelectricity of a material. The shapes of the loop and the values of remanent polarization and coercive field mainly depend on the preparation conditions, mechanical stress, nature of dopants, charged defects and crystallographic orientation. Figure 2.16 shows the set up made for the measurement of ferroelectric hysteresis using TF analyser (Model: aix ACCT 2000, Germany). Usually a sinusoidal voltage is applied on the sample and the corresponding polarization, displacement are recorded. Actually it involves the measurement of displacement field $D(E)$ or charge density. An ideal hysteresis loop will be symmetrical (Figure 2.17) so that the positive and negative remanent polarizations and the positive and negative coercive fields will be equal. The contribution of intrinsic and extrinsic factors towards ferroelectric properties can be distinguished via the study of field amplitude dependence of the response.

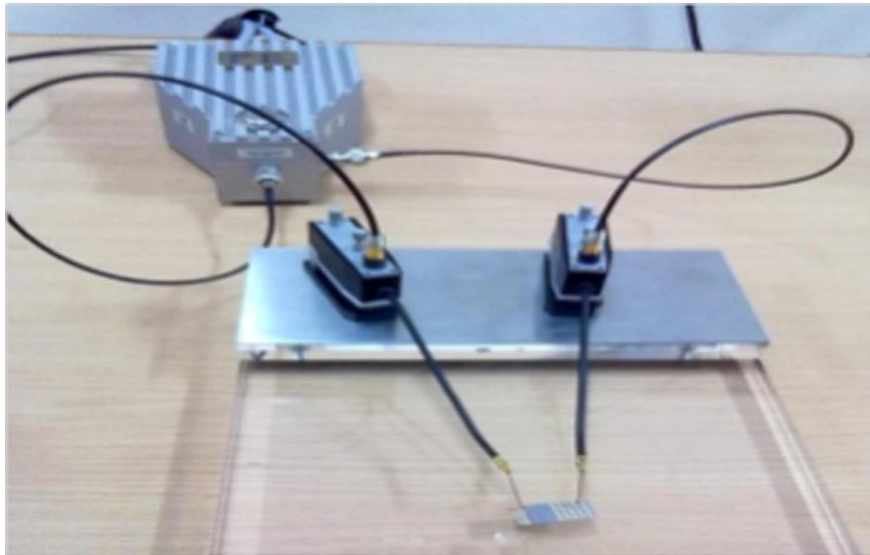


Figure 2.16: Set up for the measurement of P-E hysteresis using TF analyser (Model: aix ACCT 2000, Germany).

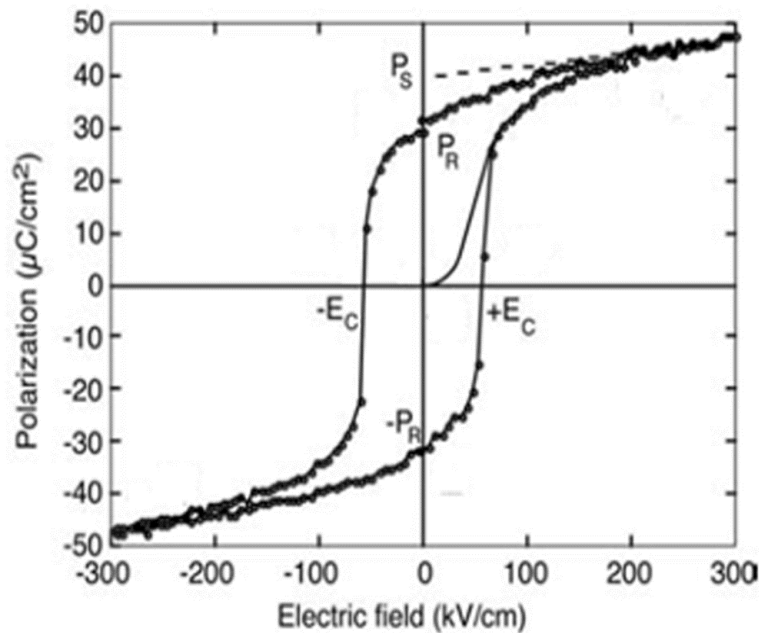


Figure 2.17: Ferroelectric P-E hysteresis loop.

[Source: D. Damjanovic, "Hysteresis in piezoelectric and Ferroelectric materials," *The science of Hysteresis*, vol.3, I. Mayergoz and G. Bertotti (Eds): Elsevier (2005)]

Normal ferroelectrics usually exhibits large remanent polarization (P_r) and coercive field (E_c), antiferroelectrics possess low P_r and E_c with wide hysteresis loop leading to large energy loss. Relaxor ferroelectrics on the other hand exhibits slim hysteresis loop with low P_r and E_c allowing high energy storage density^{34,35,36}.

For preferentially oriented thin films, the 'Optimum orientation' provides the crystallographic direction not only for poling but also for actuators to obtain low hysteresis and high strain as possible as illustrated in Figure 2.18. Eventhough $\langle 100 \rangle$ orientation is superior to $\langle 111 \rangle$, multidomain rhombohedral crystals will also allow other crystallographic directions as optimum for achieving higher strain and lower hysteresis³⁷.

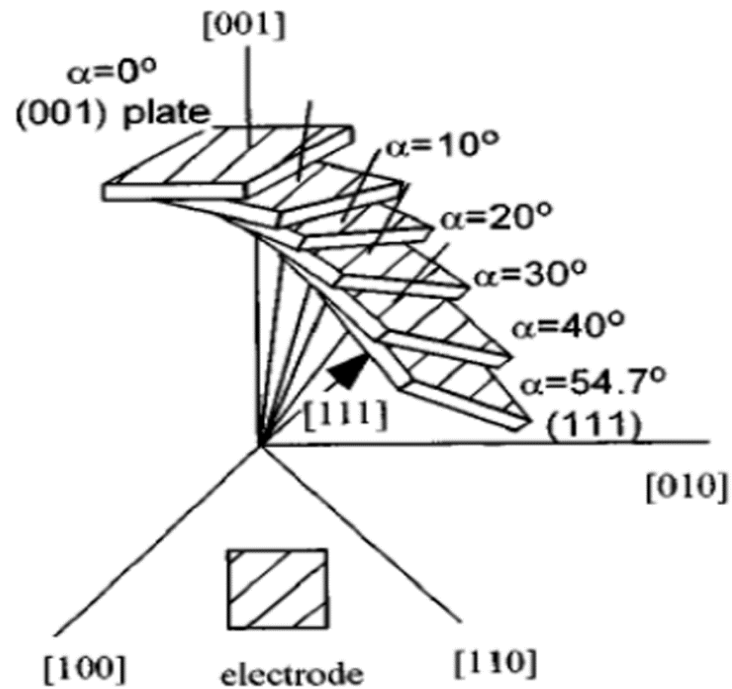


Figure 2.18: Schematic diagram of sample preparation for investigating optimum crystallographic orientation.

[Source: S. E. Park, T. R. Shrout, "Ultrahigh strain and piezoelectric behavior in relaxor based ferroelectric single crystals," *J. Appl. Phys.* 82 (1997) 1804].

At low fields, when $\alpha \neq 0$, the strain values do not vary significantly as a function of α due to strain induced by domain reorientation. There will be increased domain motion with increased α and is depicted in the hysteresis versus α plot given in Figure 2.19. The amount of hysteresis can be converted to the degree of depoling because more depoling causes more domain reorientation resulting in increased hysteresis.

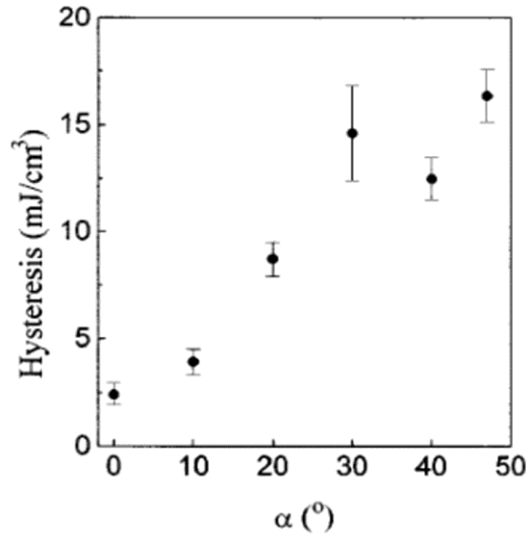


Figure 2.19: Hysteresis is plotted as a function of α , where α is the degree of deviation from $\langle 001 \rangle$ toward $\langle 111 \rangle$.

[Source: S. E. Park, T. R. ShROUT, "Ultrahigh strain and piezoelectric behavior in relaxor based ferroelectric single crystals," *J. Appl. Phys.* 82 (1997) 1804].

2.11 Measurement of piezoelectric properties

The transverse piezoelectric coefficient $|e_{31,f}|$, is defined as the in-plane stress developed in the piezoelectric thin film on applying an external electric field along the film thickness. Based on the theory developed by Smith and Choi³⁸, Kanno *et al*³⁹ gave an expression to $|e_{31,f}|$.

$$|e_{31,f}| = \frac{d_{31}}{s_{11,p}^E + s_{12,p}^E} \cong - \frac{h_s^2}{3s_{11,s}(1-\nu_s)L^2} \frac{\delta}{V} \quad (2.15)$$

where h_{si} is the thickness of the substrate, δ is the tip displacement, V is the applied voltage, L is the length of the cantilever and S_{11}^S is the elastic compliance of the substrate.

Various techniques such as atomic force microscopy, cantilever beam method, normal loading method, laser interferometric technique are available for the measurement of piezoelectric properties. In laser interferometric

technique method, the edge of the beam was clamped using a small vise grip and unimorph cantilevers composing the film and the substrate was made.

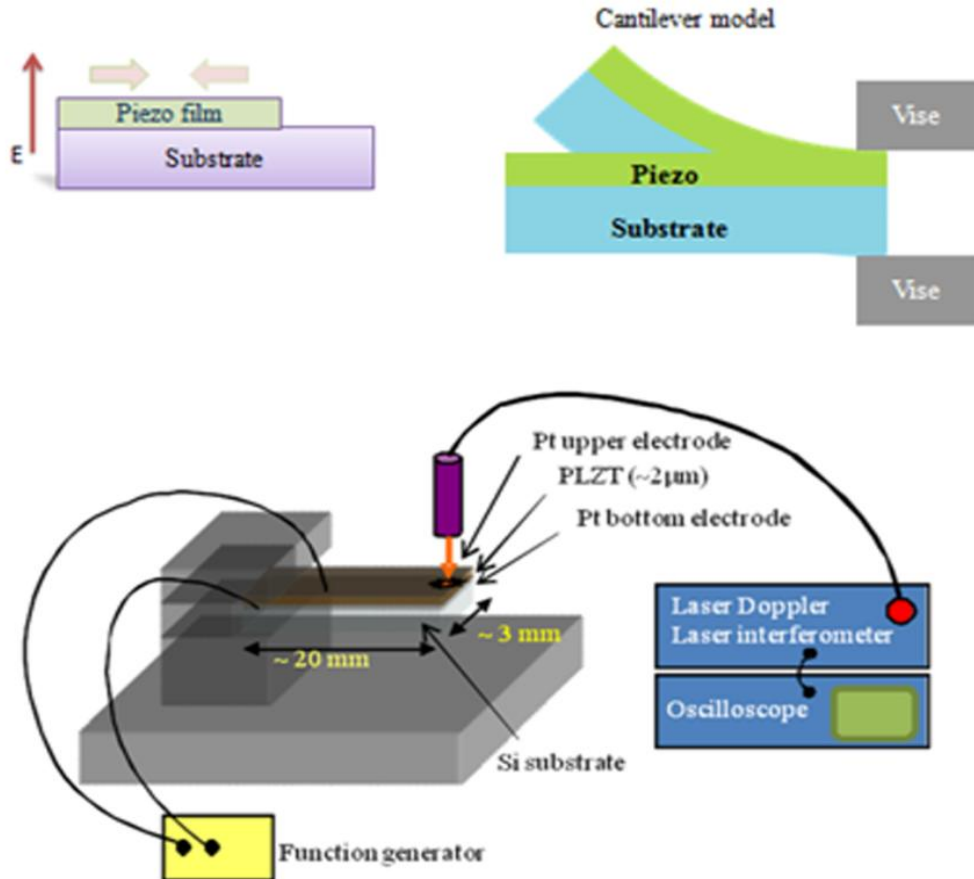


Figure 2.20: Measurement system of the transverse piezoelectric properties of PLZT thin films.

Piezoelectric vibration was generated by applying sine wave voltage between upper and bottom electrodes (Figure 2.20). Tip displacement was measured using a laser Doppler vibrometer (Model: AT-3500, Graphtec, Japan) and a laser interferometer (Model: AT-1100, Graphtec, Japan). Interferometers are configured either as single or as double beam setups. The interference of monochromatic laser light in response to a piezoelectrically induced strain results

in change of the optical path length. This can be achieved by comparing the interference light intensity of a reference laser beam to a laser beam striking surface of the sample before and after the strain developed. This can resolve very small changes in displacement of about 10^{-3} Å.

References

- [1] N. Izyunskaya, Y. -I Alivov, S. -J Cho, H. Morkoe, H. Lee and Y. -S Kang, "Processing, structure, properties and Applications of PZT thin films," *Crit. Rev. Solid State.*, **32** (2007) 111.
- [2] H. N. Naumann, "Studies on vacuum evaporation and distillation," *Biochem J.*, **29** (1935) 994.
- [3] J. L. Vossen and J. J. Cuomo, "Thin Film Processes," J. L. Vossen and W. Kern, eds., Academic Press, New York (1978).
- [4] W. D. Westwood, "Microelectronic Materials and Processes," R. A. Levy, ed., Kluwer Academic, Dordrecht (1989).
- [5] G. K. Wehner, "Controlled sputtering of metals by low-energy Hg ions," *Phys. Rev.*, **102** (1956) 690.
- [6] H. H. Anderson and H. L. Bay, "Sputtering by Particle Ion Bombardment," I. R. Behrisch, ed., Springer-Verlag, Berlin (1981).
- [7] D. B. Fraser, "Thin Film Processes," J. L. Vossen and W. Kern, eds., Academic Press, New York (1978) 115.
- [8] J. A. Thornton and A. S. Penfold, "Thin Film Processes," J. L. Vossen and W. Kern, eds., Academic Press, New York (1978).
- [9] W. Tsai, J. Fair and D. Hodul, "Ti/TiN Reactive Sputtering: Plasma Emission, X-Ray Diffraction and Modeling," *J. Electrochem Soc.*, **139** (1992) 2004.
- [10] J. M. Molarius and M. Orpana, "Issues in Semiconductor Materials and Processing Technologies," S. Coffa, F. Priolo, E. Rimini and J.M. Poate, eds., Kluwer, Dordrecht (1991).
- [11] J. R. Arthur, "Physical and chemical methods for thin-film deposition and epitaxial growth, specimen handling, preparation and treatments in surface characterization," edited by Czanderna et al. Kluwer Academic/plenum publishers, New York (1998) 239.

- [12] J. E. Crowell, "Chemical methods of thin film deposition: chemical vapour deposition, atomic layer deposition, and related technologies," *J. Vac. Sci. Technol., A.*, **21** (2003) S88.
- [13] F. Jansen and S. Krommenhoek, "Thin film deposition on inside surfaces by plasma enhanced chemical vapour deposition," *Thin solid films.*, **252** (1994) 32.
- [14] R. L. Puurunen "Surface chemistry of atomic layer deposition: A case study for the trimethylaluminium water process," *J. Appl. Phys.*, **97** (2005) 9.
- [15] W. Zhu, Z.Q. Liu, M. S. Tse and H. S. Tan, "Raman, FT-IR and dielectric studies of PZT 40/60 films deposited by MOD technology," *J. Mater. Sci.-Mater. Electron.*, **6** (1995) 369.
- [16] R. W. Vest, "Metallo-Organic decomposition (MOD) processing of ferroelectric and electrooptic films: A review," *Ferroelectrics.*, **102** (1990) 53.
- [17] H. Schmidt, "Chemistry of material preparation by the sol-gel process," *J. Non-Cryst. Solids.*, **100** (1988) 51.
- [18] J. Livage and C. Sanchez, "Sol-gel chemistry," *J. Non-Cryst. Solids.*, **145** (1992) 11.
- [19] C. Sanchez, J. Livage, M. Henry and F. Babonneau, "Chemical modification of alkoxide precursors" *J. Non-Cryst. Solids.*, **100** (1988) 65.
- [20] C. J. Brinker, "Hydrolysis and condensation of silicates: effects on structure" *J. Non-Cryst. Solids.*, **100** (1988) 31.
- [21] B. A. Vaartstra, J. C. Huffman, P. S. Gradeff, L. Hubert-Pfalzgraf, J. C. Daran, S. Parraud, K. Yunlu and K.G. Caulton, "Alcohol adducts of alkoxides: intramolecular hydrogen bonding as a general structural feature," *Inorg. chem.*, **29** (1990) 3126.

- [22] C. Sanchez and J. Livage, "Sol-gel chemistry from metal alkoxide precursors" *New J. Chem.*, **14** (1990) 513.
- [23] J. Livage, M. Henry and C. Sanchez, "Sol-gel chemistry of transition metal oxides" *Prog. Solid State Chem.*, **18** (1988) 259.
- [24] J. Livage and M. Henry, "Ultrastructure Processing of Advanced Ceramics," ed. J.D. Mackenzie and L.L. Hench, Wiley, New York, (1988) 183.
- [25] A. Lèaustic, F. Babonneau and J. Livage, "Structural investigation of the hydrolysis-condensation process of titanium alkoxides $Ti(OR)_4$ (OR= OPr-iso, OEt) modified by acetylacetone. 1. Study of the alkoxide modification," *Chem. Mater.*, **1** (1989) 240.
- [26] G. D. Smith, C. N. Caughlan and J. A. Campbell, "Crystal and molecular structures of di- μ -Oxo-bis (diacetylacetonatotitanium (IV))bisdioxane, $(TiO)(C_5H_7O_2)_2)_2 \cdot 2C_4H_8O_2$, di- μ -Oxo-bis (diacetylacetonatotitanium (IV)), $(TiO)(C_5H_7O_2)_2)_2$," *Inorg. Chem.*, **11** (1972) 2989.
- [27] D. Ambika, V. Kumar, C. S. S. Sandeep and R. Philip, "Non-linear optical properties of $(Pb_{1-x}Sr_x)TiO_3$," *Appl. Phys. B.*, **97** (2009) 661.
- [28] V. Kumar, I. Packiaselvam, K. Sivanandan, M. A. Vahab and A. K. Sinha, "Chemical solution deposition of $(Ba_{1-x}Sr_x)TiO_3$," *J. Am. Ceram. Soc.*, **89** (2006) 1136.
- [29] D. Ambika, V. Kumar, C. S. S. Sandeep and R. Philip, "Tunability of third order nonlinear absorption in $(Pb,La)(Zr,Ti)O_3$ thin films," *Appl. Phys. Lett.*, **98** (2011) 011903.
- [30] T. Schuler and M. A. Aegerter, "Optical, electrical and structural properties of sol gel ZnO:Al coatings," *Thin Solid Films.*, **351** (1999) 125.
- [31] Y. Ohya, H. Saili, T. Tanaka and Y. Takahashi, "Microstructure of TiO_2 and ZnO films fabricated by the sol-gel method," *J. Am. Ceram. Soc.*, **79** (1996) 825.

- [32] M. T. Postek, K. S. Howard, A. H. Johnson and K. L. McMichael, "Scanning Electron Microscopy: A Student's Handbook," Ladd Research Ind., Inc. Wiliston, VT., (1980).
- [33] K. Hirota, S. Wakimoto and D. E. Cox, "Neutron and X-ray scattering study of relaxors," *J. Phys. Soc. Jpn.*, **75** (2006) 111006.
- [34] S. Tong, B. Ma, M. Narayanan, S. Liu, R. Koritala, U. Balachandran, and D. Shi, "Lead lanthanum zirconate titanate ceramic thin films for energy storage," *Acs. Appl Mater. Inter.*, **5** (2014) 1474.
- [35] L. E. Cross, "Relaxor ferroelectrics: an over view," *Ferroelectrics.*, **151** (1994) 305.
- [36] N. Ortega, A. Kumar, J. F. Scott, D. B. Chrisey, M. Tomazawa, S. Kumari, D. G. B. Diestra and R. S. Katiyar, "Relaxor-ferroelectric super lattices: high energy density capacitors," *J. Phys-Condens. Mat.*, **24** (2012) 445901.
- [37] S. E. Park and T. R. Shrout, "Ultra high strain and piezoelectric behaviour in relaxor based ferroelectric single crystals", *J. Appl. Phys.*, **82** (1997) 1804.
- [38] J. G. Smits and W. Choi, "The constituent equations of piezoelectric heterogeneous bimorphs," *IEEE Trans. Ultrason. Ferroelectr. Freq. Control.*, **38** (1991) 256.
- [39] I. Kanno, H. Kotera, K. Wasa, "Measurement of transverse piezoelectric properties of thin films," *Sens. Actuators A Phys.*, **107** (2003) 68.

LAXMI PRIYA S. "FERROELECTRIC THIN FILMS FOR MICROACTUATOR APPLICATIONS". THESIS. CENTRE FOR MATERIALS FOR ELECTRONICS TECHNOLOGY (C-MET), UNIVERSITY OF CALICUT, 2018.

Preferentially oriented PLZT thin films suitable for MEMS applications

• Contents •	3.1 Introduction
	3.2 Preferentially {100}-oriented $(\text{Pb}_{1-x}\text{La}_x)(\text{Zr}_{0.65}\text{Ti}_{0.35})_{1-x/4}\text{O}_3$ thin films
	3.3 Transverse piezoelectric properties of {110}-oriented PLZT thin films
	3.4 Conclusion
	References

Some of the contents of this chapter have appeared in the following research publication

- [1] **S. Laxmi Priya**, V. Kumar, Fumiya Kurokawa, Isaku Kanno, “Transverse piezoelectric properties of {100}-oriented PLZT[x/65/35] thin films,” *Materials Chemistry and Physics* 151, (2015) 308-311.
- [2] **S. Laxmi Priya**, V. Kumar, Takuya Teramoto, Isaku Kanno, “Transverse Piezoelectric properties of {110}-oriented PLZT thin films” *Integrated Ferroelectrics* (Under review).

3.1 Introduction

Micro electromechanical systems (MEMS) have been receiving greater attention as an actively researched area since the needs for micro devices are increasing. MEMS using piezoelectric thin films are important for developing micro sensors and actuators¹⁻⁵. For MEMS applications like micro actuators, development of dense, crack-free thin films integrated on silicon substrates is essential. Thin film texture and composition are also significant from the point of device applications. In the case of piezoelectric single crystals, preferential crystallographic orientation significantly enhances their piezoelectric characteristics. In this context, there arises the importance of preferentially orientated thin films that offers the possibility of achieving maximum piezoproperties.

3.2 Preferentially {100}-oriented $(\text{Pb}_{1-x}\text{La}_x)(\text{Zr}_{0.65}\text{Ti}_{0.35})_{1-x/4}\text{O}_3$ thin films

Of the various possible crystallographic orientations, preferentially {100}-oriented thin films having compositions with rhombohedral structure near morphotropic phase boundary (MPB) are of interest for electromechanical applications^{6,7,8}. According to Park and Shrout⁸, closer to $\langle 001 \rangle$ rhombohedral crystal orientation, more stable will be the domain configuration and hence higher strain values are possible.

Figure 3.1 demonstrates domain configurations in $\langle 001 \rangle$ oriented rhombohedral crystals under bias. When electric field is applied along $\langle 001 \rangle$ direction, the polar direction is expected to be inclined close to the electric field direction in each domain⁸. At higher electric fields, the observed high

strain in such crystals is due to an electric field-induced rhombohedral \rightarrow tetragonal phase transition (step B)⁸.

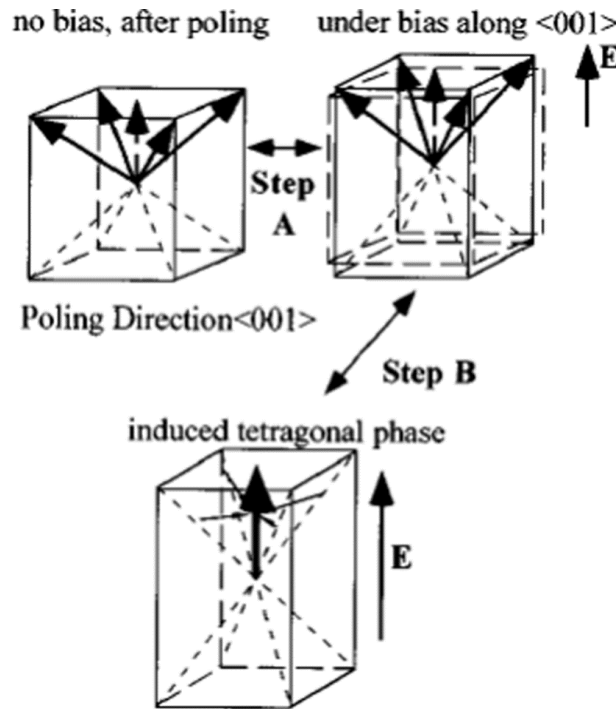


Figure 3.1: Schematic diagram of domain configurations in $\langle 001 \rangle$ oriented rhombohedral crystals under bias.

[Source: S. E. Park and T. R. ShROUT, "Ultrahigh strain and piezoelectric behavior in relaxor based ferroelectric single crystals," *J. Appl. Phys.*, 82 (1997) 1804].

Among ferroelectric materials, lead based perovskites such as PZT (Lead Zirconate Titanate), PLZT (Lanthanum doped Lead Zirconate Titanate) acquires greater significance due to their high dielectric constant, large spontaneous polarization, excellent optical transparency and optical nonlinearity⁹. PZT exhibits a cubic paraelectric phase above Curie point (T_C) and undergoes a phase transition below T_C to either rhombohedral or tetragonal phase depending upon the composition. The greatest advantage of PZT is the presence of a stable bridging monoclinic phase near morphotropic

phase boundary that can provide a suitable path for polarization rotation between the coexisting rhombohedral and tetragonal phases.

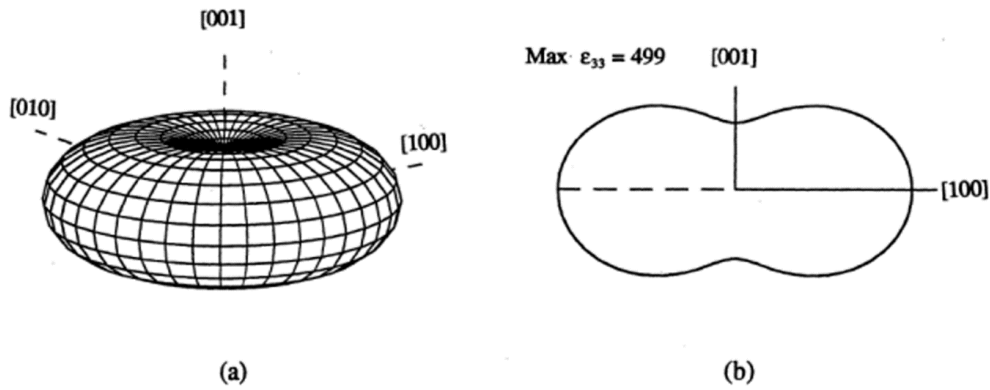


Figure 3.2: (a) Dielectric constant of tetragonal PZT 40/60. (b) shows the cross section curve when fig (a) is cut by (010) plane. Here maximum value of ϵ_{33} is obtained in a direction perpendicular to [001].

[Source: X. Du, U. Belegundu and K. Uchino, "Crystal orientation dependence of piezoelectric properties in Lead Zirconate Titanate: Theoretical expectation for thin films," *Jpn. J. Appl. Phys.*, 36 (1997) 5580].

Uchino *et. al*⁷ phenomenologically calculated crystal orientation dependence of piezoelectric properties of PZT in three dimensional space for tetragonal PZT (40/60) and rhombohedral PZT (60/40). The dielectric constant (ϵ_{33}) values obtained for tetragonal PZT (40/60) and rhombohedral PZT (60/40) are depicted in Figures 3.2 and 3.3 respectively.

The maximum value was obtained in a direction perpendicular to [001] ie, in a direction perpendicular to the polarization direction and the dielectric constant becomes minimum along the polarization direction. The orientation dependence of longitudinal piezoelectric constant d_{33} , electro mechanical coupling factor k_{33} , transverse piezoelectric constant d_{31} , electro mechanical coupling factor k_{31} in tetragonal PZT 40/60 and rhombohedral PZT 60/40 estimated by Uchino *et. al*⁷ are illustrated in Figures 3.4, 3.5, 3.6 and 3.7 respectively.

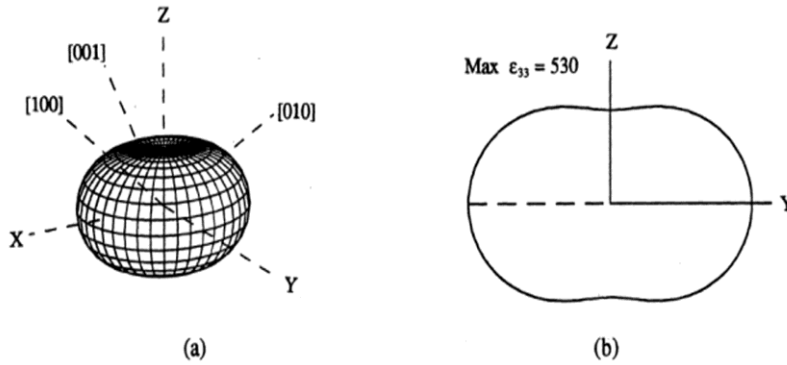


Figure 3.3: Dielectric constant of rhombohedral PZT 60/40. (b) shows the cross section curve when the figure is cut by Y-Z plane.

[Source: X. Du, U. Belegundu and K. Uchino, "Crystal orientation dependence of piezoelectric properties in Lead Zirconate Titanate: Theoretical expectation for thin films," *Jpn. J. Appl. Phys.*, 36 (1997) 5580].

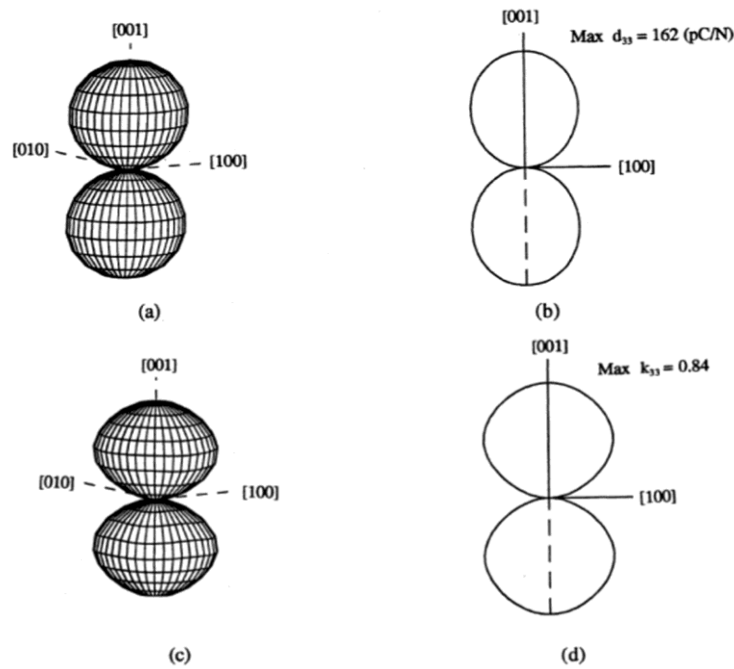


Figure 3.4: (a) shows the piezoelectric constant d_{33} of tetragonal PZT 40/60. (b) gives the cross section curve when fig (a) is cut by (010) plane. (c) gives the electromechanical coupling factor k_{33} of tetragonal PZT 40/60 and (d) gives the cross section curve when fig (c) is cut by (010) plane.

[Source: X. Du, U. Belegundu and K. Uchino, "Crystal orientation dependence of piezoelectric properties in Lead Zirconate Titanate: Theoretical expectation for thin films," *Jpn. J. Appl. Phys.*, 36 (1997) 5580].

The physical properties of PZT single crystal mainly depends on crystal orientation. For tetragonal PZT 40/60, maximum values of d_{33} and k_{33} occur along the polarization direction in Figure 3.4. For orientation perpendicular to polarization direction, d_{33} is found to be zero and k_{31} shows maximum value when axis 1 is along $[110]$.

The results obtained for rhombohedral PZT 60/40 (Figure 3.6) was found to be different (Figure 3.5). For rhombohedral single crystals of PZT, maximum d_{33} and k_{33} values are obtained along cubic perovskite equivalent axis $[001]$ at angles 56.7° and 51.3° respectively from the spontaneous polarisation direction.

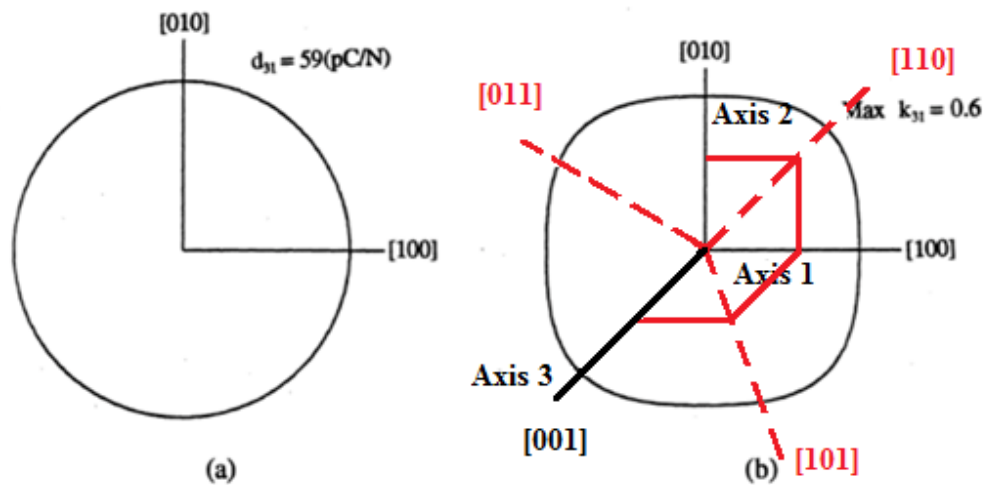


Figure 3.5: (a) shows the piezoelectric constant d_{31} of tetragonal PZT 40/60. (b) shows the electromechanical coupling factor k_{31} of tetragonal PZT 40/60.

[Source: X. Du, U. Belegundu and K. Uchino, "Crystal orientation dependence of piezoelectric properties in Lead Zirconate Titanate: Theoretical expectation for thin films," *Jpn. J. Appl. Phys.*, 36 (1997) 5580].

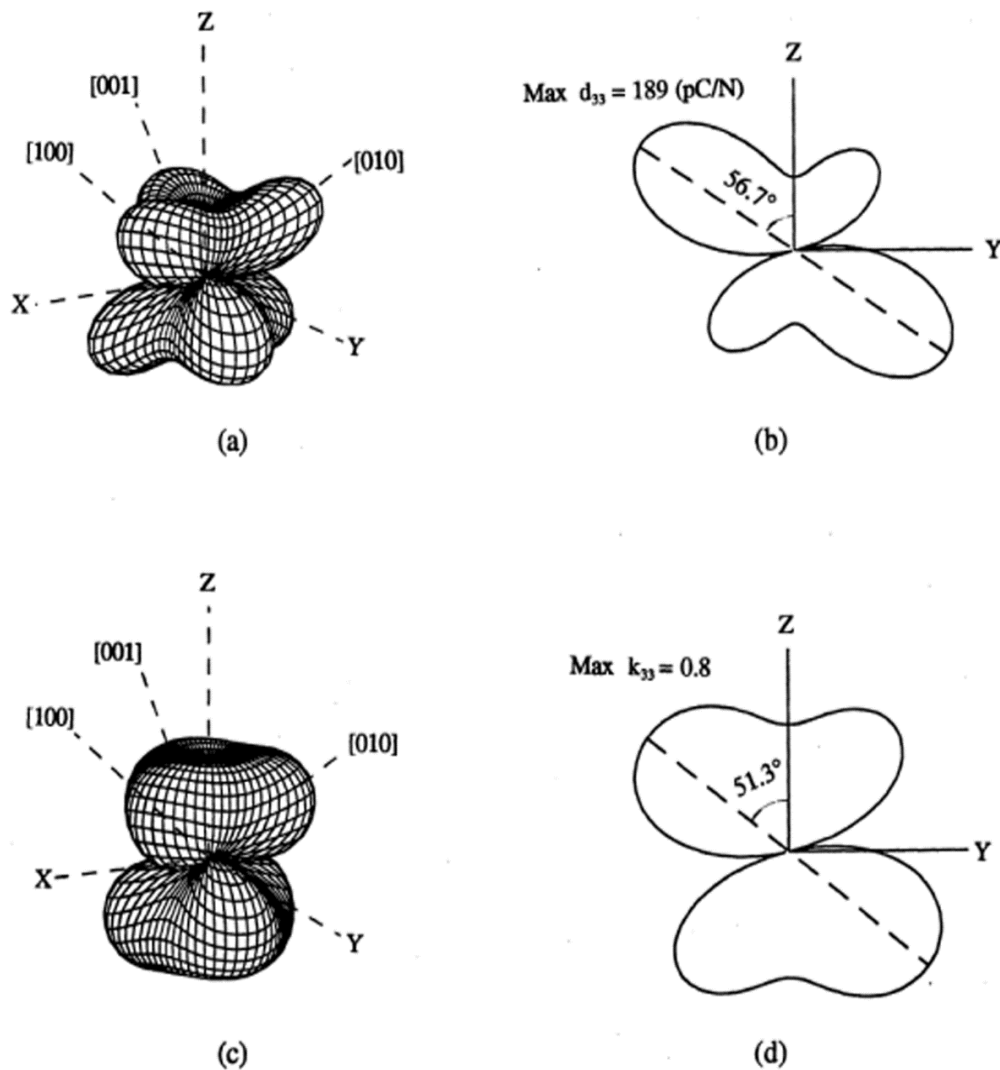


Figure 3.6: (a) Piezoelectric constant d_{33} of rhombohedral PZT 60/40, (b) Cross section curve when Fig in (a) is cut by Y-Z plane, (c) Electromechanical coupling factor K_{33} , (d) Cross section curve when fig in (c) is cut by Y-Z plane.

[Source: X. Du, U. Belegundu and K. Uchino, "Crystal orientation dependence of piezoelectric properties in Lead Zirconate Titanate: Theoretical expectation for thin films," *Jpn. J. Appl. Phys.*, 36 (1997) 5580].

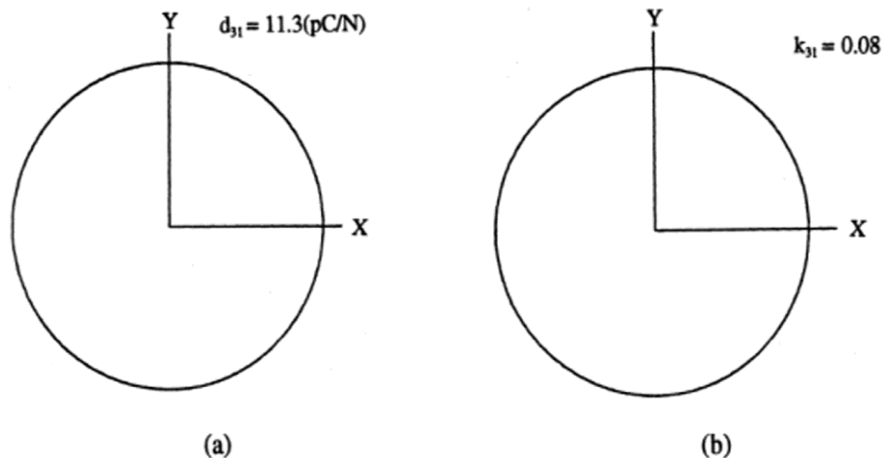


Figure 3.7: (a) Piezoelectric constant d_{31} of rhombohedral PZT 60/40. (b) Electro mechanical coupling factor k_{31} of rhombohedral PZT 60/40.

[Source: X. Du, U. Belegundu and K. Uchino, "Crystal orientation dependence of piezoelectric properties in Lead Zirconate Titanate: Theoretical expectation for thin films," *Jpn. J. Appl. Phys.*, 36 (1997) 5580].

The orientation dependence of d_{31} and k_{31} in rhombohedral PZT 60/40 with direction 3 along Z-direction perpendicular to the plane of paper and the direction 1 is rotated which is depicted in Figure 3.7. Both d_{31} and k_{31} are independent of the choice of direction 1. Hence Uchino *et. al*⁷ suggested that for piezoelectric thin film actuators and sensors, development of [100] epitaxially oriented rhombohedral compositions are preferable.

In PLZT ABO_3 perovskite, La^{3+} ion replaces Pb^{2+} ions creating A site vacancies. Lanthanum doping in PLZT can soften domain wall motion thereby improving the dielectric, piezoelectric and ferroelectric properties¹⁰. Hence we have fabricated prepared {100}- preferentially oriented PLZT thin films with rhombohedral composition near MPB and investigated their piezoelectric characteristics that are suitable for MEMS application^{11,12}.

The room temperature phase diagram of PLZT system¹³ is depicted in Figure 3.8 with PLZT(x/65/35); x= 6, 7 and 8 belonging to the rhombohedral composition. We have used sol-gel method for the fabrication of thin films since it offers numerous advantages such as excellent control of composition,

texture, uniform film thickness and also offers lower processing temperatures. As discussed¹³ previously, the in-plane transverse piezoelectric coefficient $e_{31,f}$ is the most important parameter to be considered for MEMS applications since large deformation can be obtained perpendicular to the applied field due to larger lateral dimension than small thickness of the film. Therefore the aim of the present work is the sol-gel deposition of preferentially {100}-oriented $(\text{Pb}_{1-x}\text{La}_x)(\text{Zr}_{0.65}\text{Ti}_{0.35})\text{O}_3$ [PLZT(x/65/35)]; $x = 6, 7, \text{ and } 8$ thin films and determination of their transverse piezoelectric characteristics.

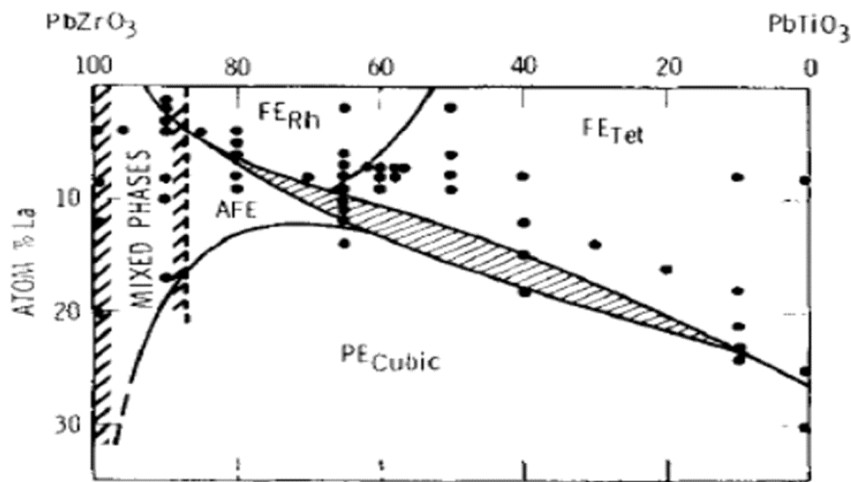


Figure 3.8: Room temperature phase diagram of PLZT system.

[Source: G. H. Haertling and C. E. Land, "Hot pressed $(\text{Pb},\text{La})(\text{Zr},\text{Ti})\text{O}_3$ ferroelectric ceramics for electrooptic applications," *J. Am. Ceram. Soc.*, 54 (1971) 1].

3.2.1 Experimental work

Stable precursor solutions corresponding to the composition $(\text{Pb}_{1-x}\text{La}_x)(\text{Zr}_{0.65}\text{Ti}_{0.35})_{1-x/4}\text{O}_3$, $x = 0.06, 0.07, 0.08$ were prepared by sol-gel process, as per the procedure adapted from our previous work¹⁴. The flow chart is shown in Figure 3.9. Sol-gel process makes use of metal alkoxide precursors that are water sensitive. Therefore control over hydrolysis and condensation reactions are important while adopting sol-gel route for synthesis. The reactants, lead acetate (99%, Merck, India), lanthanum acetyl acetonate

hydrate (Sigma Aldrich, India) and zirconium acetyl acetonate (98%, Merck, India) were refluxed in ethanol at 50°C for 1 hr. The clear solution thus obtained was mixed with a solution of titanium (IV) isopropoxide (97%, Sigma Aldrich, India) in isopropyl alcohol containing equimolar amounts of diethanolamine (98%, Merck, India) as the chelating agent thereby forming a highly stable PLZT precursor solution.

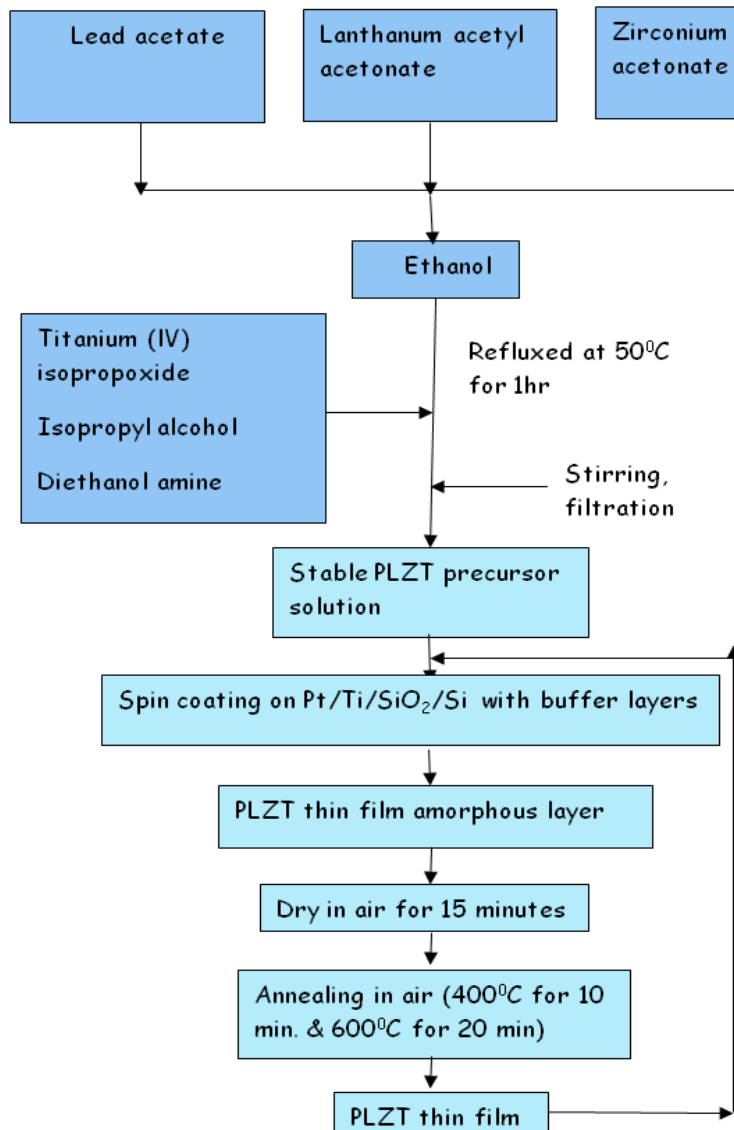


Figure 3.9: Synthesis of PLZT precursor solution

Preferential crystallographic orientation of the precursor could be controlled with the use of buffer layers and by controlling the annealing temperatures. According to Muralt *et. al*^{15,16}, introduction of PbTiO_3 (PT) layer between Pt/Ti/SiO₂/Si substrate and PZT film could produce {100}-preferentially oriented PZT films whereas the introduction of Pt/TiO₂ buffer layer can provide {111}-preferential orientation¹⁷. In another paper¹⁸, he gave reports regarding the role of PbO layer in achieving {100}-orientation and the role of TiO₂ layer in attaining {111}-preferential orientation on Pt/Ti/SiO₂/Si substrate. Hence for obtaining {100}-preferentially oriented films, we first spin-coated TiO₂ layer having a thickness of 10 nm on (111) Pt/Ti/SiO₂/Si substrate (Inostek, Korea), dried at 110⁰C for 15 min and then subjected to annealing at 600⁰C for 30 min^{19,20}. Later SrTiO₃ (ST) layer having a thickness of ~50 nm was coated over TiO₂ layer with the same annealing conditions. ST has a perovskite structure and possesses only a smaller lattice mismatch with PZT. So in addition to attaining preferential orientation, ST layer can also reduce the crystallization temperature of PZT since small activation energy is only required for inducing nucleation between two perovskites. Thus annealing conditions of buffer layers will control the nucleation and growth steps and preferred orientation could be achieved by carefully controlling the annealing temperatures. Buffer layers can also act as effective barriers preventing inter diffusion^{15,16,21}. The TiO₂ layer can decrease the surface roughness of the film thereby leading to an increase in dielectric constant and tunability with a decrease in dielectric loss and leakage current density. Also the surface of TiO₂ buffer allows the precursor layer to remain intact on the surface while spin coating, thereby leading to an increase in film thickness. Hence film surface deposited on TiO₂ layer seems to be more flat than films deposited directly on platinum electrodes²⁰. Finally, PLZT films were coated above the buffer layers by spin-coating process using a Spin coater (Model:

KW-4A, Chemat technologies, USA) at a speed of 4000 rpm for 25 s. The coated PLZT layers were dried at 110⁰C for 15 min and then annealed in two stages, initially at 400⁰C for 10 min and then at 600⁰C for 20 min. Thus preferentially {100}-oriented thin films of lead lanthanum zirconate titanate, (Pb_{1-x}La_x)(Zr_{0.65}Ti_{0.35})_{1-x/4}O₃ [PLZT(x/65/35)] with compositions near the morphotropic phase boundary (MPB) were prepared on platinised silicon substrates (111)Pt/Ti/SiO₂/Si by sol-gel spin coating technique.

Crystalline orientation and microstructure of the prepared films were determined using X-ray diffraction (X-ray diffractometer, Model: D5005, Bruker, Germany), Scanning electron microscopy, respectively. The structural, micro structural and electrical characteristics have been studied as a function of thin film composition. Raman spectra were recorded using a Raman Spectrometer (Model: DXR, Thermo scientific, USA). Gold top electrodes of 350 nm thickness were deposited on the PLZT films using a Vacuum Coater (Model: 12A4D, Hind High Vacuum, India). Ferroelectric and dielectric properties were determined using a piezoelectric evaluation system (Model: FT Analyser 2000, aixACCT, Germany). Leakage current measurements were recorded on PLZT thin films with positive voltage applied on the top gold electrode and negative voltage on the bottom electrode.

For the measurement of piezoelectric properties of the PLZT films, rectangular beams of substrate with PLZT films were diced out and transverse piezoelectric properties were measured as described in our earlier studies^{22,23}. The transverse piezoelectric properties of the PLZT thin films were evaluated using unimorph cantilevers of PLZT/Si. Piezoelectric vibration was generated by applying sine wave voltage between upper and bottom electrodes. Tip displacement was measured using a laser Doppler vibrometer (Model: AT-3500, Graphtec, Japan) and a laser interferometer (Model: AT-1100, Graphtec, Japan). Micro structural analysis of thin films was carried out using a High

Resolution Scanning Electron Microscope (HRSEM, Model: Genesis Apex 2, Ametek, Japan).

3.2.2 Results and discussion

The X-ray diffraction patterns and Raman spectra of {100}-oriented PLZT (6/65/35), (7/65/35) and (8/65/35) films are given in Figure 3.10 (A) and (B) respectively. It is seen that all the three films exhibited {100}-preferred orientation. The introduction of TiO_2 and SrTiO_3 bottom layers and the modification of heat treatment conditions played a prominent role in accomplishing the preferred crystallographic orientation^{19,20}. From the Raman spectra [Figure 3.10(B)], it is clear that thin films of PLZT (x/65/35); x = 6, 7 are purely rhombohedral as evidenced by E, E' modes at $\sim 65\text{cm}^{-1}$ and E mode at 285cm^{-1} . But in the case of PLZT (8/65/35) thin film [Figure 3.10 B(c)], the broad peak at 140cm^{-1} [$A_1(1\text{TO})$] and 326cm^{-1} [$A_1(2\text{TO})$] are sensitive indications of the presence of some fractions of tetragonal phase²⁴⁻²⁸. All the three films exhibited dense columnar microstructures as revealed by the SEM of their cross-sections as shown in Figure 3.11.

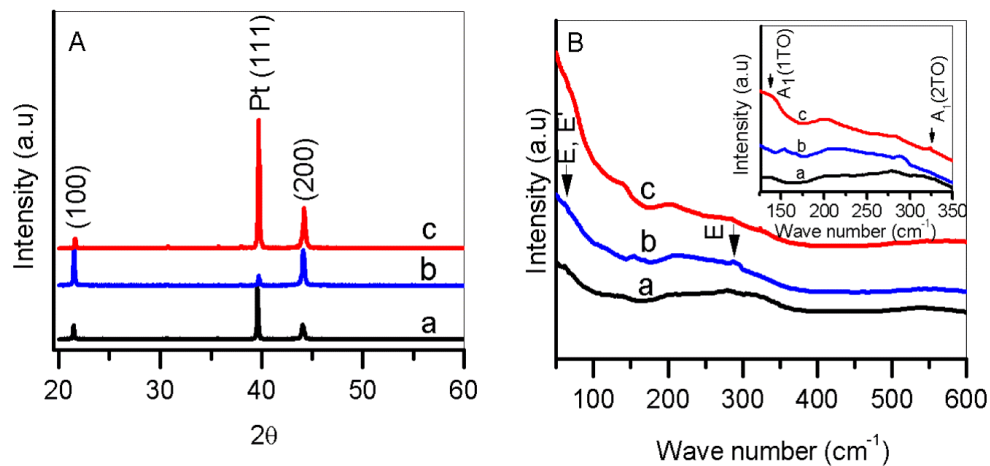


Figure 3.10: (A) XRD patterns and (B) Raman spectra of PLZT films with varying lanthanum concentrations (a) 6/65/35, (b) 7/65/35, and (c) 8/65/35 on Pt/Ti/SiO₂/Si substrate.

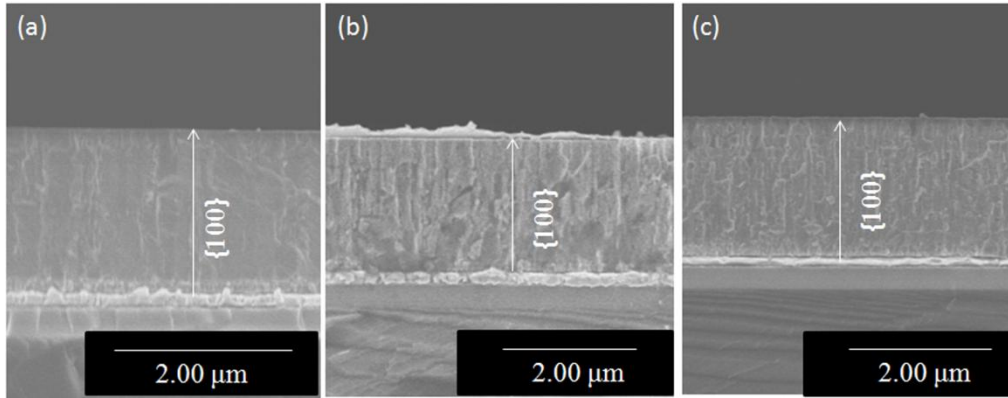


Figure 3.11: HRSEM of the PLZT (a) 6/65/35, (b) 7/65/35, and (c) 8/65/35 thin films.

Transverse piezoelectric properties of the thin films were evaluated from the deflection of PLZT/Pt/Ti/SiO₂/Si cantilevers by applying unipolar sine wave voltage between upper and bottom electrodes. In this experiment, we measured the tip displacement at the frequency of 700Hz. From the piezoelectric displacement, the transverse piezoelectric coefficient $|e_{31,f}|$ was evaluated as per equation (3.1) given below;

$$|e_{31,f}| = \frac{d_{31}}{s_{11,p}^E + s_{12,p}^E} \cong -\frac{h_s^2}{3s_{11,s}(1-\nu_s)L^2} \frac{\delta}{V} \quad (3.1)$$

where δ , V , L , h , ν_s and $s_{11,s}$ are the tip displacement, applied voltage between top and bottom electrodes, length of the cantilever, thickness, Poisson's ratio and the elastic compliance of the substrate respectively²⁹. The subscripts "s" and "p" denote the substrate and the piezoelectric film respectively. The elastic compliance S_{11} is given by the reciprocal of the Young's modulus. The Young's modulus and Poisson's ratio of the <110>Si, which is the length direction of the cantilevers was reported as 168GPa and 0.066, respectively^{30,31}.

Transverse piezoelectric coefficient $|e_{31,f}|$ determined from equation (3.1) for {100}-oriented films are given in Figure 3.12. It is seen that maximum

transverse piezoelectric coefficient and least nonlinearity is obtained for PLZT (7/65/35) thin film. The nonlinearity in $|e_{31,f}|$ decreases in the order, PLZT (8/65/35) > PLZT (6/65/35) > PLZT (7/65/35). This is because both PLZT (6/65/35) and (7/65/35) thin films exhibit pure rhombohedral geometry. For {100}-oriented thin films with rhombohedral structure the domains \vec{a} are stable [Figure 3.13 (A)]³². In the case of PLZT (8/65/35) thin film, which has an MPB composition, large nonlinearity in $|e_{31,f}|$ is attributed to the switching of non-180° domains \vec{b}, \vec{c} also as shown in Figure 3.13 (B). In the case of PLZT (7/65/35) thin film, higher value of $|e_{31,f}|$ may be due to an electric field enforced Rhombohedral → Tetragonal phase transformation.

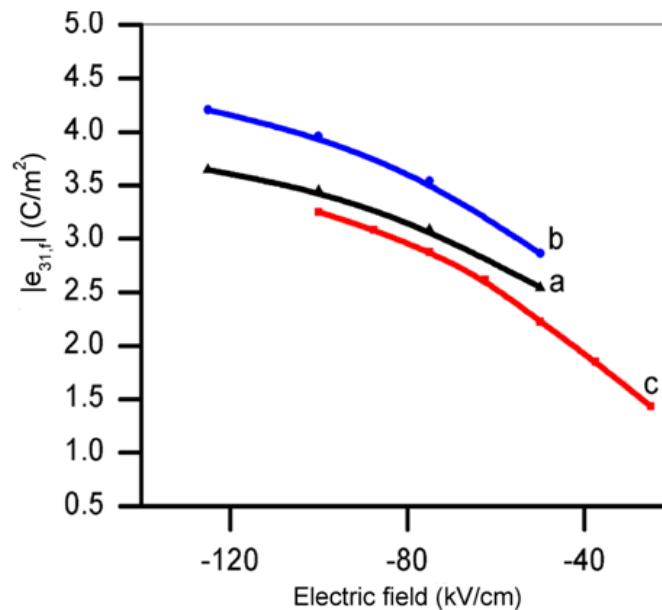


Figure 3.12: Transverse piezoelectric response in {100} - oriented PLZT (a) (6/65/35), (b) (7/65/35), and (c) (8/65/35) thin films as a function of applied voltage.

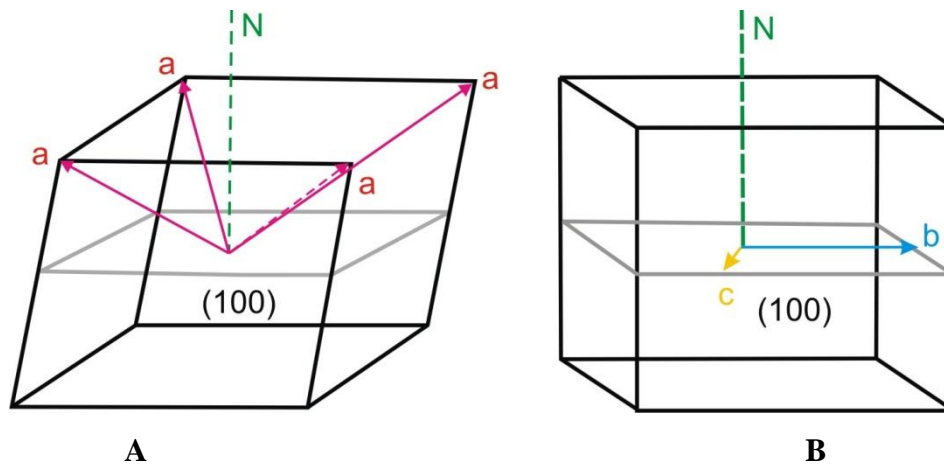


Figure 3.13: Domains in {100} - oriented PLZT thin film having (A) rhombohedral and (B) tetragonal structure.

Table 3.1 Electrical characteristics of PLZT thin films

PLZT [x/65/35]	Dielectric permittivity ϵ_r	Dielectric loss $\tan \delta$	Transverse piezoelectric coefficient $ e_{31,f} $ (C/m ²)
(6/65/35)	864	0.02	3.6
(7/65/35)	917	0.03	4.2
(8/65/35)	951	0.03	3.3

In contrast to the piezoelectric effects, the displacements of all domains (180° and non- 180°) contribute to dielectric permittivity³³. Large values of ϵ_r for PLZT (8/65/35) films (Table 3.1) obtained in our work is consistent with this. The dielectric characteristics obtained for us are better than those reported earlier^{34,35}. The room temperature dielectric constant and loss tangent values reported for PZT thin films at 10 kHz were found to be 720 and 0.045 respectively³³. But as per the reports given by Thomas *et. al*³⁴, upon lanthanum doping, these values get decreased to 440 and 0.038. For acetate derived PLZT, Haertling³⁶ reported ϵ_r and $\tan \delta$ values to be 790 and 0.092 respectively. {100}-preferentially oriented PLZT thin films prepared by us

through sol-gel route was found to exhibit better dielectric properties even at frequency of 1 kHz. Hence differences in precursor materials and processing steps can bring about dramatic variations in dielectric and ferroelectric properties of materials with the same composition.

Among our prepared PLZT compositions, the leakage current density was found to be minimum ($\sim 10^{-2} \mu\text{A}/\text{cm}^2$) for PLZT (7/65/35) thin film (Figure 3.14) indicating its suitability for micro actuator applications.

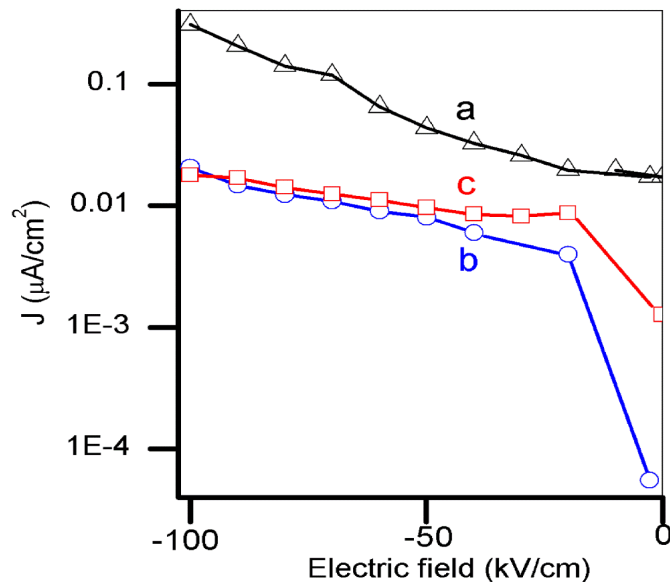


Figure 3.14: Leakage current of PLZT thin films (a) 6/65/35, (b) 7/65/35, and (c) 8/65/35 on $\text{TiO}_2/\text{ST}/\text{Pt}/\text{Ti}/\text{SiO}_2/\text{Si}$ substrate.

Slim P-E hysteresis loops obtained in Figure 3.15 (A) are characteristic of high – La. substituted PZT films. Figure 3.15 (B) shows the strain curves (S-E) of PLZT films by applying bipolar sine wave voltage of $\pm 30\text{V}$ at 100Hz. All the curves are butterfly shaped indicating domain switching of ferroelectricity.

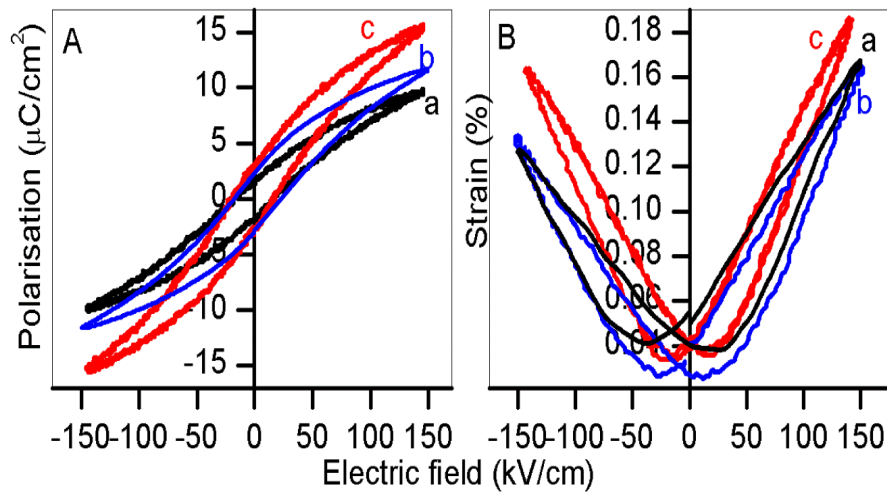


Figure 3.15: (A) P-E hysteresis loop and (B) S-E curve under bipolar excitation in PLZT thin films (a) 6/65/35, (b) 7/65/35, and (c) 8/65/35

Thus it is observed that, down the group, PLZT (7/65/35) thin films are found to exhibit the optimum characteristics such as minimum nonlinearity in $|e_{31,f}|$ and minimum leakage current density.

3.3 Transverse piezoelectric properties of {110}-oriented PLZT thin films

Lead zirconate titanate $\text{Pb}(\text{Zr}_{1-x}\text{Ti}_x)\text{O}_3$ (PZT) ferroelectric thin films, having compositions at or near the morphotropic phase boundary region of $\text{Zr}/\text{Ti} = 52/48$ have received greater attention in MEMS applications due to the excellent piezoelectric properties offered by them³⁶. Hence PLZT ceramic compositions across the morphotropic phase boundary, having a constant A-site La^{3+} concentration are of interest for studying their piezoelectric properties and multifunctionality^{7,8,36}. We have selected three PLZT compositions across the MPB region with different Zr/Ti ratios at a constant La content $(\text{Pb}_{0.93}\text{La}_{0.07})(\text{Zr}_{0.65}\text{Ti}_{0.35})_{0.9825}\text{O}_3$ PLZT (7/65/35), $(\text{Pb}_{0.93}\text{La}_{0.07})(\text{Zr}_{0.60}\text{Ti}_{0.40})_{0.9825}\text{O}_3$ PLZT (7/60/40) and $(\text{Pb}_{0.93}\text{La}_{0.07})(\text{Zr}_{0.56}\text{Ti}_{0.44})_{0.9825}\text{O}_3$ PLZT (7/56/44). Even

though studies have been conducted on synthesis and characterisation of these materials in the bulk form³⁷⁻⁴⁰, no study has yet been reported on the determination of the transverse piezoelectric coefficient, ($|e_{31,f}|$) of the thin films, especially on the correlation with their crystal structure and texture. For piezoelectric thin films having compositions across MPB, achieving preferential {110} orientation enhances their piezoelectric applications in view of the co-existence of tetragonal, monoclinic and rhombohedral phases^{41,42} as depicted in Figure 3.8. Therefore the sol-gel deposition of preferentially {110}-oriented PLZT thin films of compositions across the MPB at a constant La content and the determination of their transverse piezoelectric characteristic ($|e_{31,f}|$) have also been carried out and are reported here.

3.3.1 Experimental

Stable precursor solutions of PLZT corresponding to the compositions PLZT (7/65/35), PLZT (7/60/40) and PLZT (7/56/44) were prepared by sol-gel process as per the procedure adapted from our previous work¹⁴. In order to achieve {110}-preferential orientation, SrTiO₃ (ST) buffer layer having a thickness of ~50 nm was first spin-coated on the platinised silicon substrate. This buffer layer can prevent inter diffusion reactions between the PLZT layer and the substrate and also minimise the thermal mismatch between the substrate and the PLZT film layers^{15,20,42,43}. Each coated film layer was dried at 110⁰C for 15 min and then annealed at a temperature of 400⁰C for 10 min and finally at 600⁰C for 20 min⁴². This process was repeated to get perfectly {110}-oriented PLZT thin films having 1.5 μ m thickness.

3.3.2 Results and discussion

Figure 3.16 shows the X-ray diffraction (XRD) patterns of PLZT (7/60/40), PLZT (7/56/44) and PLZT (7/65/35) thin films on silicon substrates. Here all the films exhibit pure perovskite phase with a high degree of {110}-preferred orientation. Such a preferred {110}-orientation was achieved with the use of SrTiO₃ (ST) as the buffer layer⁴².

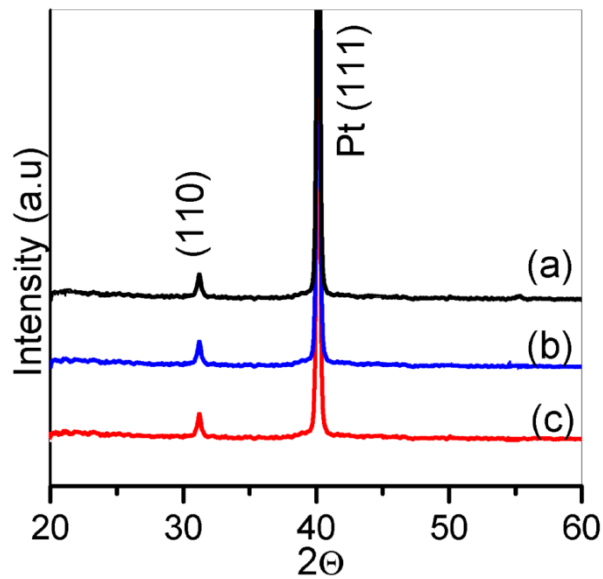


Figure 3.16: XRD patterns of PLZT thin films (a) 7/60/40, (b) 7/56/44, and (c) 7/65/35 on Pt/Ti/SiO₂/Si substrate.

Since different phases are known to coexist in compositions near MPB, in order to get a clear understanding of them, detailed Raman spectral studies were undertaken. The Raman spectra given in Figure 3.17 reveal a clear picture of the crystal structure of PLZT thin films. It is seen that {110} oriented PLZT (7/65/35) thin film [Figure. 3.17 (c)] has a rhombohedral structure as evidenced by the presence of the E mode at 285cm⁻¹. In the case of PLZT (7/56/44) thin films, it is seen that the rhombohedral phase is prominent as evidenced by the presence of E mode at 285 cm⁻¹. Presence of small

amounts of tetragonal phase is also indicated by the $[A_1(1TO)]$ mode at 140 cm^{-1} [Figure 3.17 (b)]. In the case of PLZT (7/60/40) [Figure 3.17 (a)], the MPB composition is very clear from the Raman spectra with rhombohedral E mode at 285 cm^{-1} and two sharp modes at $140 [A_1(1TO)]$ and $326 [A_1(2TO)]\text{ cm}^{-1}$ respectively due to the tetragonal modification^{24,25,26,27}. Also on comparing the spectra, it is clear that the intensity of E(2TO) mode at 210 cm^{-1} is higher for PLZT (7/56/44) [Figure 3.17 (b)] while the intensities of both $[A_1(1TO)]$ and $[A_1(2TO)]$ modes are higher for PLZT (7/60/40) [Figure 3.17 (a)]. This clearly suggests that PLZT (7/56/44) has a higher rhombohedral content and PLZT (7/60/40) has a higher tetragonal content²⁸.

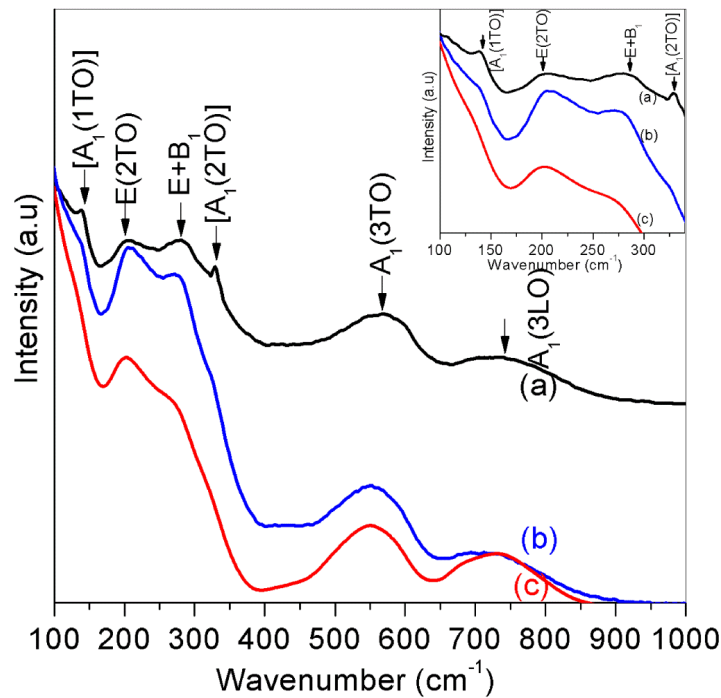


Figure 3.17: Raman spectra of PLZT thin films (a) 7/60/40 (b) 7/56/44 and (c) 7/65/35 on Pt/Ti/SiO₂/Si substrate

The dielectric characteristics obtained for the PLZT thin films are given in Table 3.2. The dielectric measurements were recorded at a frequency of 1kHz. Higher dielectric permittivity, ϵ_r are obtained for all the three compositions, since the displacement of both 180 and non-180⁰ domains contribute to dielectric permittivity. The dielectric characteristics obtained are better than those reported for the corresponding bulk ceramics^{37,38,39}. This is attributed to their dense and columnar microstructures as revealed by the SEM cross sectional images [Figure 3.18].

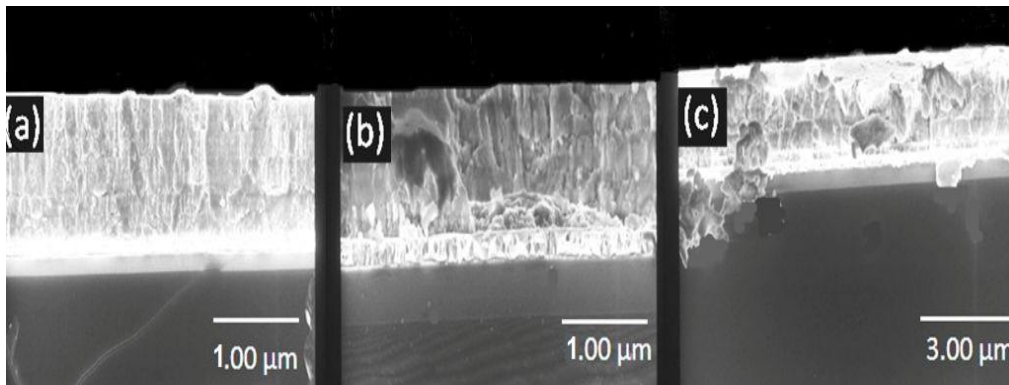


Figure 3.18: HRSEM images of (a) 7/60/40, (b) 7/56/44, and (c) 7/65/35 thin films on Pt/Ti/SiO₂/Si substrate.

Table 3.2 Electrical characteristics of PLZT thin films

PLZT thin films	Dielectric permittivity, ϵ_r	Dielectric loss, $\tan \delta$	Remanent Polarization $2P_r$ ($\mu\text{C}/\text{cm}^2$)	Transverse piezoelectric coefficient $ e_{31,f} $ (C/m^2)
(7/60/40)	2220	0.01	24	2.4
(7/56/44)	1780	0.02	23	1.5
(7/65/35)	1500	0.01	19	1.3

Transverse piezoelectric properties of the prepared PLZT thin films were measured from the deflection of PLZT/Ti/SiO₂/Si cantilevers by applying unipolar sine wave voltage between the top and bottom electrodes.

Here the tip displacement was measured at a frequency of 500Hz which is far away from the resonance frequency of the cantilever. The transverse piezoelectric coefficient $|e_{31,f}|$ was evaluated from tip deflection as per equation (3.1) indicated earlier in this chapter. The electric field dependence of $|e_{31,f}|$ is shown in Figure 3.19.

It is seen that maximum transverse piezoelectric coefficient ($|e_{31,f}|$) is obtained for PLZT (7/60/40) thin films. This is because PLZT (7/60/40) has the morphotropic phase boundary composition and has a higher tetragonal content. When they are preferentially {110}-oriented, there are two different domains, domains \vec{a} which are at an angle of 45° and \vec{b} at an angle of 90° with the film normal [Figure 3.20 (B)]. Out of these, 90° domain switching lead to more strain. This gives rise to increased $|e_{31,f}|$ values as shown in Figure 3.19 (a). In the case of PLZT (7/56/44) and (7/65/35) thin films which have higher rhombohedral content, the switching of \vec{c} domains which are at an angle of $35^\circ 16'$ [Figure 3.20 (A)] leads to only reduced strain. Comparing PLZT (7/56/44) and (7/65/35), the former exhibits increased $|e_{31,f}|$ value due to the presence of small amounts of tetragonal phase along with the predominant rhombohedral phase.

The domain switching mechanism is confirmed from the dielectric data obtained for the thin films (Table 3.2) as well as from the P-E characteristics in Figure 3.21. Comparatively larger polarization values are obtained for all the three films. The maximum remanent polarization of $2P_r = 24 \mu\text{C}/\text{cm}^2$ is obtained for PLZT (7/60/40) having an MPB composition with increased tetragonal content. PLZT (7/56/44) and (7/65/35) exhibited $2P_r$ values of 23 and $19 \mu\text{C}/\text{cm}^2$ respectively.

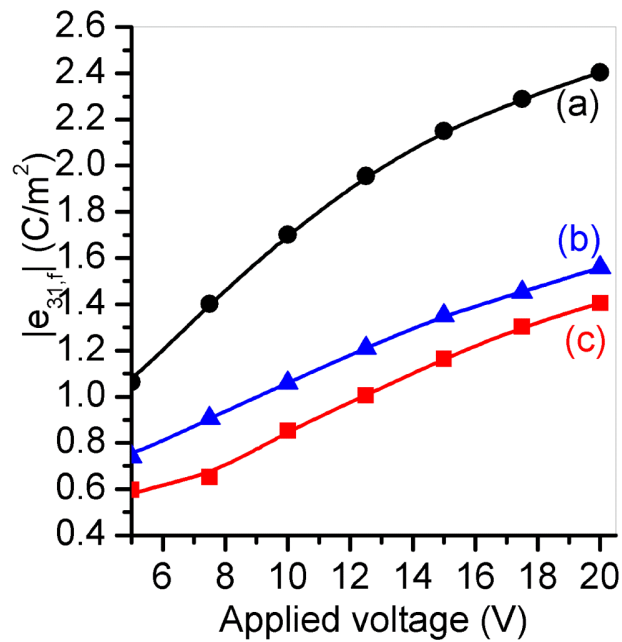


Figure 3.19: Transverse piezoelectric coefficient, $|e_{31,f}|$ in $\{110\}$ - oriented PLZT thin films (a) (7/60/40), (b) (7/56/44), and (c) (7/65/35) as a function of applied voltage.

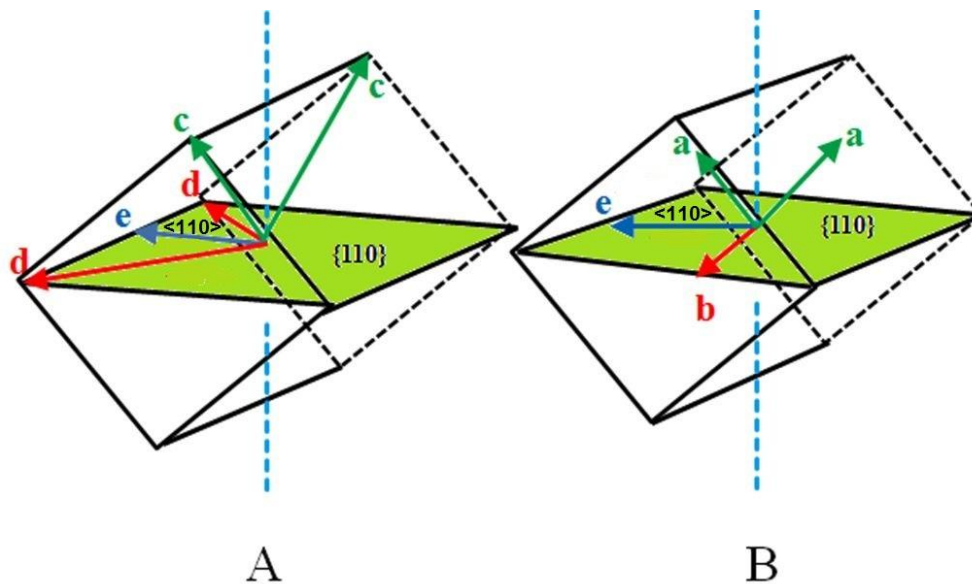


Figure 3.20: Domains in $\{110\}$ - preferentially oriented PLZT thin films having (A) rhombohedral and (B) tetragonal structure.

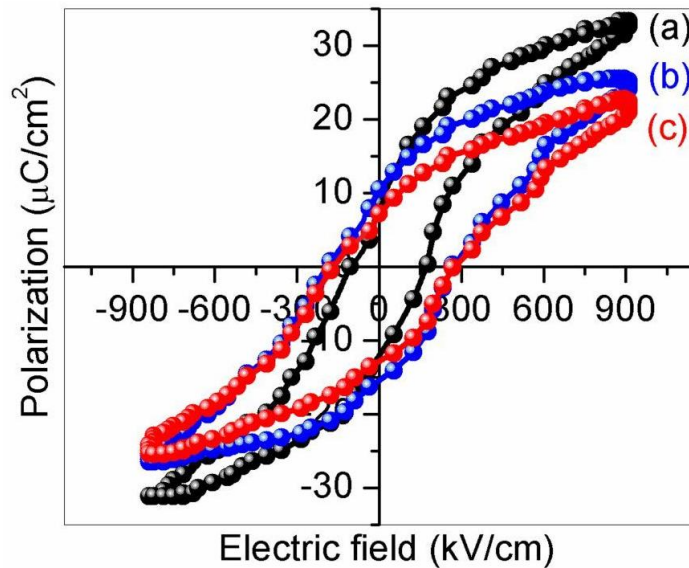


Figure 3.21: P-E characteristics of {110}-oriented PLZT thin films (a) 7/60/40, (b) 7/56/44, (c) 7/65/35.

3.4 Conclusion

Crystallographically {100}-preferentially oriented PLZT films having thickness of 2.0 μm were prepared on Pt/Ti/SiO₂/Si substrates by sol-gel spin coating technique. The TiO₂ and ST bottom layers facilitated preferred {100}-orientation of PLZT. {100}-oriented PLZT (6/65/35) and PLZT (7/65/35) thin films having rhombohedral symmetry have stable domains and exhibit minimum nonlinearity in $|e_{31,f}|$. In the case of PLZT (8/65/35) thin films having MPB composition, switching of non-180° domains contribute to large nonlinearity in $|e_{31,f}|$. PLZT (7/65/35) thin films are found to exhibit the optimum characteristics such as minimum nonlinearity in $|e_{31,f}|$ and minimum leakage current density.

In the case of PLZT thin films of (7/60/40), (7/56/44) and (7/65/35), preferential {110}-orientation was achieved. The influence of crystallographic orientation and thin film composition on their electrical characteristics was

investigated. All the three films exhibited good dielectric, ferroelectric and piezoelectric properties indicating their suitability for MEMS applications. By combining the structural information obtained from their Raman spectra, the domain switching mechanism was established. PLZT (7/60/40) thin films exhibited the highest transverse piezoelectric coefficient, $|e_{31,f}|$. Also an increase in piezoelectric properties was observed on moving from left to right across the MPB, due to the increased contribution from strain causing 90° domain switching.

References

- [1] C. Ma, B. Ma, S. B. Mi, M. Liu, J. Wu, "Enhanced dielectric nonlinearity in epitaxial $\text{Pb}_{0.92}\text{La}_{0.08}\text{Zr}_{0.52}\text{Ti}_{0.48}\text{O}_3$ thin films," *Appl. Phys. Lett.*, **104** (2014) 162902.
- [2] K. Kanda, J. Inoue, T. Saito, T. Fujita, K. Higuchi, K. Maeneka, "Fabrication and characterization of double-layer $\text{Pb}(\text{Zr},\text{Ti})\text{O}_3$ thin films for micro-electromechanical systems" *Jpn. J. Appl. Phys.*, **51** (2012) 09LD12.
- [3] R. A. Wolf and T. S. McKinstry, "Temperature dependence of the piezoelectric response in lead zirconate titanate films," *J. Appl. Phys.*, **95** (2004) 1397.
- [4] K. Kanda, I. Kanno, H. Kotera and K. Wasa, "Simple Fabrication of Metal-Based Piezoelectric MEMS by Direct Deposition of Thin Films on Titanium Substrates," *J. Microelectromech. Syst.*, **18** (2009) 610.
- [5] S. K. Pandey, O. P. Thakur, D. K. Bhattacharya, Harsh C. Prakash and R. Chatterjee, "Effect of double doping in lead zirconate titanate (PZT) lattices by sol-gel technique for MEMS applications," *Integr. Ferroelectr.*, **121** (2010) 65.
- [6] Z. Hu, B. Ma, S. Liu, M. Narayanan and U. Balachandran, "Relaxor behavior and energy storage performance of ferroelectric PLZT thin films with different Zr/Ti ratios," *Ceram. Int.*, **40** (2014) 557.
- [7] X. Du, U. Belegundu and K. Uchino, "Crystal orientation dependence of piezoelectric properties in Lead Zirconate Titanate: Theoretical expectation for thin films," *Jpn. J. Appl. Phys.*, **36** (1997) 5580.
- [8] S. E. Park and T. R. Shrout, "Ultrahigh strain and piezoelectric behavior in relaxor based ferroelectric single crystals," *J. Appl. Phys.*, **82** (1997) 1804.
- [9] T. S. McKinstry and P. M. Muralt, "Thin film piezoelectrics for MEMS," *J. Electroceram.*, **12** (2004) 7.

- [10] R. Poyato, M. Algueró, M. L. Calzada and L. Pardo, "Enhancement of the 90° domain-wall mobility in sol-gel (Pb,La)TiO₃ thin films prepared by multiple deposition and crystallization," *J. Appl. Phys.*, **98** (2005) 024117.
- [11] W. J. Leng, C. R. Yang, H. Ji, J. H. Zhang, J. L. Tang and H. W. Chen, "Large third-order optical nonlinearity in (Pb,La)(Zr,Ti)O₃ ferroelectric thin film," *J. Appl. Phys.*, **100** (2006) 126101.
- [12] A. Kumar, V. V. Bhanu Prasad, K. C. James Raju and A. R. James, "Ultra high strain properties of lanthanum substituted PZT electroceramics prepared via mechanical activation," *J Alloys Compd.*, **599** (2014) 53.
- [13] G. H. Haertling and C. E. Land, "Hot pressed (Pb,La)(Zr,Ti)O₃ ferroelectric ceramics for electrooptic applications," *J. Am. Ceram. Soc.*, **54** (1971) 1.
- [14] D. Ambika, V. Kumar, C. S. Suchand Sandeep and R. Philip, "Tunability of third order nonlinear absorption in (Pb,La)(Zr,Ti)O₃ thin films," *Appl. Phys. Lett.*, **98** (2011) 011903.
- [15] P. Muralt, "Ferroelectric thin films for micro-sensors and actuators: a review," *J. Micromech. Microeng.*, **10** (2000) 134.
- [16] P. Muralt, "Texture control and seeded nucleation of nanosize structures of ferroelectric thin films," *J. Appl. Phys.*, **100** (2006) 051605.
- [17] S. Hiboux and P. Muralt, "Piezoelectric and dielectric properties of sputter deposited (111), (100) and random textures Pb(Zr_xTi_{1-x})O₃ (PZT) thin films," *Ferroelectrics.*, **24** (1999) 315.
- [18] S. Hiboux and P. Muralt, "Mixed titania-lead oxide seed layers for PZT growth on Pt(111): a study on nucleation, texture and properties," *J. Euro. Ceram. Soc.*, **24** (2004) 1593.
- [19] D. Ambika and V. Kumar, "Chemical-solution deposition and nonlinear dielectric characteristics of nanocrystalline (Pb_{0.5}Sr_{0.5})TiO₃ thin films," *J. Phys. D: Appl. Phys.*, **43** (2010) 065401.

- [20] L. Chen, M. Shen, L. Fang and Y. Xu, "Dielectric properties and IV characteristics of $(\text{Pb}_{0.4}\text{Sr}_{0.6})\text{TiO}_3$ thin films improved by TiO_2 buffer layers," *Sol-Gel Sci. Technol.*, **42** (2007) 299.
- [21] M. Jain, S. B. Majumder, R. Guo, A. S. Bhalla and R. S. Katiyar, "Synthesis and characterization of lead strontium titanate thin films by sol-gel technique," *Mater. Lett.*, **56** (2002) 692.
- [22] I. Kanno, H. Kotera and K. Wasa, "Measurement of transverse piezoelectric properties of PZT thin films," *Sens. Actuators A: Phys.*, **107** (2003) 68.
- [23] K. Sivanandan, T. A. Asha, V. Kumar and I. Kanno, "Fabrication and transverse piezoelectric characteristics of PZT thick-film actuators on alumina substrates," *Sens. Actuators A: Phys.*, **148** (2008) 134.
- [24] M. Deluca, H. Fukumura, N. Tonari, C. Capianni, N. Hasuike, K. Kisoda, C. Galassi and H. Harima, "Raman spectroscopic study of phase transitions in undoped morphotropic $\text{Pb}(\text{Zr}_{1-x}\text{Ti}_x)\text{O}_3$," *J. Raman Spectrosc.*, **42** (2011) 488.
- [25] J. Frantti and V. Lantto, "Structural studies of Nd-modified lead zirconate titanate ceramics between 11 and 680 K at the morphotropic phase boundary," *Phys Rev B.*, **56** (1997) 221.
- [26] J. Frantti, V. Lantto and J. Lappalainen, "Symmetry consideration of Raman modes in Nd-doped lead zirconate titanate thin films for structure characterization," *J. Appl. Phys.*, **79** (1996) 1065.
- [27] E. R. Camargo, J. Frantii and M. Kakihana, "Low-temperature chemical synthesis of lead zirconate titanate (PZT) powders free from halides and organics," *J. Mater. Chem.*, **11** (2001) 1875.
- [28] A. G. Souza Filho, K. C. V. Lima, A. P. Ayala, I. Guedes, P. T. C. Freire, F. E. A. Melo, J. Mendes Filho, E. B. Araujo and J. A. Eiras, "Raman scattering study of the $\text{Pb}(\text{Zr}_{1-x}\text{Ti}_x)\text{O}_3$ system: Rhombohedral-monoclinic-tetragonal phase transitions," *Phy. Rev. B.*, **66** (2002) 132107.

- [29] J. G. Smits and W. Choi, "Equations of state including the thermal domain of piezoelectric and pyroelectric heterogeneous bimorphs," *IEEE Trans.*, **38** (1991) 256.
- [30] J. J. Wortman and R. A. Evans, "Young's modulus, shear modulus, and Poisson's ratio in silicon and germanium," *J. Appl. Phys.*, **36** (1965) 153.
- [31] M. A. Hopcroft, W. D. Nix and T. W. Kenny, "What is the Young's modulus of Silicon?," *J. Micro. Electro. Mech. S.*, **19** (2010) 229.
- [32] S. Y. Chen and C. L. Sun, "Ferroelectric characteristics of oriented $\text{Pb}(\text{Zr}_{1-x}\text{Ti}_x)\text{O}_3$ films," *J. Appl. Phys.*, **6** (2001) 2970.
- [33] M. Narayanan, S. Tong, S. Liu, B. Ma and U. Balachandran, "Estimation of intrinsic contribution to dielectric response of $\text{Pb}_{0.92}\text{La}_{0.08}\text{Zr}_{0.52}\text{Ti}_{0.48}\text{O}_3$ thin films at low frequencies using high bias fields," *Appl. Phys. Lett.*, **102** (2013) 062906.
- [34] R. Thomas, S. Mochizuki, T. Mihara and T. Ishida, "PZT (65/35) and PLZT (8/65/35) thin films by sol-gel process: a comparative study on the structural, microstructural and electrical properties," *Thin Solid Films.*, **443** (2003) 14.
- [35] K. P. Rema, A. S. Divya and V. Kumar, "Influence of low lanthanum doping on the electrical characteristics of PZT (53/47)," *J. Phys D: Appl. Phys.*, **42** (2009) 075420.
- [36] G. Haertling, E. Skaar, F. Wang, J. Guha and D. Dausch, "Intelligent processing of ferroelectric thin films," Annual report CLEMSON UNIV SC DEPT OF CERAMIC ENGINEERING, (1993) AD-A272-518.
- [37] V. Priyadarshini, P. V. Salija, A. S. Divya and V. Kumar, "Influence of Strontium Substitution on Ferroelectric-Relaxor Transition in PLZT (7/60/40)," *J. Am. Ceram. Soc.*, **93** (2010) 3584.
- [38] L. B. Kong, J. Ma, R. F. Zhang and T. S. Zhang, "Fabrication and characterization of lead lanthanum zirconate titanate PLZT (7/60/40) ceramics from oxides," *J. Alloys Compd.*, **339** (2002) 167.

- [39] R. L. Withers, Y. Liu, T. R. Welberry, “Structured diffuse scattering and the fundamental 1-d dipolar unit in PLZT $(\text{Pb}_{1-y}\text{La}_y)_{1-\alpha}(\text{Zr}_{1-x}\text{Ti}_x)_{1-\beta}\text{O}_3$ (7.5/65/35) and (7.0/60/40) transparent ferroelectric ceramics,” *J. Solid State Chem.*, **182** (2009) 348.
- [40] W. Y. Pan, Q. M. Zhang, Q. Y. Jiang and L. E. Cross, “Electric field induced strain in $(\text{Pb},\text{La})(\text{Ti},\text{Zr})\text{O}_3$ ferroelectric ceramics near the tetragonal-rhombohedral morphotropic phase boundary,” *Ferroelectrics.*, **88** (1988) 1.
- [41] D. Damjanovic, “A morphotropic phase boundary system based on polarization rotation and polarization extension,” *Appl. Phys. Lett.*, **97** (2010) 062906.
- [42] A. Ghosh and D. Damjanovic, “Antiferroelectric–ferroelectric phase boundary enhances polarization extension in rhombohedral $\text{Pb}(\text{Zr},\text{Ti})\text{O}_3$,” *Appl. Phys. Lett.*, **99** (2011) 232906.
- [43] P. Muralt, “Recent progress in materials issues for piezoelectric MEMS,” *J. Am. Ceram. Soc.*, **91** (2008) 1385.

LAXMI PRIYA S. "FERROELECTRIC THIN FILMS FOR MICROACTUATOR APPLICATIONS". THESIS. CENTRE FOR MATERIALS FOR ELECTRONICS TECHNOLOGY (C-MET), UNIVERSITY OF CALICUT, 2018.

Improved piezoelectric response in {110}-oriented B – site acceptor doped PLZT (8/65/35) thin films

● Contents ●	4.1 Introduction
	4.2 Experimental
	4.3 Results and Discussion
	4.4 Conclusion
	References

Some of the contents of this chapter have appeared in the following research publication

- [1] **S. Laxmi Priya**, V. Kumar, Shogo Nishio, Isaku Kanno, “Improved piezoelectric response in {110}-oriented B-site acceptor doped PLZT (8/65/35) thin films”, *Integrated Ferroelectrics*, 176, 210-219 (2016).

4.1 Introduction

Superior piezoelectric properties of lead-based perovskite type solid solution systems such as PLZT, having compositions near the morphotropic phase boundary (MPB) are ideal candidates for MEMS applications. The dielectric, piezoelectric and ferroelectric characteristics of such perovskite based thin films are related to their structure and texture and is possible to change the nature of material from hard to soft and vice versa by varying the nature and concentration of dopants. The electrical characteristics of A-site La^{3+} substituted PZT have already been well correlated with their charge compensation mechanism¹. Aliovalent acceptor doping in the B-site of PZT have been reported to lead to degradation in the electromechanical characteristics^{2,3}. When a ferroelectric material like PZT is doped with an acceptor like Fe^{3+} or Fe^{2+} of lower valence than the host atom Ti^{4+} , a positively charged oxygen vacancy \dot{V}_O is created which neutralizes the negative charge induced by the acceptor dopant, Fe'_{Ti} or Fe''_{Ti} . When Nb^{5+} is used as the donor dopant replacing Ti^{4+} , additional electrons or lead vacancies (V''_{Pb}) are introduced as the charge compensating defect.

Consider a trivalent acceptor dopant M^{3+} at the B-site of perovskite structure, which causes charge compensation through the creation of oxygen vacancy as represented by equation (4.1)



Here M'_B represents a single negatively charged acceptor at the B-site and \dot{V}_O represents a doubly positively charged oxygen vacancy. The negatively charged trivalent B-site acceptor dopant forms a defect dipole of the type $[M'_B - \dot{V}_O]$. Figure 4.1 shows an EPR spectrum reporting signals at $g \approx 5.7$ and $g \approx$

4.3 that are characteristics of $[Fe'_{Ti} - \ddot{V}_O]$ defect-dipole in PZT of MPB composition⁴.

Such defect dipoles that are mobile cause pinning of ferroelectric domain thereby suppressing nucleation and growth of domain in the direction of the applied field.

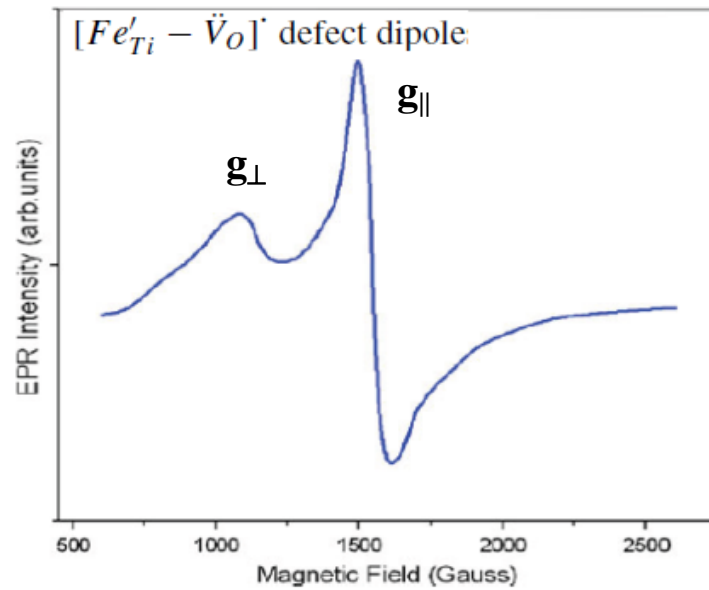


Figure 4.1: EPR spectra of $[Fe'_{Ti} - \ddot{V}_O]$ defect dipole in PSZTFe.

[Source: K. P. Rema, Vinod K. Etacheri and V. Kumar, "Influence of low trivalent iron doping on the electrical characteristics of PZT," *J. MaterSci: Mater Electron.*, 21 (2010) 1149].

However in PLZT, oxygen vacancies are not formed as charge compensation takes place through A-cation vacancies. These are represented by equations (4.2) and (4.3),



where M'_{Ti} is a negatively charged acceptor at the B-site, \ddot{V}_O is a doubly positively charged oxygen vacancy, V''_{Pb} is a doubly negatively charged A-site vacancy and La_{Pb} represents a positively charged A-site with respect to the neutral lattice according to Kröger and Vink notation. Hence PLZT are ideal host systems for B-site aliovalent acceptor dopants. Significantly most of the B-site aliovalent dopants, offer the possibility of structural distortions thereby providing a potential pathway for enhancing their electromechanical properties for sensor and actuator applications⁵⁻¹⁰. For piezoelectric thin films, preferential crystallographic orientation can also contribute much for tailoring their piezoelectric properties^{11,12}. Preferentially oriented ferroelectric films will restrict the polarization to lie in directions desired for applications thereby providing significant performance advantage over randomly oriented ones¹³. Therefore, in our study, we have investigated the influence of aliovalent B-site acceptor dopants (Fe^{3+} , Mn^{3+} and Cu^{2+}) on the structure, dielectric and piezoelectric properties in {110}-preferentially oriented PLZT (8/65/35) thin films. PLZT $(Pb_{1-x}La_x)(Zr_{0.65}Ti_{0.35})O_3$ with $x = 0.08$ lies very close to the MPB and adopts a rhombohedral structure¹⁴. In PLZT (8/65/35) thin films, {110} texture assumes significance due to the coexistence of Rhombohedral, Monoclinic and Tetragonal phases at MPB^{15,16}. The improved transverse piezoelectric coefficient, $|e_{31,f}|$ and electric field induced bipolar strain characteristics of such acceptor-doped PLZT films have been correlated with their crystal structure. Mechanism for higher bipolar strain in Cu^{2+} and Mn^{3+} doped PLZT films have also been studied and are reported.

4.2 Experimental

Highly stable precursor solutions of PLZT (8/65/35) with 0.002 moles of Fe^{3+} , Mn^{3+} and Cu^{2+} acceptor dopants at the B-site, having the general formulas $(\text{Pb}_{0.92}\text{La}_{0.08})(\text{Zr}_{0.65}\text{Ti}_{0.35})_z\text{M}_y\text{O}_3$; $z = 0.98(1-3y/4)$, $\text{M} = \text{Fe}^{3+}$, Mn^{3+} and $(\text{Pb}_{0.92}\text{La}_{0.08})(\text{Zr}_{0.65}\text{Ti}_{0.35})_z\text{N}_y\text{O}_3$; $z = 0.98(1-y/2)$, $\text{N} = \text{Cu}^{2+}$ with 10% excess lead was prepared by sol-gel method as per the procedure adopted from our previous work¹⁷. The reactants, lead acetate (99%, Merck, India), lanthanum acetyl acetonate hydrate (Sigma Aldrich, India), zirconium acetyl acetonate (98%, Merck, India) were refluxed with different acceptor dopants such as Iron (III) acetyl acetonate (tech.-grade, Sigma Aldrich, Germany), Manganese (III) acetyl acetonate (tech.-grade, Sigma Aldrich, Germany) and Copper (II) acetyl acetonate (tech.-grade, Sigma Aldrich, Germany). The three clear solutions thus obtained were mixed individually with solution of titanium (IV) isopropoxide (97%, Sigma Aldrich, India) in isopropyl alcohol with equimolar amounts of acetyl acetone ($\geq 98\%$, Merck, India) as the chelating agent. The stable precursor solution thus obtained was then spin coated on platinised silicon substrate [(111) Pt/Ti/SiO₂/Si; Inostek, Korea]. To obtain {110}-preferential orientation, SrTiO₃ layer having ~45 nm thickness and (110) orientation was used as the buffer layer since it can easily allow the effective crystallization of PZT thin films. Above it, Fe^{3+} doped PLZT (8/65/35) film layer was coated. The same procedure was adopted to obtain Mn^{3+} and Cu^{2+} doped PLZT thin films. The coating was done at a speed of 4000 rpm for 25 seconds. In the case of all the thin film layers including SrTiO₃, after coating each layer, they were dried at 110⁰C for 10 min and then annealed at temperature of 400⁰C for 10 min and finally at 600⁰C for 20

min^{12,15}. This process was repeated till the film reached 2.0 μm thickness since thickness is a very important factor in determining the ferroelectric and piezoelectric properties. Another prominent factor is internal stress inside a ferroelectric material that can contribute to hindrance in domain switching thereby resulting in increased coercive field. This was already reported by Lebedev and Akedo¹⁸ in PZT thin films with an asymmetrical hysteresis and increased electrical breakdown. Hence decrease in internal stress with increase in film thickness is very important for improving the piezoelectric properties.

The preferential crystallographic orientation of the films were determined using an X-ray diffractometer (Model: D5005, Bruker, Germany) and the crystalline phases were analysed with a Raman spectrometer (Model: DXR, Thermo Scientific, USA). Gold top electrodes of 350 nm thickness were deposited on the films using a Vacuum coater (Model: 12A4D, Hind High Vacuum, India). Dielectric characteristics were measured using an impedance analyzer (HP 4294A, Agilent, USA). For the measurement of piezoelectric properties, rectangular beams of substrate were diced out and the transverse piezoelectric properties were measured as described in our previous studies^{19,20}. The transverse piezoelectric properties of PLZT thin films were evaluated using unimorph cantilevers of PLZT/Si. Piezoelectric vibration was generated by applying sine wave voltage between top and bottom electrodes. The tip displacement was measured using a laser Doppler vibrometer (Model: AT-3500, Graphtec, Japan) and a laser interferometer (Model: AT-1100, Graphtec, Japan). The non-linearity was determined from the slope of the linear curve fits of $|e_{31,f}|$ curves.

4.3 Results and Discussion

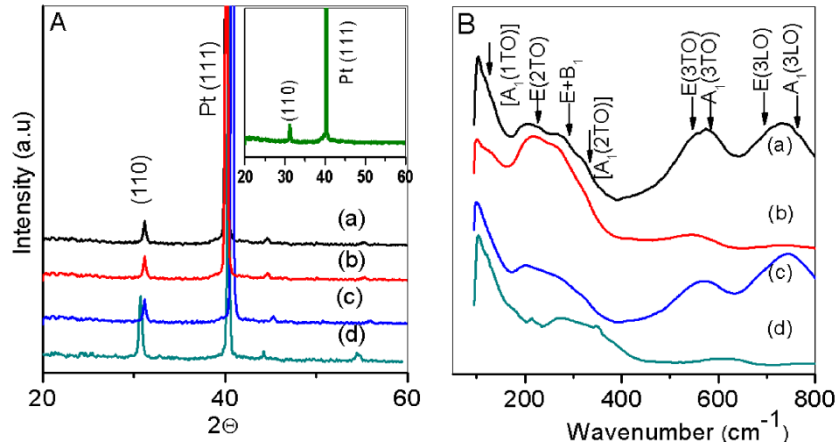


Figure 4.2: (A) XRD patterns of acceptor (X) doped PLZT (8/65/35) thin films; X= (a) Fe³⁺, (b) Cu²⁺, (c) Mn³⁺ and (d) Pure PLZT (Inset shows the XRD of ST buffer layer on Pt (111)/Ti/SiO₂/Si substrate) and (B) Raman spectra of (a) Fe³⁺-doped, (b) Cu²⁺-doped, (c) Mn³⁺-doped and (d) undoped PLZT thin films on (111)Pt/Ti/SiO₂/Si substrate.

The X-ray diffraction patterns of Fe³⁺, Cu²⁺ and Mn³⁺ doped PLZT (8/65/35) thin films are shown in Figure 4.2 (A). It is seen that all the films exhibit preferential {110}-orientation. The Raman spectra in Figure 4.2 (B) gives a clear picture of the crystalline modifications of acceptor doped PLZT (8/65/35) thin films. Raman spectral analysis of rhombohedral (R3m), monoclinic (Pm) and tetragonal (P4mm) phases near the MPB region is investigated by normal coordinate analysis and are given in Figures 4.3, 4.4 and 4.5 respectively. The symmetry and number of normal modes of vibration are determined by group theory analysis. Γ_{total} (sum of normal modes of all ions) includes both the optic and acoustic modes. It is possible to determine the numbers and symmetry of modes belonging to Γ_{acoustic} , Γ_{optic} and Γ_{raman} on the basis of selection rules presented in character table²¹.

C_{3v}	E	$2C_3$	$3\sigma_v$	Selection rules	
A_1	1	1	1	T_z	$\alpha_{xx}^z + \alpha_{yy}^z, \alpha_{zz}^z$
A_2	1	1	-1	R_z	
E	2	-1	0	$(T_x, T_y) (R_x, R_y)$	$(\alpha_{xx}^y - \alpha_{yy}^y, \alpha_{xy}^x)$ $(\alpha_{xz}^x, \alpha_{yz}^y)$
χ_T	3	0	1		

R3m

ions	site symmetry	normal modes
Pb^{2+}	1a	$A_1 + E$
$Mg^{2+} / Nb^{5+} / Ti^{4+}$	1a	$A_1 + E$
O^{2-}	3b	$2A_1 + A_2 + 3E$



$$\Gamma_{\text{total}} = 4A_1 + A_2 + 5E$$



$$\Gamma_{\text{acoustic}} = A_1 + E$$



$$\Gamma_{\text{optic}} = 3A_1 + A_2 + 4E$$



$$\Gamma_{\text{Raman}} = 3A_1 + 4E$$

Figure 4.3: Character table and symmetry modes of rhombohedral phase (R3m).

[Source: A. Słodczyk, "Structural, dielectric and vibrational studies of lead magnesium niobate-lead titanate $(1-x)PbMg_{1/3}Nb_{2/3}O_3-xPbTiO_3$ solid solutions", Ph.D Thesis, University of Silesia (Katowice) and Université du Maine (Le Mans) (2006)].

C_s	E	σ^{xy}	Selection rules	
A_1	1	1	T_x, T_y, R_z	$\alpha_{xx}^{x,y}, \alpha_{yy}^{x,y}, \alpha_{zz}^{x,y}, \alpha_{xy}^{x,y}$
A_2	1	-1	T_z, R_x, R_y	$\alpha_{xz}^z, \alpha_{yz}^z$
χ_T	3	1		

Pm

ions	site symmetry	normal modes
Pb^{2+}	1a	$2A_1+A_2$
$Mg^{2+}/Nb^{5+}/Ti^{4+}$	1b	$2A_1+A_2$
O_{I}^{2-}	1a	$2A_1+A_2$
O_{II}^{2-}	1b	$2A_1+A_2$
O_{III}^{2-}	1b	$2A_1+A_2$

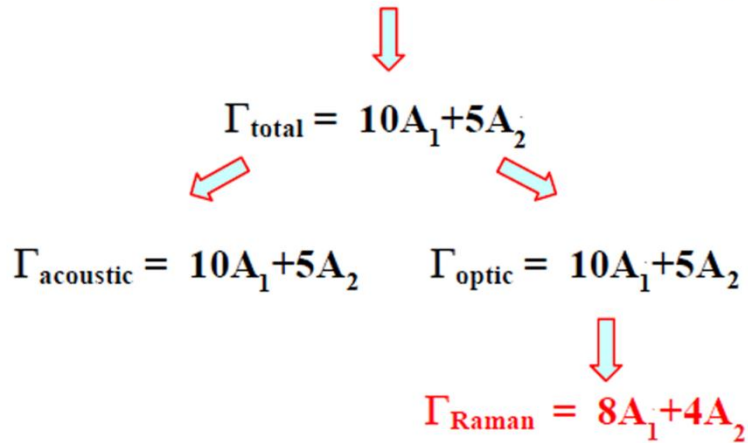


Figure 4.4: Character table and symmetry modes of monoclinic phase (Pm).

[Source: A. Słodczyk, "Structural, dielectric and vibrational studies of lead magnesium niobate-lead titanate (1-x)PbMg_{1/3}Nb_{2/3}O₃-xPbTiO₃ solid solutions", Ph.D Thesis, University of Silesia (Katowice) and Université du Maine (Le Mans) (2006)].

C_{4v}	E	$2C_4^z$	C_2^z	$2\sigma_v$	$2\sigma_d$	Selection rules	
A_1	1	1	1	1	1	T_z	$\alpha_{xx}^z + \alpha_{yy}^z, \alpha_{zz}^z$
A_2	1	1	1	-1	-1	R_z	
B_1	1	-1	1	1	-1		$\alpha_{xx} - \alpha_{yy}$
B_2	1	-1	1	-1	1		α_{xy}
E	2	0	-2	0	0	$(T_x, T_y); (R_x, R_y)$	$(\alpha_{xz}^x, \alpha_{yz}^y)$
χ_T	3	1	-1	1	1		

P4mm

ions	site symmetry	normal modes
Pb^{2+}	1a	$A_1 + E$
$Mg^{2+}/Nb^{5+}/Ti^{4+}$	1b	$A_1 + E$
O_{I}^{2-}	2c	$A_1 + B_1 + 2E$
O_{II}^{2-}	1b	$A_1 + E$



$$\Gamma_{\text{total}} = 4A_1 + B_1 + 5E$$



$$\Gamma_{\text{acoustic}} = A_1 + E$$



$$\Gamma_{\text{optic}} = 3A_1 + B_1 + 4E$$



$$\Gamma_{\text{Raman}} = 3A_1 + B_1 + 4E$$

Figure 4.5: Character table and symmetry modes of tetragonal phase (P4mm).

[Source: A. Slodczyk, "Structural, dielectric and vibrational studies of lead magnesium niobate-lead titanate $(1-x)PbMg_{1/3}Nb_{2/3}O_3-xPbTiO_3$ solid solutions", Ph.D Thesis, University of Silesia (Katowice) and Université du Maine (Le Mans) (2006)].

It is reported that for R3m, Pm and P4mm space groups, the group theory analysis predicts 7, 12 and 8 active raman lines²¹. A group theory analysis was done to interpret the Raman spectra. Two types of phonons – acoustic and optical phonons exist in solids with more than one atom in smallest unit cell. Acoustic mode exhibits Brillouin scattering resulting from scattering of photons by large scale, low-frequency phonons. Optical phonons that results from out-of-phase movements of lattice atoms can be infrared active or Raman active. Raman active optical phonons can indirectly interact with light through Raman scattering.

Therefore, for precise structure determination, the peaks in their Raman spectra were deconvoluted using Gauss-Lorentzian line shape approximation. The perfect overlap of the peak sum line with the obtained Raman peaks indicated the correctness of peak deconvolution. The deconvoluted Raman spectrum of pure PLZT is given in Figure 4.6 (D) for comparison. For Cu²⁺ and Mn³⁺ doped PLZT (8/65/35), the deconvoluted spectrum in Figures 4.6 (B) and (C) give 8 Raman active modes ($\Gamma_{\text{Raman}} = 3A_1 + B_1 + 4E$) confirming tetragonal structure (P4mm). In addition to this, the peaks obtained at ~140 cm⁻¹ and 326 cm⁻¹ are clear indications of tetragonal phase formation^{10,22}. The deconvoluted spectra of Fe³⁺ doped PLZT in Figure 4.6 (A) shows 7 Raman active modes ($\Gamma_{\text{Raman}} = 3A_1 + 4E$) indicating rhombohedral (R3m) symmetry. Interestingly, the peak at 550 cm⁻¹ in Figure 4.6 (A) is found to split in to E(3TO) and A₁(3TO) modes at 510 and 600 cm⁻¹ respectively clearly indicating the rhombohedral → tetragonal phase transformation²³. Thus in Fe³⁺ doped PLZT (8/65/35) thin films, small amounts of tetragonal phase coexist with the predominant rhombohedral phase.

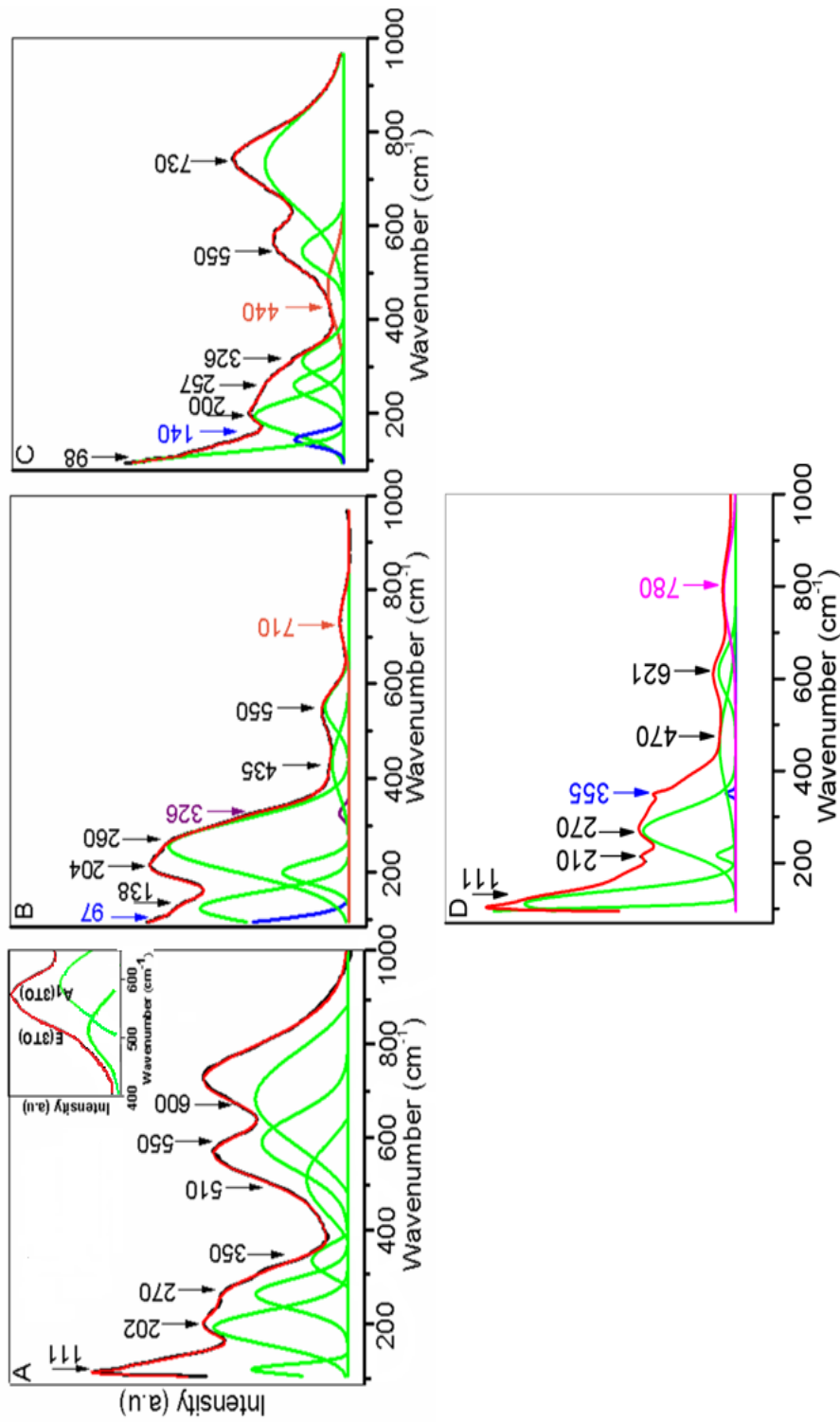


Figure 4.6: Deconvoluted Raman spectra of (A) Fe³⁺ doped PLZT (8/65/35), (B) Cu²⁺ doped PLZT (8/65/35), (C) Mn³⁺ doped PLZT (8/65/35) and (D) undoped PLZT (8/65/35).

Table 4.1 Dielectric and piezoelectric properties of acceptor doped PLZT (8/65/35) thin films

PLZT (8/65/35) thin films	Dielectric permittivity ϵ_r	Dielectric loss $\tan \delta$	Dielectric tunability at E=200kV/cm	Average $ e_{31,f} $ (C/m ²)
undoped	430	0.04	48.2%	3.3
Fe ³⁺ -doped	1050	0.03	62.1%	4.7
Cu ²⁺ -doped	740	0.04	58.9%	4.6
Mn ³⁺ -doped	500	0.04	50.3%	4.0

The dielectric permittivity, ϵ_r obtained for PLZT (8/65/35) thin films are comparable with those reported for PLZT (8/65/35) ceramics²⁴ and higher than those reported by Dutta *et. al*²⁵. Lower values of dielectric loss obtained (Table 4.1) for all the films also reflected their good quality.

Transverse piezoelectric properties of acceptor doped PLZT (8/65/35) thin films was evaluated from the deflection of PLZT/Pt/Ti/SiO₂/Si cantilevers by applying unipolar sine wave voltage. In this experiment, we measured the tip displacement at a frequency of 600Hz which was far away from the resonance frequency of the cantilevers. From the tip displacements, the transverse piezoelectric coefficient $|e_{31,f}|$ was evaluated as per equation (3.1) illustrated and explained in Chapter 3. Using the equation, we evaluated the piezoelectric properties of acceptor doped PLZT (8/65/35) thin films and the electric field dependence of $|e_{31,f}|$ is shown in Figure 4.7

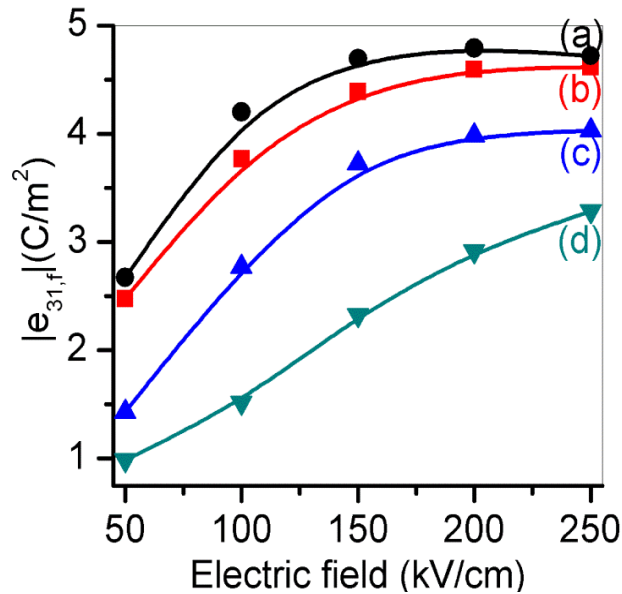


Figure 4.7: Transverse piezoelectric coefficient ($|e_{31,f}|$) in $\{110\}$ – oriented films of PL_xZT where $x =$ (a) Fe^{3+} , (b) Cu^{2+} , (c) Mn^{3+} and (d) pure PLZT (8/65/35).

All the three acceptor doped PLZT thin films showed clear piezoelectric response. From Figure 4.7, it is seen that maximum transverse piezoelectric coefficient is obtained for Fe^{3+} -doped PLZT (8/65/35). The higher $|e_{31,f}|$ value of Fe^{3+} -doped PLZT (8/65/35) is attributed to the polarisation rotation due to the coexistence of rhombohedral and tetragonal phases. This is also confirmed from its higher value of ϵ_r obtained as given in Table 4.1. Pure PLZT (8/65/35) exhibits rhombohedral symmetry with domains \vec{c} at an angle of $35^{\circ}16'$ and domains \vec{d} at an angle of 90° with the film normal as shown in figure 4.8 (A). For Cu^{2+} -doped PLZT and Mn^{3+} -doped PLZT, due to their tetragonal structure, domains \vec{a} are at an angle of 45° and \vec{b} at an angle of 90° with the film normal. The lower $|e_{31,f}|$ value of pure PLZT (8/65/35) is attributed to the predominant switching of $35^{\circ}16'$ domains which is confirmed by their relatively lower dielectric characteristics

as given in Table 4.1. The dielectric measurements were recorded at a frequency of 1 kHz.

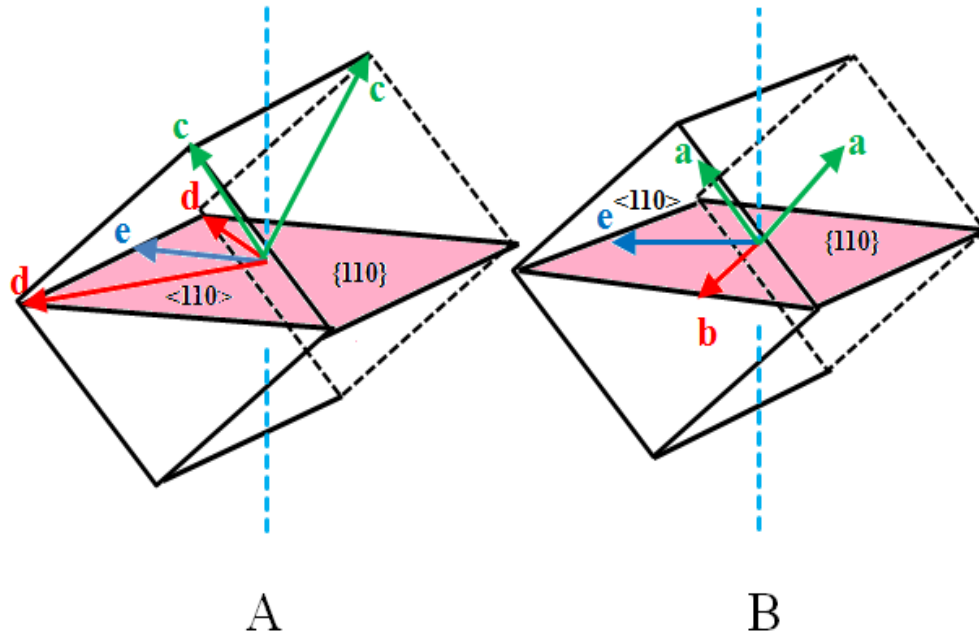


Figure 4.8: Domains in {110} - preferentially oriented PLZT thin films having (A) rhombohedral and (B) tetragonal structure.

The higher $|e_{31,f}|$ values of Cu^{2+} -doped PLZT in comparison to that of Mn^{3+} -doped one is due to the higher tetragonality of the former as evidenced from the Raman spectrum in Figure 4.6 (B). Higher tetragonality is also confirmed from the higher value of dielectric tunability and strain. In the case of Fe^{3+} -doped PLZT, where both rhombohedral and tetragonal phases coexist, the [110] polarisation vector (\vec{e}) lying in the (110) plane will be in a direction between [111] and [100] polar axis thereby promoting the polarisation to rotate from one direction to another¹².

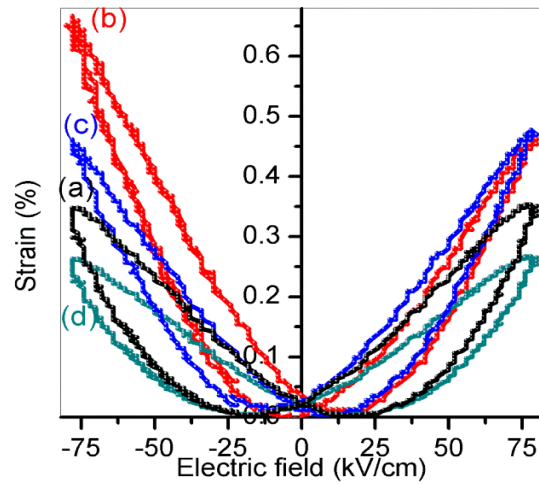


Figure 4.9: S-E curve under bipolar excitation in acceptor (X) doped PLZT (8/65/35) thin films; X= (a) Fe^{3+} , (b) Cu^{2+} , (c) Mn^{3+} and (d) Pure PLZT.

Figure 4.9 shows the field dependence of strain and Figure 4.10 shows Polarization-Electric field (P-E) curves of Fe^{3+} , Mn^{3+} and Cu^{2+} doped PLZT (8/65/35) thin films by applying bipolar sine wave voltage of ± 15 V at 50 Hz. All of them demonstrated domain switching of ferroelectricity.

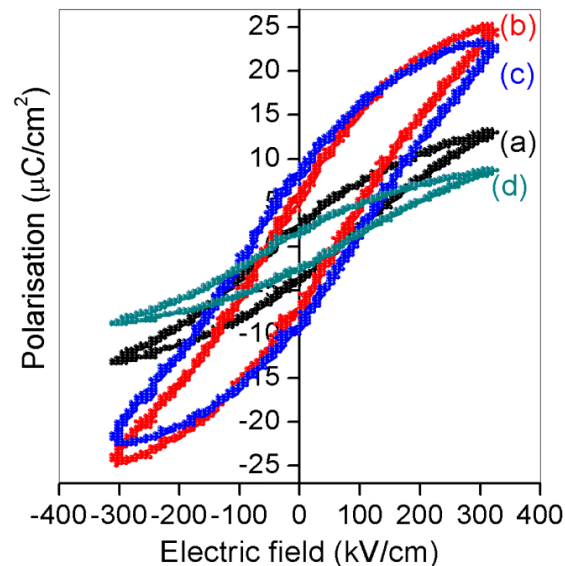


Figure 4.10: P-E hysteresis loop under bipolar excitation in acceptor (X) doped PLZT (8/65/35) thin films; X= (a) Fe^{3+} , (b) Cu^{2+} , (c) Mn^{3+} and (d) Pure PLZT.

Higher strain obtained at electric fields greater than -50kV/cm , is attributed to increased contribution from the switching of 90° domains. Here maximum strain was obtained for Cu^{2+} and Mn^{3+} doped PLZT. Hence higher tetragonality due to Jahn-Teller (J-T) distortion may be the reason for increased bipolar strain in Cu^{2+} and Mn^{3+} doped PLZT.

J-T distortion in Cu^{2+} and Mn^{3+} doped PLZT was confirmed from their absorption spectra shown in Figures 4.11 (A) and (B). The peaks in the absorption spectrum of Cu^{2+} doped PLZT observed at 13840 cm^{-1} , 15480 cm^{-1} and 17160 cm^{-1} respectively in Figure 4.11 (A) correspond to the three spin allowed transitions ${}^2\text{A}_{1g} \leftarrow {}^2\text{B}_{1g}$, ${}^2\text{B}_{2g} \leftarrow {}^2\text{B}_{1g}$ and ${}^2\text{E}_g \leftarrow {}^2\text{B}_{1g}$. The energy level diagrams are shown in Figure 4.12 (A).

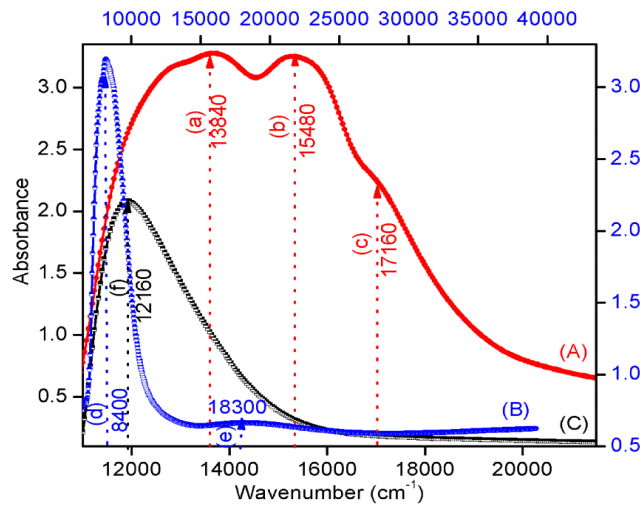


Figure 4.11: Absorption spectra obtained for (A) Cu^{2+} , (B) Mn^{3+} and (C) Fe^{3+} -doped PLZT (8/65/35) thin films.

For Mn^{3+} doped PLZT system, Mn^{3+} in MnO_6 octahedra adopts the high-spin state and hence two absorption peaks observed at 18300 and 8400 cm^{-1} in Figure 4.12 (B) correspond to ${}^5\text{B}_{2g} \leftarrow {}^5\text{B}_{1g}$ and ${}^5\text{A}_{1g} \leftarrow {}^5\text{B}_{1g}$ spin allowed transitions respectively^{26,27}. In Fe^{3+} -doped PLZT, only one absorption peak is observed in Figure 4.12 (C) corresponding to the $t_{2g} \rightarrow e_g$ transition.

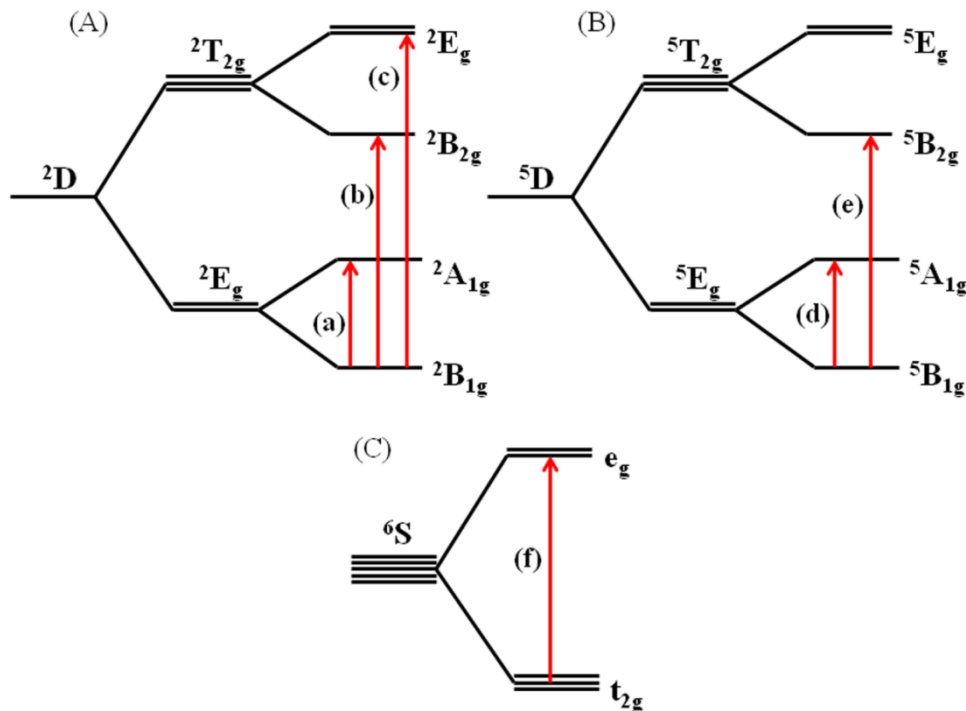


Figure 4.12: Crystal field splitting in (A) Cu^{2+} , (B) Mn^{3+} and (C) Fe^{3+} - doped PLZT thin films.

4.4 Conclusion

{110} – preferentially oriented PLZT (8/65/35) thin films of $2.0\ \mu\text{m}$ thickness with different B-site aliovalent acceptor dopants (Fe^{3+} , Cu^{2+} and Mn^{3+}) were prepared on (111) Pt/Ti/SiO₂/Si substrates using Sol-gel spin coating technique. All the prepared films exhibited clear piezoelectric response. Careful analysis of the Raman spectra, revealed the coexistence of rhombohedral and tetragonal phases in Fe^{3+} doped PLZT (8/65/35) which was found to exhibit the highest transverse piezoelectric coefficient, $|e_{31,f}|$. The increased tetragonality as a result of J-T distortion could induce increased bipolar strain in Cu^{2+} and Mn^{3+} doped PLZT(8/65/35) thin films. Cu^{2+} -doped PLZT with higher degree of tetragonality was found to exhibit maximum strain at higher electric fields indicating increased 90° domain switching.

References

- [1] K. P. Rema, A. S. Divya and V. Kumar, “Influence of low lanthanum doping on the electrical characteristics of PZT (53/47),” *J. Phys. D: Appl. Phys.*, **42** (2009) 075420.
- [2] K. H. Hardtl, “Defect structure of PLZT doped with Mn, Fe and Al,” *J. Am. Ceram. Soc.*, **64** (1981) 283.
- [3] K. P. Rema, Vinod K. Etacheri, V. Kumar, “Influence of low trivalent iron doping on the electrical characteristics of PZT,” *J. Mater Sci: Mater Electron.*, **21** (2010) 1149.
- [4] W. L. Warren, B. A. Tuttle, F. Christopher Rong, G. J. Gerardi and E. H. Poindexter, “Electron paramagnetic resonance investigation of acceptor centers in Pb(Zr,Ti)O₃ ceramics,” *J. Am. Ceram. Soc.*, **80** (1997) 680.
- [5] G. H. Haertling, “Ferroelectric Ceramics: History and technology,” *J. Am. Ceram. Soc.*, **82** (1999) 797.
- [6] V. Nagarajan, A. Roytburd, A. Stanishevsky, S. Prasertchoung, T. Zhao, L. Chen, J. Melngailis, O. Auciello and R. Ramesh, “Dynamics of ferroelastic domains in ferroelectric thin films,” *Nat. Mater.*, **2** (2003) 43.
- [7] Abdel-Baset M. A. Ibrahim, R. Murgan, M. K. A. Rahman, J. Osman, “Morphotropic phase boundary in ferroelectric materials,” *Ferroelectrics – Physical Effects*, Dr. Mickaël Lallart (Ed.) InTech (2011)
- [8] P. Muralt, “Recent progress in materials issues for piezoelectric MEMS,” *J. Am. Ceram. Soc.*, **91** (2008) 1385.
- [9] D. Damjanovic, “A morphotropic phase boundary system based on polarisation rotation and polarisation extension,” *Appl. Phys. Lett.*, **97** (2010) 062906.

- [10] S. Laxmi Priya, V. Kumar, F. Kurokawa and I. Kanno, "Transverse piezoelectric properties of {100}-oriented PLZT[x/65/35] thin films," *Mater. Chem. Phys.*, **151** (2015) 308.
- [11] S. E. Park and T. R. Shrout, "Ultrahigh strain and piezoelectric behavior in relaxor based ferroelectric single crystals," *J. Appl. Phys.*, **82** (1997) 1804.
- [12] D. Ambika, V. Kumar, K. Tomioka and I. Kanno, "Deposition of PZT thin films with {001}, {110} and {111} crystallographic orientations and their transverse piezoelectric characteristics," *Adv. Mat. Lett.*, **3** (2012) 102.
- [13] V. Vaithyanathan, J. Lettieri, W. Tian, A. Sharan, A. Vasudevaran and Y. L. Li, "C-axis oriented epitaxial BaTiO₃ films on (001) Si," *J. Appl. Phys.*, **100** (2006) 024108.
- [14] G. H. Haertling and C. E. Land, "Hot-pressed (Pb,La)(Zr,Ti)O₃ ferroelectric ceramics for electrooptic applications," *J. Am. Ceram. Soc.*, **54** (1971) 1.
- [15] B. Noheda, D. E. Cox, G. Shirane, R. Guo, B. Jones and L. E. Cross, "Stability of monoclinic phase in the ferroelectric perovskite PbZr_{1-x}Ti_xO₃," *Phys. Rev. B.*, **63** (2000) 014103.
- [16] D. Ambika, V. Kumar, H. Imai and I. Kanno, "Sol-gel deposition and piezoelectric properties of {110}-oriented Pb(Zr_{0.52}Ti_{0.48})O₃ thin films," *Appl. Phys. Lett.*, **96** (2010) 031909.
- [17] D. Ambika, V. Kumar, C. S. Suchand Sandeep and R. Philip, "Non-linear optical properties of (Pb_{1-x}Sr_x)TiO₃ thin films," *Appl. Phys. B.*, **97** (2009) 661.
- [18] M. Lebedev and J. Akedo, "Effect of thickness on the piezoelectric properties of Lead Zirconate Titanate films fabricated by Aerosol deposition method," *Jpn. J. Appl. Phys.*, **41** (2002) 6669.
- [19] I. Kanno, H. Kotera and K. Wasa, "Measurement of transverse piezoelectric properties of PZT thin films," *Sens. Actuators A Phys.*, **107** (2003) 68.

- [20] K. Sivanandan, T. A. Asha, V. Kumar and I. Kanno, “Fabrication and transverse piezoelectric characteristics of PZT thick-film actuators on alumina substrates,” *Sens. Actuators A Phys.*, **148** (2008) 134.
- [21] A. Slodczyk, P. Daniel and A. Kania, “Local phenomena of $(1-x)\text{PbMg}_{1/3}\text{Nb}_{2/3}\text{O}_3-x\text{PbTiO}_3$ single crystals ($0 \leq x \leq 0.38$) studied by Raman scattering,” *Phy. Rev. B.*, **77** (2008) 184114.
- [22] J. Frantti and V. Lantto, “Structural studies of Nd-modified lead zirconate titanate ceramics between 11 and 680 K at the morphotropic phase boundary,” *Phys. Rev. B.*, **56** (1997) 221.
- [23] J. Frantti, V. Lantto and J. Lappalainen, “Symmetry consideration of Raman modes in Nd-doped lead zirconate titanate thin films for structure characterization,” *J. Appl. Phys.*, **79** (1996) 1065.
- [24] V. I. Dimza, “Dielectric properties and structure of pure and doped (Mn,Fe,Co,Cu) PLZT 8/65/35,” *Ferroelectrics.*, **188** (1996) 53.
- [25] S. Dutta and R. N. P. Choudhary, “Effect of trivalent iron substitution on structure and properties of PLZT ceramics,” *Appl. Phys. A.*, **90** (2008) 323.
- [26] R. S. Drago, “Electronic absorption spectroscopy,” *Physical Methods in Inorganic Chemistry*, East-West Press Pvt. Ltd. New Delhi (1965) 135.
- [27] T. S. Davis, J. P. Fackler and M. J. Weeks, “Spectra of Manganese (III) complexes. The origin of the low-energy band,” *Inorg. Chem.*, **7** (1968) 1994.

LAXMI PRIYA S. "FERROELECTRIC THIN FILMS FOR MICROACTUATOR APPLICATIONS". THESIS. CENTRE FOR MATERIALS FOR ELECTRONICS TECHNOLOGY (C-MET), UNIVERSITY OF CALICUT, 2018.

Composition dependence of Transverse Piezoelectric properties of preferentially {110}- oriented (1 - x) PIN- x PT thin films

● Contents ●	5.1 Introduction
	5.2 Experimental
	5.3 Results and Discussions
	5.4 Conclusion
	References

Some of the contents of this chapter have appeared in the following research publication

S. Laxmi Priya, V. Kumar, Shogo Nishio, Isaku Kanno, “Composition dependence of transverse piezoelectric properties of preferentially {110}-oriented (1-x)PIN-xPT thin films”, *Journal of Alloys and Compounds* 688, (2016) 863-867.

5.1 Introduction

Lead-based solid solutions of relaxor ferroelectrics of the type $(1-x)\text{Pb}(\text{B}'\text{B}'')\text{O}_3-x\text{PbTiO}_3$, where $\text{B}' = \text{Mg}^{2+}, \text{Zn}^{2+}, \text{Ni}^{2+}, \text{Co}^{3+}, \text{Fe}^{3+}, \text{Sc}^{3+}, \text{In}^{3+}$; $\text{B}'' = \text{Nb}^{5+}, \text{Ta}^{5+}$ or W^{6+} are extensively used in actuators due to their excellent piezoelectric and electrostrictive properties. Such relaxor-PT piezoelectric materials provide higher dielectric permittivities, nearly twice than that of PZT ceramics. They usually possess a cubic perovskite type structure at higher temperatures and undergoes a ferroelectric phase transition at lower temperatures. Phase diagram of solid solutions of PIN with ferroelectric PT having the general formula $(1-x)\text{Pb}(\text{In}_{0.50}\text{Nb}_{0.50})\text{O}_3-x\text{PbTiO}_3$ near the morphotropic phase boundary in the range of $0.34 < x < 0.38$ that are reported to exhibit properties suitable for excellent piezoelectric applications¹ is shown in Figure 5.1.

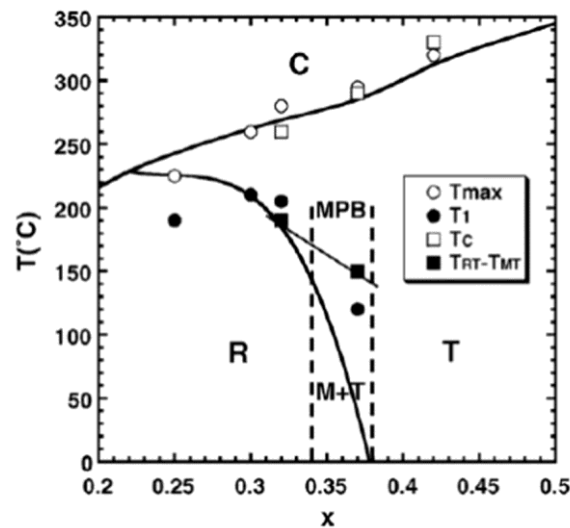


Figure 5.1: Phase diagrams of $(1-x)\text{PIN}-x\text{PT}$ system.

[Source: E. F. Alberta and A. S. Bhalla, "Piezoelectric properties of $\text{Pb}(\text{InNb})_{(1/2)}\text{O}_3-x\text{PbTiO}_3$ solid solution ceramics," *J. Korean Phys. Soc.*, 32 (1998) 1265.]

Eventhough numerous literature reports are available on relaxor ferroelectrics PMN-PT, PZN-PT and PIN-PMN-PT²⁻⁷, the dielectric and ferroelectric characteristics of them have been reported only on single crystals and ceramics²⁻⁴. H. Fu and R. Cohen⁵ reported theoretical demonstration of homogeneous polarization rotation between $\langle 111 \rangle_c$ ferroelectric rhombohedral and $\langle 001 \rangle_c$ ferroelectric tetragonal directions upon electric field application for perovskite oxides. Two different rotation pathways depicting two ferroelectric monoclinic phases were possible in them with the polarization constrained to a plane as given in Figure 5.2.

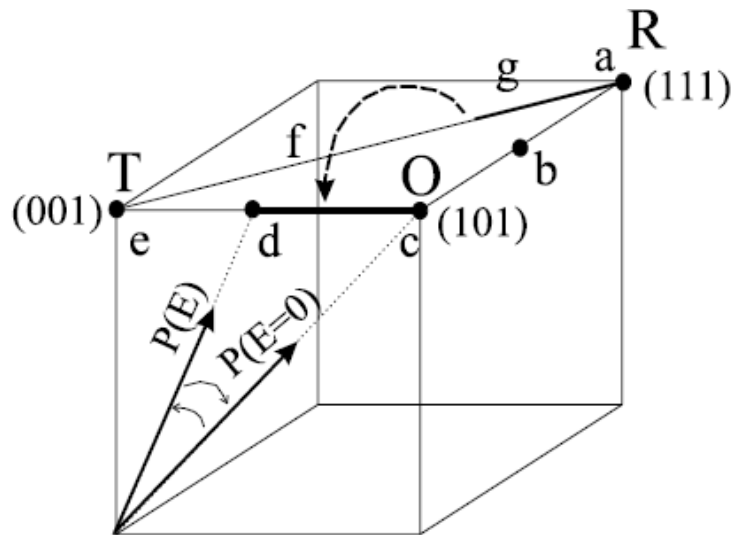


Figure 5.2: Two possible paths $R-T$ and $R-O-T$ for polarization direction to change from $[111]$ in the rhombohedral R phase to $[001]$ in the tetragonal T phase. The thickest lines represent path followed by polarization in PZN-8%PT upon electric field application. The solid arrows demonstrate the orientation of polarization in a particular domain with and without electric field.

[Source: H. Fu and R. Cohen, "Polarization rotation mechanism for ultrahigh electromechanical response in single-crystal piezoelectrics," *Nature (London)* 403 (2000) 281].

The monoclinic phase in PZT lies along the pseudocubic [110] and represents a-g-f-e path with a flat internal energy for the polarization to rotate between the rhombohedral and tetragonal phases whereas the monoclinic phase in PZN-8%PT⁸ represents the rotation path along a-c-d-e. Therefore the polarization rotation theory proposed by H. Fu and R. Cohen⁵ explained that the origin of large piezoelectric response was due to the large c-axis polarization variation facilitating polarization rotation.

The results obtained by Noheda *et al.*⁹ (Figure 5.3) is very consistent and reproduces the MPB of Jaffe *et al.*¹⁰ (Figure 5.4). On applying an electric field, the polar axis gets rotated causing monoclinic distortion which is retained even after the field is removed. This in turn can lead to the origin of high piezoelectric responses in PZT.

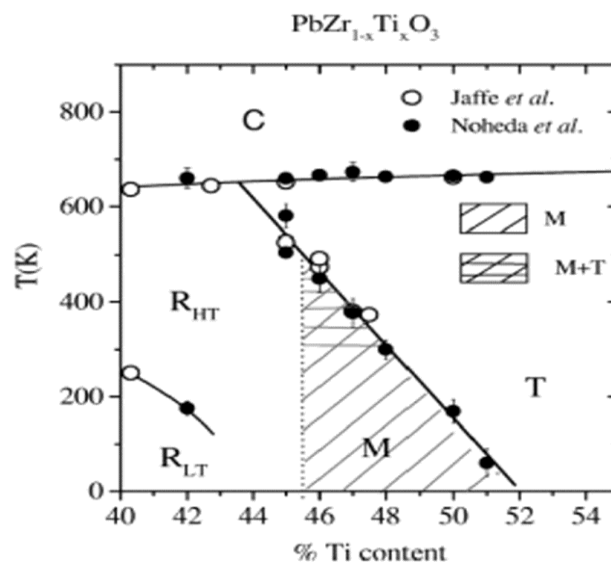


Figure 5.3: New PZT diagram around MPB.

[Source: B. Noheda, G. E. Cox and H. Shirane, "Stability of the monoclinic phase in the ferroelectric perovskite $PbZr_xTi_{1-x}O_3$," *Phy. Rev. B.*, 63 (2000) 014103].

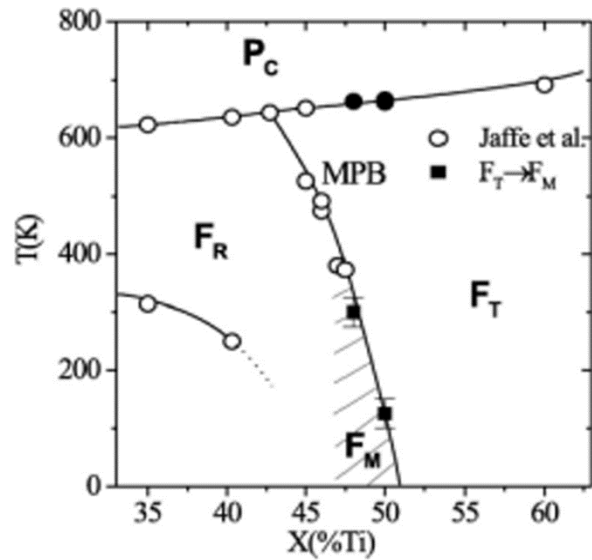


Figure 5.4: PZT phase diagram close to MPB reported by Jaffe et al.

[Source: B. Jaffe, W. R. Cook and H. Jaffe, "Piezoelectric ceramics," Academic press, London (1971)].

PMN-PT and PZN-PT single crystals were also reported to exhibit ultrahigh piezoelectric responses^{6,7,11} superior than conventional piezoelectrics and hence proved to be the most promising materials for next generation transducers and actuators. The presence of about 10-15% metastable orthorhombic phase in rhombohedral crystals was the possible reason for the extremely high electromechanical properties in PZT-PT poled along $\langle 011 \rangle$ ¹². For PMN-PT system, the MPB region lies at $x \cong 0.30$ separating the rhombohedral phase and monoclinic (M_C) phase^{13,14}. Neutron and X-ray diffraction studies in $\langle 001 \rangle$ directed field induces the presence of a monoclinic M_A phase in rhombohedral PMN-PT at room temperature and the presence of a M_C phase at higher temperatures¹⁵. The largest d_{33} value of ~ 3000 pC/N was measured in the rhombohedral phase (M_A) that are fully poled and d_{33} values in M_C region are found to be much smaller. Bokov *et. al*² suggested that PMN-PT

crystals when used as piezoelectric components should be in the rhombohedral phase close to MPB in order to obtain large d_{33} values and should be far away from MPB to avoid the appearance of M_C phase.

For piezoelectric thin films, achieving desired crystalline structure and preferential orientation¹⁶⁻¹⁹ are the two most important criteria for optimising their piezoelectric properties, especially the transverse piezoelectric coefficient, $|e_{31,f}|$ for MEMS applications^{9,20,21,22}. For thin film compositions at or near MPB, preferential {110}-orientation is significant in view of the coexistence of rhombohedral, monoclinic and tetragonal phases.

Since no study has yet been reported on PIN-PT thin films, we have focussed our attention in preparing preferentially {110}-oriented thin films of PIN-PT having compositions at the MPB region where rhombohedral, monoclinic and tetragonal structures and also studied their suitability for microactuator applications by determining their transverse piezoelectric coefficient $|e_{31,f}|$. Epitaxial growth of thin films on silicon substrates is important since the leakage current and optical scattering offered by them is lower when compared to that of polycrystalline films²³. For fabrication of thin films by spin-coating technique, a hybrid Metallo-Organic Decomposition (MOD) and Sol-gel method is adopted for the preparation of the precursor solution.

5.2 Experimental

Stable precursor solutions of $(1-x)$ PIN- x PT were prepared by a hybrid Metallo-Organic Decomposition (MOD) and Sol-gel process as per the procedure described in our earlier work^{24,25}. Metallo-organic decomposition (MOD) process uses metal carboxylate precursors with large carbon chains like 2-ethyl hexanoate, neodecanoate ligands etc^{26,27,28}. In our work, the reactants, lead acetate (99%, Merck, India) and Indium acetyl acetonate were refluxed in 2-ethyl hexanoic acid (99%, Sigma Aldrich, India). The excess 2-

ethyl hexanoic acid was removed by distillation and the resulting residue was dissolved in Isopropyl alcohol containing titanium (IV) isopropoxide (97%, Sigma Aldrich, India) and niobium (V) ethoxide (99.999%, Alfa Aesar, India) with acetyl acetone ($\geq 98\%$, Merck, India) as the chelating agent to yield a highly stable precursor solution. The obtained stable solution was spin-coated on (111) Pt/Ti/SiO₂/Si substrate (Inostek, Korea). The flow chart demonstrating the synthesis of $(1-x)$ PIN- x PT precursor solution is given in Figure 5.5.

SrTiO₃ (ST) layer having 45 nm thickness was coated on the silicon substrate as a buffer layer at a speed of 4000 rpm for 25 s. Moon *et.al*²⁹ and Brinker *et.al*³⁰ gave reports regarding the use of ST seed layer for low-temperature crystallization of PZT and also in minimizing shrinkage stresses during thin film crystallization by increasing the inorganic content in precursors. In addition to preventing inter diffusion and oxidation reactions, buffer layers act as templates for achieving the preferential crystallographic orientation in the PZT layers deposited over them^{31,32,33}.

Each coated film layer were dried at 110⁰C for 15 min and then annealed at a temperature of 400⁰C for 10 min and finally at 600⁰C for 20 min^{34,35}. This process was repeated to get perfectly {110}-oriented $(1-x)$ PIN- x PT thin films of 2.0 μ m thickness. The crystallographic orientation of the prepared films were determined using an X-ray diffractometer (Model: D5005, Bruker, Germany) and the crystalline phases were analysed with a Raman Spectrometer (Model: DXR, Thermo Scientific, USA). For precise determination of the crystal structure, deconvolution of the Raman spectra using Gauss-Lorentzian line shape approximation was done for all the three compositions. The perfect overlap of the peak sum line with the obtained Raman peaks indicated the correctness of the peak deconvolution. Gold top electrodes were deposited by a vacuum coater (Model: 12A4D, Hind High Vacuum, India) on the prepared films for dielectric and piezoelectric

characterisation. Capacitance and dielectric losses were measured at 1 kHz, using an impedance analyzer (HP 4294A, Agilent, USA). For the measurement of piezoelectric properties, rectangular specimens of dimensions of PIN-PT films were diced out from the substrate.

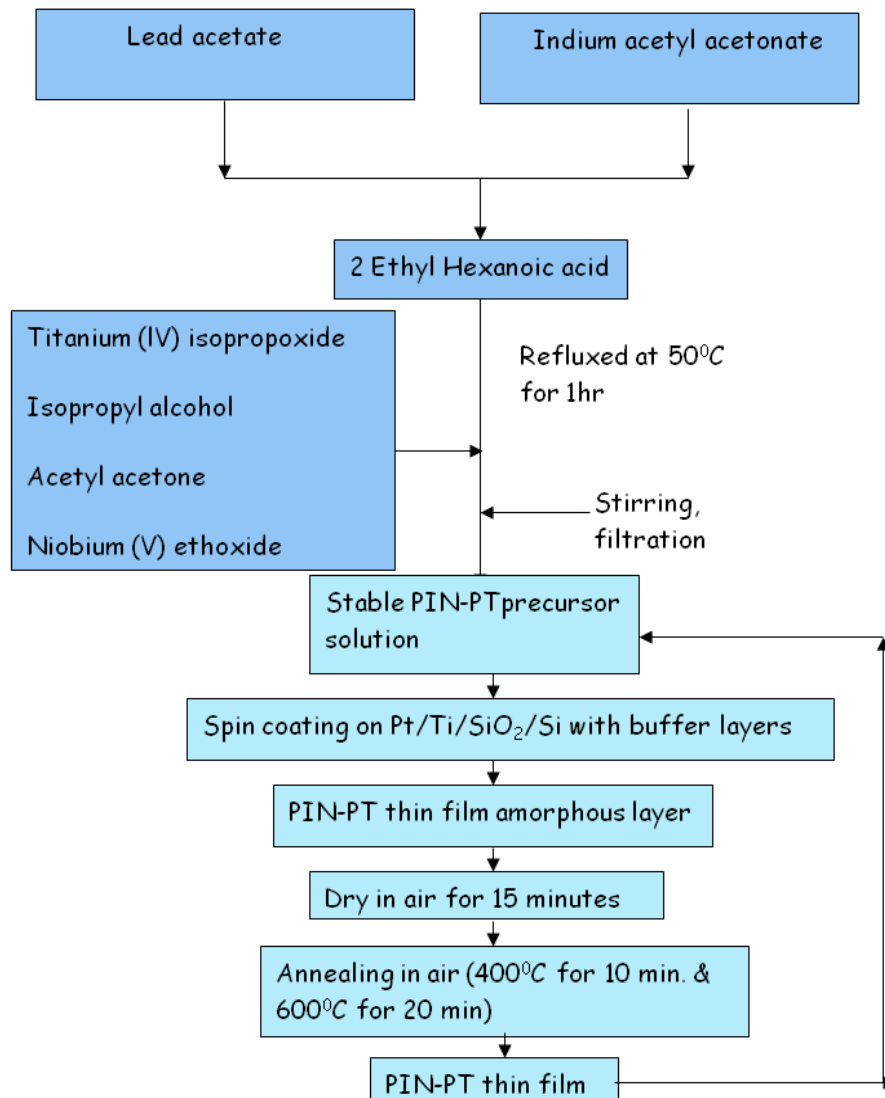


Figure 5.5: Synthesis of $(1-x)$ PIN- x PT precursor solution.

The transverse piezoelectric properties of the PIN-PT thin films were evaluated using unimorph cantilevers of PIN-PT/Pt/Ti/SiO₂/Si. The

measurement system and details of measurement have been described in the previous reports^{36,37}. Application of sine wave voltage between upper and bottom electrodes generates piezoelectric vibration and the tip displacement was measured using a laser Doppler vibrometer (Model: AT-3500, Graphtec, Japan) and a laser interferometer (Model: AT-1100, Graphtec, Japan). The non-linearity was determined from the slope of the linear curve fits of $|e_{31,f}|$ curves.

5.3 Results and Discussions

Figure 5.6 (A) shows the X-ray diffraction (XRD) patterns of $(1-x)$ PIN- x PT ($x = 0.36, 0.38, 0.40$) thin films on silicon substrates. From Figure 5.6 (A), it is clear that all the films exhibit pure perovskite phase and {110}-preferred orientation. The high degree of {110}-preferential orientation was achieved with the use of SrTiO₃ (ST) as the buffer layer^{34,35}. Increase in titanium content leads to a decrease in unit cell volume on moving from $x = 0.36$ to $x = 0.40$. The development of a shoulder in the (110) diffraction peak at $2\theta \approx 32^\circ$ also indicate structural transition to the tetragonal phase. The Raman spectra given in Figure 5.6 (B) give a clear picture of the crystalline modifications of PIN- x PT compositions across the morphotropic phase boundary.

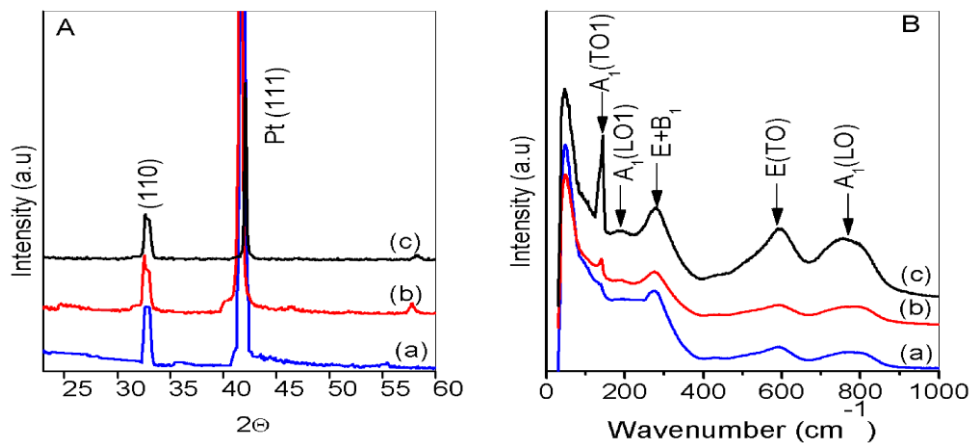


Figure 5.6: (A) XRD patterns and (B) Raman spectra of {110}-oriented $(1-x)$ PIN- x PT thin films (a) $x = 0.36$, (b) $x = 0.38$, (c) $x = 0.40$ on (111) Pt/Ti/SiO₂/Si substrate.

For rhombohedral symmetry with $R3m$ space group, there will be 7 active modes ($\Gamma_{\text{Raman}} = A_{1g} + E_g + 2F_{2g}$) in the Raman spectra. These 7 peaks are clearly evidenced from the deconvoluted Raman spectra of PIN-0.36PT as shown in Figure 5.7 (a). The spectra of PIN-0.38PT [Figure 5.7 (b)] gives 12 Raman-active modes ($\Gamma_{\text{Raman}} = 8A_1 + 4A_2$) which demonstrates it as being the monoclinic phase with space group Cm . For compositions having $x = 0.40$, the $A_1(\text{TO}_1)$ phonon mode at 140 cm^{-1} becomes more sharper. Also peaks in the Raman spectra of PIN-0.40PT could be deconvoluted with 8 Raman-active modes ($\Gamma_{\text{Raman}} = 3A_1 + B_1 + 4E$) as in Figure 5.7 (c). This clearly indicates the tetragonal phase ($P4mm$) of PIN-0.40PT³⁸.

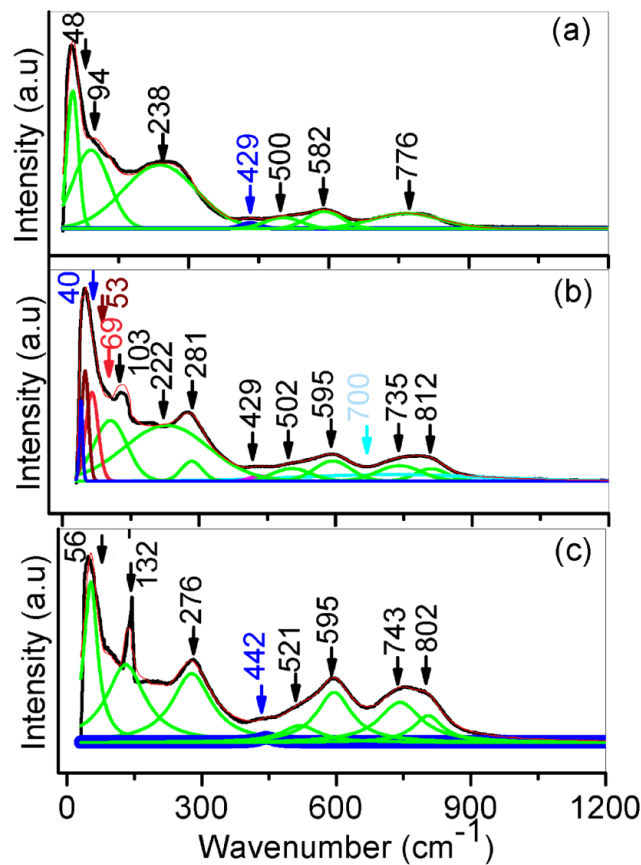


Figure 5.7: Deconvoluted Raman spectra of (a) PIN- 0.36PT, (b) PIN- 0.38PT and (c) PIN-0.40PT.

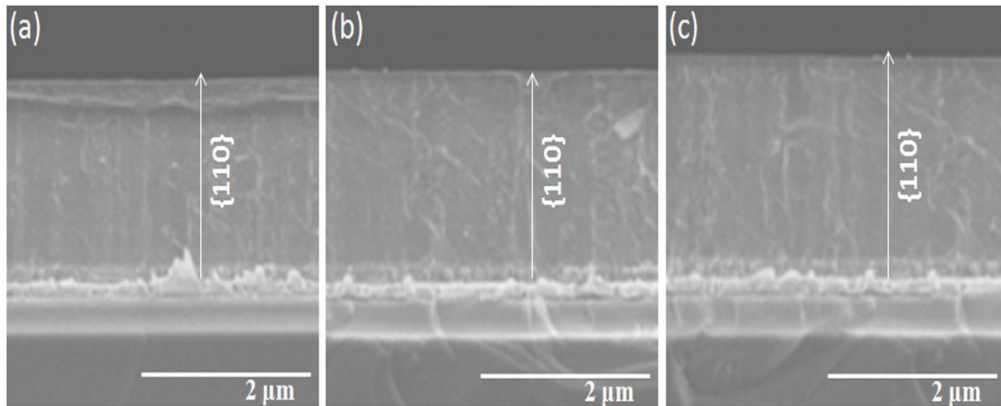


Figure 5.8: HRSEM of the cross-section of the (a) PIN- 0.36PT, (b) PIN- 0.38PT and (c) PIN-0.40PT thin films.

Here all the films exhibited dense columnar microstructure (Figure 5.8).

Transverse piezoelectric properties of the PIN-PT thin films were evaluated from the deflection of PIN-PT/Pt/Ti/SiO₂/Si cantilevers by applying unipolar sine wave voltage. In this experiment, we measured the tip displacement at a frequency of 600Hz which is far away from the resonance frequency of the cantilever. From the tip displacements, the transverse piezoelectric coefficient $|e_{31,f}|$ was evaluated as per equation (3.1) given in Chapter 3.

From Figure 5.9, it is seen that maximum transverse piezoelectric coefficient is obtained for 0.60PIN-0.40PT thin film. PIN-0.38PT [Figure. 5.9 (b)] also shows $|e_{31,f}|$ value in close proximity to PIN-0.40PT. Since the polar axis of the monoclinic phase is in the (110) plane which lies in between that of the tetragonal (001) and rhombohedral (111) polar axes, excellent piezoelectric responses are obtained in the intermediate monoclinic phase³⁹.

The domains in $\{110\}$ -oriented rhombohedral, monoclinic and tetragonal phases are shown in Figures 5.10 A, B and C respectively. Domains \vec{f} which are at an angle θ with the $[001]$ (Figure. 5.10 (B)) lying in the $\{110\}$ plane can switch by 90° , towards the film normal thereby resulting in increased strain values. But in $\{110\}$ -oriented films with tetragonal structure [Figure 5.10(C)], domains \vec{a} are at an angle of 45° and \vec{b} at an angle of 90° from the film normal. Here, in addition to 90° switching of \vec{b} domains, 45° switching of \vec{a} domains is also possible thereby resulting in increased non-linearity in $|e_{31,f}|$. For films with rhombohedral structure, the domains \vec{c} are at an angle of $35^\circ 16'$ and \vec{d} at an angle of 90° from the film normal. In this case lower $|e_{31,f}|$ value is attributed to the predominant switching of $35^\circ 16'$ domains as confirmed by their relatively lower dielectric tunability (Table 5.1).

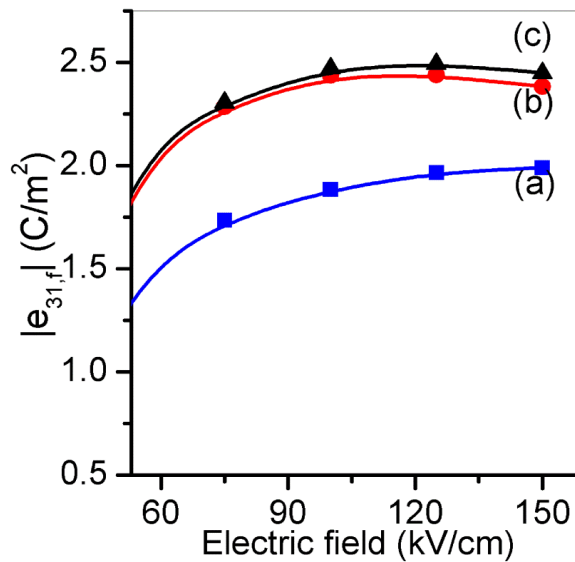


Figure 5.9: Transverse piezoelectric coefficient ($|e_{31,f}|$) in $\{110\}$ -oriented $(1-x)$ PIN- x PT films where (a) $x = 0.36$, (b) $x = 0.38$ and (c) $x = 0.40$.

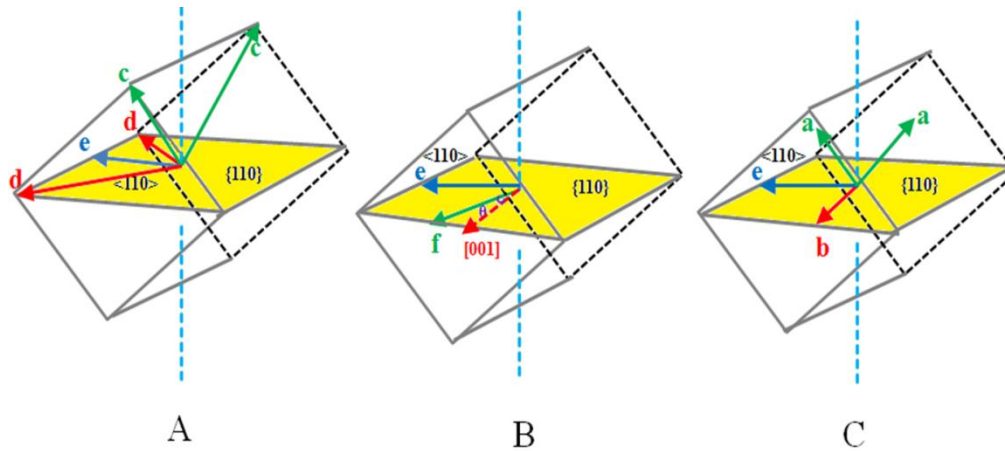


Figure 5.10: Domains in {110}-preferentially oriented $(1-x)$ PIN- x PT thin film having (A) rhombohedral (B) monoclinic and (C) tetragonal structure.

The dielectric results obtained are even better than those reported for PIN-PT ceramics⁴⁰. Figure 5.11 (a) and (b) shows the ϵ_r Vs T plots for PIN- x PT compositions measured at different frequencies with the sharpening of dielectric constant peaks with increased PT contents. The increased PT contents results in decreased relaxor behaviour by increasing size and interaction between polar nano regions.

Table 5.1: Dielectric and piezoelectric characteristics of $(1-x)$ PIN- x PT thin films

$(1-x)$ PIN- x PT	Crystal structure	Dielectric permittivity ϵ_r	Dielectric loss $\tan \delta$	Dielectric tunability at $E=200\text{kV/cm}$	Average transverse piezoelectric coefficient, $ e_{31,f} $ (C/m^2)
PIN-0.36PT	Rhombohedral	1800	0.07	43.0%	1.9
PIN-0.38PT	Monoclinic	1950	0.05	67.5%	2.4
PIN-0.40PT	Tetragonal	2000	0.05	59.7%	2.5

The dielectric characteristics obtained for $(1-x)$ PIN- x PT thin films are given in Table 5. 1. Here an increase in ferroelectric properties with increasing PT content can be seen. Also it is observed that the dielectric permittivities are higher as all domains including 180° domains contribute to it.

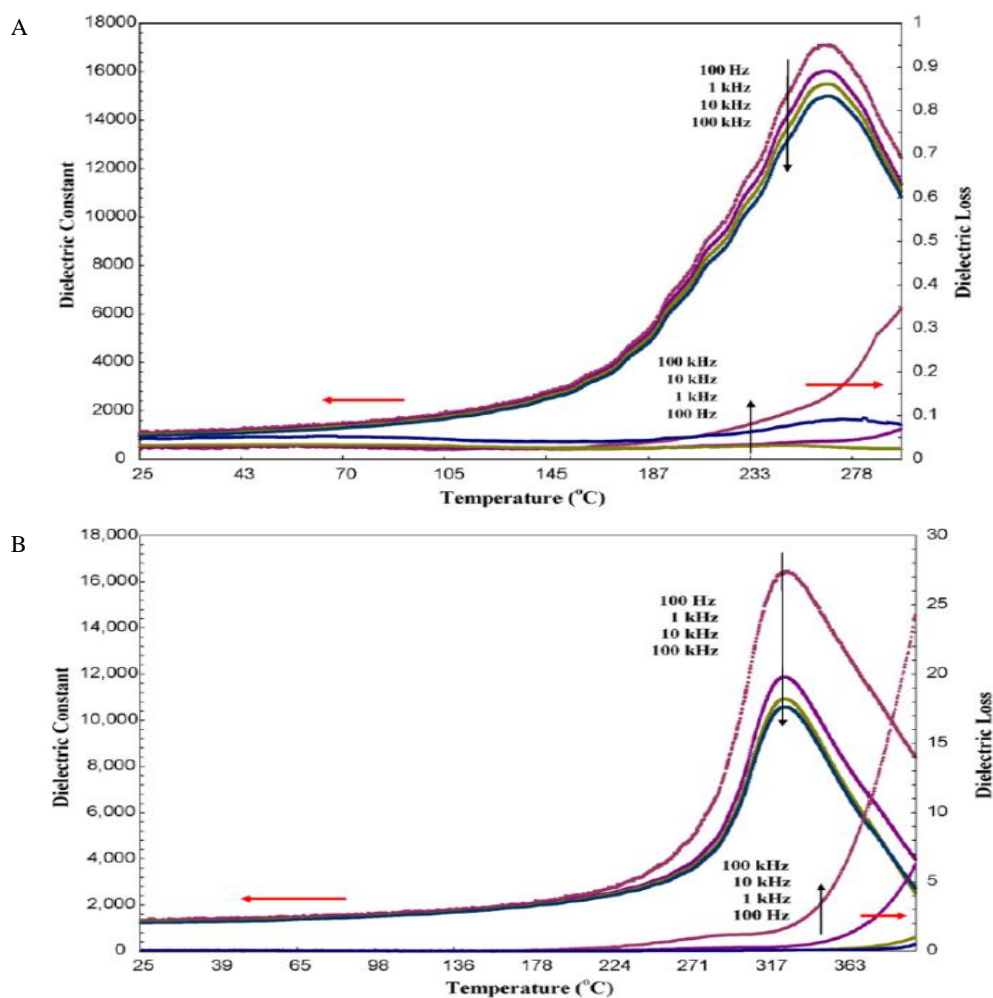


Figure 5.11: Temperature and frequency dependence of dielectric properties in (A) PIN-0.30PT, (B) PIN-0.40PT. Frequencies from top to bottom are 100 Hz, 1 kHz, 10 kHz and 100 kHz respectively.

[Source: S. Wongsanmai, X. Tan, S. Ananta and R. Yimnirun, "Dielectric and ferroelectric properties of fine grains $Pb(In_{1/2}Nb_{1/2})O_3$ - $PbTiO_3$ ceramics," *J. Alloys Compd.*, 454 (2008) 331].

Figure 5.12 shows the Strain-Electric field (S-E) and Figure 5.13 shows Polarisation-Electric field (P-E) curves of $(1-x)$ PIN- x PT thin films by applying bipolar sine wave voltage of ± 40 V at 30 Hz. Clear butterfly shaped curves are obtained for all the three films demonstrating domain switching of ferroelectricity. Higher bipolar strain is obtained for PIN-0.38PT thin film having the monoclinic phase. With increasing PT contents (from $x = 0.38$ to $x = 0.40$), the P_r value is found to increase from 5.0 to $7.2 \mu\text{C}/\text{cm}^2$ (Figure 5.13). The P_r values obtained are higher than those reported on PIN-PT ceramics⁴⁰. These results imply that the film composition and therefore the crystal structure as well as the film texture influence the piezoelectric properties.

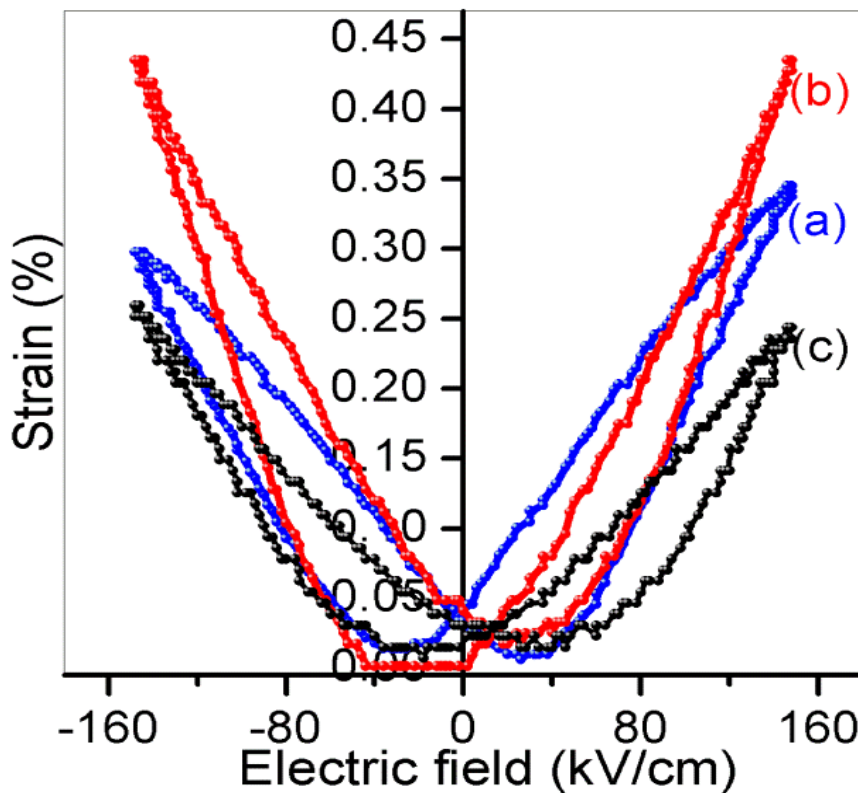


Figure 5.12: S-E curves under bipolar excitation in {110}-oriented $(1-x)$ PIN- x PT thin films (a) $x = 0.36$, (b) $x = 0.38$, (c) $x = 0.40$.

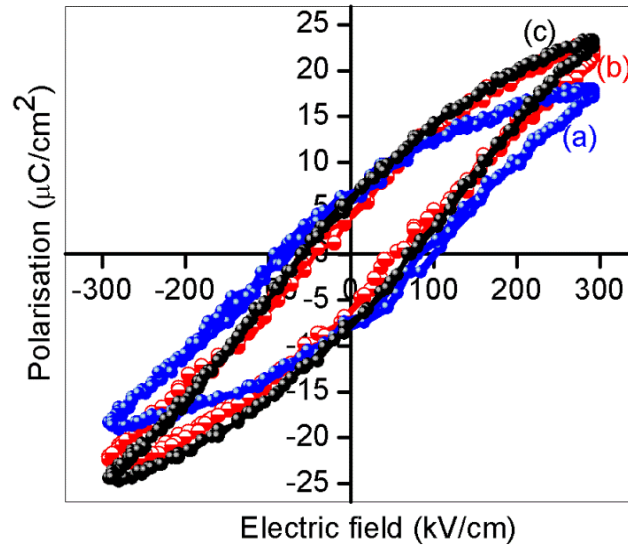


Figure 5.13: P-E hysteresis loop under bipolar excitation in $\{110\}$ -oriented $(1-x)$ PIN- x PT thin films (a) $x = 0.36$, (b) $x = 0.38$, (c) $x = 0.40$.

5.5 Conclusion

In this study we fabricated $\{110\}$ -preferentially oriented $(1-x)$ PIN- x PT thin films of $2.0 \mu\text{m}$ thickness on platinised silicon substrates using a hybrid MOD and sol-gel spin coating technique. The ST buffer layer was found to facilitate the $\{110\}$ -preferential orientation. The influence of thin film texture and composition on the transverse piezoelectric properties was established. The presence of discrete rhombohedral, monoclinic and tetragonal phases across the MPB could be identified through Raman spectral studies. All the thin films exhibited good dielectric, ferroelectric and piezoelectric properties indicating their suitability for MEMS. The $\{110\}$ -oriented PIN-0.36PT thin film was found to exhibit minimum nonlinearity in $|e_{31,f}|$ due to the presence of stable domains. A sharp increase in transverse piezoelectric coefficient was observed on moving from rhombohedral to monoclinic and tetragonal compositions as a result of the increased contribution of switching of the 90° domains.

References

- [1] E. F. Alberta and A. S. Bhalla, "Piezoelectric properties of $\text{Pb}(\text{InNb})_{(1/2)}\text{O}_3\text{-PbTiO}_3$ solid solution ceramics," *J. Korean Phys. Soc.*, **32** (1998) 1265.
- [2] A. A. Bokov and Z. G. Ye, "Field – induced shift of morphotropic phase boundary and effect of overpoling in $(1-x)\text{Pb}(\text{Mg}_{1/3}\text{Nb}_{2/3})\text{O}_3\text{-}x\text{PbTiO}_3$ piezocrystals," *Appl. Phys. Lett.*, **92** (2008) 082901.
- [3] F. Fang, W. Jing and W. Yang, "Interplay between polarisation rotation and crack propagation in PMN-PT relaxor single crystals," *Theor. Appl. Mech. Lett.*, **4** (2014) 051003.
- [4] J. A. Gallagher, J. Tian and C. S. Lynch, "Composition dependence of field induced phase transformations in [011]c PIN-PMN-PT relaxor ferroelectric single crystals with d_{322} piezoelectric mode," *Acta Mater.*, **81** (2014) 512.
- [5] H. Fu and R. Cohen, "Polarization rotation mechanism for ultrahigh electromechanical response in single-crystal piezoelectrics," *Nature.*, **403** (2000) 281.
- [6] J. Kuwata, K. Uchino and S. Nomura, "Phase transitions in the $\text{Pb}(\text{Zn}_{1/3}\text{Nb}_{2/3})\text{O}_3\text{-PbTiO}_3$ system," *Ferroelectrics.*, **37** (1981) 579.
- [7] [7] J. Kuwata, K. Uchino and S. Nomura, "Dielectric and piezoelectric properties of $0.91\text{Pb}(\text{Zn}_{1/3}\text{Nb}_{2/3})\text{O}_3\text{-}0.09\text{PbTiO}_3$ single crystals," *Jpn. J. Appl. Phys.*, **21** (1982) 1298.
- [8] B. Noheda, D. E. Cox, G. Shirane, S. E. Park, L. E. Cross and Z. Zhang, "Polarization rotation via a monoclinic phase in the piezoelectric $92\%\text{PbZn}_{1/3}\text{Nb}_{2/3}\text{O}_3\text{-}8\%\text{PbTiO}_3$," *Phy. Rev. Lett.*, **86** (2001) 3891.

- [9] B. Noheda, G. E. Cox and H. Shirane, "Stability of the monoclinic phase in the ferroelectric perovskite $\text{PbZr}_x\text{Ti}_{1-x}\text{O}_3$," *Phys. Rev. B.*, **63** (2000) 014103.
- [10] B. Jaffe, W. R. Cook and H. Jaffe, "Piezoelectric ceramics," Academic press, London, (1971).
- [11] S. E. Park and T. R. ShROUT, "Ultrahigh strain and piezoelectric behavior in relaxor based ferroelectric single crystals," *J. Appl. Phys.*, **82** (1997) 1804.
- [12] K. K. Rajan, J. Jin, W. S. Chang and L. C. Lim, "Transverse-mode properties of [011]-poled $\text{Pb}(\text{Zn}_{1/3}\text{Nb}_{2/3})\text{O}_3$ - PbTiO_3 single crystals: Effects of composition, length orientation, and poling conditions," *Jpn. J. Appl. Phys.*, **46** (2007) 681.
- [13] D. Zekria and A. M. Glazer, "Automatic determination of the morphotropic phase boundary in lead magnesium niobate titanate $\text{Pb}(\text{Mg}_{1/3}\text{Nb}_{2/3})(1-x)\text{Ti}_x\text{O}_3$ within a single crystal using birefringence imaging," *J. Appl. Crystallogr.*, **37** (2004) 143.
- [14] B. Noheda, D. E. Cox, G. Shirane, J. Gao and Z. G. Ye, "Phase diagram of the ferroelectric relaxor $(1-x)\text{Pb}(\text{Mg}_{1/3}\text{Nb}_{2/3})\text{O}_3$ - $x\text{PbTiO}_3$," *Phys. Rev. B.*, **66** (2002) 054104.
- [15] F. Bai, N. Wang, J. Li, D. Viehland, P. M. Gehring, G. Xu and G. Shirane, "X-ray and neutron diffraction investigations of the structural phase transformation sequence under electric field in $0.7\text{Pb}(\text{Mg}_{1/3}\text{Nb}_{2/3})$ - 0.3PbTiO_3 crystal," *J. Appl. Phys.*, **96** (2004) 1620.
- [16] S. Zhang, F. Li, X. Jiang, J. Kim, J. Luo and X. Geng, "Advantages and challenges of relaxor- PbTiO_3 ferroelectric crystals for electroacoustic transducers - A review," *Prog. Mater. Sci.*, **68** (2015) 1.

- [17] N. Setter, D. Damjanovic, L. Eng, G. Fox, S. Gevorgian and S. Hong, "Ferroelectric thin films: Review of materials, properties, and applications," *J. Appl. Phys.*, **100** (2006) 05160.
- [18] S. Tadigadapa and K. Mateti, "Piezoelectric MEMS sensors: state-of-the art and perspectives," *Meas. Sci. Technol.*, **20** (2009) 092001.
- [19] M. Dawber, K. M. Rabe and J. F. Scott, "Physics of thin-films ferroelectric oxides," *Rev. Mod. Phys.*, **77** (2005) 1083.
- [20] S. E. Park and W. Hackenberger, "High performance single crystal piezoelectrics: applications and issues," *Curr. Opin. Solid State Mater. Sci.*, **6** (2002) 11.
- [21] S. Wada, H. Kakemoto and T. Tsurumi, "Enhanced piezoelectric properties of piezoelectric single crystals by Domain Engineering," *Mater. Trans.*, **45** (2004) 178.
- [22] M. Davis, D. Damjanovic, D. Hayem and N. Setter, "Domain engineering of the transverse piezoelectric coefficient in perovskite ferroelectrics," *J. Appl. Phys.*, **98** (2005) 014102.
- [23] M. Suzuki, "Review on future ferroelectric non-volatile memory", *J. Ceram. Soc. Jpn.*, **103** (1995) 1099.
- [24] V. Kumar, I. Packiaselvam, K. Sivanandan, M. A. Vahab and A. K. Sinha, "Chemical solution deposition of $(\text{Ba}_{1-x}\text{Sr}_x)\text{TiO}_3$," *J. Am. Ceram. Soc.*, **89** (2006) 1136.
- [25] D. Ambika, V. Kumar, C. S. S. Sandeep and R. Philip, "Tunability of third order nonlinear absorption in $(\text{Pb,Lu})(\text{Zr,Ti})\text{O}_3$ thin films," *Appl. Phys. Lett.*, **98** (2011) 011903.
- [26] J. Fukushima, K. Kodaira and T. Matsushita, "Preparation of ferroelectric PZT films by thermal decomposition of organometallic compounds", *J. Mater. Sci.*, **19** (1984) 595.

- [27] R. W. Vest, "Metallo-organic decomposition (MOD) processing of ferroelectric and electro-optical films: A Review," *Ferroelectrics*, **102** (1990) 53.
- [28] R. W. Vest, "Electronic films from metallo-organic precursors" Ceramic films and coating, edited by J. B. Wachtman and R. A. Haber. Noyes publications, Park Ridge, NJ (1993) 303.
- [29] J. W. Moon, S. Tazawa, K. Shinozaki, N. Wakiya and N. Mizutani, "Impact of thin SrTiO₃ seed layer to achieve low-temperature crystallization below 300⁰C and ferroelectricity of lead zirconate titanate thin film," *Appl. Phys. Lett.*, **89** (2006) 202907.
- [30] C. J. Brinker, A. J. Hurd, P. R. Schunk, G. C. Frye and C. S. Ashley, "Review of sol-gel thin film formation," *J. Non-cryst. Solids*, **147** (1992) 424.
- [31] P. Muralt, "Ferroelectric thin films for micro-sensors and actuators: a review," *J. Micromech. Microeng.*, **10** (2000) 136.
- [32] M. Jain, S. B. Majumder, R. Guo, A. S. Bhalla and R. S. Katiyar, "Synthesis and characterization of lead strontium titanate thin films by sol-gel technique," *Mater Lett.*, **56** (2002) 692.
- [33] S. Laxmi Priya, V. Kumar, F. Kurokawa and I. Kanno, "Transverse piezoelectric properties of {110}-oriented PLZT[x/65/35] thin films," *Mater. Chem. Phys.*, **151** (2015) 308.
- [34] D. Ambika, V. Kumar, H. Imai and I. Kanno, "Sol-gel deposition and piezoelectric properties of {110}-oriented Pb(Zr_{0.52}Ti_{0.48})O₃ thin films," *Appl. Phys. Lett.*, **96** (2010) 031909.
- [35] D. Ambika, V. Kumar, K. Tomioka and I. Kanno, "Deposition of PZT thin films with {001}, {110} and {111} crystallographic orientations and their transverse piezoelectric characteristics," *Adv. Mat. Lett.*, **3** (2012) 102.

- [36] I. Kanno, H. Kotera and K. Wasa, "Measurement of transverse piezoelectric properties of thin films," *Sens. Actuators A Phys.*, **107** (2003) 68.
- [37] K. Sivanandan, T. A. Asha, V. Kumar and I. Kanno, "Fabrication and transverse piezoelectric characteristics of PZT thick-film actuators on alumina substrates," *Sens. Actuators A Phys.*, **148** (2008) 134.
- [38] Y. Ma, F. Wu and F. Guo, "Refined crystal structures and phase transitions in relaxor ferroelectric $0.24\text{Pb}(\text{In}_{1/2}\text{Nb}_{1/2})\text{O}_3$ - $0.43\text{Pb}(\text{Mg}_{1/3}\text{Nb}_{2/3})\text{O}_3$ - 0.33PbTiO_3 single crystal," *Jpn. J. Appl. Phys.*, **53** (2014) 051502.
- [39] B. Noheda, D. E. Cox, G. Shirane, J. A. Gonzalo, L. E. Cross and S. E. Park, "A monoclinic ferroelectric phase in the $\text{Pb}(\text{Zr}_{1-x}\text{Ti}_x)\text{O}_3$ solid solution," *Appl. Phys. Lett.*, **74** (1999) 2059.
- [40] S. Wongsanmai, X. Tan, S. Ananta and R. Yimnirun, "Dielectric and ferroelectric properties of fine grains $\text{Pb}(\text{In}_{1/2}\text{Nb}_{1/2})\text{O}_3$ - PbTiO_3 ceramics," *J. Alloys Compd.*, **454** (2008) 331.

LAXMI PRIYA S. "FERROELECTRIC THIN FILMS FOR MICROACTUATOR APPLICATIONS". THESIS. CENTRE FOR MATERIALS FOR ELECTRONICS TECHNOLOGY (C-MET), UNIVERSITY OF CALICUT, 2018.

Influence of Zr/Sn ratio on the transverse piezoelectric Coefficient $|e_{31,f}|$ in Lanthanum doped Lead Zirconate Titanate Stannate Thin Films

● Contents ●	6.1 Introduction
	6.2 Experimental
	6.3 Results and Discussion
	6.4. Conclusion
	References

Some of the contents of this chapter have appeared in the following research publication

S. Laxmi Priya, V. Kumar, Isaku Kanno, “Influence of Zr/Sn ratio on the Transverse Piezoelectric Coefficient $|e_{31,f}|$ in Lanthanum doped Lead Zirconate Titanate Stannate Thin Films”, *Journal of Materials Engineering and Performance* (communicated).

6.1 Introduction

Superior ferroelectric and piezoelectric properties offered by solid solutions of PZT with various dopants are an interesting field of research since they provide wide range of applications in non-volatile memories, random access memories, microactuators etc:¹⁻⁵. The need for ferroelectric and antiferroelectric thin films in the tin-modified $\text{PbZrO}_3\text{-PbTiO}_3$ system with high piezoelectric coefficients is also increasing as a result of various applications offered by such materials⁶⁻¹⁵. Antiferroelectric materials which undergo an electric field induced phase transition to the ferroelectric phase are reported for microactuator applications^{4,5} due to the excellent strain (large volume expansion) associated with the AFE \rightarrow FE switching. In addition to large strains, low switching field and low hysteresis makes AFE compositions in the $\text{Pb}(\text{Zr}_{0.50}\text{Ti}_{0.50})\text{O}_3\text{-Pb}(\text{Zr}_{0.50}\text{Sn}_{0.50})\text{O}_3\text{-PbZrO}_3$ system ideal candidates for actuator and transducer applications^{16,17}. Mostly studied antiferroelectric systems are PbZrO_3 , $(\text{Pb},\text{La})(\text{Zr},\text{Sn},\text{Ti})\text{O}_3$, $(\text{Pb},\text{Nb})(\text{Zr},\text{Sn},\text{Ti})\text{O}_3$ ¹⁸⁻²² etc. Compositions of particular interest are in the antiferroelectric tetragonal phase (AFE_{tet}) that can be readily switched to the ferroelectric rhombohedral (FE_{rh}) phase upon application of electric field^{23,24}. For PLSnZT compositions near the AFE-FE morphotropic phase boundary, apart from the Zr:Sn:Ti ratio, the antiferroelectric phase stability is an important criterion to obtain larger strains²⁵⁻²⁸. In the AFE perovskite phase, when Pb^{2+} ($r = 1.49\text{\AA}$) is substituted by La^{3+} ($r = 1.32\text{\AA}$) at the A-site, lattice shrinkage is expected to yield large strains. Substitution of Sn^{4+} ($r = 0.69\text{\AA}$) by Zr^{4+} ($r = 0.72\text{\AA}$) in the B-site yields a tolerance factor, $t < 1$, stabilising the perovskite AFE phase^{27,28}. According to Halliyal and ShROUT²⁹, a plot of tolerance factor (t) versus average electronegativity (χ) gives information regarding the stability of perovskite family of compounds across different substitutions and solid solutions. The average electronegativity is given as

$$\chi = \frac{\chi_{A-O} + \chi_{B-O}}{2} \quad (6.1)$$

where χ_{A-O} is the electronegativity difference between A cation and oxygen anion, χ_{B-O} is the electronegativity difference between B cation and oxygen anion. Figure 6.1 illustrates the relationship between t and χ of various perovskite compounds. Solid solutions of perovskite phase will be stabilised when either t or χ are increased and complex lead perovskite compounds will favour the pyrochlore phase when both values of t and χ will be lower. But antiferroelectric phase will be stabilised in NaNbO_3 (NN) by decreasing the value of t and by keeping the value of χ fixed.

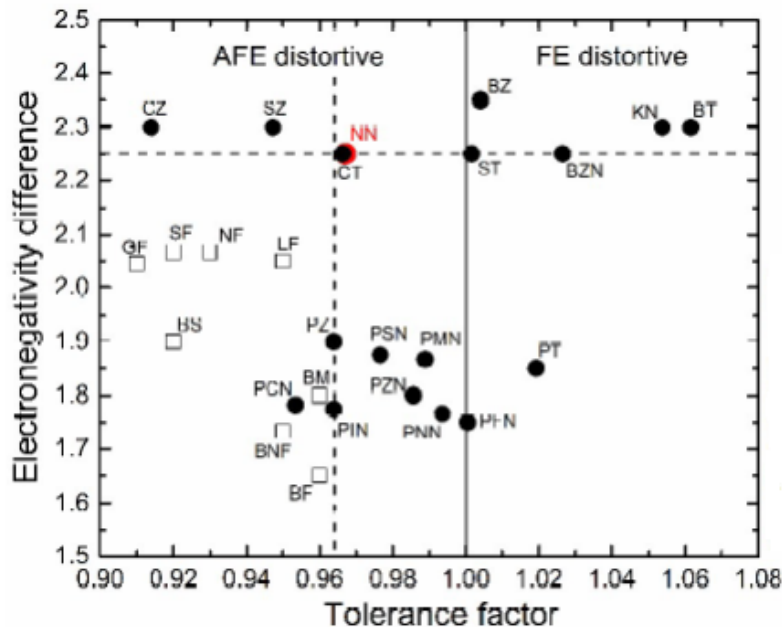


Figure 6.1: Tolerance factor versus averaged electronegativity difference for various perovskites. Here BT = BaTiO_3 , KN = KNbO_3 , BZN = $\text{Ba}(\text{Zn}_{1/3}\text{Nb}_{2/3})\text{O}_3$, BZ = BaZrO_3 , SZ = SrZrO_3 , CZ = CaZrO_3 , ST = SrTiO_3 , CT = CaTiO_3 , PT = PbTiO_3 , PMN = $\text{Pb}(\text{Mg}_{1/3}\text{Nb}_{2/3})\text{O}_3$, PSN = $\text{Pb}(\text{Sc}_{1/2}\text{Nb}_{1/2})\text{O}_3$, PZ = PbZrO_3 , PFN = $\text{Pb}(\text{Fe}_{1/2}\text{Nb}_{1/2})\text{O}_3$, PNN = $\text{Pb}(\text{Ni}_{1/3}\text{Nb}_{2/3})\text{O}_3$, PZN = $\text{Pb}(\text{Zn}_{1/3}\text{Nb}_{2/3})\text{O}_3$, PIN = $\text{Pb}(\text{In}_{1/2}\text{Nb}_{1/2})\text{O}_3$, PCN = $\text{Pb}(\text{Cd}_{1/3}\text{Nb}_{2/3})\text{O}_3$, BF = BiFeO_3 , NF = NdFeO_3 , BNF = $\text{Bi}_{0.8}\text{Nd}_{0.2}\text{FeO}_3$, LF = LaFeO_3 , SF = SmFeO_3 , GF = GdFeO_3 , BS = BiScO_3 , BM = BiMnO_3 .

[Source: A. Halliyal and T. R. Shrout, *Am. Ceram. Conf. (Regional)*, New Orleans, 1986].

Hence in this study, we focussed on the compositions with different Zr:Sn ratios, along the MPB, using the composition $\text{Pb}_{0.97}\text{La}_{0.02}(\text{Zr}_{1-x+y}\text{Sn}_x\text{Ti}_y)\text{O}_3$ as the basis and investigated the influence of electric field induced phase transition on dielectric, ferroelectric and transverse piezoelectric characteristics. In this system, the influence of electric field induced phase transition on transverse piezoelectric characteristics of thin films has not yet been reported.

6.2 Experimental

We selected the antiferroelectric compositions close to the antiferroelectric-ferroelectric phase boundary for our study. Stable precursor solutions of compositions $\text{Pb}_{0.97}\text{La}_{0.02}(\text{Zr}_{0.750}\text{Sn}_{0.150}\text{Ti}_{0.10})\text{O}_3$ [B], $\text{Pb}_{0.97}\text{La}_{0.02}(\text{Zr}_{0.775}\text{Sn}_{0.125}\text{Ti}_{0.10})\text{O}_3$ [C] and $\text{Pb}_{0.97}\text{La}_{0.02}(\text{Zr}_{0.80}\text{Sn}_{0.10}\text{Ti}_{0.10})\text{O}_3$ [D] near the morphotropic phase boundary in ternary $\text{Pb}(\text{Zr}_{0.50}\text{Ti}_{0.50})\text{O}_3$ - $\text{Pb}(\text{Zr}_{0.50}\text{Sn}_{0.50})\text{O}_3$ - PbZrO_3 phase diagram (Figure 6.2) were prepared by sol-gel method as described in our earlier work³⁰. The reactants lead acetate (99%, Merck, India), lanthanum acetyl acetonate (Sigma Aldrich, India) and zirconium acetyl acetonate (98%, Merck, India) were refluxed in ethanol for 1 hr to form a brown coloured solution. Tin (IV) isopropoxide (98%, Merck, India) was dissolved separately in an equimolar mixture of acetic acid and ethanol which was again treated with titanium (IV) isopropoxide (97%, Sigma Aldrich, India) in isopropyl alcohol containing equimolar amounts of acetyl acetone ($\geq 98\%$, Merck, India) as the chelating agent. The resulting mixture was then added to the previously obtained brown coloured solution and stirred well to make it homogeneous. The highly stable precursor solution was then spin coated on (111) Pt/Ti/SiO₂/Si substrate (Inostek, Korea). The spin coating was carried out on the substrate at a speed of 4000 rpm for 25 s. Each coated layer was dried in oven for 15 minutes and placed in furnace at 650°C for half an hour. This process was repeated to get PLSnZT thin films of 2.0 μm thickness. The crystalline phase of the

prepared films were determined by an X-ray diffractometer (Model: D5005, Bruker, Germany) and the structures of the different phases were analyzed with a Raman Spectrometer (Model: DXR, Thermo Scientific, USA). Dielectric and ferroelectric properties were measured using an impedance analyzer (HP 4294A, Agilent, USA and PE-2000 Piezoevaluation system) at 1 kHz. For this gold top electrode of 300 nm thickness were deposited on PLSnZT films by a vacuum coater (Model: 12A4D, Hind High Vacuum, India). For measuring transverse piezoelectric properties, rectangular beams of PLSnZT films were diced out along with the substrate and piezoelectric properties were evaluated using unimorph cantilevers of PLSnZT/Pt/Ti/SiO₂/Si. The details regarding measurement system have been given in our previous reports^{31,32}. By applying sine wave voltage between the top and bottom electrodes, piezoelectric vibration was generated and hence the tip displacement was measured using a laser Doppler vibrometer (Model: AT-3500, Graphtec, Japan) and a laser interferometer (Model: AT-1100, Graphtec, Japan).

6.3 Results and discussion

We selected three compositions, B, C and D in the antiferroelectric tetragonal region (AFE_T) $\text{Pb}_{0.97}\text{La}_{0.02}(\text{Zr}_{0.750}\text{Sn}_{0.150}\text{Ti}_{0.10})\text{O}_3$ [B], $\text{Pb}_{0.97}\text{La}_{0.02}(\text{Zr}_{0.775}\text{Sn}_{0.125}\text{Ti}_{0.10})\text{O}_3$ [C] and $\text{Pb}_{0.97}\text{La}_{0.02}(\text{Zr}_{0.80}\text{Sn}_{0.10}\text{Ti}_{0.10})\text{O}_3$ [D] as reported earlier in the ternary phase diagram (Figure 6.2)³³. These three compositions which are very close to the morphotropic phase boundary separating the AFE_T and FE_R phases as indicated in Figure 6.2, differ in their Zr/Sn ratios. In such thin films, application of a sufficient electric field induces AFE → FE phase transition since they are very close to the boundary separating the two phases.

Figure 6.3 shows the X-ray diffraction (XRD) patterns obtained for the PLSnZT compositions. It is observed that all the films crystallise in the pure perovskite phase. Interestingly, thin films of composition B is found to

exhibit a higher degree of {110}-orientation than those of composition C which in turn exhibit a higher {110} orientation than D.

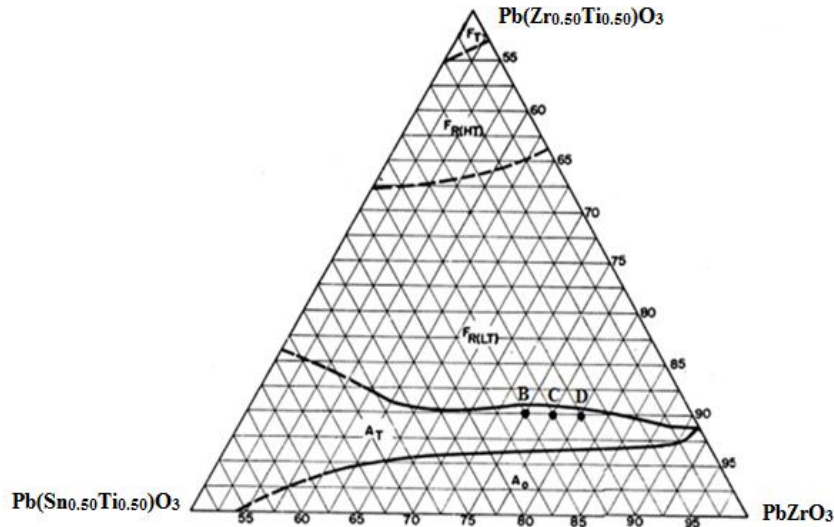


Figure 6.2: PZT-PZSn-PZ ternary phase diagram showing antiferroelectric orthorhombic (A_0), antiferroelectric tetragonal (A_T) and ferroelectric rhombohedral (FE_R) phases. Compositions studied in the present work are marked B, C and D respectively.

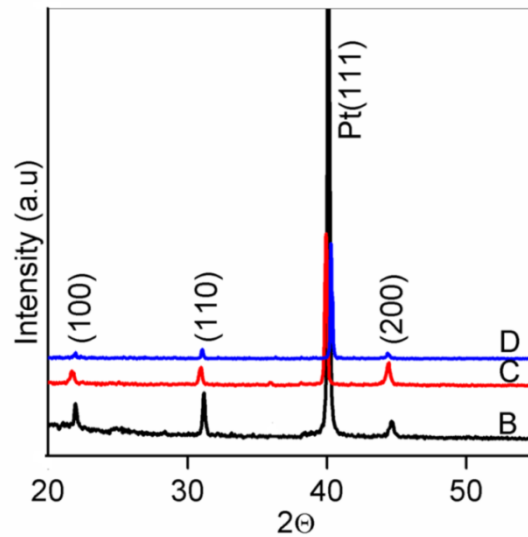


Figure 6.3: X-ray diffraction pattern of $\text{Pb}_{0.97}\text{La}_{0.02}(\text{Zr}_x\text{Sn}_y\text{Ti}_z)\text{O}_3$ thin films. (B) $x = 0.750$, $y = 0.150$, $z = 0.10$; (C) $x = 0.775$, $y = 0.125$, $z = 0.10$ and (D) $x = 0.80$, $y = 0.10$, $z = 0.10$ on (111)Pt/Ti/SiO₂/Si substrate.

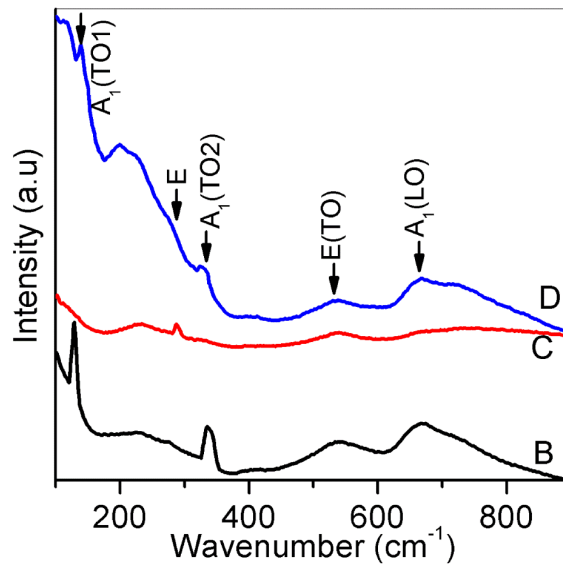


Figure 6.4: Raman spectra of $\text{Pb}_{0.97}\text{La}_{0.02}(\text{Zr}_x\text{Sn}_y\text{Ti}_z)\text{O}_3$ thin films. (B) $x = 0.750$, $y = 0.150$, $z = 0.10$; (C) $x = 0.775$, $y = 0.125$, $z = 0.10$ and (D) $x = 0.80$, $y = 0.10$, $z = 0.10$ on (111)Pt/Ti/SiO₂/Si substrate.

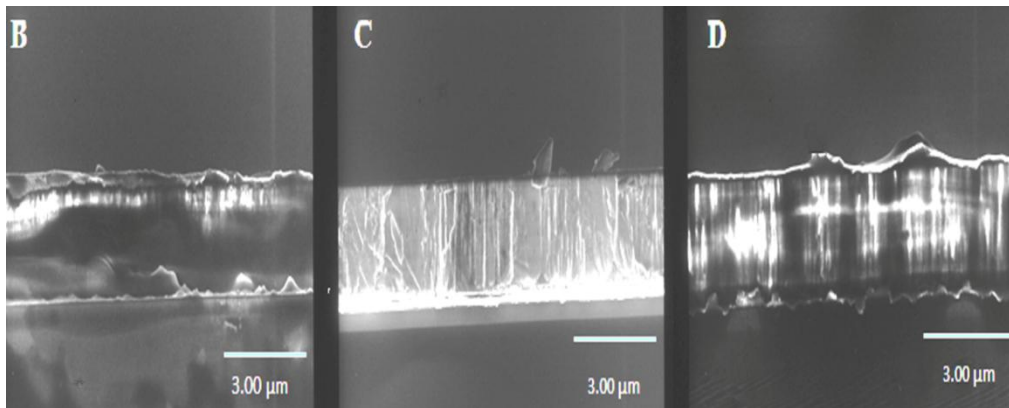


Figure 6.5: HRSEM of $\text{Pb}_{0.97}\text{La}_{0.02}(\text{Zr}_x\text{Sn}_y\text{Ti}_z)\text{O}_3$ thin films. (B) $x = 0.750$, $y = 0.150$, $z = 0.10$; (C) $x = 0.775$, $y = 0.125$, $z = 0.10$ and (D) $x = 0.80$, $y = 0.10$, $z = 0.10$ on (111)Pt/Ti/SiO₂/Si substrate.

From the Raman spectral data depicted in Figure 6.4, it is clear that compositions B and D are purely tetragonal as evidenced from the $A_1(\text{TO}1)$ mode at 140 cm^{-1} and $A_1(\text{TO}2)$ mode at 326 cm^{-1} . It can also be clearly seen

that the tetragonal content is higher for thin films of B. But for composition C, these peaks are absent. The SEM cross sectional images of the thin films in Figure 6.5 reveal a columnar microstructure.

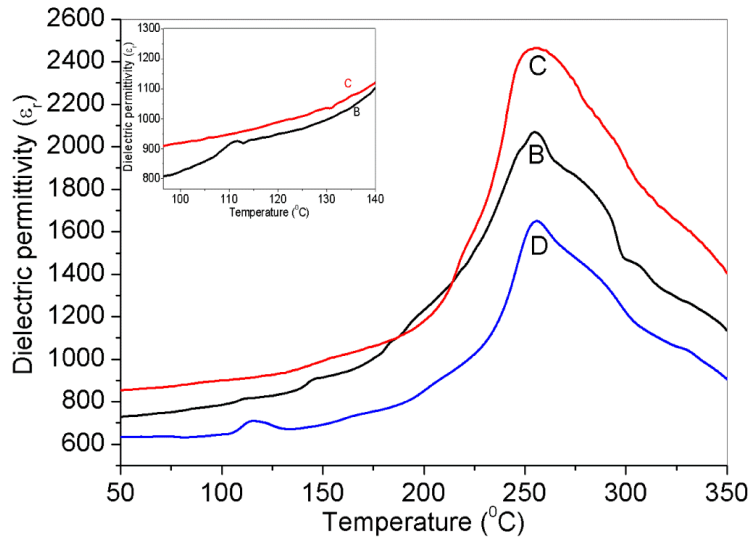


Figure 6.6: Temperature dependence of dielectric permittivity of (B) $x = 0.750$, $y = 0.150$, $z = 0.10$; (C) $x = 0.775$, $y = 0.125$, $z = 0.10$ and (D) $x = 0.80$, $y = 0.10$, $z = 0.10$ on (111)Pt/Ti/SiO₂/Si substrate.

The room temperature dielectric permittivity and dielectric loss of PLSnZT thin films measured as a function of frequency at 1 kHz are given in Table 6.1. The values obtained reveal the good quality of the thin films. Figure 6.6 demonstrates the variation of dielectric permittivity ϵ_r as a function of temperature. In the case of thin films having compositions B and D, the dielectric anomaly around 110⁰C correspond to the AFE-FE transition²⁷. It is also clearly seen that the AFE-PE transition temperature around 250⁰C shifts to higher values with increasing Zr⁴⁺ content (Table 1). For composition C, absence of dielectric anomaly in this temperature region (inset of Figure 6.6) confirms the stability of the AFE composition.

Table 6.1 Dielectric and piezoelectric properties of thin films

$\text{Pb}_{0.97}\text{La}_{0.02}(\text{Zr}_{1-x+y}\text{Sn}_x\text{Ti}_y)\text{O}_3$	Tolerance factor, t	AFE- FE $T(^{\circ}\text{C})$	AFE- PE $T(^{\circ}\text{C})$	Dielectric permittivity ϵ_r	Dielectric loss, $\tan \delta$	Transverse piezoelectric coefficient, $ e_{31,f} $ (C/m^2)	Nature (at RT)
$\text{Pb}_{0.97}\text{La}_{0.02}(\text{Zr}_{0.750}\text{Sn}_{0.150}\text{Ti}_{0.10})\text{O}_3$ [B]	0.8192	110	252	1400	0.01	3.8	FE
$\text{Pb}_{0.97}\text{La}_{0.02}(\text{Zr}_{0.775}\text{Sn}_{0.125}\text{Ti}_{0.10})\text{O}_3$ [C]	0.8191	-	255	1000	0.02	1.2	AFE
$\text{Pb}_{0.97}\text{La}_{0.02}(\text{Zr}_{0.80}\text{Sn}_{0.10}\text{Ti}_{0.10})\text{O}_3$ [D]	0.8190	110	256	1156	0.02	2.6	FE

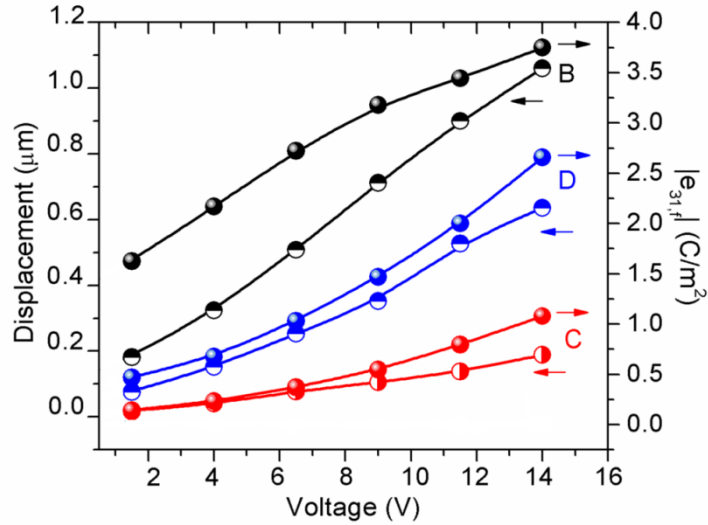


Figure 6.7: Tip displacement of PLSnZT/Si unimorph cantilever and $|e_{31,f}|$ as a function of applied unipolar voltage. (B) $x = 0.750$, $y = 0.150$, $z = 0.10$; (C) $x = 0.775$, $y = 0.125$, $z = 0.10$ and (D) $x = 0.80$, $y = 0.10$, $z = 0.10$ on (111)Pt/Ti/SiO₂/Si substrate.

For measuring the transverse piezoelectric properties of PLSnZT films, unipolar sine wave voltage was applied between the top and bottom electrodes. In this experiment we measured the tip displacement at a frequency of 500Hz. Figure 6.7 shows the tip displacements obtained for PLSnZT thin films as a function of applied electric field.

At low electric fields, the low tip displacement obtained indicates the stability of AFE phase. With increasing electric field, the AFE \rightarrow FE phase transformation is confirmed by a relatively large increase in displacement values obtained in the case of B and D as shown in Figure 6.7. From the tip displacements obtained, the transverse piezoelectric coefficient $|e_{31,f}|$, was evaluated as per equation (6.2) given below

$$|e_{31,f}| = \frac{d_{31}}{s_{11,p}^E + s_{12,p}^E} \cong -\frac{h_s^2}{3s_{11,s}(1-\nu_s)L^2} \frac{\delta}{V} \quad (6.2)$$

Here δ , V , L , h_s , $s_{11,s}$ and ν_s are the tip displacement, applied voltage between top and bottom electrodes, length of the cantilever, thickness, elastic compliance and Poisson's ratio respectively³⁴. The subscripts "s" and "p" indicates the substrate and the piezoelectric film respectively. The elastic compliance of the substrate is $5.9E-12 \text{ m}^2/\text{N}$ which is the reciprocal of Young's modulus. The Poisson's ratio of $\langle 110 \rangle$ Si. is reported as 0.066 ³⁵. Transverse piezoelectric coefficient $|e_{31,f}|$ obtained using the above equation is also plotted in Figure 6.7.

It is seen that the $|e_{31,f}|$ values obtained for compositions B and D are higher when compared to that of C. This can be explained as follows: Thin films exhibiting $\{110\}$ -orientation having rhombohedral and tetragonal phases exhibit different domain switching mechanisms as illustrated in Figures 6.8 (a) and (b) respectively.

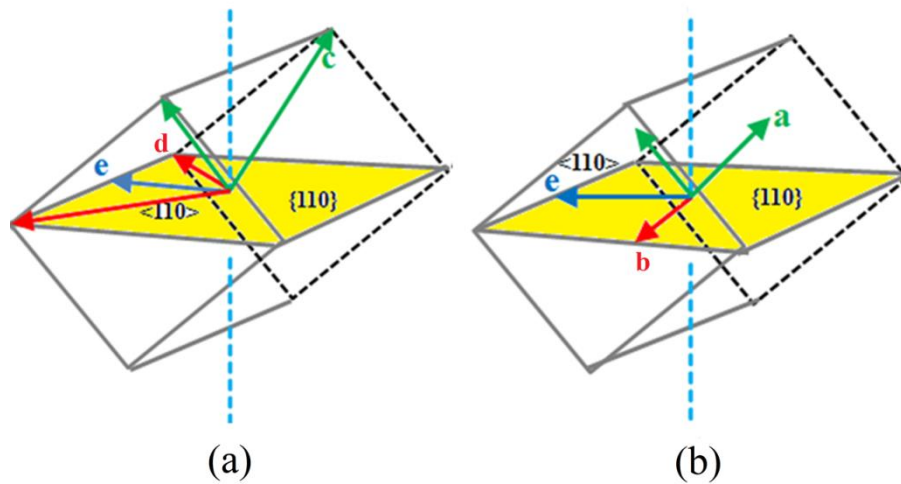


Figure 6.8: Domains in $\{110\}$ - preferentially oriented PLZT thin films having (A) rhombohedral and (B) tetragonal structure

Composition B with tetragonal structure is found to exhibit the highest degree of $\{110\}$ -orientation. In such thin films with a higher degree of $\{110\}$ -orientation and having tetragonal structure, domains \vec{a} are at an angle of 45°

and \vec{b} at an angle of 90° with the film normal as shown in Figure 6.8 b. Out of these, 90° domain switch will yield higher strains giving rise to increased $|e_{31,f}|$ values^{36,37,38}. Higher values of $|e_{31,f}|$ obtained for thin films of B is attributed to the higher tetragonal content. The lower $|e_{31,f}|$ values of composition C shows higher stability of the AFE state due to its higher Zr/Sn ratio.

The polarization-electric field (P-E) curves of PLSnZT films are shown in Figure 6.9. The P-E loops indicate that the PLZST thin films exhibit ferroelectric nature, in spite of their AFE nature for bulk ceramics. This is attributed to the compressive/tensile stresses due to mismatch in the coefficient of thermal expansion of the film and the underlying substrate. Here maximum remanent polarization, $2P_r = 38 \mu\text{C}/\text{cm}^2$, is obtained for thin films of composition B, where as those of D and C showed $2P_r$ values of 36 and $28 \mu\text{C}/\text{cm}^2$ respectively. The larger remanent polarization values of B and D are due to the ferroelectric phase. In the case of C lower values of P_r and higher values of E_{A-F} (field required for AFE-FE transition) reveal the stability of the antiferroelectric phase.

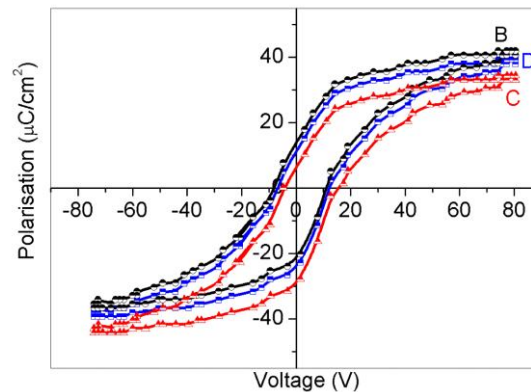


Figure 6.9: P-E hysteresis loop under bipolar excitation in PLSnZT thin films. (B) $x = 0.750$, $y = 0.150$, $z = 0.10$, (C) $x = 0.775$, $y = 0.125$, $z = 0.10$ and (D) $x = 0.80$, $y = 0.10$, $z = 0.10$ on (111)Pt/Ti/SiO₂/Si substrate.

6.4. Conclusion

Antiferroelectric lead lanthanum stannate zirconate titanate thin films having thickness of 2.0 μm were prepared on (111)Pt/Ti/SiO₂/Si substrate by sol-gel spin coating technique. The electric field induced AFE \rightarrow FE phase transition for three different compositions along the AFE_(T)-FE_(R) phase boundary were investigated by studying the differences in their dielectric, ferroelectric and transverse piezoelectric characteristic ($|e_{31,f}|$). The AFE \rightarrow FE transition was also confirmed by structural investigations through Raman spectroscopy. The AFE \rightarrow FE field induced transition was correlated with the stability of the AFE_(T) state in these compositions.

References

- [1] K. Kanda, I. Kanno, H. Kotera and K. Wasa, "Simple Fabrication of Metal-Based Piezoelectric MEMS by Direct Deposition of Pb(Zr,Ti)O₃ Thin Films on Titanium Substrates," *J. Microelectromech. Syst.*, **18** (2009) 610.
- [2] S. K. Pandey, O. P. Thakur, D. K. Bhattacharya, Harsh C. Prakash and R. Chatterjee, "Effect of double doping in lead zirconate titanate (PZT) lattices by sol-gel technique for MEMS applications," *Integr. Ferroelectr.*, **121** (2010) 65.
- [3] R. A. Wolf and T. S. McKinstry, "Temperature dependence of the piezoelectric response in lead zirconate titanate films," *J. Appl. Phys.*, **95** (2004) 1397.
- [4] J. P. George, J. Beckman, W. Woestenborghs, P. F. Smet, W. Bogaerts and K. Neyts, "Preferentially oriented BaTiO₃ thin films deposited on silicon with thin intermediate bufferlayers," *Nanoscale Res. Lett.*, **8** (2013) 62-1-7.
- [5] N. Izyumskaya, Y. I. Alivov, S. J. Cho, H. Morkoc, H. Lee & Y. S. Kang, "Processing, structure, properties and Applications of PZT Thin films," *Crit. Rev. Solid State Mater. Sci.*, **32** (2007) 111.
- [6] D. Berlincourt, H. Jaffe, H. H. A. Krueger and B. Jaffe, "Release of Electric energy in PbNb(Zr,Ti,Sn)O₃ by Temperature and by Pressure-Enforced phase transitions," *Appl. Phys. Lett.*, **3** (1963) 90.
- [7] L. E. Cross, "Antiferroelectric–Ferroelectric switching in simple 'Kittle' Antiferroelectrics," *J. Phys. Soc. Jpn.*, **23** (1967) 77.

- [8] B. Jaffe, W. R. Cooke, Jr., and H. Jaffe, "Piezoelectric Ceramics; Monographs on Non-metallic Solids," Edited by J.P. Roberts and P. Popper, Academic Press, London, (1971) 135.
- [9] D. Berlincourt, H. H. Krueger and B. Jaffe, "Stability of phase in modified Lead Zirconate with variation in pressure, Electric field, Temperature and Composition," *Phys. Chem. Solids.*, **25** (1964) 659.
- [10] K. Uchino and S. Nomura, "Shape Memory Effect Associated with the Forced phase transition in Antiferroelectrics," *Ferroelectrics.*, **50** (1983) 517.
- [11] S. S. N. Bharadwaja, S. B. Krupanidhi, "Growth and study of antiferroelectric lead zirconate thin films by pulsed laser ablation," *J. Appl. Phys.*, **86** (1999) 5862.
- [12] D. Berlincourt, "Transducers using Forced Transitions between Ferroelectric and Antiferroelectric state," *IEEE Trans Ultrason Ferroelectr Freq Control.*, **SU-13(4)** (1966) 116.
- [13] K. Uchino, "Digital displacement transducer using antiferroelectrics," *Jpn. J. Appl. Phys.*, **24** (1985) 460.
- [14] W. Y. Pan, C. Q. Dam, Q. M. Zhang and L. E. Cross, "Large displacement transducers based on electric field forced phase transition in the tetragonal $(\text{Pb}_{0.97}\text{La}_{0.02})(\text{Ti,Zr,Sn})\text{O}_3$ family of ceramics," *J. Appl. Phys.*, **66** (1989) 6014.
- [15] Y. Li, Q. Li, X. Chu, "Domain dielectric and optical studies in antiferroelectric $(\text{Pb,L a})(\text{Zr,Sn,Ti})\text{O}_3$ single crystals," *Solid State Commun.*, **152** (2012) 1791.
- [16] B. Xu, Y. Ye and L. E. Cross, "Dielectric properties and field-induced phase switching of lead zirconate titanate stannate antiferroelectric thick films on silicon substrates," *J. Appl. Phys.*, **87** (2000) 2507.

- [17] C. J. Gaskey, K. R. Udayakumar, H. D. Chen and L. E. Cross, "Antiferroelectric to ferroelectric phase switching thin films in the lead zirconate stannate titanate solid solution system," in: Proceedings of the 9th IEEE International symposium, Application of Ferroelectrics., (1994) 416.
- [18] K. Y. Yamakawa, T. S. Mc Kinstry, J. P. Dougherty and S. B. Krupanidhi, "Reactive magnetron co-sputtered antiferroelectric lead zirconate thin films," *Appl. Phys. Lett.*, **67** (1995) 2014.
- [19] B. Xu, P. Moses, N. G. Pai and L. E. Cross, "Charge release of lanthanum-doped lead zirconate titanate stannate antiferroelectric thin films," *Appl. Phys. Lett.*, **72** (1998) 593.
- [20] B. Xu, Y. Ye and L. E. Cross, "Dielectric properties and field-induced phase switching of lead zirconate titanate stannate antiferroelectric thick films on silicon substrates," *J. Appl. Phys.*, **87** (2000) 2507.
- [21] B. Xu, L. E. Cross and J. J. Bernstein, "Ferroelectric and antiferroelectric films for microelectromechanical systems applications," *Thin Solid Films.*, **377** (2000) 712.
- [22] J. H. Jang and K. H. Yoon, "Electric fatigue in antiferroelectric and ferroelectric $\text{Pb}(\text{Zr}, \text{Sn}, \text{Ti})\text{NbO}_3$ thin films prepared by sol-gel process," *Jpn. J. Appl. Phys.*, **37** (1998) 5162.
- [23] D. Berlincourt, "Transducers using the electric field-forced antiferroelectric-ferroelectric transition," *Ultrasonics.*, **6** (1968) 48.
- [24] D. Berlincourt, H. H. A. Krueger and B. Jaffe, "Stability of phases in modified lead zirconate with variation in pressure, electric field, temperature and composition," *J. Phys. Chem. Solids.*, **25** (1964) 659.

- [25] K. A. Markowski, S. E. Park, S. Yoshikawa and L. E. Cross, "Effect of compositional variations in the lead lanthanum zirconate stannate titanate system on electrical properties," *J. Am. Ceram. Soc.*, **79** (1996) 3297.
- [26] M. J. Pan, S. E. Park, K. A. Markowski, W. S. Hackenberger, S. Yoshikawa and L. E. Cross, "Electric field induced phase transition in Lead lanthanum stannate zirconate titanate (PLSnZT) antiferroelectrics: Tailoring properties through compositional modification," *Ferroelectrics.*, **215** (1998) 153.
- [27] Y. Feng, Z. Xu, H. Li, X. Yao, "Effects of La modifier on the electric hysteresis of lead zirconate stannate titanate compounds," *Ceram. Int.*, **30** (2004) 1393.
- [28] W. Pan, Q. Zhang, A. Bhalla and L. E. Cross, "Field-Forced Antiferroelectric-to-Ferroelectric Switching in Modified Lead Zirconate Titanate Stannate Ceramics," *J. Am. Ceram. Soc.*, **72** (1989) 571
- [29] A. Halliyal and T. R. Shrout, "Preparation of lead based ferroelectric relaxors for capacitors," *Am. Ceram. Soc. Bull.*, **66** (1987) 704.
- [30] K. G. Brooks, J. Chen, K. R. Udayakumar and L. E. Cross, "Electric field forced phase switching in La modified lead zirconate titanate stannate thin films," *J. Appl. Phys.*, **75** (1994) 1699.
- [31] I. Kanno, H. Kotera, K. Wasa, "Measurement of transverse piezoelectric properties of thin films," *Sens. Actuators, A.*, **107** (2003) 68.
- [32] K. Sivanandan, T. A. Asha, V. Kumar, I. Kanno, "Fabrication and transverse piezoelectric characteristics of PZT thick-film actuators on alumina substrates," *Sens. Actuators, A., Physical*, **148** (2008) 134.

- [33] D. Berlincourt, “Transducers using forced transitions between ferroelectric and antiferroelectric states”, presented at IEEE, 1965 Ultrasonics symposium (1965).
- [34] J. G. Smits, W. Choi, “The constituent equations of piezoelectric heterogenous bimorphs,” *IEEE Trans.*, **38** (1991) 256.
- [35] M. A. Hopcroft, W. D. Nix and T. W. Kenny, “What is the Young’s modulus of silicon?”, *J. Micro. Electro. Mech. S.*, **19** (2010) 229.
- [36] M. S. Mirshekarloo, L. Zhang, K. Yao, T. Sritharan, “Electromechanical properties and fatigue of antiferroelectric (Pb,La)(Zr,Sn,Ti)O₃ thin film cantilevers fabricated by micromachining,” *Sens. Actuators, A.*, **187** (2012) 127.
- [37] D. Ambika, V. Kumar, H. Imai and I. Kanno, “Sol-gel deposition and piezoelectric properties of {110}-oriented PZT thin films,” *Appl. Phys. Lett.*, **96** (2010) 031909.
- [38] S. Laxmi Priya, V. Kumar, S. Nishio and I. Kanno, “Improved transverse piezoelectric properties in {110}-oriented B-site acceptor doped PLZT (8/65/35) thin films,” *Integr. Ferroelectr.*, **176** (2016) 210.

HIGHLIGHTS OF THE PRESENT WORK

The major outcomes of the present work are:

- ✚ High quality, dense, crack free and preferentially oriented ferroelectric thin films based on PZT having compositions near the $FE_{(R)}$ - $FE_{(T)}$ morphotropic phase boundary PLZT (6/65/35), (7/56/44), (7/60/40), (7/65/35), (8/65/35) and antiferroelectric thin films near the $AFE_{(T)}$ - $FE_{(R)}$ phase boundary have been prepared by Chemical solution deposition method using spin coating technique.
- ✚ Transverse piezoelectric coefficient, $|e_{31,f}|$ of such thin films have been determined by Cantilever method.
- ✚ Correlation of thin film structure and texture with their dielectric and piezoelectric properties have been established.
- ✚ Mechanism for higher bipolar strain in B-site Cu^{2+} and Mn^{3+} doped PLZT thin films has been established.
- ✚ In the case of thin films of compositions near MPB $(1-x)$ PIN- x PT, where $x = 0.36-0.40$, the stabilisation of discrete rhombohedral, monoclinic and tetragonal crystalline phases have also been established through detailed Raman spectral investigations.
- ✚ In thin films of antiferroelectric compositions $Pb(Zr_{0.50}Ti_{0.50})O_3$ - $Pb(Zr_{0.50}Sn_{0.50})O_3$ - $PbZrO_3$, the $AFE \rightarrow FE$ field induced transition was also correlated with the stability of the $AFE_{(T)}$ state in these compositions.

LIST OF RESEARCH PUBLICATIONS

Following are the research publications that have been published in different international journals

1. **S. Laxmi Priya**, V. Kumar, Fumiya Kurokawa, Isaku Kanno, “Transverse piezoelectric properties of {100}-oriented PLZT[x/65/35] thin films,” **Materials Chemistry and Physics**, 151, (2015) 308-311.
2. **S. Laxmi Priya**, V. Kumar, Shogo Nishio, Isaku Kanno, “Composition dependence of transverse piezoelectric properties of preferentially {110}-oriented ($I-x$) PIN- x PT thin films,” **Journal of Alloys and Compounds**, 688, (2016) 863-867.
3. **S. Laxmi Priya**, V. Kumar, Shogo Nishio, Isaku Kanno, “Improved piezoelectric response in {110}-oriented B-site acceptor doped PLZT (8/65/35) thin films,” **Integrated Ferroelectrics**, 176, (2016) 210-219.
4. **S. Laxmi Priya**, V. Kumar, Isaku Kanno, “Influence of Zr/Sn ratio on the Transverse Piezoelectric Coefficient $|e_{31,f}|$ in Lanthanum doped Lead Zirconate Titanate Stannate Thin Films,” **Journal of Materials Engineering and Performance** (communicated).
5. **S. Laxmi Priya**, V. Kumar, Takuya Teramoto, Isaku Kanno, “Transverse Piezoelectric properties of {110}-oriented PLZT thin films,” **Integrated Ferroelectrics** (under review).
